MECHANISMS AND IMPLICATIONS OF THE LOW DOSE INTRINSIC

RADIATION SURVIVAL RESPONSE

by

BRADLY GARRY WOUTERS

B.Eng., The University of Saskatchewan, 1991

A THESIS SUBMITTED IN PARTIAL FULFILLMENT OF

THE REQUIREMENTS FOR THE DEGREE OF

DOCTOR OF PHILOSOPHY

in

THE FACULTY OF GRADUATE STUDIES

(Department of Physics and Astronomy)

We accept this thesis as conforming
to the required standard

THE UNIVERSITY OF BRITISH COLUMBIA

April, 1996

©Bradly Garry Wouters, 1996

In presenting this thesis in partial fulfilment of the requirements for an advanced degree at the University of British Columbia, I agree that the Library shall make it freely available for reference and study. I further agree that permission for extensive copying of this thesis for scholarly purposes may be granted by the head of my department or by his or her representatives. It is understood that copying or publication of this thesis for financial gain shall not be allowed without my written permission.

Department of _PHYSICS_

The University of British Columbia
Vancouver, Canada

Date _APRIL 08, 1996_

ABSTRACT

Previous studies in this laboratory using a precise assay for measurement of cell survival revealed substructure in the radiation response of asynchronously growing cells. The substructure appeared to result from selective killing of sensitive cells in the cell-cycle, such that the radiosensitivity of the surviving population decreased with increasing dose. Accurate characterization of the low dose response with the linear quadratic (LQ) model resulted in smaller α/β ratios than predicted from a fit to the entire response, suggesting that survival at low doses must be measured, rather than extrapolated, in order to evaluate particular treatment strategies. We have used this same assay in an *in vitro* model system, based on a panel of several human tumour cell lines, to investigate the efficacy of two hypoxic radiosensitizers, etanidazole (2-(2-nitro-1-imidazolyl)-N-(2-hydroxyethyl) acetamide) and RB6145 (1H-imidazole-1-ethanol, α-([(2-bromoethyl) amino]methyl) -2-nitro-,monohydrobromide). The results reveal a cell line and radiation dose dependence for the sensitizing ability of these drugs. Modeling the low dose data indicates that sensitization by RB6145 and etanidazole results primarily from modification of the α and β parameters, respectively. Consequently, the efficacy and dose dependence of these sensitizers are tumour specific, determined more by differences in the low dose α and β values than by overall radiosensitivity.

In order to understand the variability of radiosensitivity and α/β ratios among different cell lines, the radiation dose-response relationship was investigated at very low doses ($\sim$0-4 Gy) in 3 human tumour cell lines. The results indicate a region of hypersensitivity below doses of $\sim$0.5 Gy. This is followed by an increase in resistance from $\sim$0.3 to 0.7 Gy, beyond which the response follows that predicted by the LQ model.

Modeling the radiation responses, and survival measurements in synchronous populations, suggest it is unlikely that this phenomenon is due to a small sub-population of sensitive cells (*e.g.,* mitotic), but rather that it reflects the ability of the cells to initiate a radiation resistance mechanism. The results also suggest a lack of sub-lethal damage repair following doses within the hypersensitive region. Together, these results suggest that a dose-dependent alteration in the processing of DNA damage at low doses may contribute to intrinsic radiosensitivity.

The implications of the low dose response were also evident in measurements of the relative biological effectiveness (RBE) of the 70 MeV proton spread out Bragg peak (SOBP) at TRIUMF. V79-WNRE Chinese hamster cell survival responses were measured as a function of dose and depth within the SOBP and compared with the response to ^{60}Co γ-rays. The shapes of the low dose responses (α/β ratios) following proton and ^{60}Co irradiation exhibited significant differences which impacted on the absolute value and dose dependence of the RBE. Above doses of 5 Gy, the RBE throughout the SOBP was relatively constant (1.21 ± 0.05), but below 4 Gy it increased significantly with decreasing dose. Based on the results with radiosensitizers, we argue that the RBE value and its dose dependence will be *cell line* dependent, and should be predicted, in part, by the low dose α and β values determined from the X-ray or ^{60}Co response. A consistent increase in RBE with increased depth in the SOBP was also observed, and at the distal edge of the stopping distribution it increased to an extent that may be of concern when this region of the treatment volume is close to sensitive tissues. These results illustrate the oversimplification of the use single RBE values for irradiation protocols, and argues for the use of proton gray doses rather than cobalt-equivalent grays.

TABLE OF CONTENTS

LIST OF FIGURES

LIST OF TABLES

LIST OF ABBREVIATIONS

ABS	Acrylonitrile Butadiene Styrene
ADIR	Accumulated Damage Induced Radioresistance
AT	ataxia telangectasia
ATCC	American Type Culture Collection
bp	base pairs
BrdU	Bromodeoxyuridine
BSA	Bovine Serum Albumin
CHO	Chinese Hamster Ovary
CT	Computed Tomography
$\overline{D}$	mean inactivation dose
DMIPS	Dynamic Microscopic Image Processing Scanner
DNA	Deoxyribonucleic Acid
DSB	Double-Strand Break
E0-9	3-hydroxymethyl-5-aziridinyl-1-methyl-2-(1H-indole-4,7-dione)prop-β-en-α-ol
ECHED	European Clinical Heavy Particle Dosimetry Group
EDTA	Ethylenediamine-Tetraacetic Acid
FACS	Fluorescence Activated Cell Sorter
FITC	Fluorescent Isothiocyanate
G	radiochemical yield
GSH	Glutathione (reduced form)
Gy	Gray
HCl	Hydrochloric Acid
HEPES	N-(2-Hydroxyethyl)piperazine-N'-(2-ethanesulfonic acid)
kbp	kilobase pairs
LET	Linear Energy Transfer
LET_d	Dose-Averaged Linear Energy Transfer
LQ	Linear Quadratic
LSS	Lifespan Study
m.w.	molecular weight
MEM	Minimum Essential Medium
MeV	Mega electron Volts
MI	Mithramycin
mitomycin C	[1aS-(1aα,8β,8aα,8bα)]-6-amino-8-[[(aminocarbonyl)oxy]methyl]-1,1a,2,8,8a,8b-hexa-hydro-8a-methoxy-5-methylazirino[2',3':3,4]pyrrolo[1,2-a]-indole-4,7-dione
mm Hg	millimeters of mercury
MRI	Magnetic Resonance Imaging
nA	nanoamperes
OER	Oxygen Enhancement Ratio
PBS	Phosphate Buffered Saline
PCD	Programmed Cell Death
PE	Plating Efficiency
PI	Propidium Iodide
PI-3	Phosphatidylinositol 3
PKC	Protein Kinase C
ppm	parts per million
RBE	Relative Biological Effectiveness
RMS	Root Mean Squared
S	Survival

S	Survival
SER	Sensitizer Enhancement Ratio
SF_2	Surviving Fraction at 2 Gy
SLDR	Sublethal Damage Repair
SOBP	Spread Out Bragg Peak
t_c	cell-cycle transit time
t_d	tumour volume doubling time
t_{pot}	tumour potential doubling time
tirapazamine	3-amino-1, 2, 4-benzotriazine-1, 4-di-N-oxide
TPLQ	Two Population Linear Quadratic
TRIUMF	Tri-University Meson Facility
ZPE	Zero-Dose Plating Efficiency

Misonidazole: 3-Methoxy-1-(2-nitro-1-imidazolyl)-2-propanol
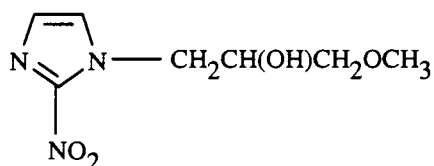
Etanidazole: 2-(2-nitro-1-imidazolyl)-N-(2-hydroxyethyl) acetamide
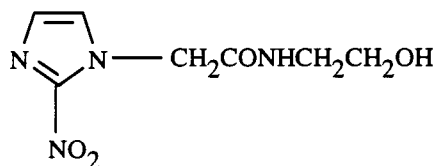
RSU1069:   1-(2-nitro-1-imidazolyl)-3-(1-aziridinyl)-2-propanol
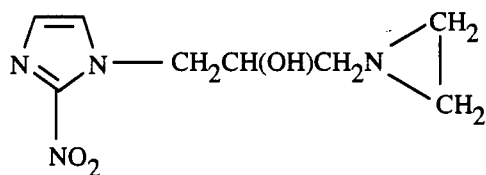
RB6145:   1H-imidazole-1-ethanol, α-([(2-bromoethyl)amino]methyl)-2-nitro-,monohydrobromide

ACKNOWLEDGMENTS

I am grateful to Dr. Graeme Dougherty for his assistance and support, and for his attempt to teach a physicist molecular biology. I also thank Dr. Brian Marples, Dr. Peter Johnston, Jeff Mathews, and Mark Skwarchuk, for stimulating and thought-provoking discussions over the past few years.

I express a special thank-you to my parents, who have always allowed me to pursue my endeavors through their caring support and encouragement.

Finally, I express my deepest gratitude to my spouse, Anna, who, perhaps unknowingly, continues to remain patient. Anna has provided her love and support without which I could not have completed this work. Consequently, it is to Anna that I dedicate this thesis.

The investigation of nature is an infinite pasture-ground,

where all may graze, and where the more bite, the longer

the grass grows, the sweeter is its flavor, and the more it

nourishes.

-Thomas Henry Huxley (1871)

1

INTRODUCTION

1.1 Radiation Interaction with Matter

It has now been 100 years since the discovery of X-rays in 1895 by Wilhelm Conrad Röntgen. This discovery is probably one of the earliest that fostered the relationship between researchers in the fields of physics, chemistry, biology and medicine that is so prevalent today. The discovery that X-rays could produce biological damage within the tissues through which they passed was made by the early investigators of this new phenomenon, often to their own detriment. However, this realization provided the stimulus for the use of X-rays as a therapeutic agent, and within 1 year of their discovery X-rays were first used to treat cancer. This medical application occurred prior to the understanding of the physical, chemical and biological processes involved. The science of radiobiology has grown out of this early discovery, and has always been closely linked with the study of cancer.

1.1.1 Physical Events

Since this early discovery, intensive study has led to a thorough understanding of the physical interaction of ionizing radiations with matter. The biological damage that occurs after radiation exposure is the result of a chain of events that begins with the physical deposition of energy. Radiation energy is deposited by processes that are capable of creating ionization and excitation events within the material of interest. These radiations may be classified either as directly ionizing (*e.g.*, fast charged particles), or as indirectly ionizing (*e.g.*, X-rays, γ-rays, and neutrons). Indirectly ionizing radiations create damage through the production of secondary ionizing charged particles. In the case

of electromagnetic radiation, this occurs through the well-described photoelectric, Compton and pair production processes in which secondary electrons are set in motion. In the case of neutrons, especially below 15 MeV, interaction occurs primarily through elastic collisions with hydrogen nuclei, resulting in the projection of secondary electrons. (For higher energy neutrons, interactions occur with other nuclei as well.) The total amount of energy deposited within a given mass of material is defined as the radiation dose, and is expressed in the units of grays (Gy), where 1 Gy=1 joule/kilogram.

Virtually all of the radiation dose that is deposited within a cell is derived from charged particle tracks. The probability of ionization events occurring in any particular small target volume (*i.e.*, intracellular structures, molecules) is extremely small until one reaches very large radiation doses, tens to hundreds of grays (Goodhead 1989). However, when direct damage at a site does occur, the actual amount of energy deposited varies widely from a single ionization to many tens of ionizations (Goodhead 1989). The rate of energy loss along the path of the charged particles (primary and secondary) is defined as the linear energy transfer (LET), and is expressed in keV/μm. Electromagnetic radiation and electrons are considered low LET radiations, whereas neutrons, and other heavier charged particles are generally of much higher LET (see fig. 1-1). The LET strongly affects both the patterns of energy deposition and biological damage within the cell (Goodhead 1989, 1994). The absolute value of the LET at any given point along the track of a charged particle is dependent on the energy of the particle at that point, and is highest at low energy levels where the particles give up the largest amount of energy in the smallest space. This gives rise to what is referred to as the Bragg peak, and for heavy

particles, the range of the particle, and thus the position of this peak, is a well-defined quantity, dependent only on the initial energy of the particle and the nature of the absorbing medium.

A dose of 1 Gy
corresponds to
~1000 tracks

Low-LET tracks in cell nucleus
e.g. fast electrons from γ-ray
interactions

A dose of 1 Gy
corresponds to
~4 tracks

~1μm

High-LET tracks in cell nucleus
e.g. α particles
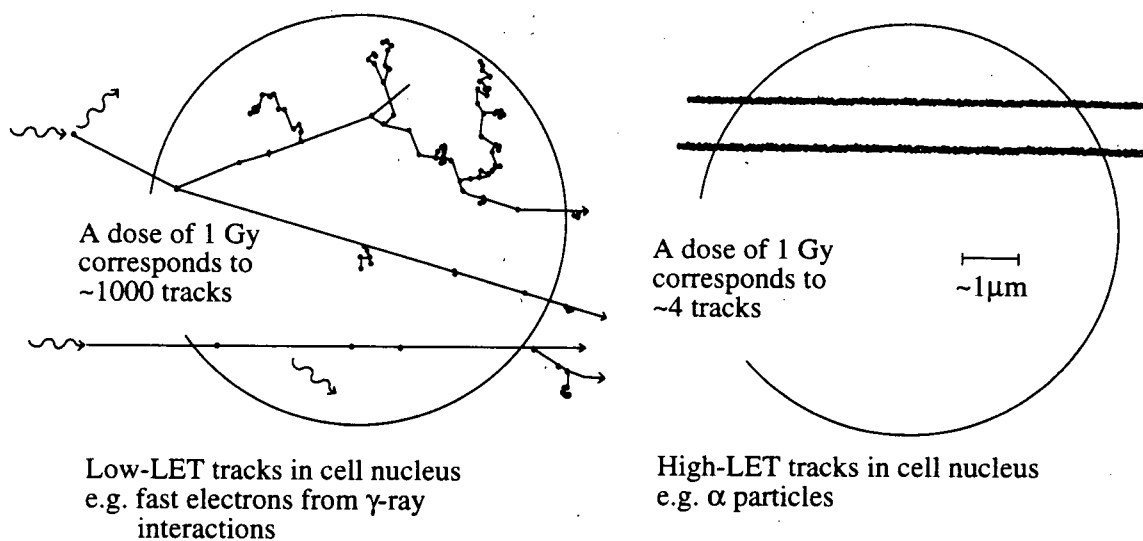
Figure 1-1 Track Structures of Low and High LET Radiations.
Schematic representation of a cell nucleus irradiated with two electron tracks from γ-rays (low LET) or two α-particle tracks (high LET) (redrawn from Goodhead 1988).

1.1.2 Chemical Events

The energy deposited in ionization events is much larger than the chemical energy that binds biological molecules in the form of covalent bonds, and is thus capable of breaking these bonds and causing dissociation of molecular species. In biological material, the chemical changes which result are due both to direct damage from energy deposition by the particle track within a given target (termed the direct effect), and by the production, in the particle track, of reactive molecular species which subsequently interact with the target of interest (termed the indirect effect). Damage produced via the direct effect can result, for example, from the breakage of a covalent bond within the critical target, and the creation of two reactive species ($R:R \rightarrow R^{\bullet}+R^{+}$ + fast electron). However, in biological material most of the radiation energy is deposited first in water, primarily through the ionization of water molecules. This creates highly reactive molecular species such as $HO^{\bullet}$, $H^{\bullet}$, e_{aq}^{-}, H_2, H_2O_2, and $HO_2^{\bullet}$. The proportions of each of these species are dependent on the incident radiation (*i.e.*, LET), and are described by the radiochemical yield G. This value indicates the number of molecules of each species produced per 100 eV of deposited energy, and in table 1-1 the G values for radiations of several different LETs are given.

The chemical reactions which result from the highly reactive molecules produce biological damage, some of which may not be expressed for several days or weeks. Several authors have summarized temporally distinct radiation-induced phenomena (*e.g.*, Hart and Platzman 1961, Chapman 1980), and in figure 1-2, the approximate time-scale for some of the physical, chemical, and biological effects of radiation is given. The

science of radiobiology is concerned with developing an understanding of the many biological phenomena which result in response to the deposition of energy from ionizing radiations.

Table 1-1 Radiochemical Yield G in Water For Several Different Radiations of Different LET
(taken from Buxton 1982)

LET	G						
keV/μm	H_2O	e^-_{aq}	$HO^\bullet$	$H^\bullet$	H_2	H_2O_2	$HO_2^\bullet$
0.23	4.08	2.63	2.72	.55	.45	.68	.008
12.3	3.46	1.48	1.78	.62	.68	.84	
61	3.01	.72	.91	.42	.96	1.00	.05
108	2.84	.42	.54	.27	1.11	1.08	.07

1.2 Radiation-Induced Lethality

Measurement of the loss of reproductive or clonogenic capacity has become one of the most useful endpoints for assessment of radiation damage, and in the field of radiobiology this has become synonymous with cell lethality. Part of the reason for this popularity may be due to the relative ease with which this assay can be performed quantitatively in mammalian cell lines with today's cell culture systems. A more important reason, perhaps, is the fact that the loss of clonogenic capacity, or more accurately, the loss of unlimited proliferative ability, is one of the primary biological effects of ionizing radiation in mammalian systems. The loss of proliferative ability occurs at relatively low X-ray doses (the dose required to reduce this ability to 50%, D_{50}, is ~ 3 Gy) in comparison to radiation inactivation of other cellular activities such as protein synthesis (D_{50}~1000 Gy).

TIME

10^{-18} s — Excitations Ionizations
Intratrack Reactions

10^{-12} s — Indirect effect of water
radicals: $OH^{\bullet}$, e^{-}_{aq}, $H^{\bullet}$

10^{-6} s — Target Radical
Reduction/Oxidation

10^{0} s — Enzyme removal of damaged
targets

10^{6} s — Cell Viability

Late Tissue Effects
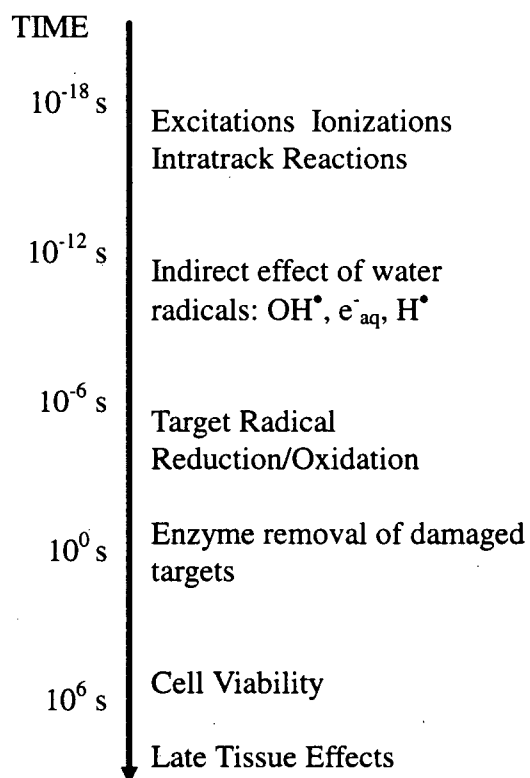
Figure 1-2 Time-Scale of Radiation-Induced Phenomena
The approximate time-scale of radiation-induced events following irradiation is shown (adapted from Chapman 1980).

It is widely believed that the primary radiation target within the cell is the DNA, which must be faithfully replicated and segregated between the two daughter cells prior to cell division. The loss of clonogenic ability is thought to arise primarily from damage to DNA, and indeed DNA single strand breaks, DNA double strand breaks, and chromosome aberrations are prevalent and can be easily measured after irradiation with relatively small doses, similar to those which result in cell lethality. The importance of radiation-induced damage to the DNA in determining the lethal effect of radiation is high-lighted by the greatly enhanced sensitivity to radiation observed in mammalian cells that are deficient in the repair of DNA double strand breaks (Jeggo and Kemp 1983, Kemp *et al.* 1984). Furthermore, some studies have shown that the dose response relationship for cell lethality agrees with that for chromosome aberrations (Skarsgard *et al.* 1967, Dewey *et al.* 1970, Carrano 1973, Joshi *et al.* 1982, Bedforth and Cornforth 1987) and for the induction and repair of DNA double strand breaks (Iliakis 1991, Powell and McMillan 1994, Ruiz de Almodovar *et al.* 1994, Whitaker *et al.* 1995, Nunez *et al.* 1995).

1.2.1 Reproductive Cell Death

Cell lethality, defined as the loss of unlimited proliferative ability, is an endpoint that can be easily and quantitatively measured, but unfortunately is relatively broad in scope. In most cases, radiation-induced cell death is characterized by mitotic or reproductive cell death. This type of cell kill specifically reflects the inability of a cell to continue to proliferate as it otherwise normally would. Cells that suffer this form of death often will retain metabolic activity, and may appear morphologically similar to unirradiated cells for several days. Cells undergoing reproductive death may also

continue to divide a few times following irradiation before the complete loss of reproductive ability. This observation has influenced the definition of cell lethality to mean the loss of *unlimited* proliferative ability. Thus an irradiated cell is generally classified as a 'survivor' only if it will continue to divide at least 5 or 6 times following irradiation and thus produce a 'colony' of at least 50 cells.

1.2.2 Interphase Cell Death and Apoptosis

Radiation-induced cell lethality can also result from a more immediate form of cell death that is morphologically distinct from reproductive cell death. The term 'interphase cell death' has been used to describe cell degradation which occurs prior to mitotic division. This generally occurs only after irradiation with very high doses, resulting in the lysis of the plasma membrane.

A morphologically distinct form of cell death can also occur at relatively low radiation doses in some cell types. This form of cell death is known as apoptosis, and can be responsible for mitotic as well as interphase death. It is the result of an active, genetically controlled pathway that is thought to regulate the balance between cell proliferation and cell death during normal development and in tissue homeostasis (Kerr *et al.* 1972, Arends and Wyllie 1991, Wyllie 1992). However, apoptosis can also be triggered in some cells by external stimuli including chemo-therapeutic agents (Barry *et al.* 1990, Hickman 1992, Gorczyca *et al.* 1993, Solary *et al.* 1994) and ionizing radiation (Payne *et al.* 1992, Shinohara and Nakano 1993, Olive *et al.* 1993b, Nakano and Shinohara 1994, Ling *et al.* 1994, Stapper *et al.* 1995, Hendry *et al.* 1995, Schwartz *et al.* 1995, Soldatenkov *et al.* 1995). Apoptosis in the normal course of development has been

most extensively studied in the nematode Caenorhabditis elegans (C. elegans), where it is characterized by an orderly cascade of events which is initiated by induction and repression of several apoptosis related genes (Hengartner and Horvitz 1994a). Some of these genes have homologues that have been implicated in apoptosis in human cells (Yuan *et al.* 1993, Hengartner and Horvitz 1994b). These genetic changes result in the activation of enzymes that cleave double-stranded DNA into 50 kbp, and subsequently 200 bp (internucleosomal) fragments. Following internucleosomal cleavage, the nucleus will often fragment into many small, condensed subunits. The final step of apoptosis is the fragmentation of the cell itself into several membrane-bound apoptotic bodies. The importance of this process in radiation-induced cell death has not been fully established, and its potential influence in terms of cancer therapy is actively being pursued (Stephens *et al.* 1993, Meyn *et al.* 1993a, Meyn *et al.* 1993b, D'Amico and McKenna 1994).

1.3 Survival Curves

The first *in vitro* mammalian cell radiation survival response was published in 1956 by Puck and Marcus. They devised a method of mammalian cell culture that allowed measurement of the quantitative relationship between cell survival and radiation treatment (the dose response). Prior to this measurement, most experiments in more simple organisms such as haploid yeast, viruses, and some bacteria, produced survival curves that exhibited an exponential form of cell killing. This type of response could be adequately explained by target theory, which hypothesized that the survival of cells following a radiation dose could be explained by that fraction in which the critical target had not been 'hit' by radiation. This could be described by a Poisson relationship:

$$P(a,n) = \sum_{i=1}^{n} \frac{a^n e^{-a}}{n!}$$

Equation 1-1

such that the probability of not being hit ($n=0$) after a dose resulting in an average number

of hits per cell (a) was equal to the surviving fraction (S) of the cells irradiated:

$$P(a,0) = S = e^{-a}$$

Equation 1-2

It was assumed that the number of hits was proportional to the dose (*i.e.*, $a=kd$), and thus

the survival could be written as a function of dose:

$$S = e^{-kd} = e^{-d/d_0}$$

Equation 1-3

where d_0 was equal to the dose that produced an average of 1 hit per cell. The concept of

target theory was expanded to include the possibility that either more than one hit per

target, or more than one target needed to be hit, to cause the inactivation of cells by

irradiation. Thus the expression shown in equation 1-2 is referred to as the single-hit,

single-target model.

The response that was measured by Puck and Marcus could not be explained by a

single-hit single-target model. Their response exhibited a 'shoulder' on the survival

curve (plotted on an exponential scale), such that at low doses cells were not as sensitive

per unit dose as they were at higher doses. In their report, they fitted their response to the

multi-target model:

$$S = 1 - (1 - e^{-d/d_0})^n$$

Equation 1-4

and derived the best-fit value for the number of targets (n) to be equal to 2. This value

has also been termed the extrapolation number in view of the fact that at high doses,

equation 1-4 can be simplified to:

$$S = ne^{-d/d_0}$$ Equation 1-5

This equation intercepts the y-axis at zero dose at the target or extrapolation number (n), and for most survival responses is not an integer value.

The presence of a shoulder on the mammalian survival curve is common for cells irradiated with low LET radiation, and the cause of this shoulder have been the source of much scientific debate in the radiobiological field in the 40 or so years since Puck and Marcus's experiment. The response of most types of cells to low LET radiation is characterized by shouldered survival curves that have an initial slope at low doses. There has been a plethora of models proposed to explain and understand this phenomenon, developed primarily on the premise of target theory (Lea 1955, Bender and Gooch 1962, Sinclair 1966, Elkind and Whitmore 1967, Wideroe 1971). However, several models have also been proposed to explain shouldered survival curves on the basis of damage interaction or biological repair (Kellerer and Rossi 1972, Chadwick and Leenhouts 1973, Tobias 1985, Curtis 1986). Repair models propose that cells are better able to withstand radiation damage at low doses because the damage is more effectively repaired at those dose levels. At higher doses the repair capacity of the cell is compromised due either to repair saturation, or alternatively to an increased complexity of the lesions created. However, due to statistical uncertainty present in radiation survival data, it has been difficult to accurately distinguish between the ability of these models to fit, universally, the responses of different cells. Despite this fact, the linear quadratic (LQ) model:

$$S = e^{-\alpha d - \beta d^2}$$ Equation 1-6

has arguably gained the widest acceptance because of its success in describing the radiation survival response in a broad range of mammalian cell studies. The LQ model was suggested on theoretical grounds by Kellerer & Rossi (1972) and by Chadwick and Leenhouts (1973), but was used empirically prior to that by Sinclair (1966). Kellerer & Rossi's theory of dual radiation action proposed that inactivation of targets took place either by a single track high LET process (proportional to dose - single hit single target) or by interaction of two low LET tracks (proportional to dose squared). Since irradiation with X-rays produces a spectrum of primary electrons that have both high and low LET components, the resultant response was a superposition of these two processes. Similarly, Chadwick and Leenhouts proposed that radiation lethality resulted from the induction of unrepairable DNA double strand breaks. They proposed that these breaks could occur from the passage of a single particle creating two DNA breaks in opposing strands (proportional to dose) or by the interaction of DNA breaks in opposing stands created by the passage of two particles (proportional to the square of the dose).

The LQ model is also useful empirically for defining the response of cells to radiation since, to a first approximation, any survival model can be expanded in a Taylor series similar to the LQ function:

$$ln(S) = -(a + bD + cD^2 + dD^3 + ...)$$
<div align="right">Equation 1-7</div>

Thus, if higher order terms are ignored, the parameters in any model can be related to the α and β values in the LQ model. This is especially true at low dose where the higher order terms have less influence on the measured survival.

1.4 Determinants of Radiation Treatment Success

Cancer is characterized by the uncontrolled proliferation of cells within different sites in the body, and it was realized shortly after the discovery of X-rays that radiation could be an effective treatment for this condition. Radiation therapy for the treatment of cancer was initiated within 1 year after the discovery of X-rays, and has become a standard therapy for the treatment of many different types of cancer. Despite our extensive use of this modality, there remains a large degree of variability in response to treatment within the general population. The failure of local control of a tumour by radiation is thought to arise primarily from one or a combination of three distinct factors: tumour cell proliferation, tumour hypoxia, and intrinsic cell radiosensitivity.

1.4.1 Tumour Cell Proliferation

The rate of cell proliferation within a tumour is governed by three factors. The first is the cell-cycle time, designated t_c, and is equal to the average time a cell requires to complete 1 round of cell division. This defines the maximum rate at which a tumour cell population can proliferate. However, the fraction of cells within the tumour that are actively progressing through the cell cycle is normally less than 100%, and thus the doubling time of the tumour will be less than the measured cell-cycle time. The growth fraction (Mendelsohn 1960) defines the fraction of cells that are proliferating, and when this is taken into account, the potential doubling time, t_{pot}, can be calculated. The actual doubling time of the tumour, or the volume doubling time (t_d), also takes into account cell loss (Steel 1967), and for large tumours, t_d will be significantly greater than the potential doubling time. The relationship between these parameters will depend to a large degree

on the size and type of tumour involved. Small tumours generally have adequate nutrient supply, and will grow at rates governed largely by the cell-cycle time, whereas large tumours may grow at rates that are almost independent of the cell-cycle time. In a typical treatment schedule, in which the radiation dose is given in small daily fractions over several weeks, the success of the treatment will be severely compromised if the tumour grows rapidly during this time period.

1.4.2 Tumour Oxygenation

A second important factor that is relevant to treatment success is the oxygen status within the tumour. Due to the rapid growth of cancerous cells, the requirement for nutrients and oxygen may often exceed that which is available via the blood supply. This results in the establishment of oxygen gradients in the proximity of blood vessels, with well-oxygenated cells adjacent to the blood supply, and poorly oxygenated (hypoxic) cells at greater distances. At a critical distance the oxygen concentration and nutrient supply will drop to levels that are low enough to cause cellular necrosis. This was first identified by Thomlinson and Gray (1955), who calculated an approximate oxygen diffusion limit of 145 μm. In addition to this 'chronic hypoxia', regions in some tumours may also suffer 'acute hypoxia' as a result of transient fluctuations in blood perfusion (Chaplin *et al.* 1986). The importance of oxygen as a determinant of radiation sensitivity is well established, and it was known very early that hypoxic conditions reduced the degree of radiation damage to mammalian cells (Gray *et al.* 1953). In terms of survival, it is generally accepted that hypoxic cells are approximately 3 times more resistant to radiation as compared to fully oxygenated cells. This sensitization is termed the oxygen

effect, and is described quantitatively by the oxygen enhancement ratio (OER). The OER is calculated by taking the ratio of the doses that produce equal levels of cell kill for the anoxic and aerobic cells respectively. The oxygen effect can be largely explained in terms of the radical species produced by irradiation of biological material (see 1.1.2). The highly reactive radical species will form hydroxyls, hydroperoxides and peroxides in the presence of oxygen (a powerful oxidizing agent). These molecules are far more stable than the initial radical species, and can also be very toxic. This results in the so called 'fixation' of radiation damage, and prevents the recombination of radicals (chemical repair) which could occur in the absence of oxygen. The sensitizing ability of oxygen is a function of the oxygen partial pressure, increasing sharply at partial pressures between 0 and 20 mm Hg. Above 30 mm Hg, tissues are considered well-oxygenated with respect to radiation treatment, and are essentially fully sensitized. Half-maximum sensitization is realized at a level of approximately 3 mm Hg.

1.4.3 Intrinsic Radiosensitivity

A more recent discovery that was shown to be potentially important in the success of radiotherapy is the intrinsic radiosensitivity of the cells in question. The radiosensitivity of a particular cell line is governed by many factors. These include chemical composition differences such as the levels of protective molecules that are able to 'scavenge' radical species before they can inflict damage to critical structures. Cellular thiols are an example of these molecules, and modification of their levels has been shown to modify radiosensitivity (Bridges 1969, Biaglow 1983, Durand 1984b). Other factors implicated in determination of radiosensitivity are those which produce differences in the

biological response *following* the radiation-induced chemical events. Most of the biological damage that is present shortly after irradiation is faithfully repaired by cell systems through complex repair mechanisms, however in cell lines where this repair system is compromised, the lethal effects of radiation are greatly enhanced (Taylor *et al.* 1975, Jeggo and Kemp 1983, Kemp *et al.* 1984). The biological response is now recognized as a very complex process that involves cell signaling events (Stephens *et al.* 1993, Little 1994, Weichselbaum *et al.* 1994, Szumiel 1994), induction or repression of genes (Boothman *et al.* 1989, Prasad *et al.* 1994, Chen *et al.* 1995), and alterations in chromatin structure (Olive 1992, McMillan and Peacock 1994). In addition, cells (even of the same type) have been shown to die by different mechanisms (apoptosis and necrosis), and the proportion attributable to these different modes is both dose and cell line dependent (Payne *et al.* 1992, Shinohara and Nakano 1993, Olive *et al.* 1993b, Ling *et al.* 1994). The intrinsic radiation response refers to the culmination of all these factors, which are inherent to the cells in question.

1.4.3.1 Sublethal Damage Repair

The composite survival response that results following irradiation is determined by the intrinsic radiosensitivity, and results from the creation of lethal lesions that are not repaired by the cell. However, following irradiation with a given dose, mammalian cells will also sustain a level of 'sublethal' damage in addition to lethal radiation events. This damage is that which can be repaired if sufficient time is available, but which can interact with additional radiation damage from a subsequent dose to become lethal damage if sufficient time is not available for repair between doses. The sublethal damage repair

(SLDR) that occurs in a fractionated irradiation regime where the total radiation dose is split into many small fractions, is an important factor in modern radiotherapy. Elkind and Sutton (1960) were the first to show that irradiation given in two fractions separated by several hours was less effective in terms of cell killing than the same dose given in a single fraction. Furthermore, they showed that the cells that survived the first fraction responded identically (had the same shoulder) as the original population did to the first dose provided there was sufficient time between fractions. This finding implies that those cell types with a small α/β ratio (large shoulder) will exhibit more sublethal damage repair than cells with a large α/β ratio (small shoulder), and will thus be selectively spared in a fractionated irradiation regime.

Most early studies of radiosensitivity, as defined by the radiation survival dose response curve, were carried out with rodent tumour cells. An analysis of much of this data showed little difference in the radiation response of different tumour types (Berry 1974). Similarly, early studies of *in vitro* radiation responses from human cell lines derived from different tumour types of widely differing curability, showed no significant correlation with the clinical responsiveness (Weichselbaum *et al.* 1976a, 1976b, 1980, Weininger *et al.* 1978). However, most of these studies used the multi-target model (equation 1-4) to characterize the radiation response, and although the parameters derived from these fits, n and D_0, can adequately characterize the response at high dose, they often fit poorly at low doses. Subsequently, a re-evaluation of over 100 published survival curves measured *in vitro,* suggested that the differences in responsiveness were sufficient to explain the diverse clinical response of human tumours to radiotherapy, and

furthermore that it was the initial, low dose region, of the *in vitro* radiation survival curve that best correlated with the clinical response of different tumour types (Fertil and Malaise, 1981, 1984, Deacon *et al.* 1984, Fertil and Malaise 1985, Deschavanne *et al.* 1986, Malaise *et al.* 1987, Steel 1988). While acknowledging that inherent radiosensitivity was only one of many factors which influence clinical outcome, these authors showed that the parameters which describe the low dose response, specifically the mean inactivation dose, $\overline{D}$, the α value derived from a LQ fit to the data, and the measured surviving fraction at 2 Gy, SF_2, were the parameters that best correlated with clinical response. In hindsight, it is perhaps not surprising that these low dose parameters are better indicators of the clinical response, since 2 Gy is typical of the daily doses given in a fractionated radiation regime. Although one would expect the most resistant cells in the tumour to determine the overall outcome after a cumulative dose of 60 Gy (depending on cell cycle redistribution and kinetic factors), the results of these studies led the authors to suggest that the inherent radiosensitivity of the tumour does not change significantly during a fractionated treatment schedule (Fertil and Malaise 1981). This suggestion has led to considerable interest in the use of *in vitro* measurements as a predictive assay for clinical response (Rofstad *et al.* 1987, Brock *et al.* 1989, West *et al.* 1989, Weichselbaum *et al.* 1990).

1.5 Substructure in the Radiation Survival Response

The *in vitro* radiation response of cells is known to vary as a function of cell age. An exponentially growing population contains cells in different phases of the cell cycle which are designated as G1 (the time spent after division and before initiation of DNA

replication), S (the time during which DNA synthesis takes place), G2 (the time between the completion of DNA synthesis and mitotic division) and M (mitosis or cell division) (Howard and Pelc 1953). Synchronization of cells in these different phases has shown that the relative sensitivity to X-ray irradiation varies as a function of cell-cycle position (Terasima and Tolmach 1961, Sinclair and Morton 1966, Sinclair 1972, Skwarchuk *et al.* 1993). Figure 1-3 shows the relative radiosensitivity of Chinese hamster cells in different phases of the cell cycle (Sinclair and Morton 1966). This figure demonstrates that cells in late S-phase are the most resistant, while cells in G2-M are the most sensitive. The response of an entire asynchronous population is thus a composite of the response of many subpopulations. The use of models to characterize such a response, then, is valid only to the extent that the variation within the cell cycle is small, or that the composite response can be accurately characterized by average parameter values in the respective models. The applicability of the LQ model to the fitting of exponentially growing populations was investigated by Gillespie *et al.* (1975). They measured the responses of synchronized cells at different points in the cell cycle, and then calculated hypothetical mixed population responses on the basis of these results. Seven dose points along this hypothetical response were then used as data to which the LQ model was applied, and their results suggested that such a response could be adequately described by a single LQ function. Acceptable fits were also found for experimentally measured asynchronous cell survival responses with 9 different dose points.
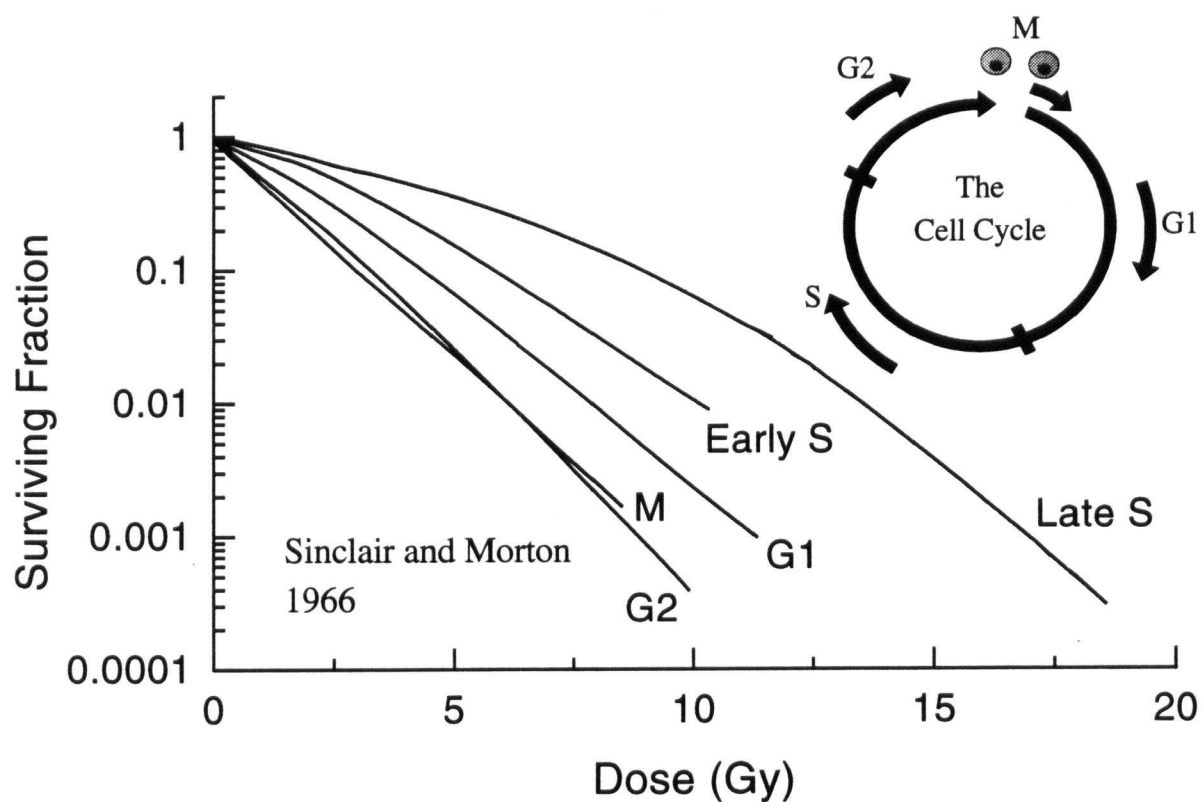
Figure 1-3 Cell-cycle Radiosensitivity
A schematic representation of the cell cycle is shown (above). Cell populations in exponential growth proceed through G1, undergo DNA replication in S, proceed through G2, and then each cell divides into two daughter cells in mitosis (M). The relative sensitivity to X-rays in each of these different phases is also shown (below) (redrawn from Sinclair and Morton 1966).

In recent years, the development of the cell sorting assay for more precise measurement of the survival of mammalian cells, after low doses of radiation (clinically relevant and below) has called into question the ability of a single LQ function to describe accurately, the response of asynchronously growing mammalian cells throughout a large dose range (representing three to four logs of cell inactivation) (Skarsgard *et al.* 1991, 1992, 1993, 1994a, 1995, Skwarchuk *et al.* 1993, Wouters and Skarsgard 1994). With the more precise data available with this technique, it has been shown that for some asynchronously growing cell lines the LQ model cannot precisely describe the entire response, and that a better description of the survival curve can be obtained if the data in the low dose and high dose regions are fitted separately (Skarsgard *et al.* 1991, 1992, 1993, 1994a, 1995, Skwarchuk *et al.* 1993). This "substructure" has been attributed to the variation of radiosensitivity throughout the cell cycle, (*i.e.*, sensitive G1 and G2 phase cells are preferentially killed at low dose leaving a more resistant, S phase enriched population at higher doses), and it has been subsequently shown that the substructure is not present in well-synchronized cell populations (Skarsgard *et al.* 1992, 1993, Skwarchuk *et al.* 1993). Hence the failure of the LQ equation is not surprising, given that if the model does accurately describe the response of the original mixed population at low dose, then it should deviate from the response at higher dose where the cell-cycle makeup of the population has changed due to selective killing of sensitive cells. Excellent fits to survival data can be obtained at low dose only (0.4-4 Gy), or alternatively by using a sum of two LQ equations representing two populations of cells, each with its own characteristic radiosensitivity (Skarsgard *et al.* 1994a). When the LQ model is applied to

the full dose response, a consistent misfit occurs, manifested as an over-prediction of the amount of cell kill at low doses. A fit to the low dose data that accurately characterizes the initial response, generally results in significantly smaller values for the α parameter and significantly larger values for the β parameter than determined from fits to either the high dose or full dose response.

The use of the cell sorting assay in a panel of asynchronously growing human tumour cell lines exhibiting a wide range in radiosensitivity at high doses has revealed both a wide range in the shape of the cell survival curve (*i.e.*, the α/β ratio), as well as in the degree of substructure present in the response (Skarsgard *et al.* 1992, 1995). Both of these factors have important implications for the evaluation of radiosensitivity, and therefore for the evaluation of agents that are capable of modifying the radiation response. Although the high dose response is strongly influenced by the most resistant fraction of cells, the parameters that are derived from a LQ fit to the data at high doses are not indicative of this resistant population. Rather they are simply an empirical description of the data. However, parameters that are derived from a fit to the data at low doses, where significant cell-killing has not taken place and thus where the make-up of the population has not changed significantly, describe quantitatively the initial response of the entire asynchronous population. Modification of these parameters by alternative treatment strategies, then, may be more reflective of the mechanisms by which this modification takes place. Moreover, it will accurately describe the effects at clinically relevant doses, which have been shown to correlate best with clinical outcome.

1.6 Thesis Objectives

In light of the importance of low dose survival measurements for accurate evaluation of radiation treatment strategies, an investigation into the implications and nature of the low dose response is warranted. The specific aims of this thesis include:

(i)   Tests of the importance of low dose intrinsic radiosensitivity for predicting the efficacy of two hypoxic radiosensitizers. Evaluation will be carried out in an *in vitro* model, consisting of a panel of human tumour cell lines, and will focus particularly on the effects of low (clinically relevant) radiation doses. Modeling these radiation responses should provide insight into mechanisms that are responsible for hypoxic cell sensitization, and factors that determine the very different inherent sensitivity of human tumour cells to low doses of radiation.

(ii)   Development of a better understanding of the radiation dose-response relationship by accurate measurement of cell survival at very low doses (0.05-4 Gy). Survival will be assessed following single and split-dose treatments in one synchronous, and several asynchronous human tumour cell lines. Several mathematical models will be used to test different hypotheses regarding the nature of these responses.

(iii)   Determination of the relative biological effectiveness (RBE) of the 70 MeV proton beam at TRIUMF. Accurate characterization of the low (clinically relevant) dose response to protons will be compared to conventional radiation treatment, in order to understand the implications of the high LET component of dose in the proton beam. An attempt will also be made to evaluate the influence of the low dose intrinsic radiation response on the determination and variability of RBE values.

2

MATERIALS AND METHODS

2.1 Cell Culture

2.1.1 Maintenance of Cell Lines

Several mammalian cell lines were chosen for these studies. The human tumour cell lines HT-29 colon adenocarcinoma, DU145 prostate carcinoma, A549 lung carcinoma and HT-144 malignant melanoma were obtained from the American Type Culture Collection (ATCC, Rockville, MD). The Chinese hamster cell line, V79-WNRE, was provided by Dr. J.D. Chapman, and is a strain of the widely studied V79-379A cell line that can be grown in monolayer or in suspension culture (Chapman *et al.* 1970, 1972). All cell lines were maintained in monolayer culture *in vitro*, in either McCoy's 5A modified medium (HT-29, DU145, and A549 : Gibco BRL) or minimal essential medium (MEM) (HT-144 and V79-WNRE: Gibco BRL) supplemented with fetal bovine serum (10% by volume: Gibco), sodium bicarbonate (2.2 g/l), and sodium pyruvate (0.122 g/l - for MEM only). The routine maintenance cultures did not generally contain antibiotics, to facilitate early detection of contamination. Cultures were grown in 75 cm^2 plastic tissue culture flasks (Falcon, Corning, or Nunc), and passaged twice weekly with trypsin. The trypsinization protocol was optimized for each cell line to reduce trypsin exposure while maintaining acceptable monodispersed cell populations. HT-29, DU145, and A549 cells were trypsinized by rinsing twice with 0.05% trypsin containing 0.53 mM EDTA (Gibco BRL) in phosphate buffered saline (PBS), followed by a 3 minute incubation with 1 ml of the trypsin solution at 37°C. HT-144 cells were similarly trypsinized with 0.03% trypsin without EDTA for 1.5 minutes and V79-WNRE cells were trypsinized with

0.1% trypsin without EDTA for 3 minutes. Following the incubation period, cells were detached from the surface of the flask by gentle agitation, and the trypsin was neutralized with growth medium containing serum. Cultures were grown at $37^{\circ}C$ in a humidified atmosphere of 95% air and 5% CO_2.

2.1.2 Asynchronous Cell Survival Experiments

Most experiments were carried out using exponentially growing cells. This type of population is distributed throughout the cell-cycle, and so is said to be 'asynchronously' growing as opposed to a cell population synchronized in one particular point in the cell cycle. For asynchronous experiments, exponentially growing cultures were seeded into large tissue culture flasks (225 cm^2: Corning or 175cm^2: Falcon) in appropriate growth medium containing either penicillin (80 units/ml) and streptomycin (80 $\mu g/ml$) or gentamycin (50 $\mu g/ml$). To ensure exponentially growing populations, cell cultures were seeded 48 hours (human tumour cell lines HT-29, HT-144, DU145, and A549) or 40 hours (V79-WNRE) prior to each experiment at appropriate densities to produce monolayers which covered only 50% to 70% of the growth surface of the flasks at the time of the experiment. Additionally, cultures were fed 24 hours prior to the experiment with fresh growth medium at $37^{\circ}C$.

2.1.3 Induction of Plateau-Phase in HT-29 cells

For experiments that employed synchronous cells, an exponential population of cells was forced into growth arrest by a combination of cell-contact inhibition, and nutrient deprivation. Cells that undergo this growth arrest exit the active cell cycle, and

populations are said to be in the plateau or G0 phase of the cell cycle. In order to maximize the percentage of cells in this phase, a series of different growing conditions were tested. HT-29 cells were seeded at high cell densities (3×10^6 cells in 25 cm^2 Falcon flasks) and allowed to grow for 3 days, during which time they reached maximum confluency. These cultures were then fed daily with McCoy's 5A modified medium (pH 7.4) with 20 mM Hepes (to help regulate pH) and either 10%, 5%, 1%, .1%, or 0% fetal bovine serum. A population of cells was also maintained which had no medium replacement over this time period. After 8 days from initial seeding, cells were analyzed for DNA content using flow cytometry (see section 2.5).

2.2 Experimental Technique

2.2.1 Radiosensitizer Studies

For each radiation survival response, a population of asynchronous (exponentially growing) cells was harvested by trypsinization, neutralized in growth medium, centrifuged at 90g for 7 minutes and resuspended in 45-50 ml of pH-balanced culture medium modified for suspension culture (Ca^{++} free : S14 for HT-144, McCoy's 5A-S for HT-29 and DU 145). To maintain a neutral pH during these experiments, sodium bicarbonate was replaced with 20 mM HEPES buffer (Sigma). Cell suspensions were loaded into a water-jacketed irradiation vessel fitted with a rubber stopper (see figure 2-1). The stopper was designed with two ports to allow for gas exchange and sampling. The sampling port was extended 7-10 cm above the surface of the stopper to prevent turbulence during sampling and thus avoid introducing outside air. Cell suspensions were

stirred at 350 RPM with a glass-encased metal bar by a rotating magnet coupled to an electric motor placed beneath the flask, and maintained at 37°C with a recirculating, thermostatically controlled water-bath equipped with a pump connected to the water jacket on the flask. During this time, cell populations could be gassed either with air or nitrogen to create aerobic or hypoxic conditions, respectively.

2.2.1.1 Aerobic Survival Response

For irradiation under aerobic conditions, cell suspensions were loaded into the water-jacketed irradiation vessels at a density of 5-6 $\times 10^5$ cells/ml and gassed with humidified air for 20 minutes prior to and during irradiation. The irradiation procedure was conducted in an incremental fashion (see 2.3.1). Control samples were taken prior to irradiation, and two samples taken after each dose increment. These aliquots of cells (0.5-2 ml) were transferred into test tubes containing 3 to 4 ml of appropriate growth medium (see 2.1.1), and placed on ice. Between 35 and 37 samples (17-18 dose points) were accumulated for each survival response in 15-20 minutes. Appropriate doses were used in each cell line to allow for measurements of survival over a 3-4 log range in survival, with extra points in the first log of cell kill to more accurately define the low dose region.

2.2.1.2 Hypoxic Survival Response

For survival responses obtained under hypoxic conditions a combination of oxygen diffusion and cellular respiration was used to reach low levels of oxygen. For this purpose, cell suspensions were loaded at a concentration of 1×10^6 cells/ml and were

gassed with humidified nitrogen gas (<10 ppm oxygen) for 1 hour prior to and during irradiation. (The humidifier was separately degassed for 1 hour prior to this procedure). To ensure that adequate levels of hypoxia were reached using this protocol, measurements of dissolved oxygen concentration within the stirred cell suspensions were made under identical experimental conditions (see 2.6). Irradiation and sampling were performed as for aerobic samples (2.2.1.2), with doses resulting in a similar range in survival (3-4 logs). No toxicity was observed after induction of hypoxic conditions.

2.2.1.3 Hypoxic Survival Response With a Radiosensitizer

For measurement of cell survival in experiments using hypoxic radiosensitizers, cells were preincubated with the drug for 1 hour prior to irradiation. Drugs were prepared at 10 times concentration, and diluted to the final concentration in the cell suspension at the same time that gassing with nitrogen was initiated. Solutions of etanidazole (kindly provided by the Drug Synthesis and Chemistry Branch, Developmental Therapeutics Program, Division of Cancer Treatement, National Cancer Institute) were prepared fresh the morning of each experiment; the drug was dissolved in cold suspension medium, stirred for 30 minutes, and then filtered through a 0.22 μm membrane. This drug solution was then kept on ice prior to use. Solutions of RB6145 (kindly provided by Dr. P. J. Sebolt-Leopold) were prepared only 20 minutes prior to addition to the cell suspension due to the instability of this drug in solution. The drug was dissolved in ice-cold suspension medium under low light conditions, and then stirred on ice in a light tight container for 10 minutes. The drug solution was then filtered (as with etanidazole) and immediately added to cell suspensions.

2.2.1.4 Preparation of Samples for Sorting

Following irradiation, samples that were placed on ice during sampling were spun down at 90g for 7 minutes, the supernatant discarded, and the pellet resuspended in ice-cold growth medium at a concentration of approximately 1×10^6 cells/ml. This procedure was employed to remove any drug present in the cell samples, but was also carried out on non-drug treated samples for consistency. After resuspension, samples were ready for cell sorting and plating (section 2.4).
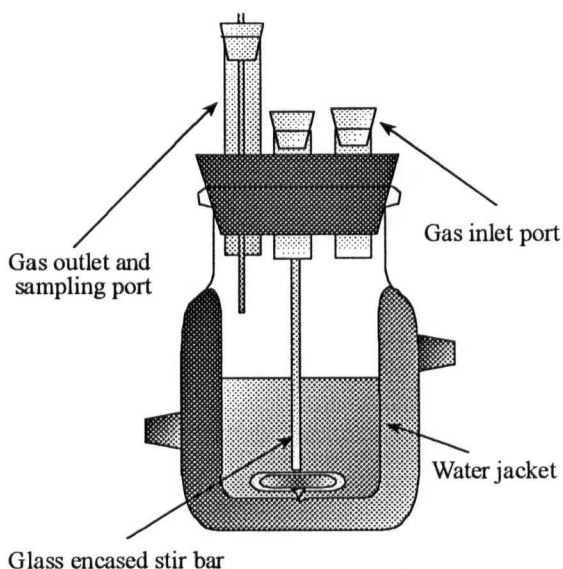
Figure 2-1 Water-Jacketed Irradiation Vessel
Irradiations in suspension were performed in a water-jacketed irradiation vessel. Water was circulated through the jacket at the desired temperature. The sampling port was extended 7-10 cm to reduce the risk of outside air entering during the sampling procedure.

2.2.2 Low Dose Survival Studies

2.2.2.1 Asynchronous Low Dose Survival Assay

Approximately 1.5 hours before the start of irradiation, exponentially growing cells were harvested by trypsinization, centrifuged at 90g for 7 minutes, resuspended in pH-balanced medium (lacking sodium bicarbonate) with 20 mM Hepes buffer, and loaded into water-jacketed (37°C) irradiation vessels at a concentration of 5-6 x 10^5 cells/ml. These cell suspensions were used to measure the low dose radiation survival response using one of two protocols. In the first, termed the postsort protocol, an experimental procedure was adopted similar to the radiosensitizer experiments of irradiation under aerobic conditions in suspension (2.2.1). To improve upon the precision in the data, a refinement to this procedure, termed the presort protocol, was later adopted.

2.2.2.2 Postsort Protocol

Cell populations were stirred and gassed with humidified air at 37°C for 15 minutes prior to and during irradiation. Careful attention was given to maintaining 37°C conditions during and following X-ray exposure until all cell samples were plated for survival assessment. The dose range used was designed to result in cell survival in the first log of cell kill. Three samples (0.5 ml) were removed prior to irradiation to serve as controls, and two samples were removed after each dose increment, with between 37 and 43 samples (17-20 dose points) being accumulated in under 20 minutes, over the dose range of interest (0 to 4 Gy). Samples were placed in a rotary shaker bath at 37°C prior to

cell sorting and plating. Sorting began approximately 10 minutes after initiation of irradiation, and lasted for approximately 1 hour for each survival response.

2.2.2.3 Presort Protocol

A new protocol for irradiating cell populations termed the presort protocol, was subsequently developed, in which the sorting and irradiation steps were reversed. Cell populations were maintained in a stirred suspension at 37°C following trypsinization, and after 45-60 minutes an aliquot of cells was used for cell sorting (see 2.4). Following sorting, samples containing known numbers of cells were immediately irradiated in a 37°C warm bath and plated for survival. In this protocol samples were sorted, irradiated and plated within a 6-8 minute period for all dose points. Furthermore, all cell samples received single doses rather than an accumulation of small incremental doses.

2.2.2.4 Priming Studies

The low dose radiation response of HT-29 cells following a small priming dose was measured using two different protocols, monolayer priming, and spinner culture priming.

2.2.2.4.1 Monolayer Priming

Exponentially growing HT-29 cells were seeded 2 days prior to the experiment from a common population into four 225 cm^2 flasks. Each of these flasks was used to obtain a cell population for 1 survival response, such that a total of 2 control (unprimed) and 2 test (primed) survival responses were measured during the experiment. For delivery of the priming dose, the flask was removed from the incubator and 100 ml of

additional growth medium was added (150 ml total) to prevent backscatter artifacts and to ensure a uniform dose distribution. The flask was then irradiated with 0.3 Gy (see 2.3.1.3), after which the excess medium was removed, and the flask was placed back into the incubator for 6 hours. After this period, the monolayer was harvested by standard trypsinization protocols (see 2.1.1), and the radiation response of the cells was measured using the presort protocol as previously described (see 2.2.2.3). Control responses were treated identically, except that the priming dose was zero (mock irradiation).

2.2.2.4.2 Suspension Culture Priming

The monolayer procedure did not allow an assessment of the plating efficiency of cells before and immediately after the priming dose, and for this reason a second protocol was employed. In this procedure, asynchronous, exponentially growing HT-29 cells from four monolayer flasks were harvested, collected into a common suspension, and transferred into four water-jacketed irradiation vessels at 37°C. Each of these irradiation vessels was then used to measure a single survival response for either the test (primed) or control (unprimed) conditions. Immediately before the priming dose, two 0.5 ml samples were withdrawn. Test populations then received the priming dose (0.3 Gy) while in spinner culture (see 2.3.1.1), and two samples were taken again immediately after irradiation. This allowed for measurement of the plating efficiency immediately before and after the priming dose was given. After the priming dose, cell populations were maintained in suspension culture for 4 hours, during which time they were gassed with air, stirred, and maintained at 37°C. After this incubation, the radiation response was measured with the presort protocol (see 2.2.2.3). In addition to the extra controls that

could be taken by this priming procedure, this protocol also had the advantage that it used

a common starting suspension of cells for all of the measured survival responses. With

this procedure, the survival following the priming dose could be assessed before and after

the 4 hour priming period. However the protocol required the maintenance of HT-29

cells in a suspension culture for up to 6 hours before irradiation. For this reason, the

ability of these cells to maintain exponential growth while in suspension was assessed

with flow cytometric techniques (see 2.5).

2.2.3 Proton RBE Studies

2.2.3.1 Gelatin Preparation

The sliced gel technique of Skarsgard *et al.* (1974, 1982, 1983) was adopted for

these studies. A 20% w/w solution of gelatin was prepared several weeks prior to the

experiment by dissolving gelatin (Fisher G-8 Type A) in cold minimal essential medium

(MEM) without serum or sodium bicarbonate, and slowly warming to $37^{\circ}C$ with

intermittent mixing. The gel solution was heated to $70^{\circ}C$ for an additional 40 minutes to

completely dissolve the gelatin, during which time the solution was mixed every 5 to 10

minutes to avoid clumping. While still hot, the gelatin solution was vacuum filtered

through a Millipore AP prefilter to remove small particulate material that can interfere

with cell sorting. The filtered gel solution was then sterilized by autoclaving.

In order to reduce the toxicity of the gelatin (presumably due to low molecular

weight components) it was necessary to dialyze the gelatin extensively. Warm gelatin

was poured into sterile dialysis tubes (25 cm in height, 2.7 cm in diameter, m.w. cutoff =

1200-1400), the tubes were sealed to preserve sterility, and the gel was dialyzed in MEM at low temperature (4°C) to reduce uptake of fluid by the gel. The medium was changed daily for 2 weeks. This procedure produced a sterile, relatively non-toxic, 15% gelatin solution. Medium was added to yield the desired 12% gelatin solution.

2.2.3.2 Preparation of Samples for Irradiation

For each experiment, asynchronous, exponentially growing V79-WNRE cells were harvested by trypsinization, neutralized with growth medium, centrifuged, and resuspended in medium with 12% gelatin at 37°C at a concentration of 7×10^5 cells/ml. At this temperature the gelatin solution was a viscous fluid. Samples which were to receive proton irradiation were prepared by pouring the viscous gel into ABS (acrylonitrile butadiene styrene) plastic tubes, 17.7 cm long, 1.2 cm in diameter, with a piston at one end. Samples receiving ^{60}Co irradiation were prepared by depositing 0.5-1.0 ml of the same cell/gel suspension into 5 ml plastic test tubes through a stainless steel cannula fitted to a 25 ml plastic syringe. All samples were then allowed to solidify at 4°C. After solidification the proton tubes were sealed (2.1 mm nylon cap, $\rho=1.14$ g/cm^3) and stored on ice until irradiation (see 2.3.3). Samples receiving ^{60}Co irradiation were also kept on ice. To avoid non-uniform scattering during ^{60}Co irradiation, the sample tubes were filled with ice-cold MEM medium just prior to irradiation (see 2.3.2).

2.2.3.3 Preparation of Samples for Cell Sorting

After proton irradiation, the ABS gel tubes were maintained on ice until they could be assessed for survival. For each tube, the nylon cap was removed, and the gel extruded and trimmed using a taught wire (0.2 mm diameter) slicer. The gel was then alternatively extruded and sliced at 2 mm intervals. Gel slices (0.2 ml) were dissolved in warm medium (1.0 ml of MEM) and maintained at 37°C prior to sorting and plating (see 2.4). ^{60}Co-irradiated samples were also melted in warm medium (ratio of medium to gel equal to 5), and maintained at 37°C prior to cell sorting and plating (see 2.4).

2.3 Irradiation and Dosimetry

2.3.1 250 kVp X-rays

Due to fluctuations in the dose rate of our X-ray unit (Philips RT-250, HVL 1.5 mm Cu), the prescribed dose was monitored with a dose integrator that was calibrated with a combination of Fricke ferrous sulfate dosimetry, and ionization chamber measurements (Victoreen Model 500, 0.6 cm^3 chamber). Appropriate numbers of monitor counts were then prescribed to obtain the chosen dose increments. Thus all dose rates quoted for irradiation under different conditions are only approximate, and represent an average dose rate.

2.3.1.1 Irradiation in Spinner Flasks

Irradiation in spinner cultures was carried out using a custom-designed aluminum jig attached to the head of the X-ray unit (see figure 2-2). Cell populations were alternatively sampled and irradiated in small dose increments in water-jacketed (37°C)

irradiation vessels with 250 kVp X-rays. Several different positions were available for

irradiation, providing a choice of dose rates to allow accurate delivery of small doses.

For irradiation of aerobic populations of cells, dose rates of approximately 2.3 Gy/minute

(HT-29 and DU145) and 0.9 Gy/minute (HT-144) were used. Irradiation under hypoxic

conditions required larger doses, and thus dose rates of approximately 4.6 Gy/minute

(HT-29 and DU145) and 2.3 Gy/minute (HT-144) were used. For low dose studies, dose

rates of approximately 0.5 Gy/minute and 2.3 Gy/minute were used. For delivery of a

small priming dose to suspension cultures, a dose rate of approximately 0.5 Gy/minute

was used.
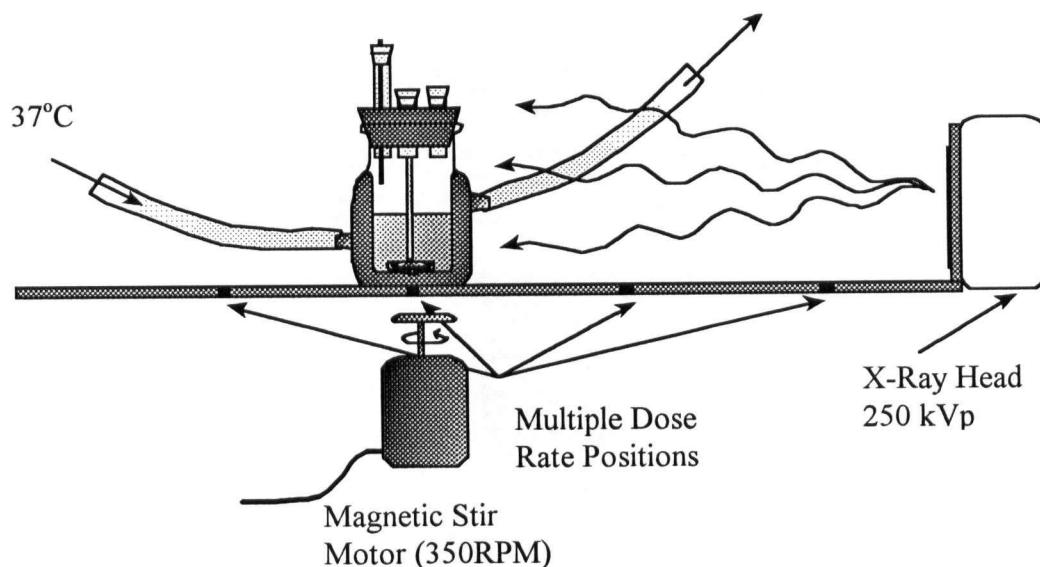
Figure 2-2 X-ray Irradiation in Suspension
Irradiation vessels were stirred at 350 RPM using a magnetic stirrer and maintained at 37°C by recirculating heated water through the water-jacket of the flask. The irradiation vessel was placed in a custom designed jig, and could be positioned at several distances from the head of the X-ray unit allowing for irradiation at different dose rates. Irradiation was carried out with a Philips RT-250 kVp, HVL 1.5 mm Cu X-ray unit.

2.3.1.2 Irradiation in Test Tubes

Irradiation of samples using the presort protocol required the use of a phantom. A plexiglass jig that accommodated six 5 ml test tubes was used (see fig. 2-3). The dose delivered to the six tubes was uniform ($\pm 1\%$) as determined from ionization chamber measurements (Victoreen Model 500, 0.6 cm^3 chamber). This phantom was filled with water, and maintained at 37°C using a thermostatically controlled recirculating water bath. All samples received single doses of radiation immediately after cell sorting. The phantom could be placed at several positions from the X-ray unit, allowing for several dose rates. For low dose hypersensitivity measurements in HT-29, DU 145 and A549 cell lines, dose rates of approximately 0.5 Gy/minute and 3.0 Gy/minute were used.

37°C Water Phantom

250kVp X-rays
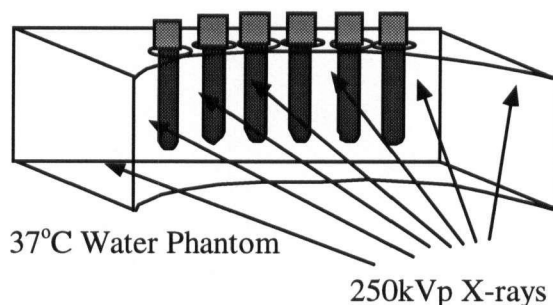
Figure 2-3 X-ray Irradiation in Test Tubes in a Phantom.
Six cell sorts could be irradiated with a uniform dose within a phantom. The phantom was maintained at 37°C with a recirculating pump. The phantom could be placed at several positions from the X-ray unit allowing for multiple dose rates.

2.3.1.3 Irradiation of Cell Monolayers

The original priming experiments required irradiation of monolayers of cells in 225 cm^2 flasks. For this purpose, a small priming dose of 0.3 Gy was required. Culture flasks containing 150 ml of medium were placed into a plexiglass box containing 37^{0}C water to a depth equal to the height of medium in the flask. The plexiglass box was located at a fixed distance above the target of the X-ray unit resulting in a dose rate of 0.54 Gy/minute.

2.3.2 Cobalt-60 γ-Irradiation

Samples were γ-irradiated in a phantom similar to that shown in figure 2-3. In this case, the phantom was filled with ice-water at 0°C, and gel samples were irradiated two at a time with single doses of ^{60}Co γ-rays. A ^{60}Co Theratron unit at the Vancouver Cancer Centre was used to deliver dose rates of approximately 2.1 Gy/minute or 3.7 Gy/minute. Due to decay of the ^{60}Co source, these dose rates varied somewhat from one experiment to another. Dosimetry was performed using the Medical Biophysics Victoreen Model 500 Electrometer and ionization chamber (0.6 cm^3) which had previously been calibrated against the Vancouver Cancer Centre Baldwin-Farmer chamber (0.6 cm^3) and Keithley Electrometer, which is the dosimetry standard used by the Physics Department in the Cancer Centre. The Baldwin-Farmer/Keithley instrument was calibrated at the National Research Council of Canada Institute for National Measurement Standards. The dosimetry and calibration were done with the assistance of Dr. Ken Yuen and Dr. Lloyd Skarsgard.

2.3.3 Proton Beam Irradiation

For proton irradiation samples, each ABS tube was placed in a phantom, with the axis of the tube collinear with the central axis of the proton beam. The phantom contained 19.3% glycerol in water, designed to have the same density (ρ=1.05 g/cm^3), and stopping power as the ABS plastic and the 12% gelatin. This ensured a constant stopping power throughout the entire phantom and thus avoided any artifacts that could have resulted from protons scattered from points outside the gel. The phantom was maintained at a temperature of ~2°C using a refrigerated circulating bath.

The 70 MeV proton beam at TRIUMF, designed for the treatment of uveal melanoma, was used for irradiation of all samples. The beam is extracted from the TRIUMF cyclotron and directed into the proton therapy facility. The proton beam is of relatively low intensity, and has an adjustable energy range of 65 - 120 MeV, with a corresponding range of 4 to 10 cm in water (Blackmore *et al.* 1995). The beam control and shaping system used to create the physical dose profile for these irradiations is the same as that used for clinical treatments. A proton beam current of ~5 nA was used, corresponding to a dose rate of about 5 Gy/minute. Slightly lower dose rates were used for the low dose points (0.5, 1, 1.5, and 2 Gy) to ensure accurate dose delivery. Uniform dose in the depth direction (*i.e.*, throughout the proton stopping peak) was provided by the standard method of range modulation using a rotating lucite wheel with sectors of different thickness. Laterally, a uniform field was generated by passive scattering using a 0.8 mm lead foil placed 1.2m upstream, and a circular brass collimator placed at 10 cm from the irradiation sample. The delivered dose was monitored by a parallel plate

transmission ionization chamber whose output was calibrated for the specific irradiation configuration used in these experiments. The lateral beam uniformity was monitored by a quadrant chamber during irradiation.

The proton dose was measured using a small 0.05 cm^3 air-filled thimble chamber (Exradin model T1) and Keithley Digital Electrometer (Model 616), which was operated as an absolute dosimeter using the known sensitive volume calculated from the exposure calibration factor, N_x, obtained from an Accredited Dosimetry Calibration lab. The particular values of the dosimetry parameters such as the W values and stopping powers were obtained from the Code of Practice published by the European Clinical Heavy Particle Dosimetry Group (ECHED) (Vynckier *et al.* 1991). This calibration factor was cross-checked at a recent international dose intercomparison at the Medical Centre of Loma Linda University. It was within 0.7% of the average dose reported from a group of 13 charged particle facilities throughout the world. The relative dosimetry measurements were made using small diodes for the lateral profiles and a parallel plate chamber for the depth dose profiles. These profiles were measured in a water tank phantom using a custom-built high resolution scanner with a precision of 0.05 mm. The proton SOBP design and dosimetry was done by the BCCA/TRIUMF clinical physics group: Dr. Gabe Lam, Mr. Ivan Liu, Dr. Uwe Oelfke, and Dr. Kaye Gardey.

2.4 Cell Sorting and Plating

For assessment of cell survival, a cell sorter (Becton-Dickinson 440) was used to sort an accurately known number of cells from each sample of interest by identifying single cells on the basis of forward and perpendicular light scatter without the use of a

cell stain (Durand 1986). Although this cell sorter is capable of delivering cells into test tubes located on both sides of the cell stream, sorting was restricted to one side only, because early experiments revealed a small but consistent difference in the number of cells delivered to each side. For radiosensitizer studies, 3 sorts were dispensed from each irradiated sample (two samples per dose point) into 5 ml test tubes containing 4.5 ml of growth medium. Each of these sorts was then plated into a 100 mm Petri dish with an additional 10 ml of warm growth medium and with 70,000 heavily irradiated feeder cells (70 Gy). The 10 ml of medium was added by rinsing the sorting tube twice with 5 ml, such that any residual sorted cells not plated during the initial emptying of the tube would subsequently be plated. For each dose point and each cell line, appropriate numbers of cells were plated to produce 300-600 colonies/Petri dish after 10-14 days of incubation. The Petri dishes were stained with malachite green or methylene blue, and colonies containing greater than 50 cells were scored as survivors. A similar procedure was carried out for studies of low dose hypersensitivity using the postsort protocol.

For studies utilizing the presort protocol, an aliquot of unirradiated cells was sorted into six 5 ml test tubes containing 4.5 ml of 37°C growth medium. These six sorts were irradiated together, and then plated as previously described.

Following preparation of the proton and ^{60}Co irradiated V79-WNRE/gel samples, 2-3 sorts were dispensed from each sample using the cell sorter. These sorts were plated as described previously, but did not require irradiated feeder cells. For this cell line, Petri dishes were incubated for 6-7 days prior to cell staining and colony counting.

2.5 Flow Cytometry

The DNA distributions of the cell populations used during asynchronous irradiation experiments were measured to ensure that cells were growing exponentially. Approximately 1×10^6 cells were centrifuged at 90g for 7 minutes, and the supernatant was discarded. Cells were then fixed by either paraformaldehyde or ethanol. Paraformaldehyde fixation was carried out by resuspending pellets in 2 ml of 0.5% paraformaldehyde for 10 minutes. The cells were then spun down and resuspended in PBS and maintained at 4°C prior to staining and analysis. Ethanol fixation was carried out by resuspending pellets in 0.25 ml of PBS. Cold (-20°C) ethanol was then slowly added while vortexing to a final concentration of 70% ethanol. Samples were maintained at -20°C prior to staining and analysis. One hour prior to analysis, fixed samples were spun down and resuspended in PBS containing either 10 μg/ml mithramycin (MI) or 50 μg/ml propidium iodide (PI). Samples labeled with PI were incubated for an additional 30 minutes with 200 units of Ribonuclease A (Sigma). Stained samples were then analyzed on a Coulter Elite ESP FACS.

In order to measure both the DNA distributions of cells, as well as the active S-phase fractions, a flow cytometric technique utilizing a monoclonal antibody to 5-bromodeoxyuridine (BrdU) was used (Gratzner 1982). This technique is based on the ability of cells to incorporate the thymidine analog BrdU during semi-conservative DNA replication. The S-phase fraction of cells can then be detected with a monoclonal antibody to BrdU conjugated to a fluorescent molecule. Counterstaining with propidium iodide allows for simultaneous measurement of S-phase fraction and DNA content. For

these measurements, the cells of interest were incubated with 10 µM BrdU for 20-30 minutes to label S-phase cells. At time points of interest, samples were taken and fixed in ethanol as previously described. Following fixation samples were centrifuged, the supernatant was aspirated off, and the cell pellet was resuspended in 1 ml of 2N HCL with 0.5% Triton-X100 (v/v) and incubated at room temperature for 30 minutes (to denature the DNA). Samples were then recentrifuged, the medium was aspirated, and the pellet resuspended in 1 ml of 0.1M $Na_2B_4O_7 \cdot 10H_2O$, pH 8.5. After a minimum of 15 minutes, cell suspensions were centrifuged again, and cell pellets resuspended in 1 ml of PBS with 1% bovine serum albumin (BSA). A monoclonal antibody conjugated to a FITC molecule (fluorescent isothiocyanate) from Becton Dickinson was added to each sample for 30 minutes. Samples were centrifuged, washed twice in PBS, and finally stained with 5 µg/ml propidium iodide (PI). After an additional 30 minutes on ice, samples were analyzed with a Counter Elite FACS. The fluorescence of both green (FITC) and red (PI) light was recorded, and analyzed later with software packages from MODFIT, and/or Coulter.

2.6 Dissolved Oxygen Measurement

To ensure that adequate levels of hypoxia could be attained for evaluation of radiosensitizers, measurements of dissolved oxygen concentration within the stirred cell suspensions were made as a function of time with a Clark-type oxygen electrode coupled to a sensitive amplifier designed and fabricated by Dr. Cameron Koch (Koch and Kruuv 1972). For these purposes the probe was inserted through a modified stopper into an irradiation vessel containing 65 ml of medium, which allowed sufficient penetration of

the probe into the suspension. Calibration of the probe was done by gassing with known concentrations of humidified oxygen (in N_2) at 37°C and allowing solutions without cells to reach equilibrium. During the gassing procedure the electrode output was recorded with a chart recorder. The background current (low level detection limit) of the probe was measured by two procedures. The oxygen concentration was measured in 65 ml of medium in the water-jacketed irradiation vessels during an extended nitrogen (O_2 free) gassing period of 20 hours, allowing for complete out-gassing of the oxygen in the system. Secondly, an enzymatic depletion of oxygen was carried out using 25 ml of phosphate buffer (5 mM KH_2PO_4, 15 mM K_2HPO_4) containing 10 mM glucose to which catalase (0.5 mg) and glucose oxidase (0.05 mg) were added. The oxygen probe and solution were placed in an airtight container, and the probe current monitored as a function of time. Following calibration, the oxygen concentration under experimental conditions could be recorded with a chart recorder.

2.7 Data Analysis

For each survival response, the plating efficiency for each individual Petri dish was calculated as the number of surviving colonies (defined as >50 cells) divided by the number of cells seeded:

$$p.e._{ij} = \frac{colonies\ counted}{cells\ seeded} \qquad \text{Equation 2-1}$$

The surviving fraction for each dish was determined by dividing the measured plating efficiency by the average of the plating efficiencies of all samples that received zero dose:

$$S_{ij} = \frac{p.e._{ij}}{ZPE}$$

Equation 2-2

$$ZPE = \sum_{j=1}^{r} \frac{p.e._{0j}}{r}$$

Equation 2-3

Here S_{ij} is the survival at dose point i in repeat j, and r is the number of samples at 0 Gy in the survival response. The data from several experiments were usually pooled, and the mean survival and the standard error of the mean computed for each individual dose point:

$$\overline{S_i} = \sum_{j=1}^{n} \frac{S_{ij}}{n}$$

Equation 2-4

$$\sigma_i = \sqrt{\frac{\sum_{j=1}^{n} (\overline{S_i} - S_{ij})^2}{n(n-1)}}$$

Equation 2-5

Here n is the total number of measurements (Petri dishes) at each dose point i.

The survival responses were fitted with several different mathematical models in the course of these studies. The best-fit parameters in these models were determined by a non-linear curve fitting program. This program used the Levenberg-Marquardt method (Press *et al.* 1989) to efficiently minimize the chi-squared value:

$$\chi^2 = \sum_{i=1}^{m} \frac{(\overline{S_i} - S_{fit})^2}{\sigma_i^2}$$

Equation 2-6

for all m data points in the survival response. Minimization of this expression allowed for appropriate weighting of survival data based on the measured scatter in the data. Since a chi-squared minimization method was used for finding best-fit values, the 95% confidence limits in each parameter separately, were determined by varying the best-fit

values until the χ^2 value changed by an amount of 4.0 (Press *et al.* 1989). To determine the joint 95% confidence limits in two parameters, this value was allowed to change by an amount of 6.17 (Press *et al.* 1989).

3

LINEAR QUADRATIC MODELING IS

PREDICTIVE FOR HYPOXIC RADIOSENSITIZER

EFFICACY IN DIFFERENT HUMAN TUMOUR

CELLS

3.1 Introduction

3.1.1 The Hypoxia Problem

Following the demonstration of the oxygen effect in mammalian cells and its proposed implications for radiotherapy (Gray *et al.* 1953, Thomlinson and Gray 1955), it was widely accepted that the presence of hypoxia could be responsible for many cases of radiation treatment failure. However, it was not until 1963 that the detrimental effect of the presence of hypoxic cells within tumours was experimentally demonstrated. Powers and Tolmach (1963) showed that a mouse tumour irradiated *in vivo* exhibited a biphasic survival response, with an initial sensitive region followed by a resistant 'tail'. From this curve they determined that approximately 1% of the cells were roughly 3 times more resistant than the remaining 99%, and they postulated that these were hypoxic cells. Since that time, the 'hypoxic fraction' of many other experimental tumours has been measured, with results ranging from 0% to greater than 50% (Moulder and Rockwell 1984). It is obviously not possible to perform similar experiments in humans to prove that clonogenically viable hypoxic cells exist, however studies with oxygen probes (Hockel *et al.* 1991, Vaupel *et al.* 1991), hypoxic cell labeling techniques (Koh *et al.* 1992, Wilson and Cerniglia 1992, Lord *et al.* 1993), and the comet assay (Olive and Durand 1992, Olive *et al.* 1993a, 1994, Olive 1995) have indicated the presence of regions of low oxygen tension in human tumours. Furthermore, it has also been shown that the presence of regions of low oxygen tension can be predictive for treatment failure

or success (Overgaard *et al.* 1986, Gatenby *et al.* 1988, Okunieff *et al.* 1993, Hockel *et al.* 1993) for some human tumours.

3.1.2 Hypoxia Selective Radiation Modifying Agents

These observations led to the development of several approaches for solving the hypoxia problem. The first attempt at reducing hypoxia was simply to increase the oxygen partial pressure within tissues, and thereby increase the diffusion limit of oxygen (Churchill-Davidson *et al.* 1955). However, clinical trials using hyperbaric oxygen (HBO), in which patients were exposed to up to 3 atmospheres of oxygen, have produced variable results. This may be due to an exacerbation of acute hypoxia that can develop from vasoconstriction, and correspondingly a reduction in blood flow through the tumour. Even a minor reduction in blood flow resulting from vasoconstriction would offset the gains from increased oxygen diffusion (Duncan and Nias 1977). The best results with hyperbaric oxygen treatment were those reported by Henk (1986), however this trial utilized somewhat larger radiation doses (4.1-4.5 Gy/fraction) as compared to more standard treatment protocols (~2 Gy/fraction). Consequently, the differential in cell kill between a fully oxygenated tumour and one with a remaining fraction of hypoxic cells would be larger than in a more typical fractionated regime using doses of approximately 2 Gy/fraction.

Another approach for solving the hypoxia problem was the development of drugs that could act as chemical radiosensitizers, mimicking the radiosensitizing effects of oxygen. The biggest advantage of these agents, as compared to hyperbaric oxygen, is that they are not as rapidly metabolized by cells as oxygen, and can thus potentially penetrate

to all chronically hypoxic cells. The largest class of agents investigated as radiosensitizers are the 2-nitroimidazoles. The first of these which showed substantial promise in the laboratory was misonidazole. This agent is highly electron-affinic (Adams *et al.* 1976), and at concentrations of 10 mM can provide sensitization that is similar to that observed with oxygen (Fowler *et al.* 1976). In the clinic, this drug has been involved in a large number of trials, the individual results of which have been largely disappointing (Dische 1985). Some of these disappointing results can be attributed to the fact that the dose limiting toxicity (peripheral neuropathy) resulted in less than optimum achievable concentrations of misonidazole (Dische *et al.* 1977, Dische 1985). This toxicity can be partially attributed to the octanol partition coefficient for misonidazole, which describes the relative affinity of the compound for lipids and water. For misonidazole this value was relatively high (0.43), and as a result this agent could easily cross the blood-brain barrier. Furthermore, the relatively long half life of misonidazole increased the toxicity of the drug (proportional to concentration and exposure time), without increasing the radiosensitizing ability (proportional to concentration only). Etanidazole was developed to counteract these disappointing results in the clinic. This drug is far more hydrophilic, with a partition coefficient of only 0.02 and, although it can still cross cell membranes, has more difficulty crossing the blood-brain barrier, resulting in a reduced concentration in neural tissues (Brown 1984). In addition, the half life of etanidazole is smaller than for misonidazole, resulting in a reduced exposure and correspondingly lower toxicity. In clinical trials the dose-limiting toxicity is still peripheral neuropathy, however etanidazole can be administered at doses which experimentally result in a three to five-fold increase

in sensitization as compared to misonidazole (Dische *et al.* 1985, 1986). The results of two phase III clinical trials with etanidazole have been published (Chassagne *et al.* 1991, Lee *et al.* 1995), both of which have shown no significant improvement in survival. The lack of any statistically significant improvement in the numerous clinical studies of nitroimidazole compounds has been addressed recently by Overgaard (1994). In this report, a meta-analysis of all phase III clinical trials with nitroimidazoles has been conducted, and a small, but statistically significant, benefit was identified for the use of these compounds. The results of this meta-analysis showed a significantly larger benefit for head and neck tumours (5.1% improvement in local control with an odds ratio of 1.23, p=.003) (Overgaard 1994). This meta-analysis also shows that, because the benefits achievable with hypoxic cell radiosensitizers are small, very large studies are required to demonstrate statistically significant gains, and suggests an explanation for the lack of significant gains in many individual studies. This author stressed the need for less toxic derivatives of these radiodsensitizers to circumvent many of the problems which have limited their success to such small gains.

Laboratory studies with misonidazole revealed that after several hours of incubation this agent was also *selectively toxic* to hypoxic cells, an observation that was first reported from this laboratory, and subsequently from others (Palcic *et al.* 1974, Hall and Roizin-Towle 1975, Moore *et al.* 1976). This finding spurred the development of a third strategy for dealing with hypoxic cells: agents that are selectively toxic under low oxygen conditions. These have come to be known as bioreductive agents, and are usually drugs that are converted to a toxic, often alkylating, species within the cell in a reaction

that is either inhibited or slowed by the presence of oxygen. Examples of these compounds include mitomycin C (Kennedy *et al.* 1980), tirapazamine (Zemen *et al.* 1986), and EO-9 (Oostveen and Speckamp 1987).

Another class of drugs, known as dual function agents, combines these latter two activities - selective toxicity and radiosensitization of hypoxic cells. An example is RSU1069, a 2-nitroimidazole with an alkylating aziridine ring at the end of one side chain (see abbreviations, page xiii). This ring greatly enhances its hypoxic potency, presumably by facilitating association with the DNA (Adams *et al.* 1984a, 1984b). Thus, this drug acts as a radiosensitizer and as a hypoxic cell cytotoxin at much lower concentrations than other 2-nitroimidazoles such as etanidazole. RB6145 is the prodrug of RSU1069, designed to have reduced systemic toxicity, that was developed as a candidate drug for clinical trials (Jenkins *et al.* 1990, Cole *et al.* 1990). This drug is converted to RSU1069, and has demonstrated a radiosensitizing ability and hypoxic cell selective toxicity similar to RSU1069 (Cole *et al.* 1992).

3.1.3 Radiation Modifiers at Low Doses

Investigations with chemical radiation modifiers have been carried out primarily in a limited number of different cell lines, often from rodent origin, and often at high single doses of radiation. The demonstration of the potential importance of the *in vitro* radioresponsiveness of different human tumour cells at low doses of radiation as determinants of clinical outcome by Malaise and colleagues (Fertil and Malaise 1981, 1985, Deschavanne *et al.* 1986, Malaise *et al.* 1987), suggests that the effectiveness of these radiation modifying agents should also be addressed at low radiation doses.

Furthermore, the demonstration of substructure in the radiation response showed that the intrinsic radiosensitivity at low dose can be dramatically different in terms of both absolute sensitivity and shape (*i.e.*, the α/β ratio) than would be predicted by the high dose data (Skarsgard *et al.* 1991, 1992, 1993, 1994a, 1995, Skwarchuk *et al.* 1993). In most cases, measurement of the low dose response reveals a more important role for cell death attributable to the β parameter than has been previously acknowledged, and is contradictory to the commonly held opinion that it is always the α component which is most important at low dose (Steel and Peacock 1989). Indeed it has been shown that the radiation response of some human tumour cell lines, when measured at low dose, can be dominated by the β component of cell kill even at doses as small as 2 Gy (Skarsgard *et al.* 1995).

To the extent that α and β represent different mechanisms or modes of cell killing, the modification of radiosensitivity by a particular agent should not be expected to modify each of these components to the same degree. Indeed, previous investigations into the effects of radiation modifying agents on the parameters in the linear quadratic (LQ) model have indicated selective modification of both the α (Korbelik and Skov 1989) and β parameters (Chapman *et al.* 1975a, 1975b, Palcic *et al.* 1984b). This has important implications for fractionated treatment, and in light of the very different contributions of these parameters to radiosensitivity in different human tumour cell lines at low dose (Skarsgard *et al.* 1995), it suggests that certain classes of radiosensitizing drugs may be tumour or cell type specific. It also offers the possibility that the efficacy of certain classes of sensitizers which act by primarily enhancing one of the two parameters

may, in part, be predicted on the basis of the measured *in vitro* parameters of the LQ model.

The objective of this chapter is to examine the importance of the inherent radiosensitivity as determined at low dose, on the efficacy of these types of radiation modifying agents. For this purpose, three human tumour cell lines have been chosen which are representative of cell lines with different radiation sensitivity, different α/β ratios, and different levels of cell-cycle associated substructure. Specifically, HT-29 colon carcinoma and DU145 prostate carcinoma are two resistant cell lines that have similar high dose radiosensitivity (*i.e.* similar survival levels after ~8 Gy), but extremely different α/β ratio's and levels of substructure (Skarsgard *et al.* 1995). HT-144 is a much more radiosensitive cell line, and has an α/β ratio that is intermediate between HT-29 and DU145 (Skarsgard *et al.* 1995).

3.2 Results

3.2.1 Evaluation of Hypoxia

To ensure that sufficiently low oxygen conditions could be obtained for evaluation of hypoxic cell survival to radiation, a Clarke oxygen electrode coupled to a sensitive amplifier was used to monitor oxygen levels within the water-jacketed irradiation vessels. This type of electrode has been shown previously to produce an electric current that is proportional to the oxygen concentration to levels as low as 50-100 ppm (Koch and Kruuv 1972, Koch 1975, Whillans and Rauth 1980). For the purposes of measuring oxygen depletion in the irradiation vessels, a volume of 65 ml (as opposed to the typical experimental value of 40-50 ml) was required in order to keep the electrode below the surface of the liquid. The electrode was calibrated by gassing stirred growth medium at 37°C with 20%, 1%, and 0.1% oxygen, and monitoring the amplified current output of the electrode as a function of time until equilibrium was established. The equilibrium electrometer reading could then be calibrated against the known oxygen partial pressure for each gas concentration:

$$oxygen\ partial\ pressure = \%O_2 * \left(p - c_h\right) mm\ of\ Hg \qquad \text{Equation 3-1}$$

To determine this quantity, the the partial pressure of water vapor (c_h) must be subtracted from the external air pressure (p) since all gas solutions were bubbled through distilled water to create essentially 100% humidity. At 37°C and an air pressure of 760 mm of Hg, this correction is approximately equal to 43 mm of Hg.

The low-level oxygen detection limit is determined by the background current of the probe in the absence of oxygen. This value was measured by an enzymatic oxygen-consuming reaction that was carried out in a small sealed flask, and by gassing irradiation vessels with oxygen-free nitrogen for up to 20 hours. Both of these methods resulted in the same background reading of 0.024 (arbitrary units).

Figure 3-1(a) shows the electrometer reading output as a function of time while gassing with several oxygen concentrations. Data from this figure were used to create the calibration plot shown in figure 3-1(b). This plot was subsequently fitted with a linear equation utilizing the known background current reading:

$$Electrometer\ Reading = .024 + m(O_2\ partial\ pressure)$$
<div align="right">Equation 3-2</div>

and resulted in a best-fit value for m = 0.816. The background current, which determines the minimum oxygen level that can be measured with this system, is thus approximately equivalent to an oxygen partial pressure of 0.029 mm of Hg.

Following calibration, the electrode was used to measure oxygen depletion as a function of time within the irradiation vessels under experimental conditions. To determine the rate of oxygen depletion through diffusion alone, initial measurements were made in cell culture medium without cells. A 65 ml solution was allowed to equilibrate with humidified air at 37°C until a stable electrode reading was obtained. Figure 3-2, (solid triangles) shows the results of gassing this solution with oxygen-free nitrogen for 90 minutes. The equivalent oxygen partial pressure drops exponentially (*i.e.* $\propto e^{-t/\tau}$) with a time constant (τ) of approximately 10.1 minutes, to a value of about 0.5 mm of Hg at 60 minutes.
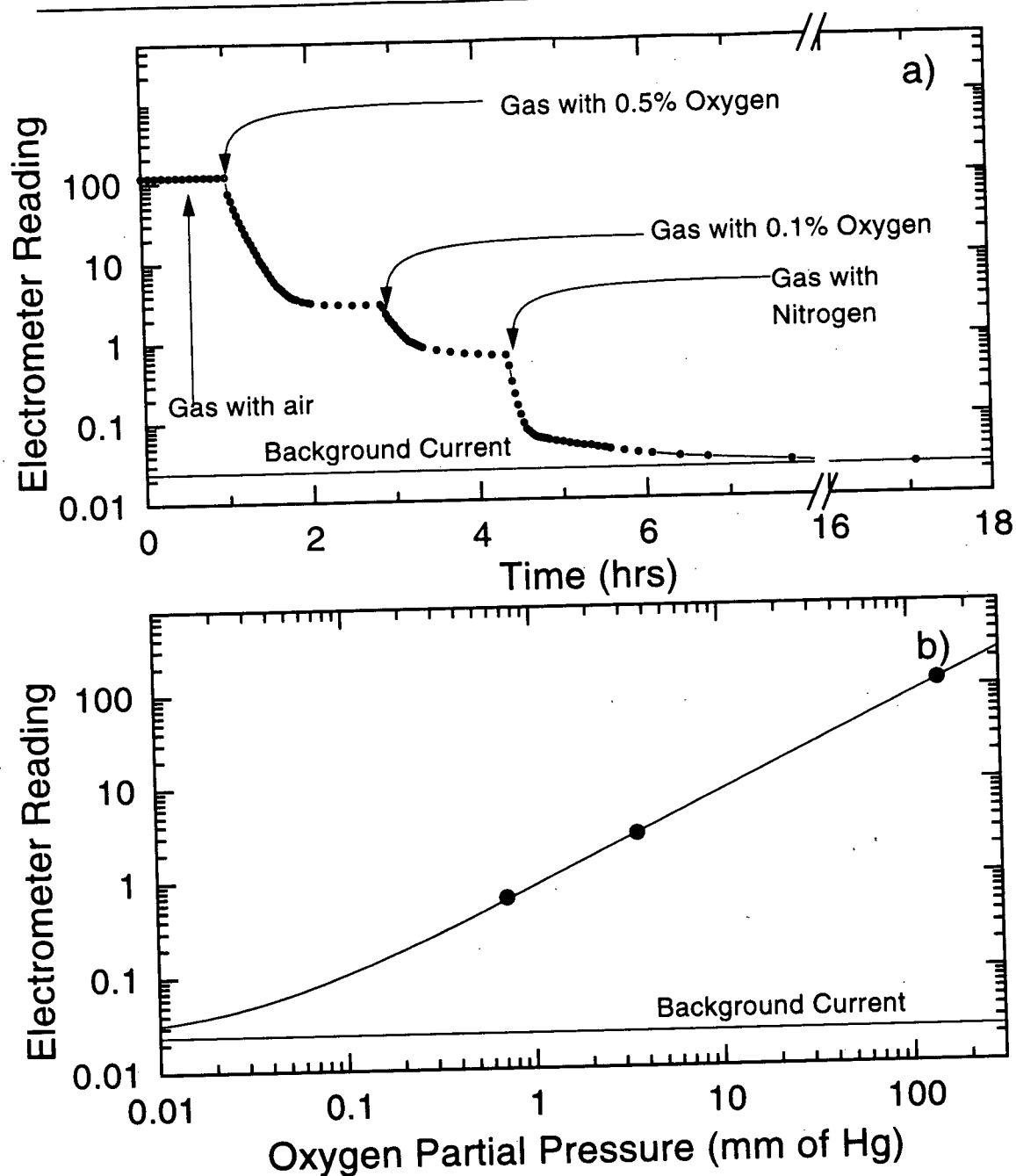
Figure 3-1 Calibration of the Oxygen Sensor
The oxygen electrode reading within an irradiation vessel containing 65 ml of stirred medium without cells was monitored while gassing with nitrogen containing the indicated amounts of oxygen (panel a). The background current of the probe was measured after extensive gassing with oxygen-free nitrogen. In panel b, the equilibrium oxygen electrode reading is shown as a function of the oxygen partial pressure in the gas used. These data were used to calibrate the electrode output with the oxygen partial pressure.
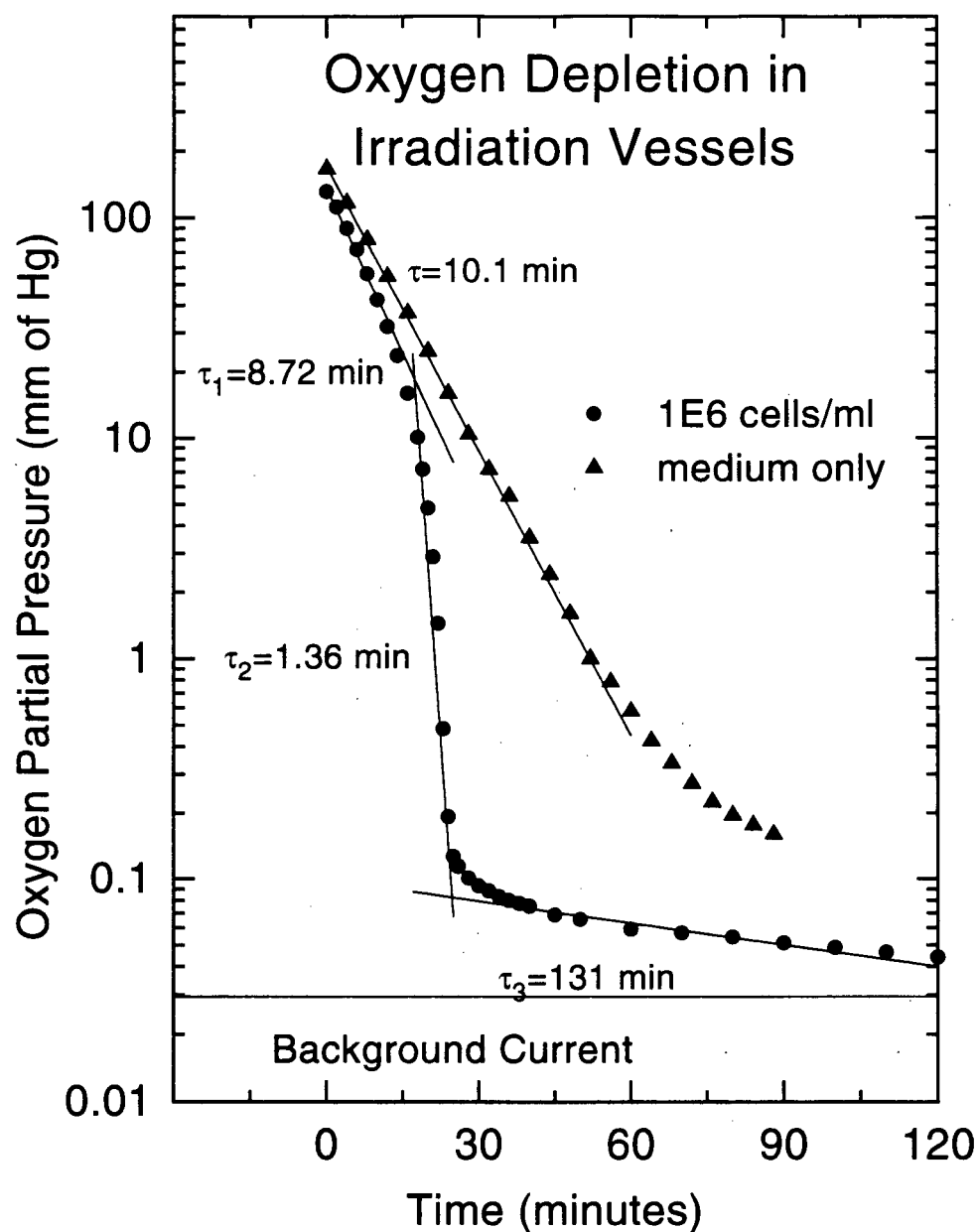
Figure 3-2 Oxygen Elimination From Irradiation Vessels

The oxygen partial pressure was measured with an oxygen electrode within an irradiation vessel containing 65 ml of stirred medium at 37°C while gassing with oxygen-free nitrogen. Oxygen elimination in medium without cells (triangles) occurred as an exponential function, with a time constant equal to 10.1 minutes. In medium with 1×10^6 cells/ml (circles) a similar initial rate of 8.72 minutes was measured. The time constant decreased to 1.36 minutes at lower oxygen concentrations due to respiratory consumption by the cells. A third time constant of 131 minutes was reached at very low levels due to oxygen outgassing of a Teflon ring on the oxygen electrode.

The rate of oxygen elimination in an equivalent solution containing 1×10^6 cells/ml, similar to experimental conditions, was also measured and is plotted as solid circles in figure 3-2. This plot exhibits a more complex response. Initially, the rate of depletion is similar to the diffusion limited value in medium alone ($\tau_1 = 8.7$ minutes) presumably because oxygen consumption by the cells is insignificant at higher oxygen concentrations. As the oxygen level drops, however, oxygen consumption by cellular respiration becomes significant and the concentration drops precipitously ($\tau_2 = 1.36$ minutes). After approximately 25 minutes a third depletion rate is reached ($\tau_3 = 131$ minutes). This third rate is most likely due to oxygen out-gassing from the Teflon ring on the oxygen electrode, a phenomenon that was also observed in an enzymatic, oxygen-consuming reaction. In any case, after 60 minutes of gassing, the equivalent oxygen partial pressure reached is approximately 0.05 mm of Hg, well within the range for radiobiological hypoxia and sufficient for the evaluation of hypoxic radiosensitizers (Ling *et al.* 1980, Whillans and Hunt 1982). The actual concentration under experimental conditions without the oxygen electrode is probably much lower than this value because the Teflon ring is absent, and because a smaller cell suspension volume (45 ml) is used.

The sequential sampling system was also tested in a mock irradiation procedure. Cell suspensions at 1×10^6 cells/ml were gassed for 1 hour with nitrogen to reach hypoxic conditions while being monitored with the oxygen electrode. A mock sequential sampling procedure without irradiation was then performed. No noticeable rise in the dissolved oxygen content within the suspension was observed during the entire

procedure. Deliberately injecting air (~2 cm^3) into the medium resulted in an increase to approximately 10% of the original oxygen level (~15 mm of Hg).

3.2.2 Survival Data

The radiation responses of HT-29, DU145, and HT-144 exponentially growing human tumour cell lines were determined using the cell sorting assay. In order to determine the nature of hypoxic cell sensitization produced by etanidazole, RB6145, or oxygen, irradiation was carried out under both aerobic and hypoxic (with and without drug), conditions. A minimum of 3 independent radiation survival responses were measured for each condition, with each of these responses comprising 4-6 repeated survival measurements (Petri dishes) at 16-17 different dose points. Hypoxic or aerobic responses were measured during each experiment as controls, and thus a proportionately higher total number of responses has been measured for these conditions. The average responses plotted for hypoxic and aerobic conditions are thus the global average of all responses measured throughout the course of these experiments. In order to characterize the initial survival region adequately, a proportionately higher number of survival measurements was carried out at high survival levels (in the first log of cell kill). Appropriate irradiation doses were chosen such as to have comparable numbers of dose points at each survival level among the different cell lines and irradiation conditions.

3.2.2.1 Etanidazole

Cell populations were made hypoxic through a combination of metabolic consumption and oxygen diffusion, by gassing with nitrogen for 1 hour prior to and

during irradiation. During this time cell suspensions were stirred and maintained at 37°C. Induction of hypoxia under these conditions did not result in any measurable reduction in plating efficiency as compared to control populations that were not hypoxic. The radiation survival response of hypoxic, asynchronously growing HT-29 cells is plotted in the upper frame of figure 3-3. Under hypoxic conditions these cells are extremely radioresistant and exhibit a large shoulder at high survival levels. These data are the average of 9 independent radiation survival curves using a dose range of 1 to 38 Gy, with 10 different dose points within the first log of cell kill.

The sensitizing ability of etanidazole was assessed by incubating cell populations with various concentrations of this drug for 1 hour prior to, and during irradiation. Figures 3-4, 3-5, and 3-6 are the average radiation survival responses of hypoxic HT-29 cells incubated with 0.5 mM, 2 mM, and 5 mM etanidazole respectively. For each of these dose responses, cell populations were irradiated with doses that resulted in survival levels similar to those found for hypoxic cell populations, and each figure is scaled appropriately to reflect these differences. Treatment with etanidazole under these conditions resulted in only minimal toxicity, and resulted in plating efficiencies that were not significantly different from those under hypoxic conditions alone.

To allow a comparison of the sensitizing ability of the two hypoxic sensitizers and oxygen, the aerobic radiation response was also determined. HT-29 cells were loaded into irradiation vessels at a reduced concentration (6×10^5 cells/ml) to prevent metabolic depletion of oxygen, and were gassed with air for 15-20 minutes prior to and during irradiation. Figure 3-7 shows the average radiation response data for 4 such survival curves.

The HT-29 radiation survival data for each of the above mentioned conditions have also been plotted in the lower frame of the corresponding figures in terms of the radiation effect per unit dose, defined as the negative logarithm of survival divided by dose:

$$-ln(S)/d \qquad\qquad \text{Equation 3-3}$$

This plot is useful for visualizing the ability of the LQ model:

$$S = e^{-\alpha d - \beta d^2} \qquad\qquad \text{Equation 3-4}$$

to adequately fit the entire dose response. On this plot, a true LQ response will yield a straight line with an intercept equal to the α parameter, and a slope equal to the β parameter:

$$-ln(S)/d = \alpha + \beta d \qquad\qquad \text{Equation 3-5}$$

These figures illustrate that for many of these responses, particularly in the hypoxic populations (with and without etanidazole: figs. 3-3 - 3-6) the survival data plotted in this form do not follow a straight line, and thus cannot be adequately fit by a single LQ function. The plots exhibit a lower effectiveness per unit dose at higher doses than would be predicted by a straight line extrapolation from the low dose data, indicating an increasing radioresistance at higher doses. Two of these plots (lower frames in fig. 3-5 and 3-7) also exhibit what could be interpreted as an unexpected low dose hypersensitivity. In these figures, the first data point shows an increased level of cell kill in comparison to the predicted LQ response. This low-dose hypersensitivity is the subject of investigation in chapter 4 of this thesis

Figure 3-3 HT-29 Hypoxic Radiation Response
Mean survival as a function of radiation dose in exponentially growing HT-29 cells irradiated at 37°C in suspension culture under hypoxic conditions (upper frame). Hypoxia was induced by a combination of nitrogen (O_2-free) gassing and cellular respiration. Data are the average of 9 survival responses determined using the cell sorting assay throughout the course of these experiments (see 3.2.2), and error bars are the standard error in the mean. The fitted lines represent the best fits of the LQ model (equation 3-4) to the mean survival data in the low dose (dashed line) and high dose (solid line) regions. Also shown are the same survival data replotted in the form -(lnS)/d (lower frame). In this plot a LQ function is a straight line with a y-intercept equal to α and a slope equal to β.

Figure 3-4 HT-29 Hypoxic Plus 0. 5 mM Etanidazole Radiation Response

Mean survival as a function of radiation dose in exponentially growing HT-29 cells irradiated at 37°C in suspension culture under hypoxic conditions with 0.5 mM etanidazole (upper frame). Cell suspensions were incubated for 1 hour prior to and during irradiation while hypoxic conditions were established. Data are the average of 4 survival responses determined using the cell sorting assay, and error bars are the standard error in the mean. The fitted lines represent the best fits of the LQ model (equation 3-4) to the mean survival data in the low dose (dashed line) and high dose (solid line) regions. Also shown are the same survival data replotted in the form -(lnS)/d (lower frame). In this plot a LQ function is a straight line with a y-intercept equal to α and a slope equal to β. Note the different dose scale.
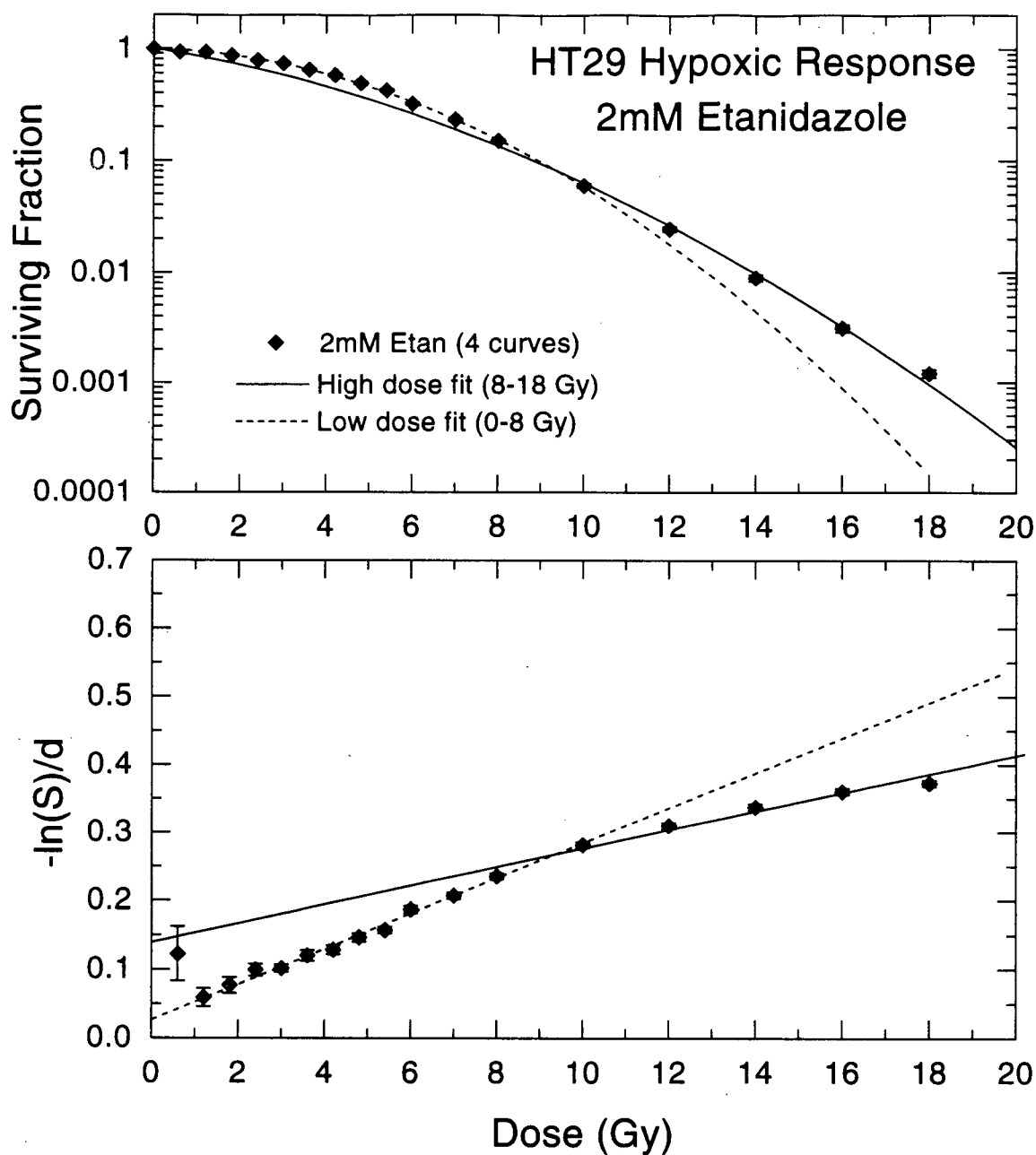
Figure 3-5 HT-29 Hypoxic Plus 2 mM Etanidazole Radiation Response
Mean survival as a function of radiation dose in exponentially growing HT-29 cells irradiated at 37°C in suspension culture under hypoxic conditions with 2 mM etanidazole (upper frame). Cell suspensions were incubated for 1 hour prior to and during irradiation while hypoxic conditions were established. Data are the average of 4 survival responses determined using the cell sorting assay, and error bars are the standard error in the mean. The fitted lines represent the best fits of the LQ model (equation 3-4) to the mean survival data in the low dose (dashed line) and high dose (solid line) regions. Also shown are the same survival data replotted in the form -(lnS)/d (lower frame). In this plot a LQ function is a straight line with a y-intercept equal to α and a slope equal to β.

Figure 3-6 HT-29 Hypoxic Plus 5 mM Etanidazole Radiation Response
Mean survival as a function of radiation dose in exponentially growing HT-29 cells irradiated at 37°C in suspension culture under hypoxic conditions with 5 mM etanidazole (upper frame). Cell suspensions were incubated for 1 hour prior to and during irradiation while hypoxic conditions were established. Data are the average of 5 survival responses determined using the cell sorting assay, and error bars are the standard error in the mean. The fitted lines represent the best fits of the LQ model (equation 3-4) to the mean survival data in the low dose (dashed line) and high dose (solid line) regions. Also shown are the same survival data replotted in the form -(lnS)/d (lower frame). In this plot a LQ function is a straight line with a y-intercept equal to α and a slope equal to β.

Figure 3-7 HT-29 Aerobic Radiation Response
Mean survival as a function of radiation dose in exponentially growing HT-29 cells irradiated at 37°C in suspension culture under aerobic conditions (upper frame). Cell suspensions were gassed with air for 20 minutes prior to and during irradiation. Data are the average of 4 survival responses determined using the cell sorting assay, and error bars are the standard error in the mean. The fitted lines represent the best fits of the LQ model (equation 3-4) to the mean survival data in the low dose (dashed line) and high dose (solid line) regions. Also shown are the same survival data replotted in the form -(lnS)/d (lower frame). In this plot a LQ function is a straight line with a y-intercept equal to α and a slope equal to β.

Figure 3-8 Sensitization With Etanidazole in HT-29 Cells

For comparison purposes, the data from figures 3-3 to 3-7 are replotted together. Mean survival is shown as a function of radiation dose in exponentially growing HT-29 cells irradiated at 37°C in suspension culture under various conditions. The data for hypoxic, aerobic, and hypoxic with 0.5 mM, 2 mM, and 5 mM etanidazole are shown together (upper frame). The fitted lines represent the best fits of the LQ model (equation 3-4) to the mean survival data in the low dose (dashed line) and high dose (solid line) regions. Also shown are the same survival data replotted in the form -(lnS)/d (lower frame). In this plot a LQ function is a straight line with a y-intercept equal to α and a slope equal to β.

To illustrate the sensitizing ability of etanidazole in HT-29 cells, the aerobic, hypoxic, and hypoxic with etanidazole survival responses have been plotted together on the same dose scale in the upper frame of figure 3-8. The -(lnS)/d plots are also shown together in the lower frame of this figure.

A similar series of experiments was carried out in DU145 cells. Under aerobic conditions DU145 cells have been shown to have a high dose radiation sensitivity similar to HT-29 cells, however the survival curve exhibits a more linear shape (Skarsgard *et al.* 1995). The radiation response of hypoxic, asynchronous, DU145 cells is shown in figure 3-9. Treatment of DU145 cells with the same concentrations of etanidazole evaluated in HT-29 cells, 0.5 mM, 2 mM, and 5 mM, resulted in the radiation survival responses plotted in figures 3-10, 3-11, and 3-12. The aerobic response is plotted in figure 3-13. For reference the survival responses under all conditions are plotted together in figure 3-14. In all figures, the corresponding -ln(S)/d plot is shown in the lower frame.

The sensitizing ability of etanidazole was also evaluated in the radiosensitive cell line, HT-144. The radiation responses of asynchronously growing hypoxic, hypoxic with 2 mM etanidazole, and aerobic cell populations were determined, and are plotted in figures 3-15, 3-16, and 3-17 respectively. The data are also shown together in figure 3-18. In all figures, the corresponding -ln(S)/d plot is again shown in the lower frame.

Figure 3-9 DU145 Hypoxic Radiation Response
Mean survival as a function of radiation dose in exponentially growing DU145 cells irradiated at 37°C in suspension culture under hypoxic conditions (upper frame). Hypoxia was induced by a combination of nitrogen (O_2-free) gassing and cellular respiration. Data are the average of 8 survival responses determined using the cell sorting assay, and error bars are the standard error in the mean. The fitted lines represent the best fits of the LQ model (equation 3-4) to the mean survival data in the low dose (dashed line) and high dose (solid line) regions. Also shown are the same survival data replotted in the form -(lnS)/d (lower frame). In this plot a LQ function is a straight line with a y-intercept equal to α and a slope equal to β.

Figure 3-10 DU145 Hypoxic Plus 0.5 mM Etanidazole Radiation Response
Mean survival as a function of radiation dose in exponentially growing DU145 cells irradiated at 37°C in suspension culture under hypoxic conditions with 0.5 mM etanidazole (upper frame). Cell suspensions were incubated for 1 hour prior to and during irradiation while hypoxic conditions were established. Data are the average of 3 survival responses determined using the cell sorting assay, and error bars are the standard error in the mean. The fitted lines represent the best fits of the LQ model (equation 3-4) to the mean survival data in the low dose (dashed line) and high dose (solid line) regions. Also shown are the same survival data replotted in the form -(lnS)/d (lower frame). In this plot a LQ function is a straight line with a y-intercept equal to α and a slope equal to β.

Figure 3-11 DU145 Hypoxic Plus 2 mM Etanidazole Radiation Response
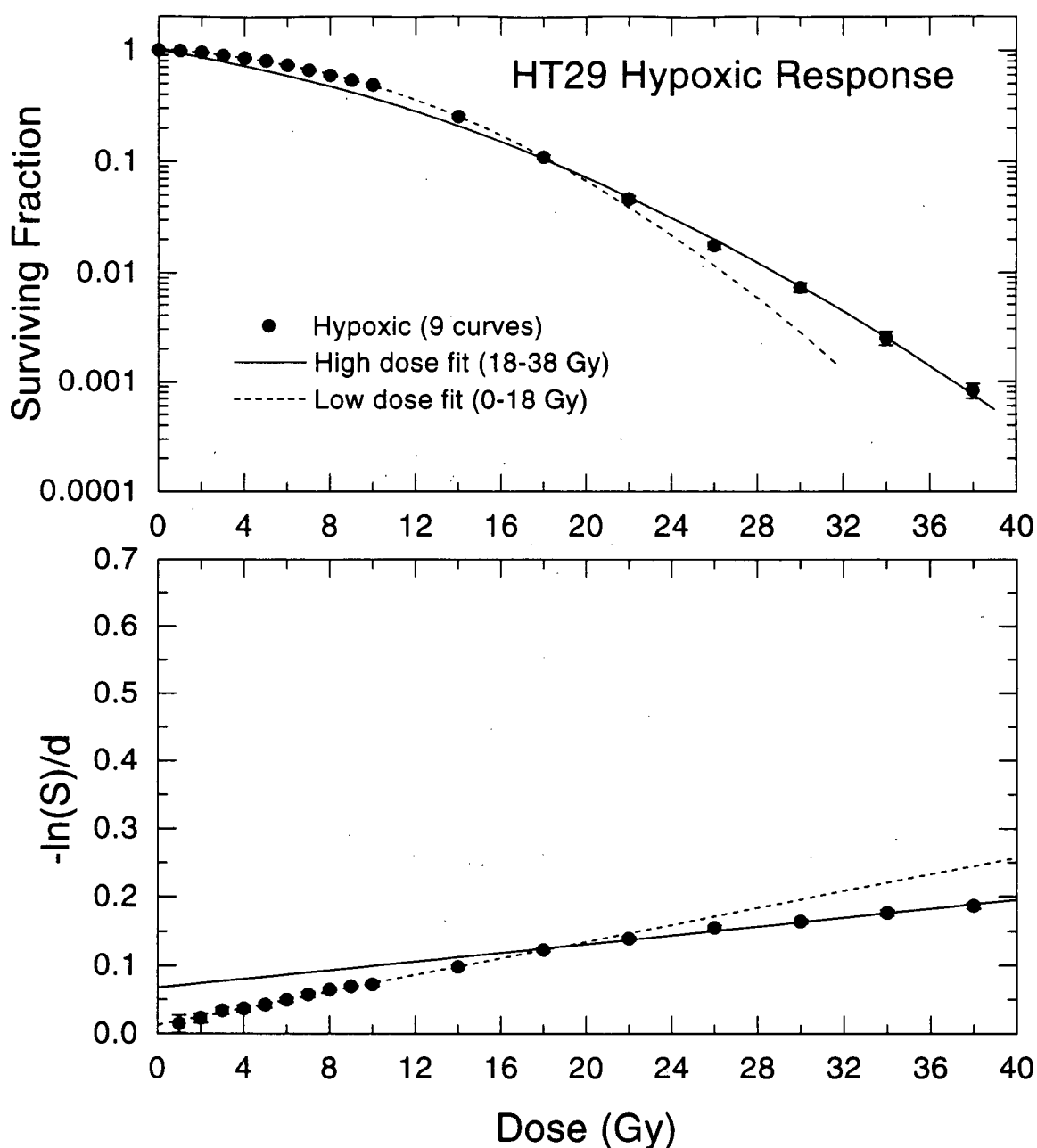Mean survival as a function of radiation dose in exponentially growing DU145 cells irradiated at 37°C in
suspension culture under hypoxic conditions with 2 mM etanidazole (upper frame). Cell suspensions were
incubated for 1 hour prior to and during irradiation while hypoxic conditions were established. Data are the
average of 4 survival responses determined using the cell sorting assay, and error bars are the standard error
in the mean. The fitted lines represent the best fits of the LQ model (equation 3-4) to the mean survival data
in the low dose (dashed line) and high dose (solid line) regions. Also shown are the same survival data
replotted in the form -(lnS)/d (lower frame). In this plot a LQ function is a straight line with a y-intercept
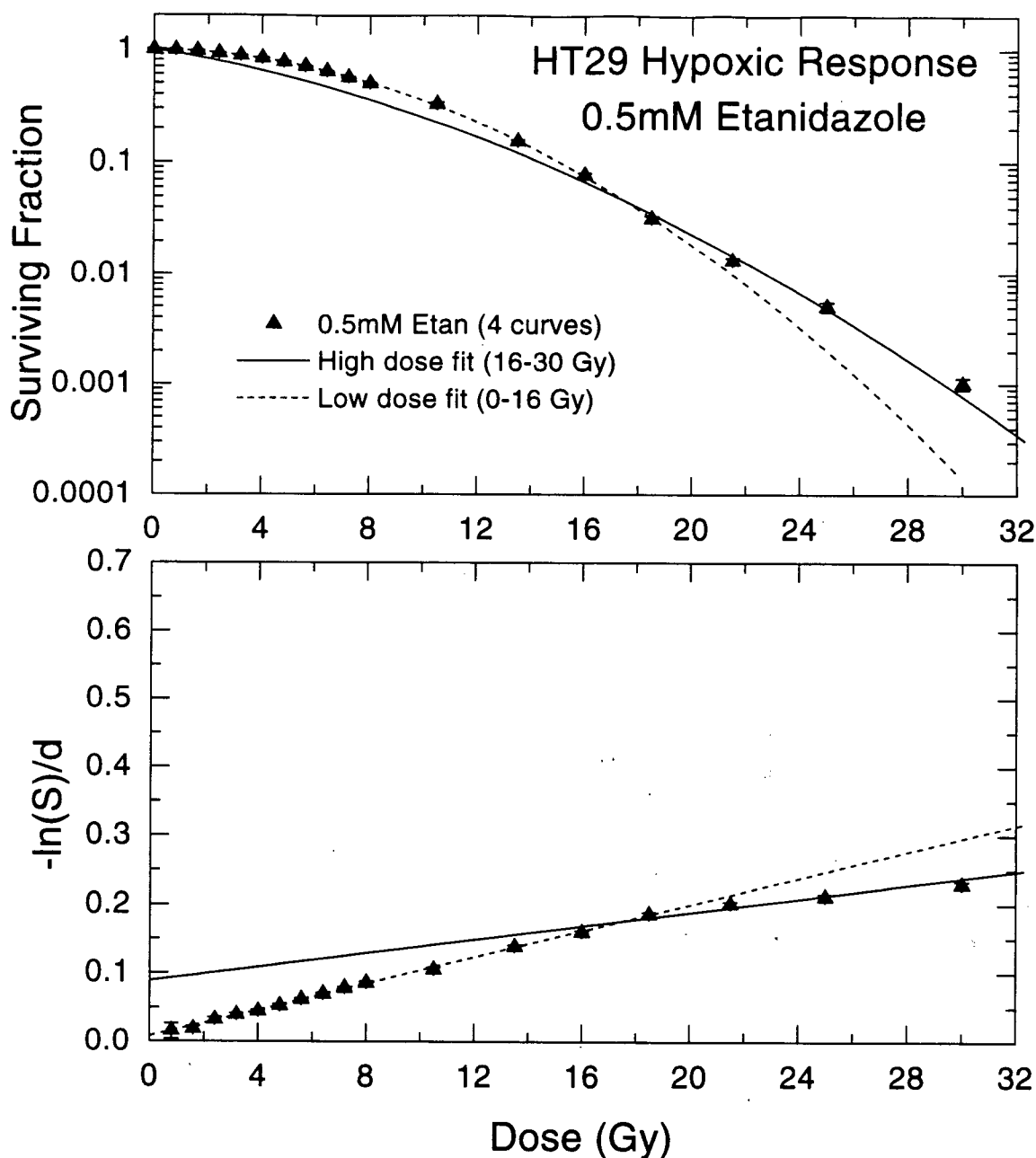equal to α and a slope equal to β.

Figure 3-12 DU145 Hypoxic Plus 5 mM Etanidazole Radiation Response

Mean survival as a function of radiation dose in exponentially growing DU145 cells irradiated at 37°C in suspension culture under hypoxic conditions with 5 mM etanidazole (upper frame). Cell suspensions were incubated for 1 hour prior to and during irradiation while hypoxic conditions were established. Data are the average of 3 survival responses determined using the cell sorting assay, and error bars are the standard error in the mean. The fitted lines represent the best fits of the LQ model (equation 3-4) to the mean survival data in the low dose (dashed line) and high dose (solid line) regions. Also shown are the same survival data replotted in the form -(lnS)/d (lower frame). In this plot a LQ function is a straight line with a y-intercept equal to α and a slope equal to β.

Figure 3-13 DU145 Aerobic Radiation Response
Mean survival as a function of radiation dose in exponentially growing DU145 cells irradiated at 37°C in suspension culture under aerobic conditions (upper frame). Cell suspensions were gassed with air for 20 minutes prior to and during irradiation. Data are the average of 4 survival responses determined using the cell sorting assay, and error bars are the standard error in the mean. The fitted lines represent the best fits of the LQ model (equation 3-4) to the mean survival data in the low dose (dashed line) and high dose (solid line) regions. Also shown are the same survival data replotted in the form -(lnS)/d (lower frame). In this plot a LQ function is a straight line with a y-intercept equal to α and a slope equal to β.

Figure 3-14 Sensitization With Etanidazole in DU145 Cells

For comparison purposes, the data from figures 3-9 to 3-13 are replotted together. Mean survival is shown as a function of radiation dose in exponentially growing DU145 cells irradiated at 37°C in suspension culture under various conditions. The data for hypoxic, aerobic, and hypoxic with 0.5 mM, 2 mM, and 5 mM etanidazole are shown together (upper frame). The fitted lines represent the best fits of the LQ model (equation 3-4) to the mean survival data in the low dose (dashed line) and high dose (solid line) regions. Also shown are the same survival data replotted in the form -(lnS)/d (lower frame). In this plot a LQ function is a straight line with a y-intercept equal to α and a slope equal to β.
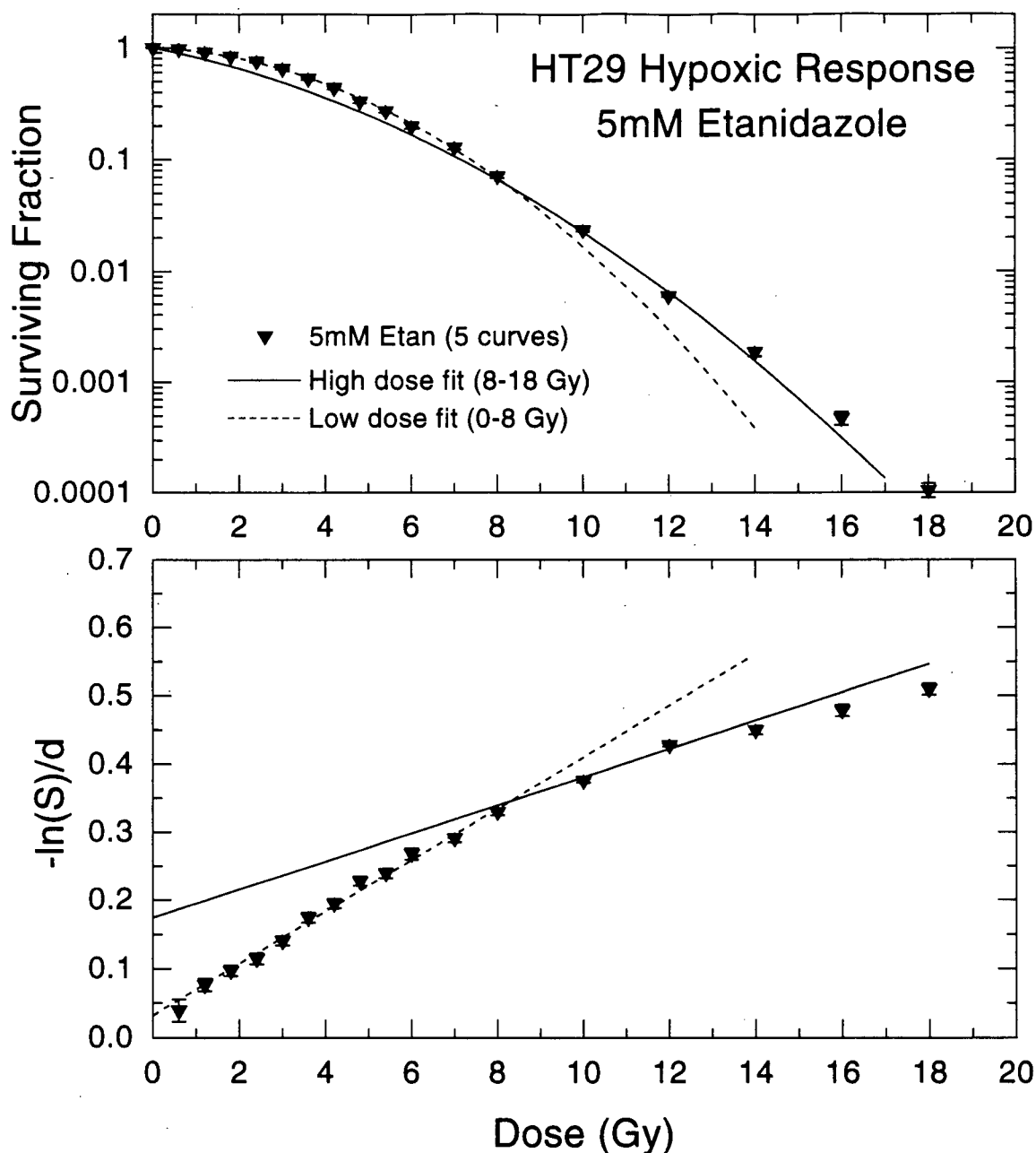
Figure 3-15 HT-144 Hypoxic Radiation Response
Mean survival as a function of radiation dose in exponentially growing HT-144 cells irradiated at 37°C in suspension culture under hypoxic conditions (upper frame). Hypoxia was induced by a combination of nitrogen (O_2-free) gassing and cellular respiration. Data are the average of 4 survival responses determined using the cell sorting assay, and error bars are the standard error in the mean. The fitted lines represent the best fits of the LQ model (equation 3-4) to the mean survival data in the low dose (dashed line) and high dose (solid line) regions. Also shown are the same survival data replotted in the form -(lnS)/d (lower frame). In this plot a LQ function is a straight line with a y-intercept equal to α and a slope equal to β.
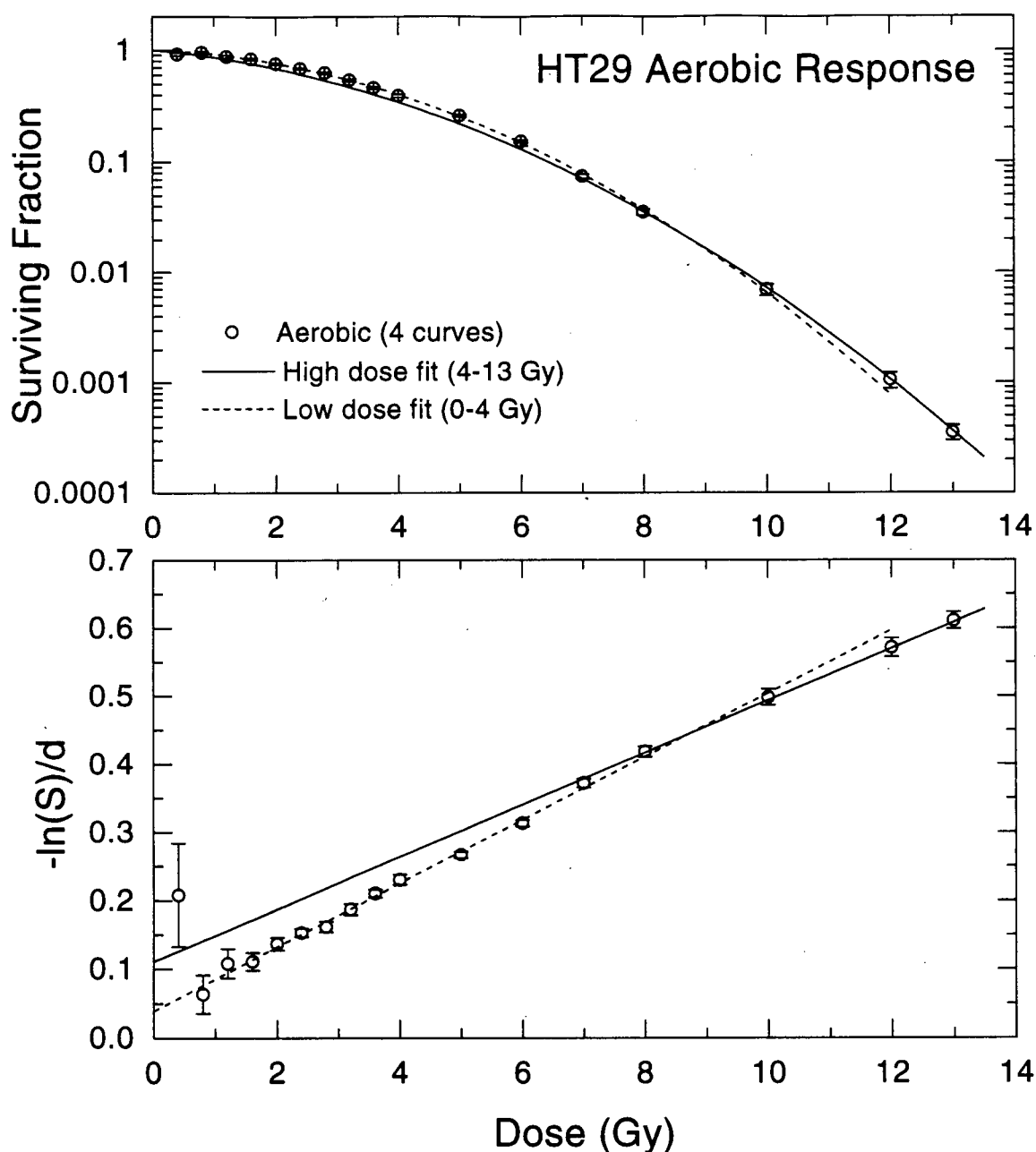
Figure 3-16 HT-144 Hypoxic Plus 2 mM Etanidazole Radiation Response
Mean survival as a function of radiation dose in exponentially growing HT-144 cells irradiated at 37°C in suspension culture under hypoxic conditions with 2 mM etanidazole (upper frame). Cell suspensions were incubated for 1 hour prior to and during irradiation while hypoxic conditions were established. Data are the average of 3 survival responses determined using the cell sorting assay, and error bars are the standard error in the mean. The fitted lines represent the best fits of the LQ model (equation 3-4) to the mean survival data in the low dose (dashed line) and high dose (solid line) regions. Also shown are the same survival data replotted in the form -(lnS)/d (lower frame). In this plot a LQ function is a straight line with a y-intercept equal to α and a slope equal to β.
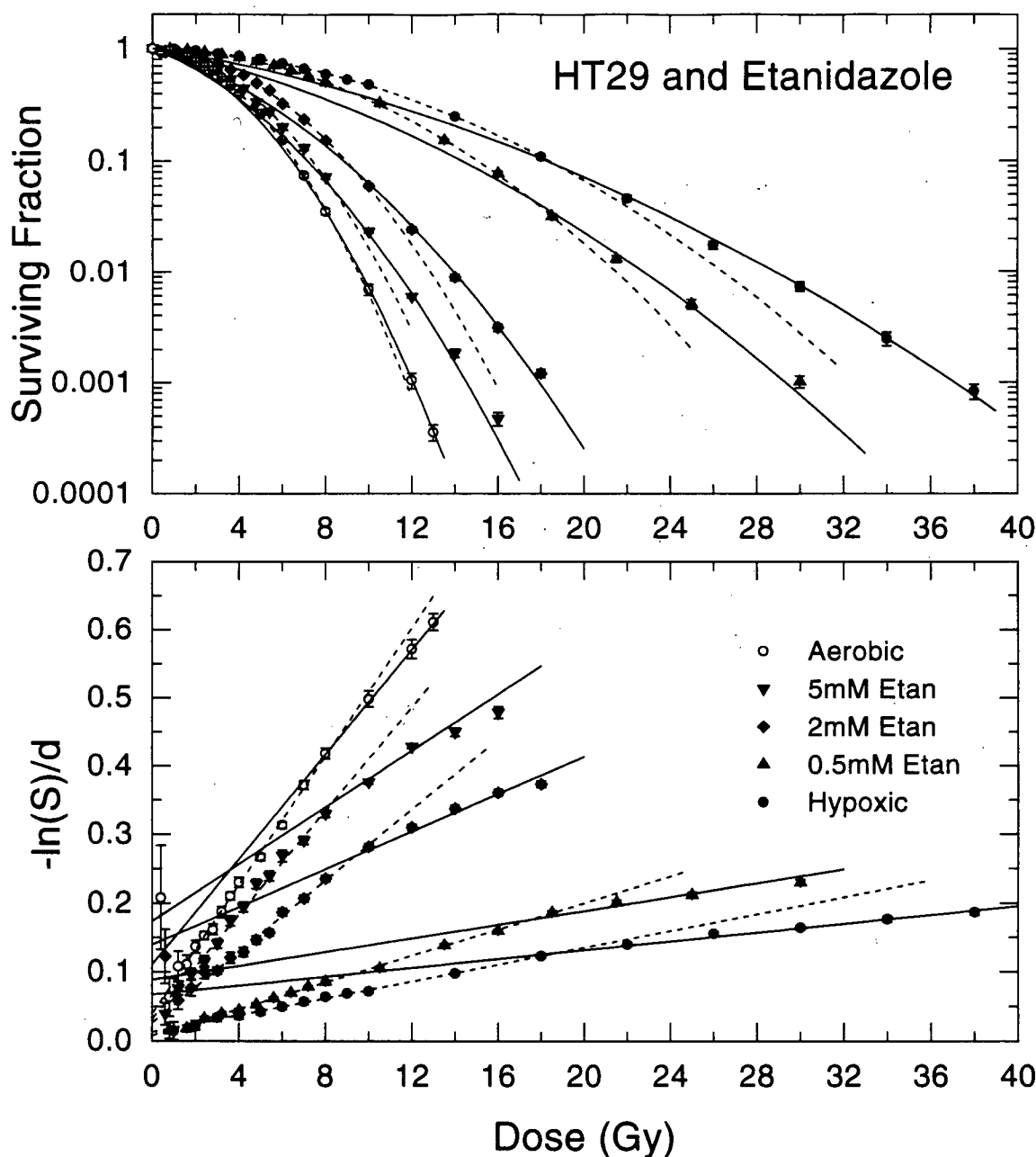
Figure 3-17 HT-144 Aerobic Radiation Response
Mean survival as a function of radiation dose in exponentially growing HT-144 cells irradiated at 37°C in suspension culture under aerobic conditions (upper frame). Cell suspensions were gassed with air for 20 minutes prior to and during irradiation. Data are the average of 3 survival responses determined using the cell sorting assay, and error bars are the standard error in the mean. The fitted lines represent the best fits of the LQ model (equation 3-4) to the mean survival data in the low dose (dashed line) and high dose (solid line) regions. Also shown are the same survival data replotted in the form -(lnS)/d (lower frame). In this plot a LQ function is a straight line with a y-intercept equal to α and a slope equal to β.

Figure 3-18 Sensitization With Etanidazole in HT-144 Cells

For comparison purposes, the data from figures 3-15 to 3-17 are replotted together. Mean survival is shown as a function of radiation dose in exponentially growing HT-144 cells irradiated at 37°C in suspension culture under various conditions. The data for hypoxic, aerobic, and hypoxic with 2 mM etanidazole are shown together (upper frame). The fitted lines represent the best fits of the LQ model (equation 3-4) to the mean survival data in the low dose (dashed line) and high dose (solid line) regions. Also shown are the same survival data replotted in the form -(lnS)/d (lower frame). In this plot a LQ function is a straight line with a y-intercept equal to α and a slope equal to β.

3.2.2.2 RB6145

A series of radiation sensitizer experiments was also carried out with RB6145. This drug is a hypoxic radiosensitizer as well as a bioreductive agent with selective toxicity for hypoxic cells. The radiation sensitizing ability of RB6145 was assessed in HT-29 cells at concentrations of 80 μM and 150 μM. Incubation with RB6145 was carried out under the same conditions as for etanidazole (1 hour at 37°C, prior to irradiation, during induction of hypoxia). In this cell line, treatment with 80 μM RB6145 under the described conditions reduced the zero dose plating efficiency to an average of 46% from approximately 75% under hypoxic conditions alone. Treatment with 150 μM RB6145 further reduced this value to an average of 20%. These values represent cyto-toxic inactivation of approximately 39% and 73% of the cells for the two concentrations.

The measured radiation survival responses of hypoxic HT-29 cells treated with 80 μM and 150 μM RB6145, corrected for this 'drug only' toxicity, are plotted in figures 3-19 and 3-20. The corresponding -ln(S)/d plots are shown in the lower frames of these figures. In figure 3-21 these responses have been plotted together with the hypoxic radiation survival response (for clarity the aerobic radiation response is not plotted). Comparison of this plot with the corresponding summary plot for etanidazole (fig. 3-8) shows substantial differences in the nature of the radiation response. With etanidazole the general shape of the survival curve remains similar to that under hypoxic and aerobic conditions. However, with RB6145, the shape of the radiation survival curve is different, exhibiting a more linear response.
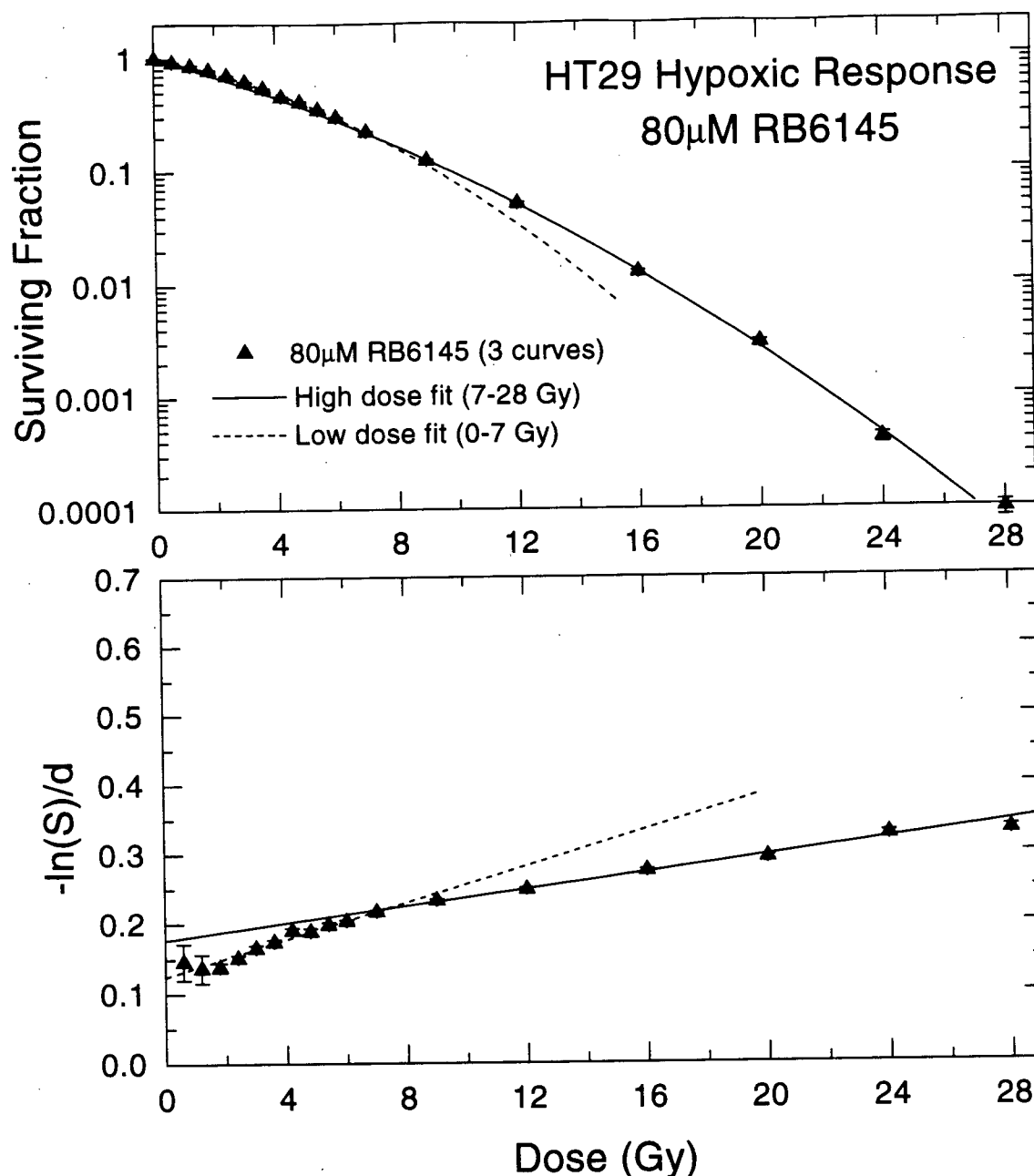
Figure 3-19 HT-29 Hypoxic Plus 80 μM RB6145 Radiation Response
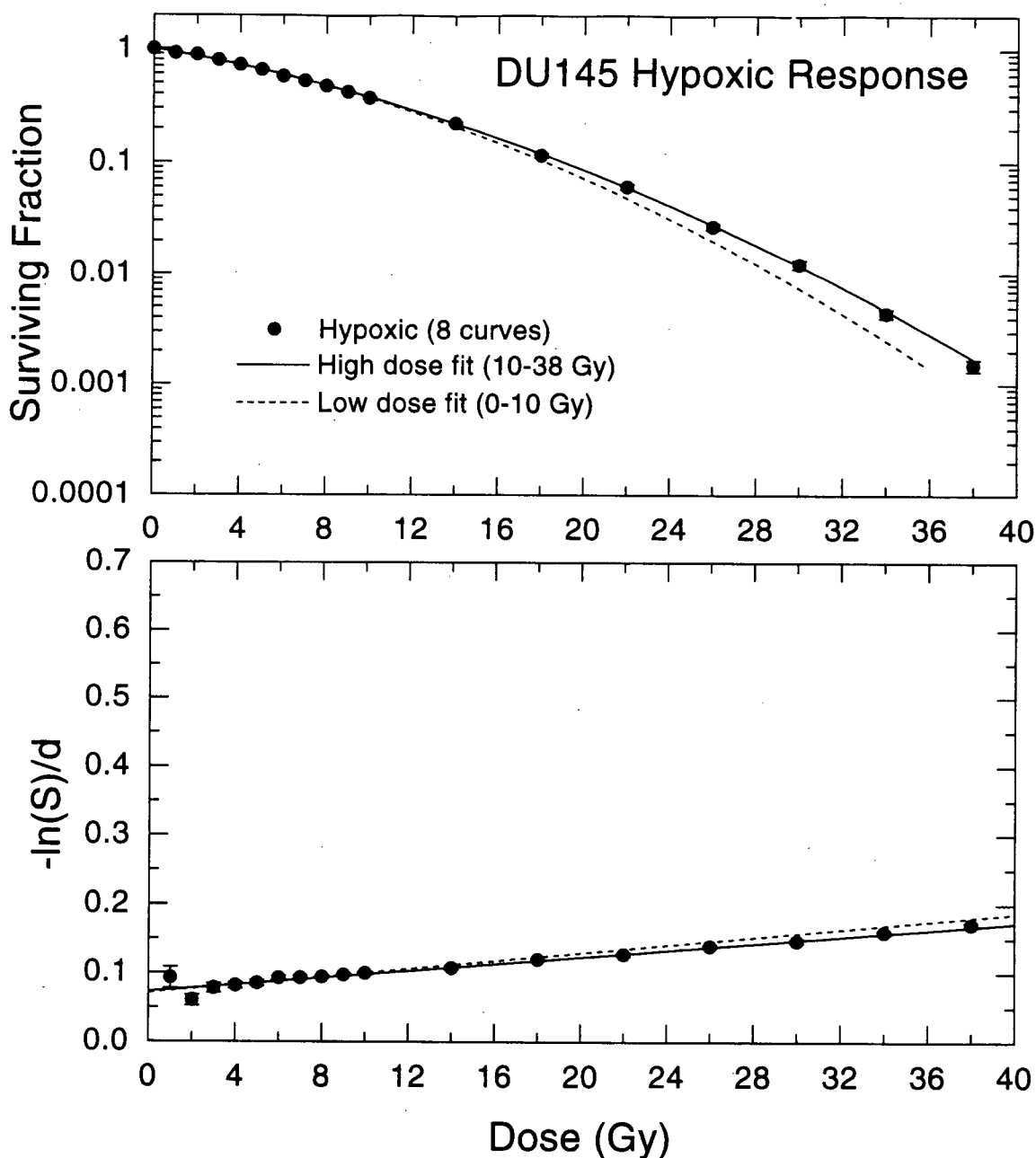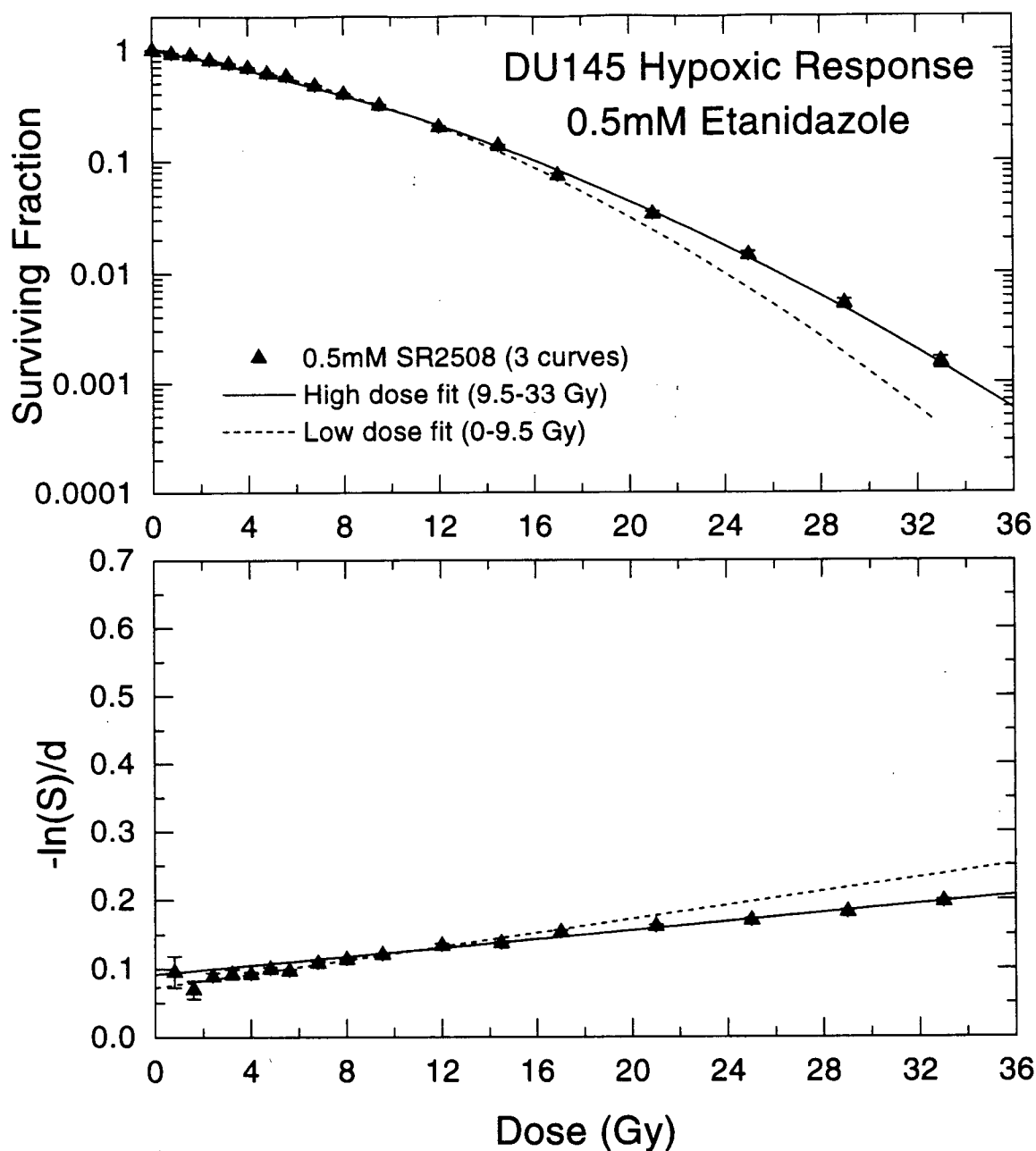Mean survival as a function of radiation dose in exponentially growing HT-29 cells irradiated at 37°C in suspension culture under hypoxic conditions with 80 μM RB6145 (upper frame). Cell suspensions were incubated for 1 hour prior to and during irradiation while hypoxic conditions were established. Data are the average of 3 survival responses determined using the cell sorting assay, and error bars are the standard error in the mean. The fitted lines represent the best fits of the LQ model (equation 3-4) to the mean survival data in the low dose (dashed line) and high dose (solid line) regions. Also shown are the same survival data replotted in the form -(lnS)/d (lower frame). In this plot a LQ function is a straight line with a y-intercept equal to α and a slope equal to β.
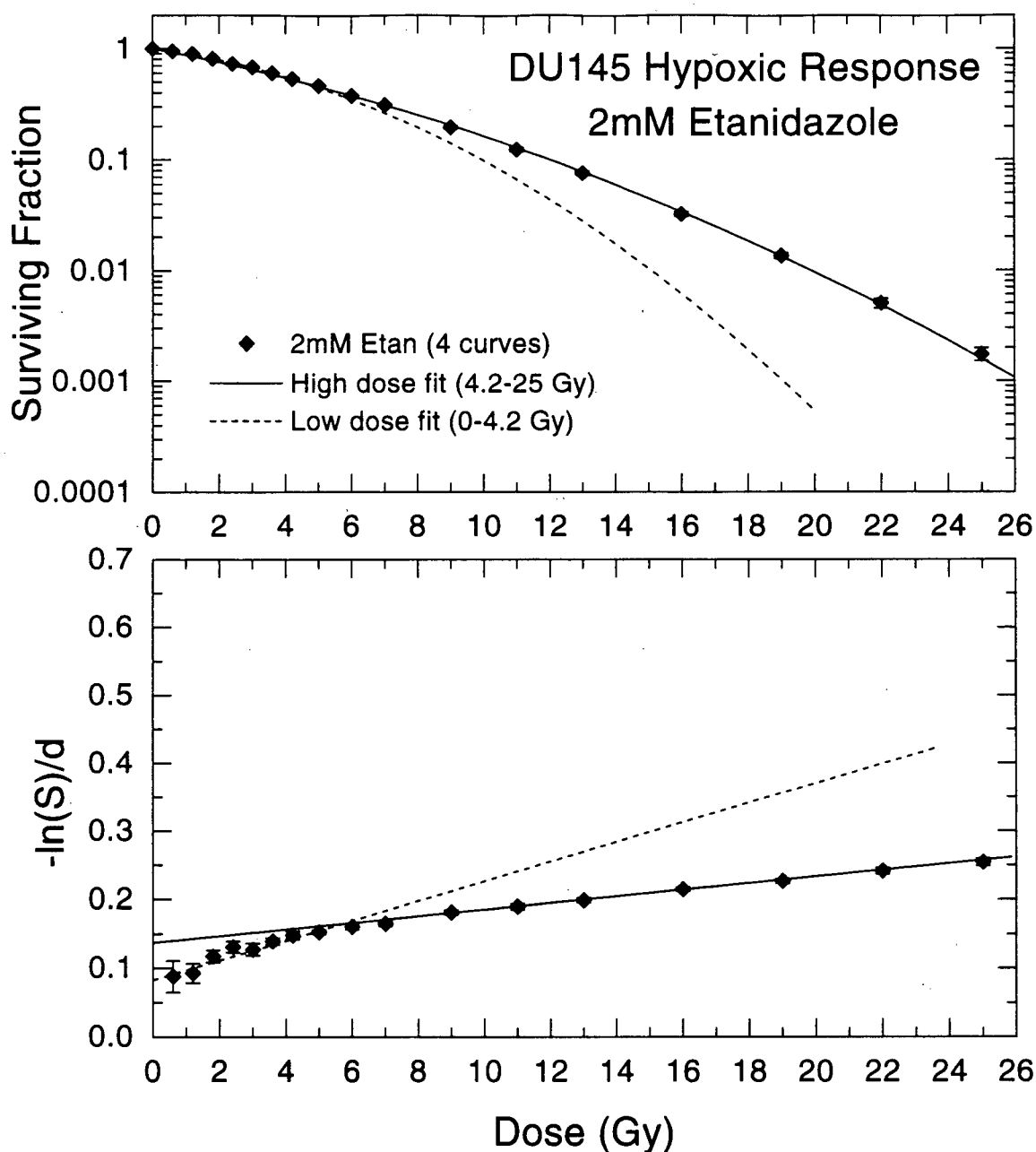
Figure 3-20 HT-29 Hypoxic Plus 150 μM RB6145 Radiation Response
Mean survival as a function of radiation dose in exponentially growing HT-29 cells irradiated at 37°C in
suspension culture under hypoxic conditions with 150 μM RB6145 (upper frame). Cell suspensions were
incubated for 1 hour prior to and during irradiation while hypoxic conditions were established. Data are the
average of 3 survival responses determined using the cell sorting assay, and error bars are the standard error
in the mean. The fitted lines represent the best fits of the LQ model (equation 3-4) to the mean survival data
in the low dose (dashed line) and high dose (solid line) regions. Also shown are the same survival data
replotted in the form -(lnS)/d (lower frame). In this plot a LQ function is a straight line with a y-intercept
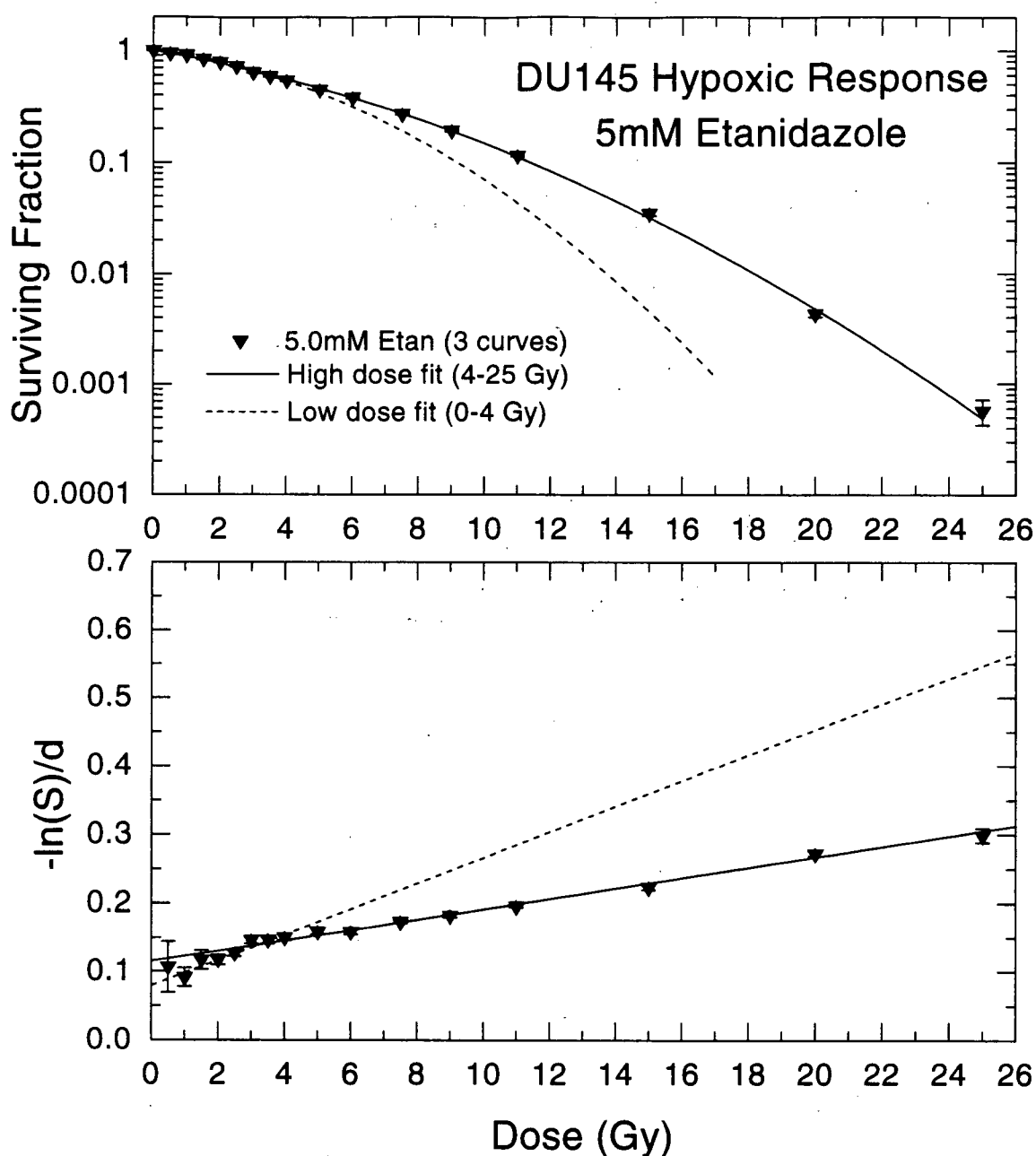equal to α and a slope equal to β.

Figure 3-21 Sensitization With RB6145 in HT-29 Cells

For comparison purposes, the data from figures 3-3, 3-19, and 3-20 are replotted together. Mean survival is shown as a function of radiation dose in exponentially growing HT-29 cells irradiated at 37°C in suspension culture under various conditions. The data for hypoxic and hypoxic with 80 μM, and 150 μM RB6145 are shown together (upper frame). The fitted lines represent the best fits of the LQ model (equation 3-4) to the mean survival data in the low dose (dashed line) and high dose (solid line) regions. Also shown are the same survival data replotted in the form -(lnS)/d (lower frame). In this plot a LQ function is a straight line with a y-intercept equal to α and a slope equal to β.
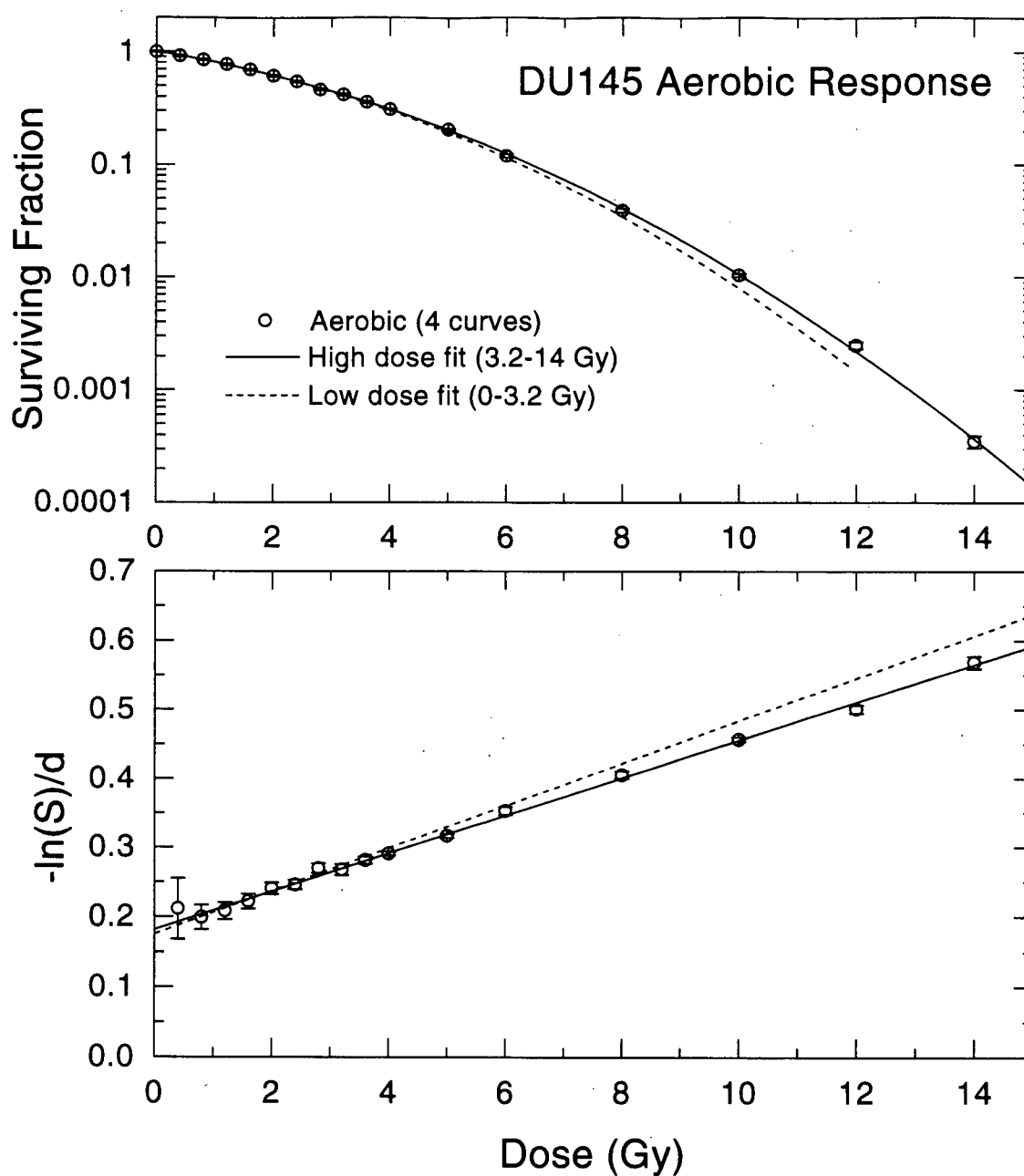
The radiation responses of hypoxic DU145 cells treated with 80 μM and 150 μM RB6145 are plotted in figures 3-22, and 3-23 respectively. In this cell line, treatment with RB6145 alone resulted in only a small reduction in the plating efficiency as compared to HT-29 cells, being toxic to only 10-25% of the cells for either concentration under these experimental conditions. For reference the data are plotted together with the aerobic and hypoxic responses in figure 3-24.

The sensitizing ability of RB6145 was also evaluated in HT-144 cells. The radiation response of asynchronously growing hypoxic cells treated with 80 μM RB6145 under identical conditions to that for etanidazole was determined, and is plotted in figure 3-25. Treatment with 80 μM RB6145 in this cell line resulted in the highest level of toxicity (lowest plating efficiency) of the three cell lines investigated, killing 80-85% of these cells. For reference these data have again been plotted together with the hypoxic and aerobic responses in figure 3-26.
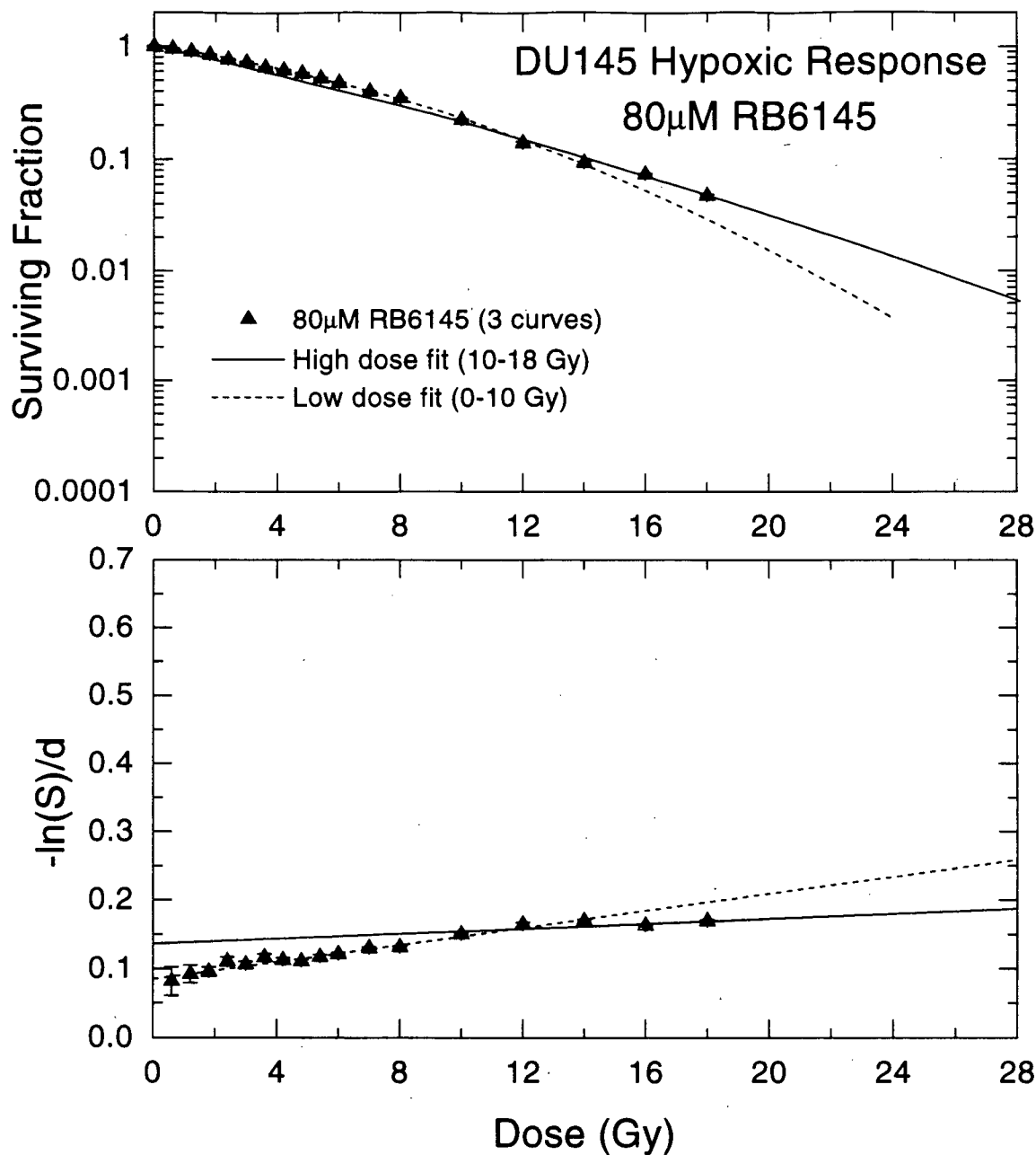
Figure 3-22 DU145 Hypoxic Plus 80 μM RB6145 Radiation Response
Mean survival as a function of radiation dose in exponentially growing DU145 cells irradiated at 37°C in suspension culture under hypoxic conditions with 80 μM RB6145 (upper frame). Cell suspensions were incubated for 1 hour prior to and during irradiation while hypoxic conditions were established. Data are the average of 3 survival responses determined using the cell sorting assay, and error bars are the standard error in the mean. The fitted lines represent the best fits of the LQ model (equation 3-4) to the mean survival data in the low dose (dashed line) and high dose (solid line) regions. Also shown are the same survival data replotted in the form -(lnS)/d (lower frame). In this plot a LQ function is a straight line with a y-intercept equal to α and a slope equal to β.
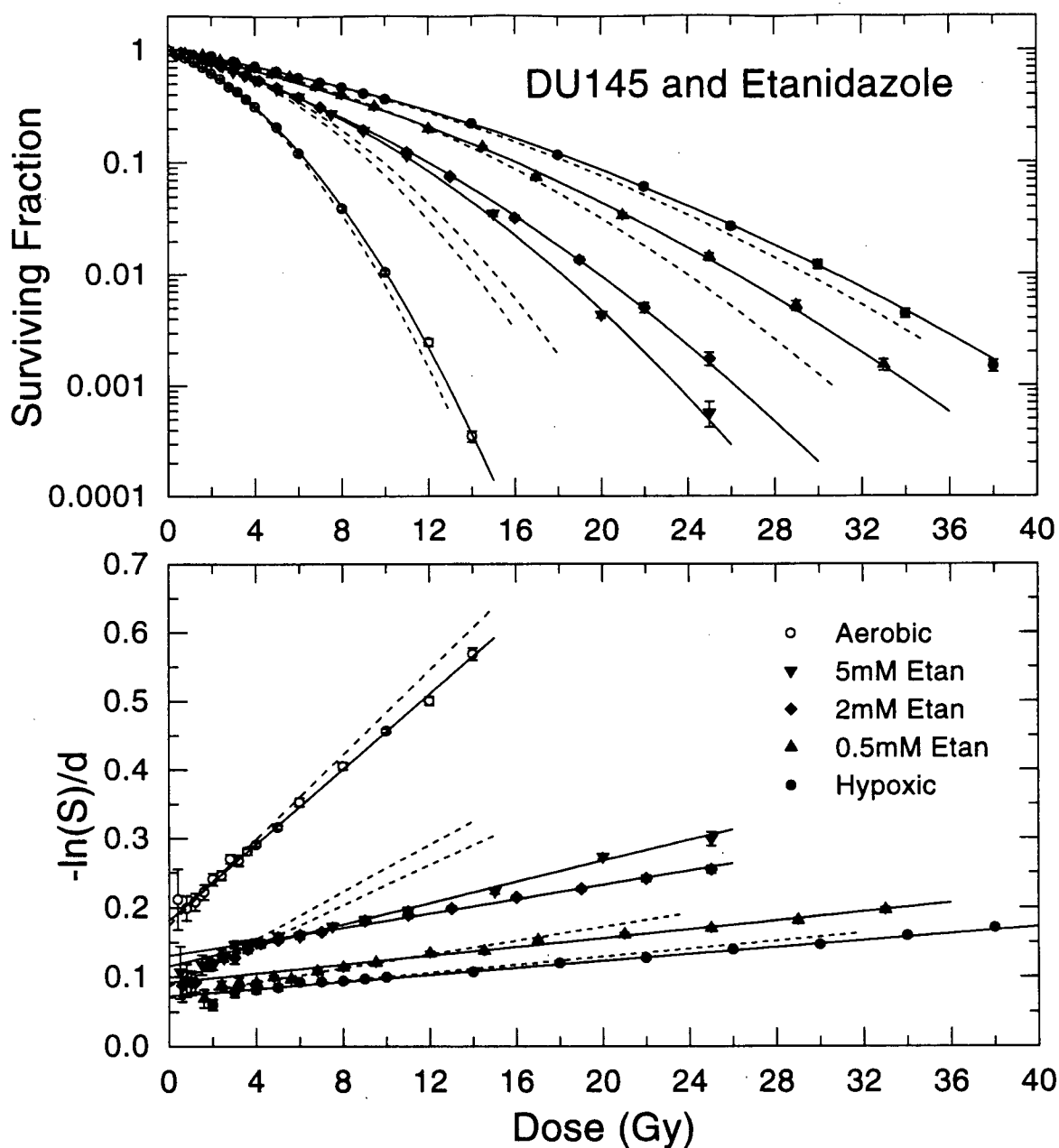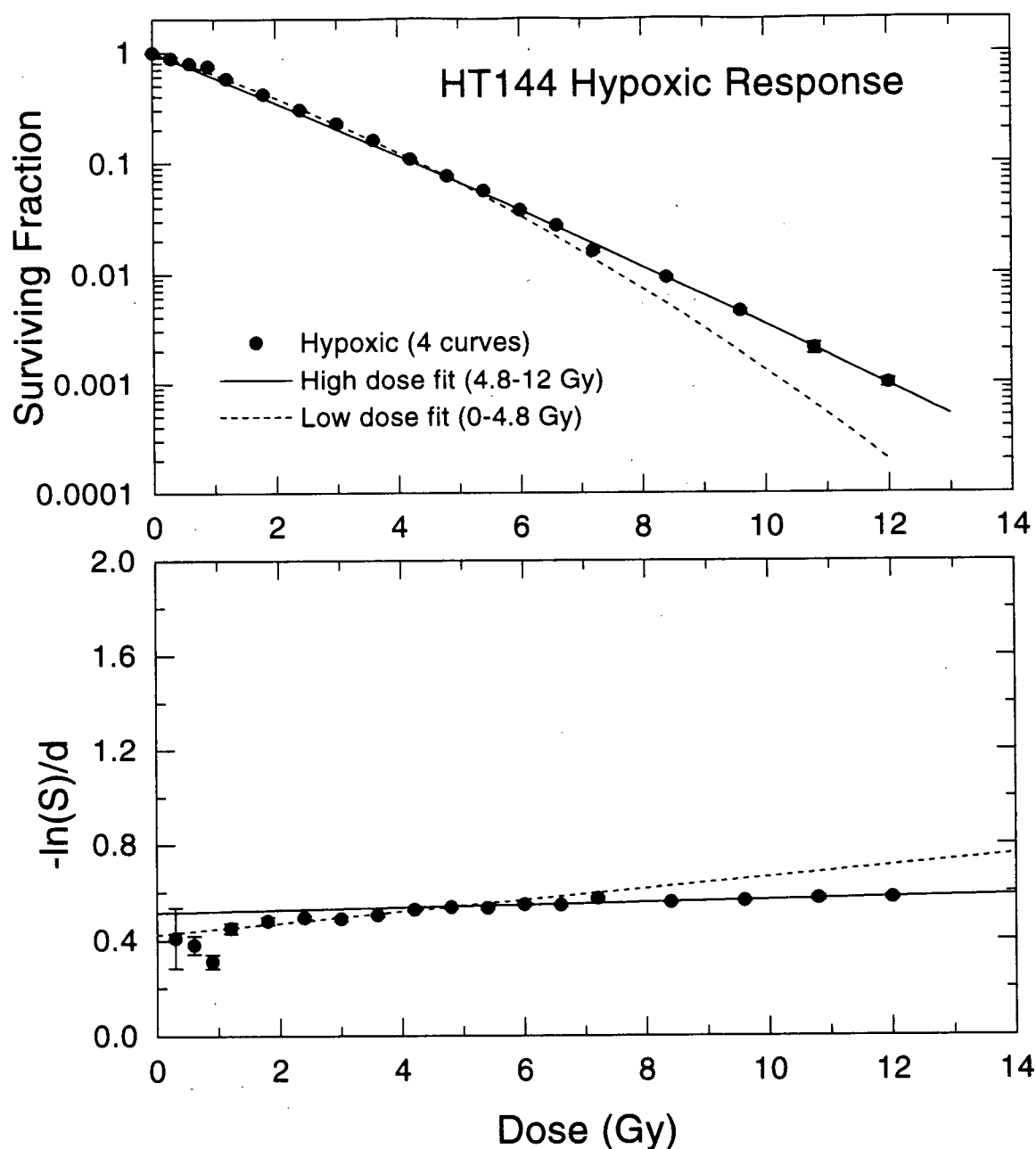
Figure 3-23 DU145 Hypoxic Plus 150 μM RB6145 Radiation Response
Mean survival as a function of radiation dose in exponentially growing DU145 cells irradiated at 37°C in suspension culture under hypoxic conditions with 150 μM RB6145 (upper frame). Cell suspensions were incubated for 1 hour prior to and during irradiation while hypoxic conditions were established. Data are the average of 3 survival responses determined using the cell sorting assay, and error bars are the standard error in the mean. The fitted lines represent the best fits of the LQ model (equation 3-4) to the mean survival data in the low dose (dashed line) and high dose (solid line) regions. Also shown are the same survival data replotted in the form -(lnS)/d (lower frame). In this plot a LQ function is a straight line with a y-intercept equal to α and a slope equal to β.

Figure 3-24 Sensitization With RB6145 in DU145 Cells

For comparison purposes, the data from figures 3-9, 3-13, 3-22, and 3-23 are replotted together. Mean survival is shown as a function of radiation dose in exponentially growing HT-29 cells irradiated at 37°C in suspension culture under various conditions. The data for hypoxic, aerobic, and hypoxic with 80 µM, and 150 µM RB6145 are shown together (upper frame). The fitted lines represent the best fits of the LQ model (equation 3-4) to the mean survival data in the low dose (dashed line) and high dose (solid line) regions. Also shown are the same survival data replotted in the form -(lnS)/d (lower frame). In this plot a LQ function is a straight line with a y-intercept equal to α and a slope equal to β.
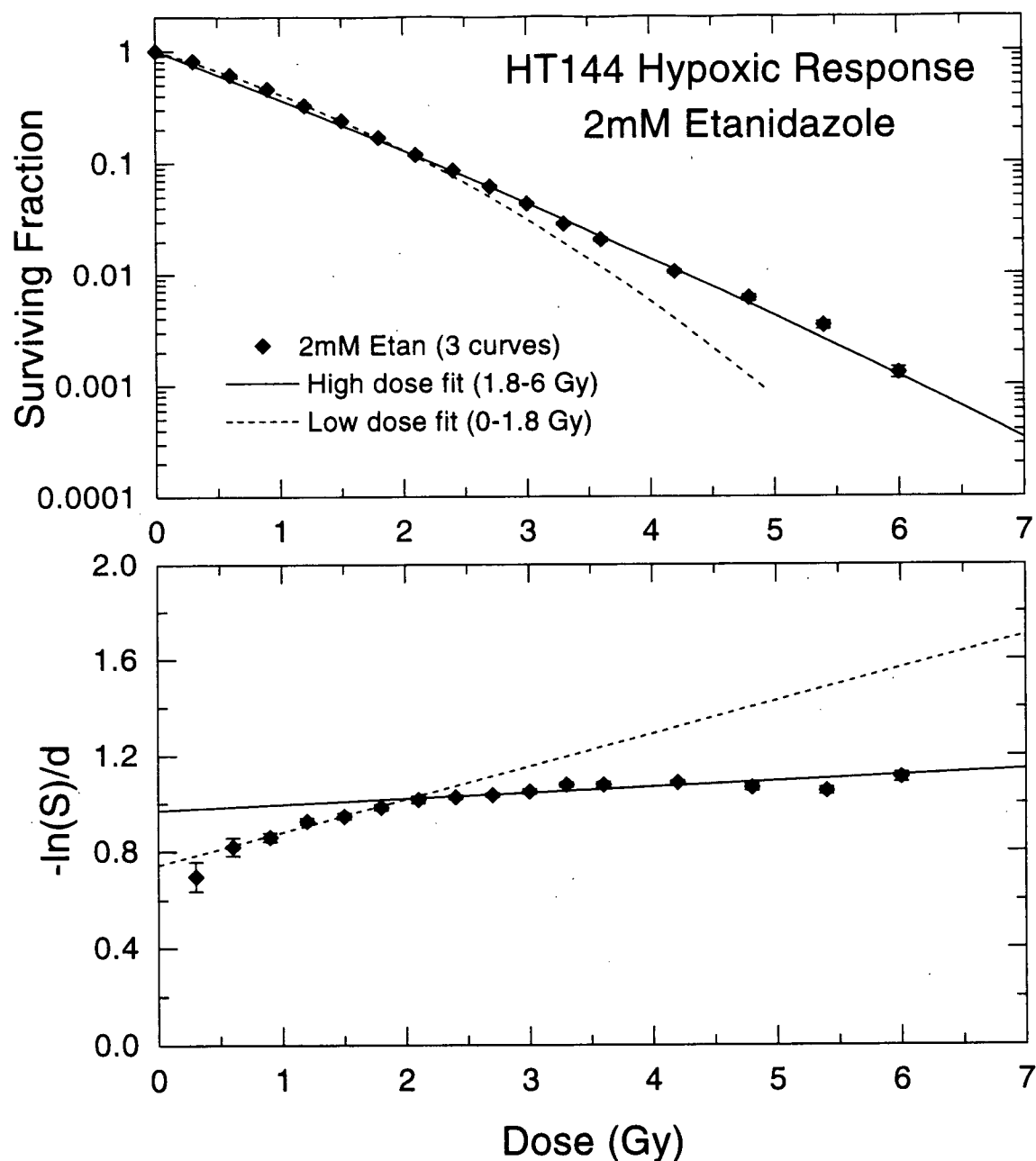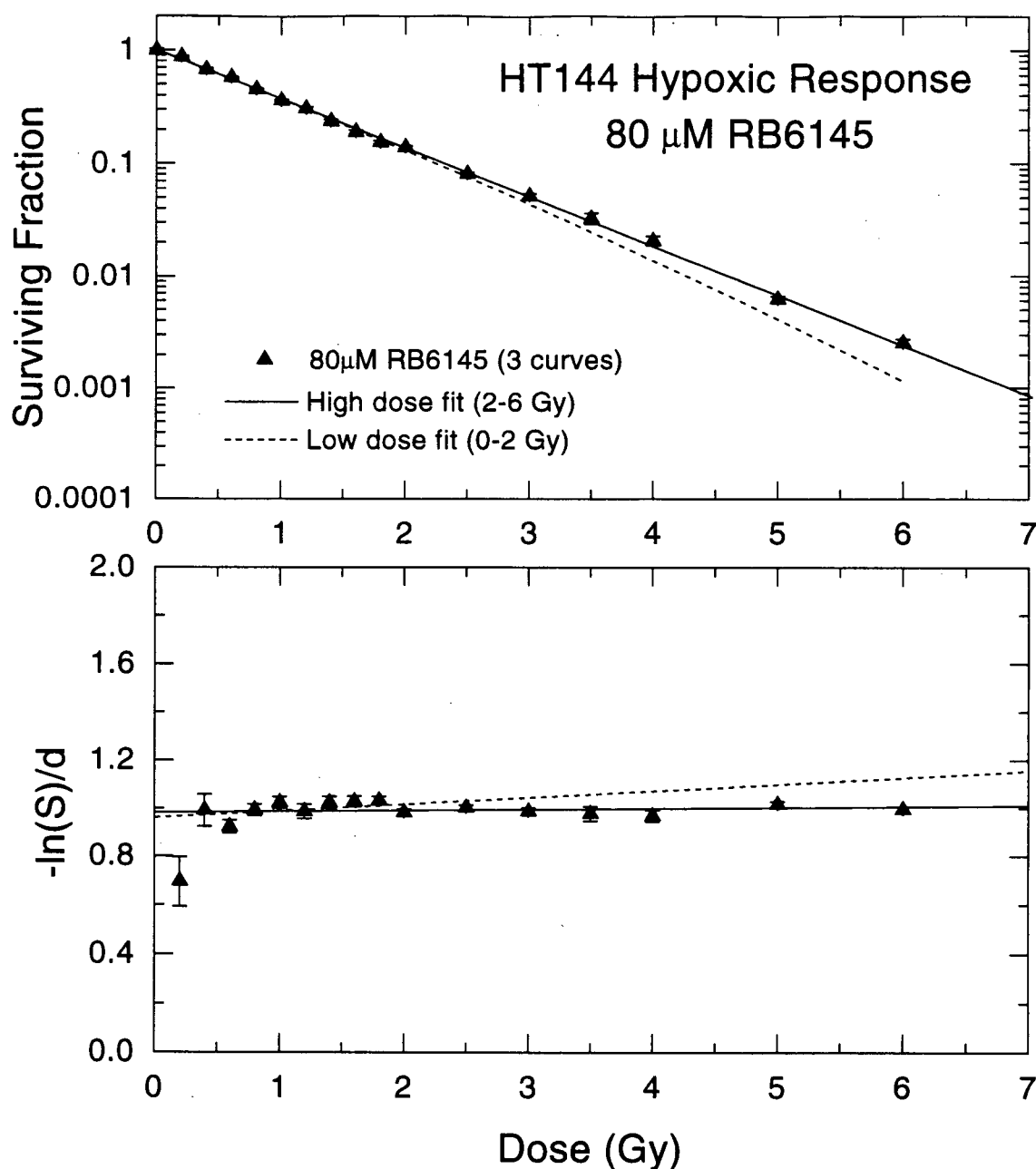
Figure 3-25 HT-144 Hypoxic Plus 80 μM RB6145 Radiation Response
Mean survival as a function of radiation dose in exponentially growing HT-144 cells irradiated at 37°C in suspension culture under hypoxic conditions with 80 μM RB6145 (upper frame). Cell suspensions were incubated for 1 hour prior to and during irradiation while hypoxic conditions were established. Data are the average of 3 survival responses determined using the cell sorting assay, and error bars are the standard error in the mean. The fitted lines represent the best fits of the LQ model (equation 3-4) to the mean survival data in the low dose (dashed line) and high dose (solid line) regions. Also shown are the same survival data replotted in the form -(lnS)/d (lower frame). In this plot a LQ function is a straight line with a y-intercept equal to α and a slope equal to β.

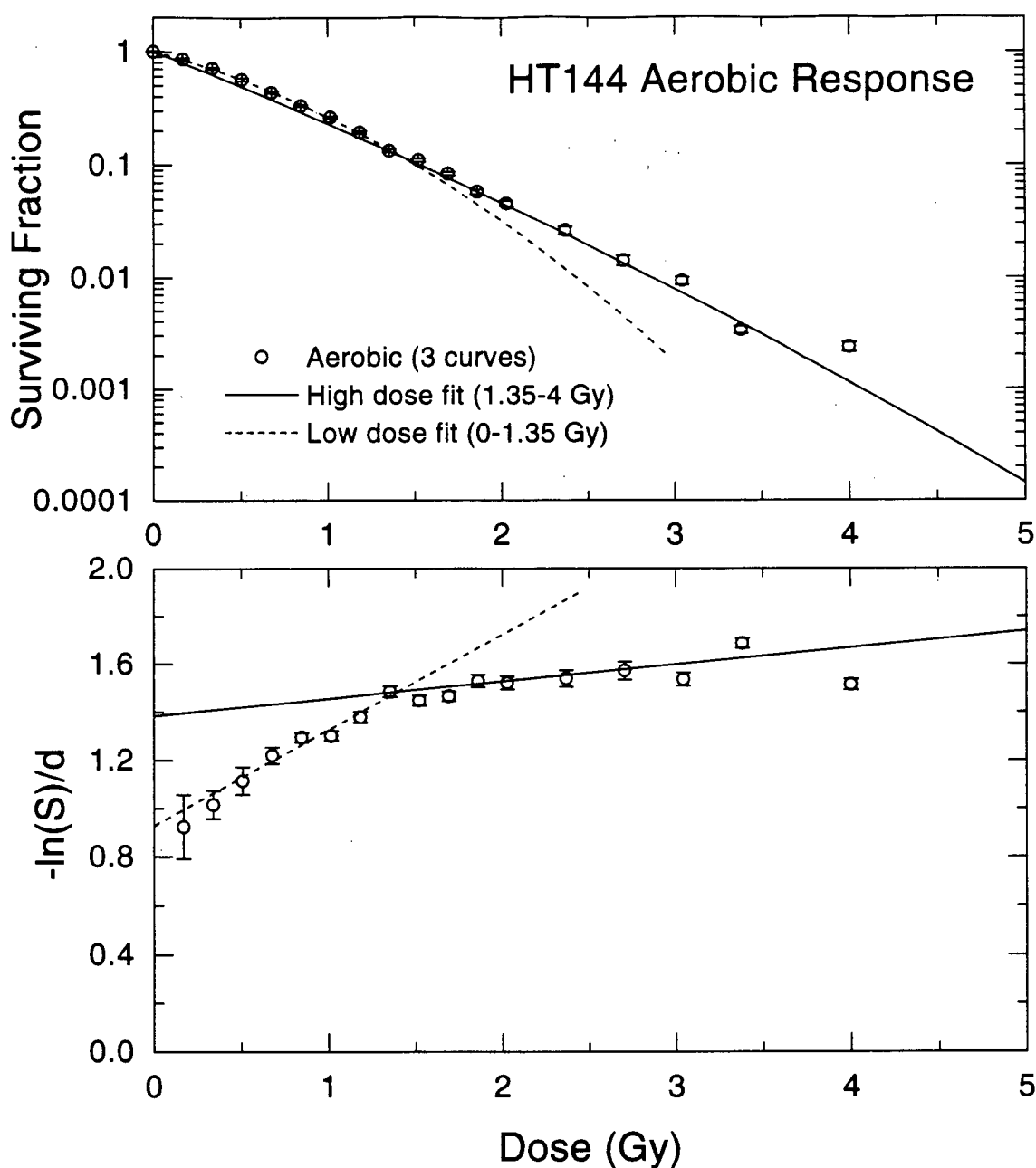**Figure 3-26 Sensitization With RB6145 in HT-144 Cells**

For comparison purposes, the data from figures 3-15, 3-17, and 3-25 are replotted together. Mean survival is shown as a function of radiation dose in exponentially growing HT-144 cells irradiated at 37°C in suspension culture under various conditions. The data for hypoxic, aerobic, and hypoxic with 80 RB6145 are shown together (upper frame). The fitted lines represent the best fits of the LQ model (equation 3-4) to the mean survival data in the low dose (dashed line) and high dose (solid line) regions. Also shown are the same survival data replotted in the form -(lnS)/d (lower frame). In this plot a LQ function is a straight line with a y-intercept equal to α and a slope equal to β.
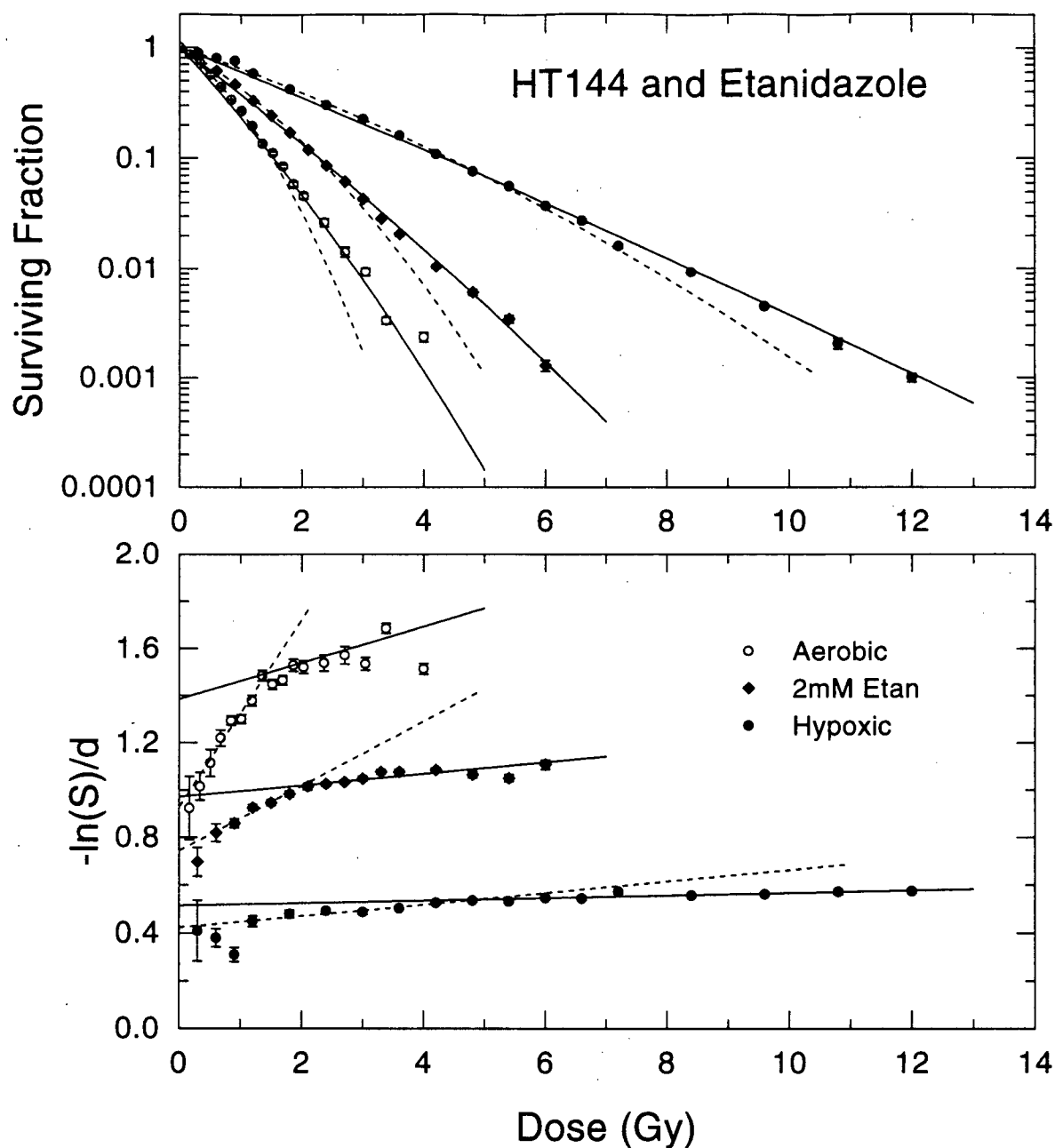
3.2.3 Modeling

An extensive effort has been made to model the observed radiation responses in an attempt to understand the mechanisms of sensitization by these two hypoxic radiosensitizers in different human tumour cell lines. As previously mentioned, the radiation response for each of the three cell lines is generally poorly described by a single LQ fit to the full dose range of data. This is most easily observable in the -ln(S)/d plots shown in figures 3-3 to 3-26. If the radiation response followed that of a LQ function, then the data points should follow a straight line on this type of plot. All of the radiation responses show some degree of substructure, which is manifested as a decreasing effectiveness per unit dose (with increasing dose) as compared to that which would be predicted from a straight line extrapolation of the low dose data. It has been previously shown that all three of these cell lines exhibit varying degrees of substructure at low dose under aerobic conditions, which has been attributed to cell-cycle variations in radiosensitivity (Skarsgard *et al.* 1995). This hypothesis suggests that the substructure results from selective elimination of sensitive cells at low doses, leaving a population enriched with resistant cells at higher doses. It was shown that because of this substructure, fits with the LQ model over the complete dose range (2-4 logs of inactivation) were inadequate, and that superior fits were possible if the data at low and high doses were modeled separately (Skarsgard *et al.* 1991, 1992, 1993, 1994a, 1995, Skwarchuk *et al.* 1993). Thus, for each cell line under investigation here, the radiation response has been characterized with LQ fits to both the low and high dose regions. Fits were made to the mean survival data, with each point weighted by the measured variance

in that data point, which in all cases was larger than the statistical variance associated with the binomial distribution inherent in this assay (see appendix 8.1 and section 4.2.2). The division between low and high dose regions was made by fitting the low dose data to an increasing dose range until a point was reached where the LQ fit produced significantly different values for the α and β parameters. In each figure, the dashed line represents the best fit to the low dose region data (determined by this procedure), and the solid line represents the best fit to the remaining high dose data. These separate fits provided an accurate description of the survival data for all 3 cell lines, and for all irradiation conditions. Tables 3-1, 3-2, and 3-3 list the best-fit α and β parameters for HT-29, DU145, and HT-144 cell lines, respectively. Parameter values are given for both the low and high dose fits, for all experimental conditions, as well as the 95% confidence limit in each parameter. The α/β ratio, and the surviving fraction calculated at 2 and 8 Gy are also shown.

3.2.4 Sensitizer Enhancement Ratio (SER)

The sensitizer enhancement ratio (SER) can be defined as the ratio of radiation doses between hypoxic (d_h) and sensitizer treated (d_s) populations that produce the same level of cell survival:

$$SER = \frac{d_h}{d_s} \qquad\qquad \text{Equation 3-6}$$

Evaluation of the SER as a function of cell survival requires a function that describes the measured survival at all radiation doses. Because of the substructure present in these

Table 3-1 HT-29 Best-Fit Parameter Values in the LQ Model

The LQ model (equation 3-4) was fit to the mean HT-29 survival data for each different irradiation condition using a non-linear χ^2 minimization routine. Uncertainty values are the 95% confidence limits in the quoted values. For each condition, the α/β ratio and the surviving fractions calculated at radiation doses of 2 and 8 Gy are also given.

Experimental Condition	Dose Range	α Gy^{-1}	β Gy^{-2}	α/β Gy	SF_2 %	SF_8 %
Hypoxic	Low (0-18)	$0.0131 \pm .0020$	$0.0061 \pm .0002$	2.1	95	61
	High (18-38)	$0.0675 \pm .0025$	$0.0032 \pm .0001$	21.1		
Aerobic	Low (0-4)	$0.0392 \pm .00418$	$0.0465 \pm .00091$	0.8	77	4
	High (4-13)	$0.1107 \pm .0110$	$0.0383 \pm .0011$	2.9		
Hypoxic+0.5mM Etan	Low (0-16)	$0.0081 \pm .0013$	$0.0096 \pm .0002$	0.8	95	51
	High (16-30)	$0.0887 \pm .0029$	$0.0050 \pm .0002$	17.7		
Hypoxic+2mM Etan	Low (0-8)	$0.0265 \pm .0037$	$0.0258 \pm .0007$	1.0	86	16
	High (8-18)	$0.1396 \pm .0038$	$0.0137 \pm .0003$	10.2		
Hypoxic+5mM Etan	Low (0-8)	$0.0322 \pm .0042$	$0.0378 \pm .0008$	0.9	81	7
	High (8-18)	$0.1740 \pm .0030$	$0.0207 \pm .0003$	8.4		
Hypoxic+80μM RB6145	Low (0-7)	$0.1251 \pm .0022$	$0.0131 \pm .0004$	9.5	74	
	High (7-28)	$0.1769 \pm .0022$	$0.0060 \pm .0002$	29.5		17
Hypoxic+150μM RB6145	Low (0-6)	$0.2765 \pm .0053$	$0.0167 \pm .0014$	16.6	54	
	High (6-18)	$0.3321 \pm .0056$	$0.0041 \pm .0005$	81.0		5

Table 3-2 DU145 Best-Fit Parameter Values in the LQ Model

The LQ model (equation 3-4) was fitted to the mean DU145 survival data for each different irradiation condition using a non-linear χ^2 minimization routine. Uncertainty values are the 95% confidence limits in the quoted values. For each condition, the α/β ratio and the surviving fractions calculated at radiation doses of 2 and 8 Gy are also given.

Experimental Condition	Dose Range	α Gy^{-1}	β Gy^{-2}	α/β Gy	SF$_2$ %	SF$_8$ %
Hypoxic	Low (0-10)	0.0710 ±.0018	0.0029 ±.0003	24.5	86	47
	High (10-38)	0.0728 ±.0017	0.0025 ±.0001	29.1		
Aerobic	Low (0-3.2)	0.1755 ±.0066	0.0308 ±.0028	5.7	62	
	High(3.2-14)	0.1816 ±.0029	0.0274 ±.0004	6.6		4
Hypoxic+0.5mM Etan	Low (0-9.5)	0.0724 ±.0017	0.0050 ±.0003	14.57	85	41
	High(9.5-33)	0.0920 ±.0017	0.0032 ±.0001	28.8		
Hypoxic+2mM Etan	Low (0-4.2)	0.0883 ±.0058	0.0144 ±.0018	6.1	79	
	High(4.2-25)	0.1304 ±.0022	0.0051 ±.0002	25.6		25
Hypoxic+5mM Etan	Low (0-4)	0.0866 ±.0046	0.0170 ±.0015	5.1	79	
	High (4-25)	0.1153 ±.0020	0.0076 ±.0002	15.2		24
Hypoxic+80μM RB6145	Low (0-10)	0.0851 ±.0016	0.0062 ±.0003	13.7	82	34
	High (10-18)	0.1366 ±.0015	0.0018 ±.0001	75.9		
Hypoxic+150μM RB6145	Low (0-7.5)	0.0944 ±.0043	0.0084 ±.0009	11.2	80	
	High (7.5-	0.1304 ±.0021	0.0038 ±.0001	34.3		28

Table 3-3 HT-144 Best-Fit Parameter Values in the LQ Model

The LQ model (equation 3-4) was fitted to the mean HT-144 survival data for each different irradiation condition using a non-linear χ^2 minimization routine. Uncertainty values are the 95% confidence limits in the quoted values. For each condition, the α/β ratio and the surviving fractions calculated at radiation doses of 2 and 8 Gy are also given.

Experimental Condition	Dose Range	α Gy^{-1}	β Gy^{-2}	α/β Gy	SF$_2$ %	SF$_8$ %
Hypoxic	Low (0-4.8)	0.4245 ±.0063	0.0238 ±.0016	17.8	39	
	High(4.8-12)	0.5155 ±.0051	0.0052 ±.0005	99.1		1.2
Aerobic	Low(0-1.35)	0.9290 ±.0191	0.3972 ±.0185	2.3		
	High(1.35-4)	1.3585 ±.0173	0.0772 ±.0066	17.6	5	
Hypoxic+2mM Etan	Low (0-1.8)	0.7435 ±.0133	0.1370 ±.0093	5.4	13	
	High (1.8-6)	0.9711 ±.0097	0.0019 ±.0016	510		.04
Hypoxic+80μM RB6145	Low (0-2)	0.9604 ±.0152	0.0278 ±.0097	34.5	13	
	High (2-6)	0.9825 ±.0117	0.0039 ±.0025	252		.03

radiation responses, a LQ fit to the full dose range will not predict accurate survival values at all radiation doses. At high survival levels, the low dose LQ fit can be used, however at high doses this function will fail to predict the measured survival values. Similarly, parameters derived from fits to the high dose would give accurate SER values at high dose, but would fail at low dose. In order to model the complete dose response with a single function, the radiation survival responses for each cell line and each sensitizer concentration were fitted with a two population model:

$$S = f \cdot e^{-\alpha_s D - \beta_s D^2} + (1 - f) \cdot e^{-\alpha_r D - \beta_r D^2} \qquad \text{Equation 3-7}$$

In this model a fraction (f) of the cell population is characterized by the parameters α_s and β_s, while the remainder of the population ($1-f$) is characterized by α_r and β_r. Figure 3-27, 3-28, and 3-29 show the radiation survival data fitted with this model for HT-29, DU145, and HT-144 cells respectively. These plots illustrate the ability of this model to accurately characterize the measured survival response for the entire cell population throughout the entire dose range. The fitted parameters for each cell line are given in table 3-4. The parameters determined from these fits were used for calculating the SER as a function of survival for each sensitizer, and for oxygen. The resulting SER and OER values are plotted in the lower frames of figures 3-30, 3-31, and 3-32.

Table 3-4 Best-Fit Parameter Values in the Two Population Model

The two population model (equation 3-7) was fitted to the mean survival data for each cell line and each different irradiation condition using a non-linear χ^2 minimization routine. In this model a fraction (f) of the cell population is characterized by the parameters α_s and β_s, while the remainder of the population $(1-f)$ is characterized by α_r and β_r. The parameter values are not unique, but do accurately describe the entire dose response for each cell line and each condition.

Cell Line and Condition	α_s (Gy^{-1})	α_r (Gy^{-1})	β_s (Gy^{-2})	β_r (Gy^{-2})	f
HT-29 Hypoxic	0.0125	0	0.00689	0.00338	0.887
HT-29 Aerobic	0	0.0940	0.0534	0.03648	0.564
HT-29 Hypoxic + 0.5 mM Etan	0	0.0555	0.0109	0.00337	0.890
HT-29 Hypoxic + 2 mM Etan	0.0186	0.0525	0.0291	0.0116	0.873
HT-29 Hypoxic + 5 mM Etan	0.0295	0.0159	0.0421	0.0206	0.891
HT-29 Hypoxic + 80 μM RB6145	0.144	0.00157	0.0190	0.0103	0.826
HT-29 Hypoxic + 150 μM RB6145	0.307	0.0307	0.0282	0.0150	0.869
DU145 Hypoxic	0.117	0.0221	0.00657	0.00347	0.487
DU145 Aerobic	0.174	0.193	0.0263	0.0314	0.661
DU145 Hypoxic + 0.5 mM Etan	0.0847	0.0587	0.00864	0.00358	0.438
DU145 Hypoxic + 2 mM Etan	0.0928	0.0692	0.0378	0.00684	0.388
DU145 Hypoxic + 5 mM Etan	0.133	0.0584	0.0658	0.00981	0.272
DU145 Hypoxic + 80 μM RB6145	0.0741	0.0834	0.0119	0.00223	0.584
DU145 Hypoxic + 150 μM	0.0922	0.122	0.00851	0.00262	0.636
HT-144 Hypoxic	0.425	0.379	0.0547	0.0107	0.555
HT-144 Aerobic	0.849	1.066	0.658	0.102	0.500
HT-144 Hypoxic + 2 mM Etan	0.791	0.652	0.204	0.0412	0.674
HT-144 Hypoxic + 80 μM RB6145	1.02	0.724	0.588	0.0367	0.379
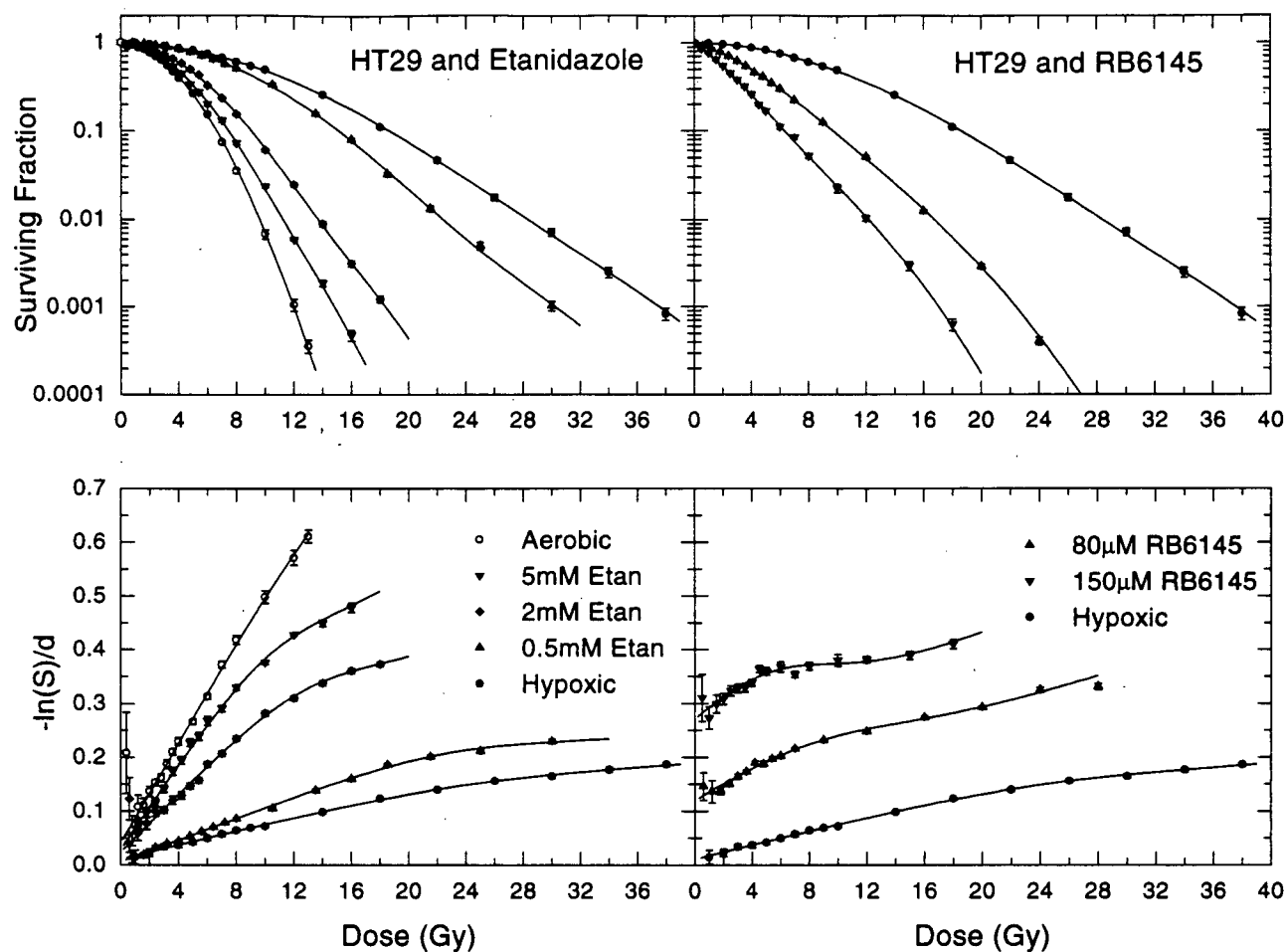
Figure 3-27 HT-29 Two Population Fits

Survival data obtained in HT-29 cells under aerobic and hypoxic conditions with etanidazole (left 2 panels) or RB6145 (right 2 panels) are replotted with the best fits of the two population model (equation 3-7). The data are plotted in both survival (upper frames) and -(lnS)/d (lower frames) forms as a function of radiation dose. The two population model is able to accurately describe the response throughout the entire dose range, though fits are not unique.
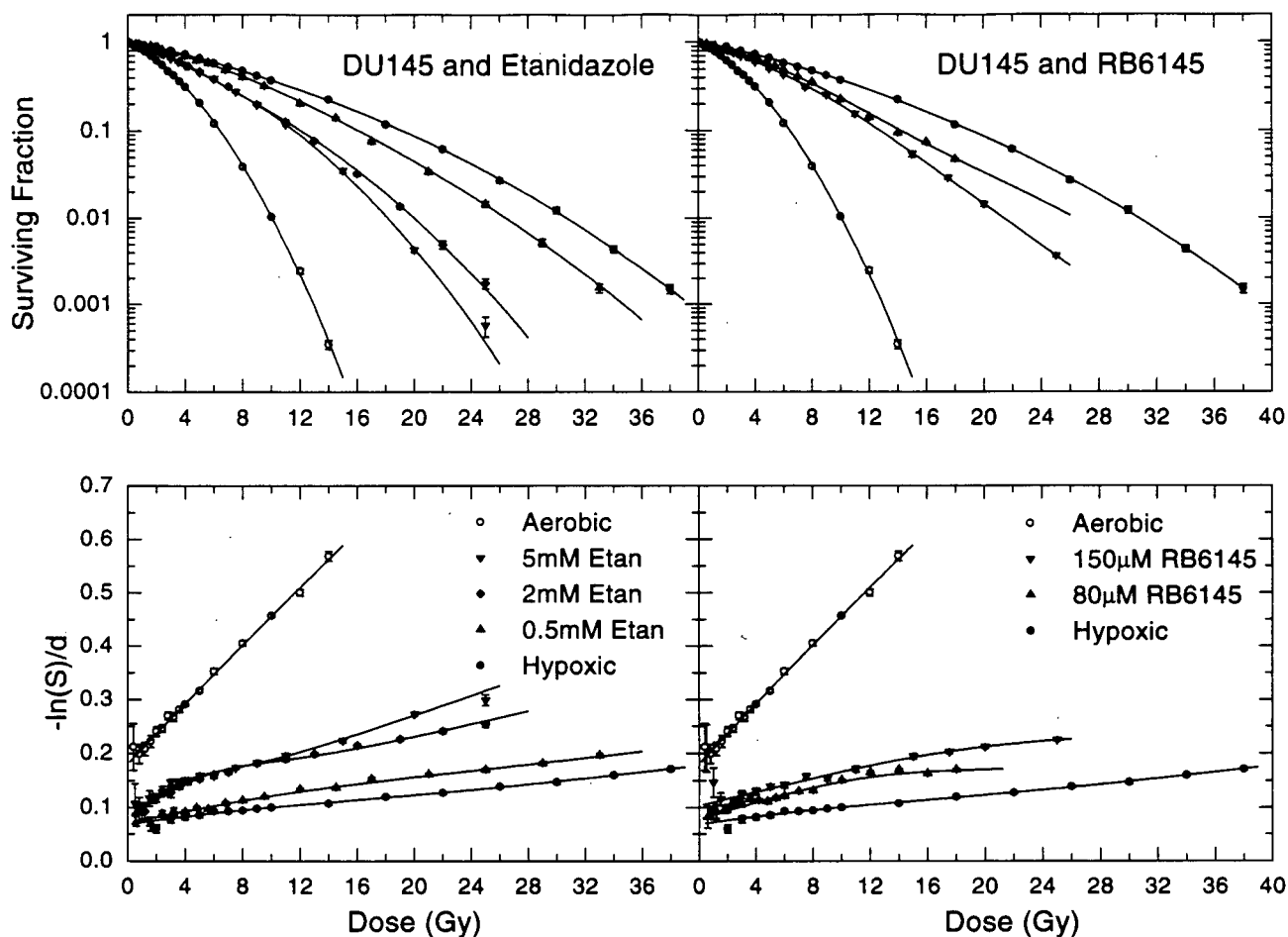
Figure 3-28 DU145 Two Population Fits
Survival data obtained in HT-29 cells under aerobic and hypoxic conditions with etanidazole (left 2 panels) or RB6145 (right 2 panels) are replotted with the best fits of the two population model (equation 3-7). The data are plotted in both survival (upper frames) and -(lnS)/d (lower frames) forms as a function of radiation dose. The two population model is able to accurately describe the response throughout the entire dose range, though fits are not unique.
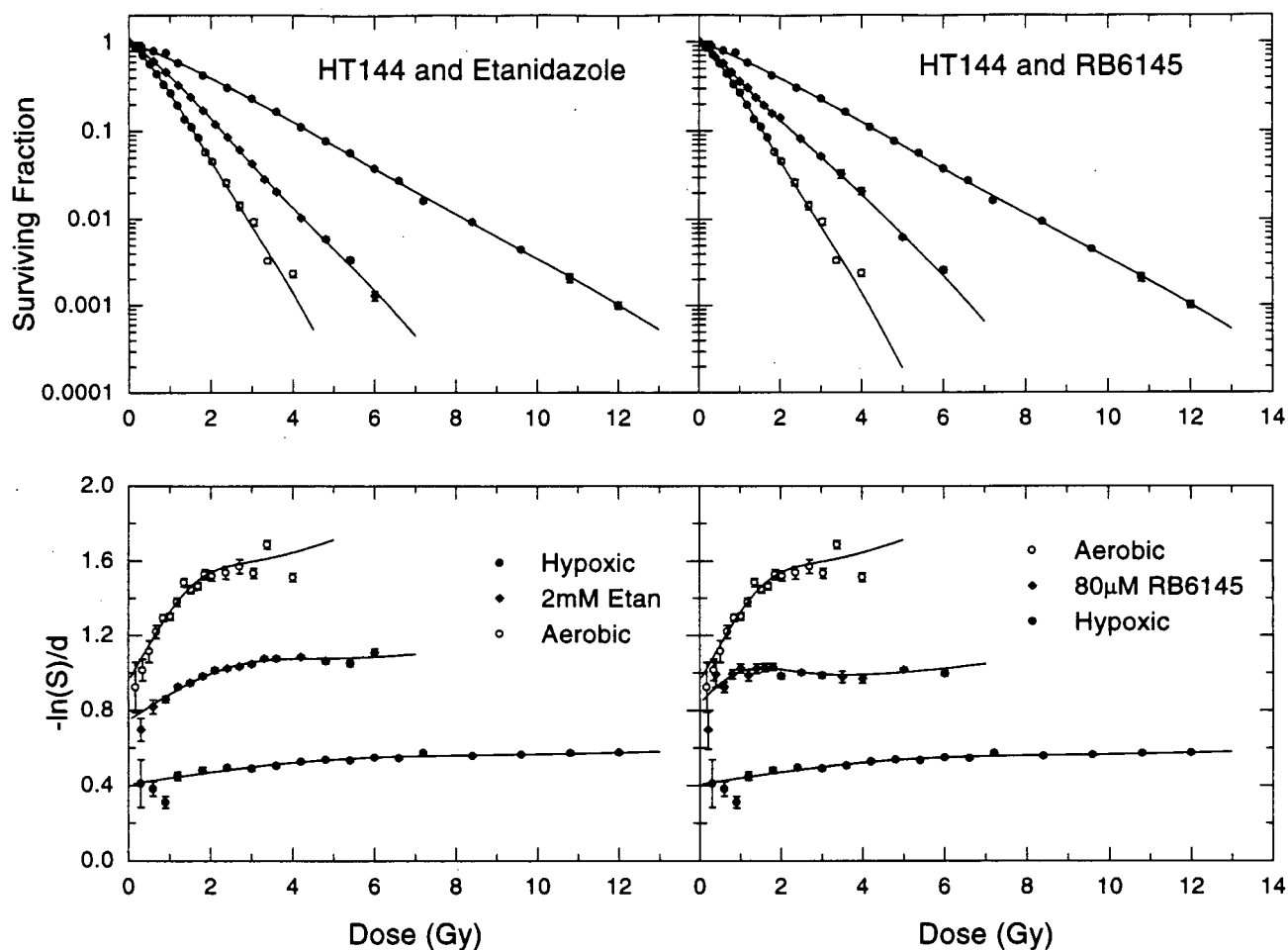
Figure 3-29 HT-144 Two Population Fits
Survival data obtained in HT-29 cells under aerobic and hypoxic conditions with etanidazole (left 2 panels) or RB6145 (right 2 panels) are replotted with the best fits of the two population model (equation 3-7). The data are plotted in both survival (upper frames) and -(lnS)/d (lower frames) forms as a function of radiation dose. The two population model is able to accurately describe the response throughout the entire dose range, though fits are not unique.

Although characterization of the radiation response data with this two population model resulted in excellent fits to the survival data, it was not useful for determining a unique fit. Correlations among the 5 parameters resulted in many possible solutions with different sets of parameters all producing very similar survival curves (data not shown). For this reason modeling the survival data with this equation did not prove useful for examining the changes in the parameters within the model after treatment under different experimental conditions. This type of analysis requires much smaller confidence regions in the parameters in order to show statistically significant changes. Thus, the simple LQ model, fitted at low dose, was chosen to analyze the changes in the fitted parameters under the different experimental conditions. This model, when fitted to the low dose data, describes the initial response of the *entire* cell population, and so proves useful for such an analysis. However, determination of the α and β values in this model is also complicated by the correlation between these parameters. Because changes in one parameter can be offset by changes in the other, it is the *joint confidence region* in both parameters that shows the true confidence in each parameter set. For this reason, the 95% joint regions of confidence for each LQ fit have also been determined, and are plotted in the upper frames of figures 3-30, 3-31, and 3-32. These regions indicate combinations of parameters that yield suitable fits to the low dose region under the different conditions as indicated on these plots.
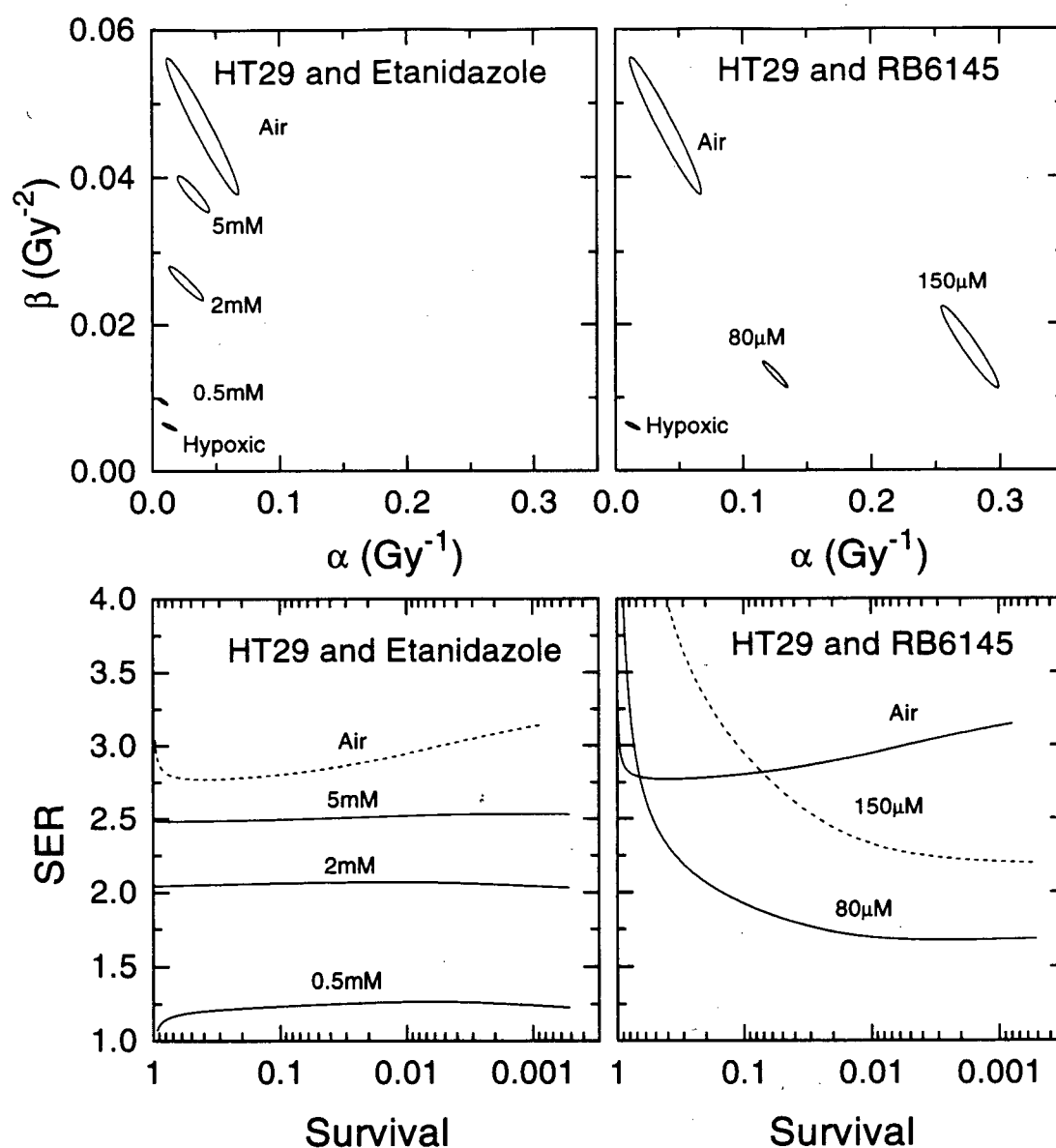
Figure 3-30 HT-29 Hypoxic Cell Sensitization
The 95% joint confidence region in the low dose fitted parameters in the LQ model for HT-29 cells are shown in the upper 2 frames. Parameter values were allowed to vary from their optimum values until a point where the resultant fit was significantly different from the best-fit function. Ellipses are plotted for both etanidazole (left frame) and RB6145 (right frame). In the lower 2 frames the OER and SER for etanidazole (left frame) and RB6145 (right frame) are shown as a function of radiation dose. These values were determined by the ratio of radiation doses under hypoxic conditions alone and under the condition of interest, as determined by the two population model fits to the data(equation 3-7).
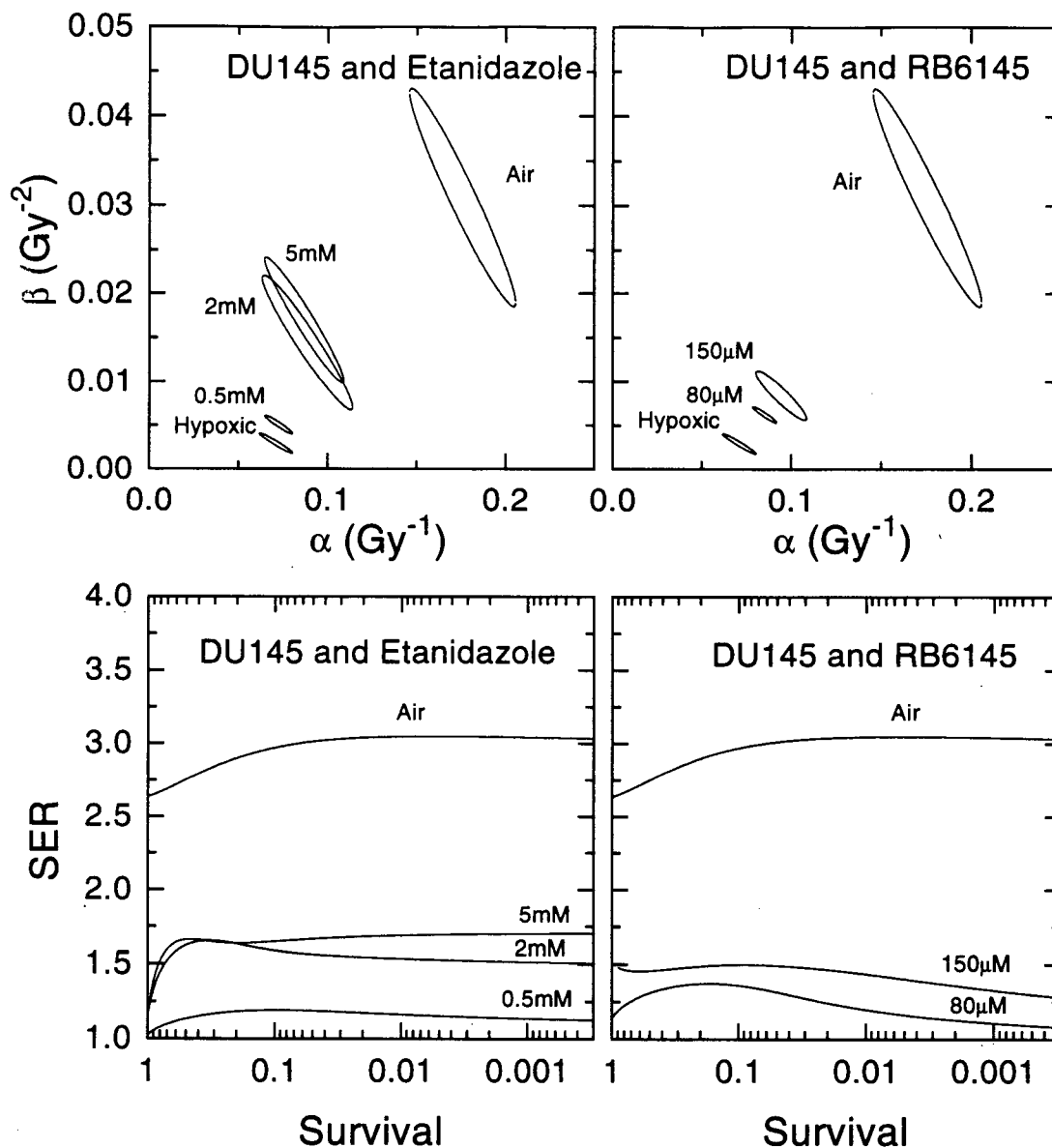
Figure 3-31 DU145 Hypoxic Cell Sensitization
The 95% joint confidence region in the low dose fitted parameters in the LQ model for DU145 cells are shown in the upper 2 frames. Parameter values were allowed to vary from their optimum values until a point where the resultant fit was significantly different from the best-fit function. Ellipses are plotted for both etanidazole (left frame) and RB6145 (right frame). In the lower 2 frames the OER and SER for etanidazole (left frame) and RB6145 (right frame) are shown as a function of radiation dose. These values were determined by the ratio of radiation doses under hypoxic conditions alone and under the condition of interest, as determined by the two population model fits to the data(equation 3-7).
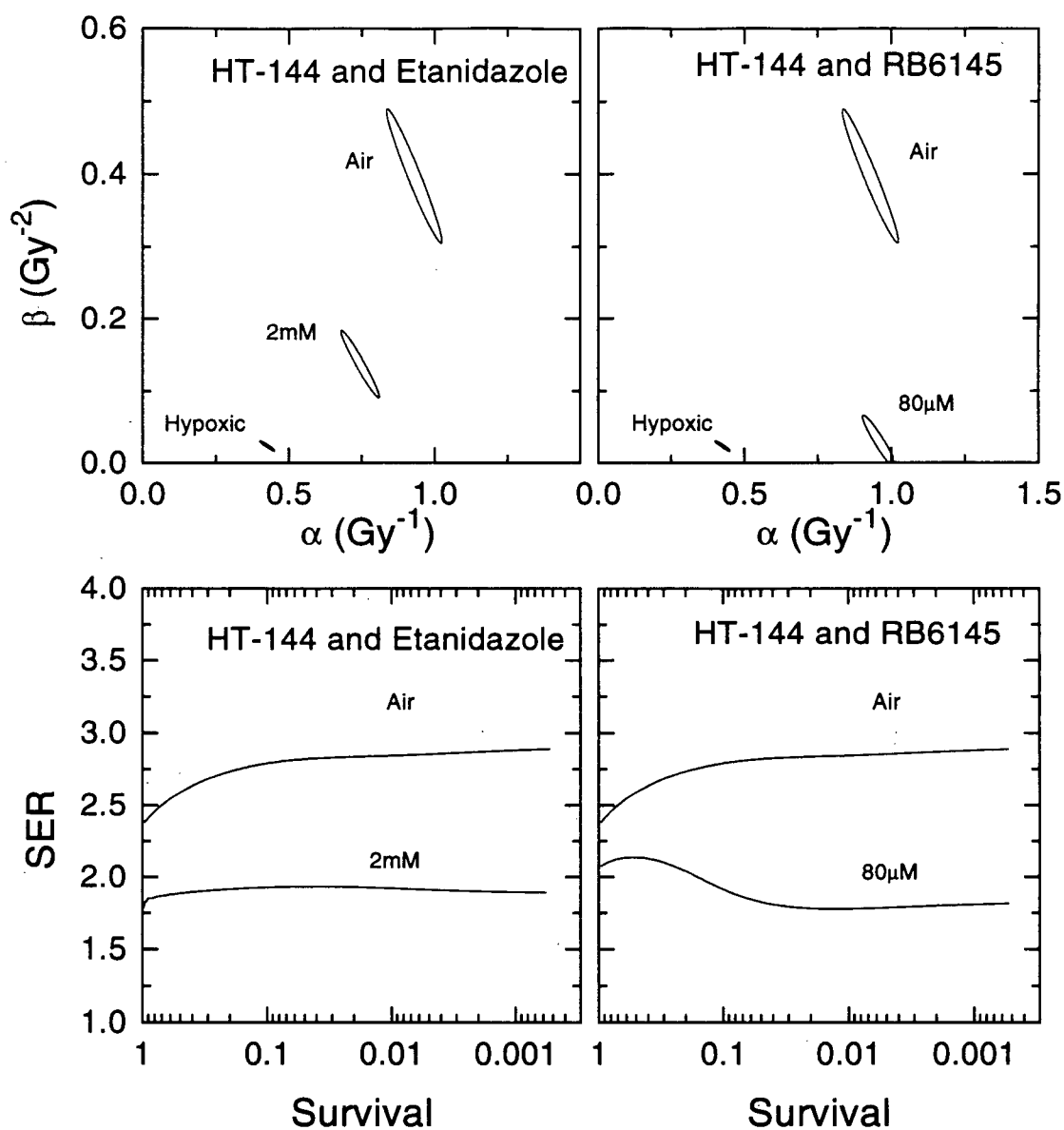
Figure 3-32 HT-144 Hypoxic Cell Sensitization
The 95% joint confidence region in the low dose fitted parameters in the LQ model for HT-144 cells are shown in the upper 2 frames. Parameter values were allowed to vary from their optimum values until a point where the resultant fit was significantly different from the best-fit function. Ellipses are plotted for both etanidazole (left frame) and RB6145 (right frame). In the lower 2 frames the OER and SER for etanidazole (left frame) and RB6145 (right frame) are shown as a function of radiation dose. These values were determined by the ratio of radiation doses under hypoxic conditions alone and under the condition of interest, as determined by the two population model fits to the data(equation 3-7).

3.3 Discussion

In order to evaluate the efficacy of the hypoxic radiosensitizers etanidazole and RB6145 at clinically relevant doses, the cell sorting assay has been used to measure the radiation survival response of a panel of human tumour cell lines. The cell sorting assay significantly improves upon the precision of survival measurements as compared to standard clonogenic assays. It has allowed a careful examination of radiation survival over three to four logs of inactivation, but with particular emphasis on the clinically relevant dose range of a few gray.

3.3.1 Substructure in the Radiation Response

The radiation survival responses of the three cell lines presented here under conditions of hypoxia or hypoxia with the sensitizers etanidazole and RB6145, cannot be adequately characterized by a single LQ response over the complete range of inactivation measured (figures 3-3 to 3-26). This 'misfit' results from the emergence of a more resistant response at higher doses than would be predicted on the basis of a LQ fit to the low dose data only. The identification of substructure in the radiation response under the hypoxic conditions of this study is consistent with the observation of substructure in mammalian cell survival curves measured previously under aerobic conditions and attributed to cell-cycle-associated changes in radiosensitivity (Skarsgard *et al.* 1991, 1992, 1993, 1994a, 1995, Skwarchuk *et al.* 1993). This substructure has been shown to be absent in well-synchronized populations of cells (Skarsgard *et al.* 1993, Skwarchuk *et al.* 1993), and has been measured in the same panel of cell lines presented here

(Skarsgard *et al.* 1995). The high dose fits in figures 3-3 to 3-26 (particularly the -(lnS)/d plots) show why, in a more conventional measurement, with very few points in the low, clinically relevant, dose range, this substructure could not be observed, and fits to the data would overestimate both the cell kill at low doses, and the value of the α parameter. It should be noted that this would occur regardless of how carefully these measurements were made. Because of the substructure present in the radiation survival curve, the response at low dose must be *measured* - it cannot be predicted.

Several of the radiation responses showed evidence of an increased effectiveness from the lowest dose of radiation delivered (see figs. 3-5, 3-7, 3-9, 3-10, 3-19, 3-20, 3-23), and this apparent low dose hypersensitivity is the subject of investigation in chapter 4 of this thesis.

In order to characterize the low, clinically relevant, dose range accurately, the data at low and high doses have been fit separately. In all cases, good fits to the low dose data with the LQ model were possible, illustrating the ability of this model to characterize correctly, the *initial* response of the heterogeneous cell population. In other words, the model predicts the correct *composite* response at low doses, until the makeup of the population changes significantly (due to selective killing of the most sensitive cells) so as to produce a predominantly resistant population. Fits to the high dose data result in larger values for α and smaller values for β (see tables 3-1, 3-2, and 3-3), and this in turn results in an overestimation of cell kill at low doses. It also results in a misinterpretation of the importance of each of these parameters in determining cell kill at low dose. In tables 3-5, 3-6, and 3-7, the contributions to cell kill at a dose of 4 Gy for each of the three cell lines

have been calculated using both the low and high dose fit parameters. Examination of the numbers in these tables shows that the high dose fit can severely underestimate the β contribution to cell kill even at this low dose. For example, in hypoxic HT-29 cells, the high dose fit attributes only 16% of the total cell kill at 4 Gy to the βd^2 term, whereas the clearly more representative low dose fit attributes 65% of cell kill to the βd^2 term. Because of the substructure present in these data, a LQ fit to the high dose data can be viewed only in an empirical sense, since the parameters derived are not reflective of any population of cells, they simply characterize the high dose data. On the other hand, the low dose fit parameters describe quantitatively the initial response of the entire mixed population. For this reason, modification of these parameters under different experimental conditions (*e.g.*, sensitizers) can be viewed in a more mechanistic fashion. While the use of a two population model can accurately describe the entire response, many equally good fits are possible due to a high degree of correlation among the parameters. This lack of uniqueness among the parameters limits the usefulness of evaluating modifications to these parameters under different experimental conditions.

3.3.2 Sensitization is Cell Line Dependent

The enhancement ratios presented in figures 3-30, 3-31, and 3-32, and tabulated in tables 3-5, 3-6, and 3-7, show clearly that the degree of sensitization with etanidazole and RB6145 is cell line dependent. In an attempt to understand the mechanistic basis of the observed cell line dependence, the radiation response data have been fitted with the LQ model and the low dose α and β values determined.

Table 3-5 Hypoxic Sensitization in HT-29 Cells

The proportion of cell kill which is attributable to the α and β parameters in the LQ model was determined as the logarithmic drop in survival at a dose of 4 Gy. Shown are the predictions for these values based on the low and high dose fits to the data (see table 3-1). Also shown are the resultant SER and OER values at survival levels of 80 % and 1 %.

Experimental Condition	Dose Range	α-kill %	β-kill %	$SER_{0.8}$	$SER_{.01}$
Hypoxic	Low (0-18)	35%	65%		
	High (18-38)	84%	16%		
Aerobic	Low (0-4)	17%	83%	2.82	2.95
	High (4-13)	22%	78%		
Hypoxic+0.5mM Etan	Low (0-16)	17%	83%	1.14	1.27
	High (16-30)	82%	18%		
Hypoxic+2mM Etan	Low (0-8)	20%	80%	2.05	2.07
	High (8-18)	72%	28%		
Hypoxic+5mM Etan	Low (0-8)	18%	82%	2.48	2.52
	High (8-18)	68%	32%		
Hypoxic+80μM RB6145	Low (0-7)	70%	30%	3.27	1.69
	High (7-28)	88%	12%		
Hypoxic+150μM RB6145	Low (0-6)	81%	19%	6.55	2.32
	High (6-18)	95%	5%		

Table 3-6 Hypoxic Sensitization in DU145 Cells
The proportion of cell kill which is attributable to the α and β parameters in the LQ model was determined as the logarithmic drop in survival at a dose of 4 Gy. Shown are the predictions for these values based on the low and high dose fits to the data (see table 3-1). Also shown are the resultant SER and OER values at survival levels of 80 % and 1 %.

Experimental Condition	Dose Range	α-kill* %	β-kill* %	SER0.8	SER.01
Hypoxic	Low (0-10)	86%	14%		
	High (10-38)	88%	12%		
Aerobic	Low (0-3.2)	59%	41%	2.67	3.05
	High (3.2-14)	62%	38%		
Hypoxic+0.5mM Etan	Low (0-9.5)	78%	22%	1.08	1.16
	High (9.5-33)	88%	12%		
Hypoxic+2mM Etan	Low (0-4.2)	61%	39%	1.45	1.53
	High (4.2-25)	86%	14%		
Hypoxic+5mM Etan	Low (0-4)	56%	44%	1.52	1.69
	High (4-25)	79%	21%		
Hypoxic+80mM RB6145	Low (0-10)	77%	23%	1.23	1.19
	High (10-18)	95%	5%		
Hypoxic+150mM RB6145	Low (0-7.5)	74%	26%	1.47	1.44
	High (7.5-25)	90%	10%		

Table 3-7 Hypoxic Sensitization in HT-144 Cells
The proportion of cell kill which is attributable to the α and β parameters in the LQ model was determined as the logarithmic drop in survival at a dose of 4 Gy. Shown are the predictions for these values based on the low and high dose fits to the data (see table 3-1). Also shown are the resultant SER and OER values at survival levels of 80 % and 1 %.

Experimental Condition	Dose Range	α-kill* %	β-kill* %	$SER_{0.8}$	$SER_{.01}$
Hypoxic	Low (0-4.8)	82%	18%		
	High (4.8-12)	96%	4%		
Aerobic	Low (1.8)	37%	63%	2.46	2.84
	High (1.8-6)	81%	19%		
Hypoxic+2mM Etan	Low (0-8)	58%	42%	1.86	1.92
	High (8-18)	99%	1%		
Hypoxic+80μM RB6145	Low (0-4)	90%	10%	2.11	1.78
	High (4-25)	98%	2%		

3.3.2.1 Etanidazole

Examination of the results with etanidazole suggests that hypoxic cell sensitization with this drug is largely due to a selective modification of the β parameter. The -ln(S)/d plots shown in the lower frames of figures 3-8, 3-14, and 3-18 illustrate the point that in all 3 cell lines, treatment of hypoxic cells with etanidazole produces only modest changes in the resulting fitted α values (the y-intercept on this type of plot), while, in general, a more substantial change occurs in the β parameters (the slopes of the lines) when compared to the hypoxic controls. These plots also show that differences in the efficacy of etanidazole among the three cell lines is dependent upon the degree to which the β parameter determines cell kill at low doses. For example, if one compares the sensitization that results from a concentration of 2 mM etanidazole, the most effective sensitization (SER=2.07 at S=1%) is in HT-29 cells, where, under conditions of hypoxia, the β parameter accounts for 65% of cell kill at a dose of 4 Gy. This sensitization is due primarily to an increase in the β parameter (it is increased by a factor of 4.2), and although there is also a modification of α (increased by a factor of 2.0), because this parameter under hypoxic conditions is very small to begin with, this change in absolute terms is also very small, and does not contribute greatly to sensitization. Furthermore, analysis of the confidence regions in figure 3-30 shows that this change is not statistically significant (the confidence limits overlap for α). By comparison, DU145 cells, which have a high dose radiosensitivity similar to HT-29 cells, are less sensitized by 2 mM etanidazole (SER=1.53 at S=1%). Here the β parameter accounts for only 14% of cell kill at 4 Gy, and although there is a highly significant modification of β by treatment with

etanidazole (see confidence ellipses in figure 3-31), because this parameter is very small under conditions of hypoxia to begin with, this increase (by a factor of 5) produces much less absolute sensitization in comparison with HT-29 cells. In DU145 cells, the α parameter changes only by a factor of 1.3, which again is not significant (see confidence ellipses in figure 3-31). In HT-144 cells, treatment with 2 mM etanidazole results in a SER of 1.92 at S=1%, between that of HT-29 and DU145 cells, despite the far greater radiosensitivity of this cell line. In HT-144 cells, there is a significant modification of both the α and β parameters (see confidence ellipses in figure 3-32). However, once again the sensitization is primarily due to the large change in the β parameter (increased by a factor of 5.8), with a more modest change in α (increased by a factor of 1.75).

Further evidence that the observed sensitization results primarily from an increase in the β parameter can be seen in tables 3-5, 3-6, and 3-7. In HT-29 cells, treatment with 2 mM etanidazole increases the amount of cell-kill attributable to the β-component from the already dominant 65% to a value of 80%. In DU145 cells, treatment with etanidazole produced far less sensitization, but still increased the amount of cell-kill attributable to the β-component from 14% to 39%. Finally in HT-144 cells, again at a dose of 4 Gy, the percentage of cell kill attributed to the β-component rises from 18% under hypoxic conditions to 42% after treatment with 2 mM etanidazole.

In figure 3-33 the SER calculated at a survival level of 80% is plotted versus the α/β ratio determined from low dose fits to survival data obtained under conditions of hypoxia. Here the α/β ratio serves as a surrogate for the importance of each of these parameters in contributing to cell kill; β is more important in those cell lines with a small

α/β ratio. This figure shows that a good correlation exists between the sensitizing ability of etanidazole, and the α/β ratio determined at low dose for all three cell lines and all three concentrations of etanidazole used, which is independent of the absolute sensitivity of each cell line. In this figure, the α/β ratio and the SER value for HT-144 cells lie between those for HT-29 and DU145 cells, despite the fact that the HT-144 cell line is far more radiosensitive (see tables 3-1, 3-2, and 3-3). This figure also suggests that the differential sensitization among cell lines with different α/β values becomes larger at higher drug concentrations. Treatment with 5 mM etanidazole produced significantly greater sensitization as compared to 2 mM in HT-29 cells (2.05 to 2.48 at S=80%), but increased the SER in DU145 cells only modestly (1.45 to 1.53 at S=80%) such that it remained smaller than the SER obtained in HT-29 cells with 2 mM etanidazole.

Figure 3-34 indicates that the dependence of the SER on the importance of the β contribution to cell kill, or alternatively the α/β ratio, is not observed if the high dose parameters are used to determine the α/β ratio. This is because of the varying degree of substructure present in the survival responses of the different cell lines, and the resulting variable correlation between the high dose fit parameters and the overall response. In HT-144 and HT-29 cells the substructure influences the high dose fit to a greater extent than it does in DU145 cells. It is, of course, expected that the SER determined at low dose (S=80%, fig. 3-34(a)) would not correlate well with the α/β values from the high dose fit, however this lack of correlation also arises if the SER is evaluated at high dose (S=1%, fig 3-34(b)).
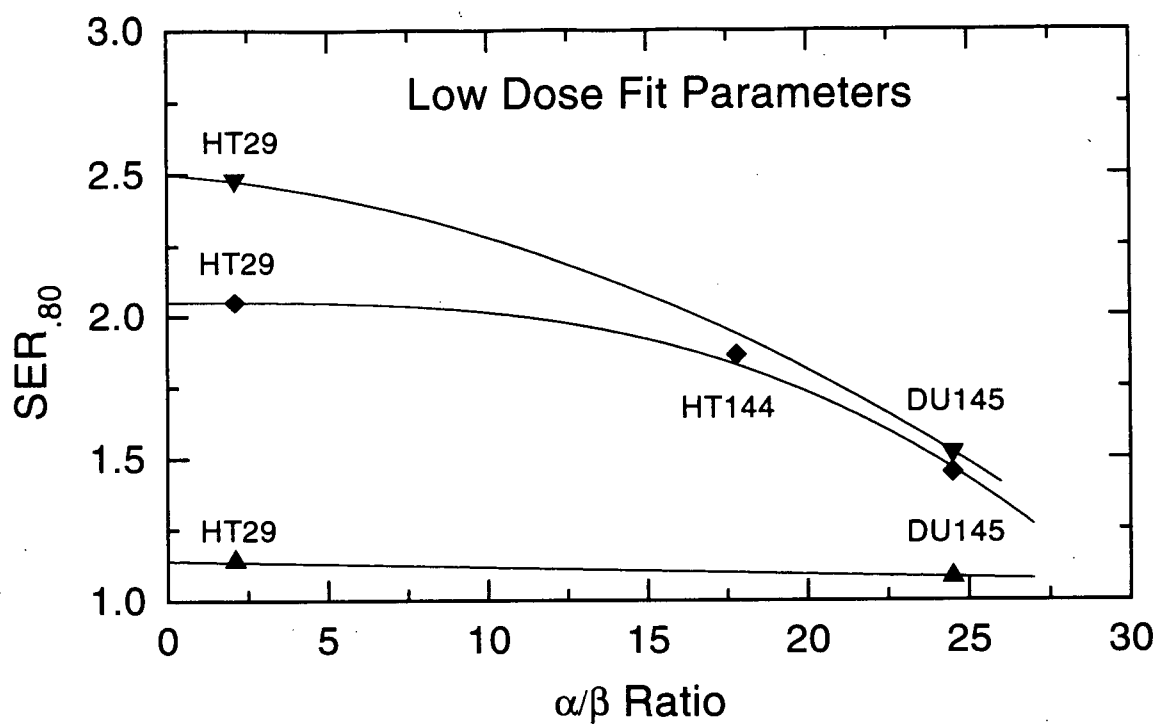
Figure 3-33 Etanidazole SER Dependence On the Low Dose α/β Ratio
The sensitizing effects of etanidazole at a survival level of 80% are plotted against the α/β ratios determined from the low dose fit LQ parameters under hypoxic conditions alone. Data are shown for HT-29, DU145, and HT-144 cell lines with etanidazole concentrations of 0.5 mM (triangles), 2 mM (diamonds) and 5 mM (inverted triangles). The data at 2 mM etanidazole were fitted with a 3rd order polynomial (solid line). Data points at 5 mM were joined with solid lines with a shape similar to that drawn for 2 mM etanidazole. The data points at 0.5 mM etanidazole were joined with a straight line.
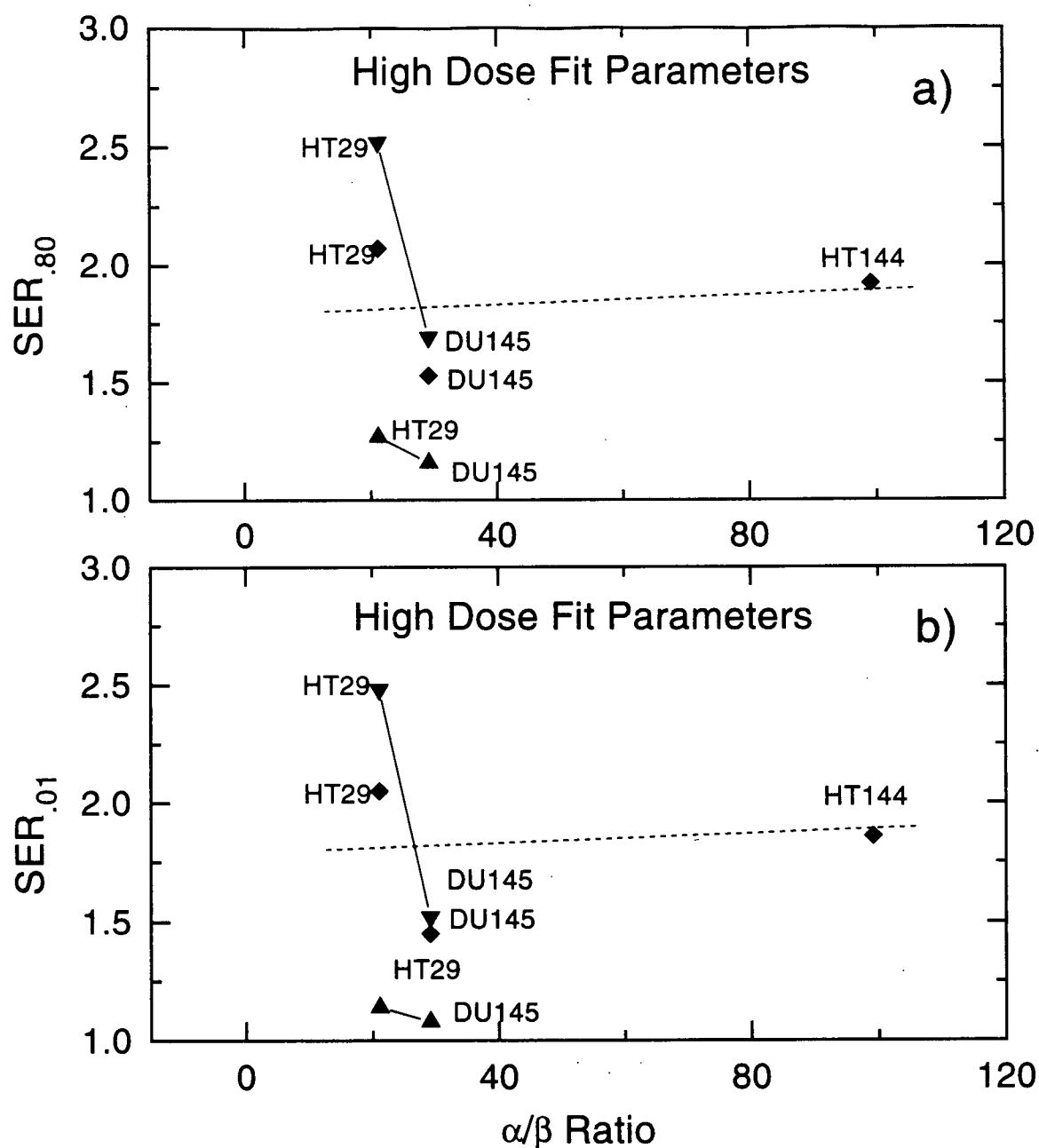
Figure 3-34 Etanidazole SER Dependence On the High Dose α/β Ratio

The sensitizing effects of etanidazole at a survival level of 80% (a) or 1% (b) are plotted against the α/β ratios determined from the high dose fit LQ parameters under hypoxic conditions alone. Data are shown for HT-29, DU145, and HT-144 cell lines with etanidazole concentrations of 0.5 mM (triangles), 2 mM (diamonds) and 5 mM (inverted triangles). The dashed line is a linear fit to the data at 2 mM etanidazole. Data points at 0.5 mM and 5 mM etanidazole were joined with straight lines.

3.3.2.2 RB6145

The data presented in figures 3-19 to 3-26 suggest that hypoxic cell sensitization with RB6145, in contrast to etanidazole, results primarily from an increase in the α-component of cell kill. The -ln(S)/d plots shown in the lower frames of figures 3-21, 3-24, and 3-26, demonstrate that the sensitization exhibited after treatment with RB6145 is largely accounted for by an increase in the y-intercept (α), with only a modest increase in the slopes of the lines (β). This modification is also illustrated by the change in the shape of the survival versus dose plots for HT-29 cells (fig. 3-21) where, after treatment with either 80 μM or 150 μM RB6145, the resulting curve has a much reduced shoulder, and thus a larger α/β ratio. However, in contrast to the results with etanidazole, the most effective sensitization was observed in cell lines in which the selectively modified parameter, in this case α, contributed the *least* to cell kill under hypoxic conditions alone. The SER data plotted in figures 3-30, 3-31, and 3-32 show that sensitization was most effective in HT-29 cells, which under hypoxic conditions exhibit the smallest α/β ratio (table 3-1), and the smallest α-contribution to cell kill (table 3-5). In this cell line, the sensitization measured after treatment with 80 μM RB6145 resulted primarily from an increase in the α-parameter from a value of 0.0131 Gy^{-1} under hypoxic conditions alone, to a value of 0.1251 Gy^{-1} (a 9.5 fold increase) after treatment. This increase is also reflected by the amount of cell kill attributable to the α-component, which rose from 35% to 70% (table 3-5). Treatment with 150 μM RB6145 in this cell line further increased the amount of cell kill attributed to this parameter to 81%. This effectively removed the

shoulder, and dramatically sensitized the cells at low doses of radiation (see fig 3-30), resulting in SER values that ranged from more than 7 at low dose to 2.32 at 1% survival. The confidence ellipse plots in the upper frames of figure 3-30 also show clearly that treatment with RB6145 results in a significant increase in the α parameter, with only a small change in the β parameter. In DU145 cells, which exhibit the most linear response under hypoxic conditions alone, and thus have the largest contribution to cell kill attributable to the α component, treatment with 80 μM RB6145 resulted in a much reduced SER (see fig 3-31), and a correspondingly smaller increase in α (from a value of 0.0710 Gy^{-1} to .0851 Gy^{-1}). In this cell line the sensitization that did result was not so much due to a selective modification of 1 parameter, but rather to a change in both α and β. However, if one compares the parameter values which result after treatment with etanidazole and RB6145 (see confidence ellipse plots in the upper frames of figure 3-31) it can be seen that sensitization with RB6145 results in a somewhat larger relative increase in the α value than does treatment with etanidazole. In HT-144 cells, the survival data in figure 3-26, and the confidence ellipse plots shown in figure 3-32 show that the sensitization that resulted from RB6145 was again primarily due to a change in the α parameter. The absolute SER values at low dose for this cell line were again intermediate between those of HT-29 and DU145, which reflected the intermediate low dose α/β ratio measured under hypoxic conditions alone. The relationship between the α/β ratio determined at low doses under hypoxic conditions alone and RB6145 efficacy is shown in figure 3-35.
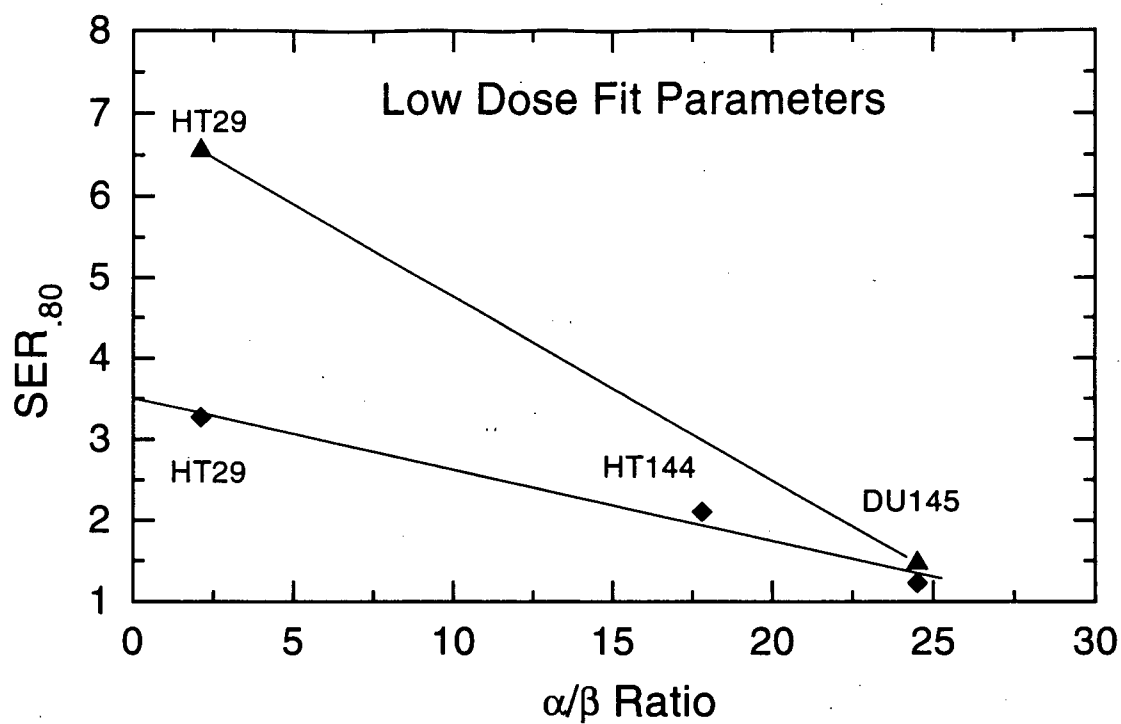
Figure 3-35 RB6145 SER Dependence On the Low Dose α/β Ratio
The sensitizing effects of RB6145 at a survival level of 80% are plotted against the α/β ratios determined from the low dose fit LQ parameters under hypoxic conditions alone. Data are shown for HT-29, DU145, and HT-144 cell lines with RB6145 concentrations of 80 μM (diamonds) and 150 μM (triangles).

3.3.2.3 Implications of Cell Line Dependence

These results suggest that sensitization of hypoxic cells by etanidazole results predominantly from a modification of the β parameter, while sensitization with RB6145 results primarily from a modification of the α parameter. For both of these drugs, this results in selectively greater sensitization in cell lines in which the β-parameter contributes significantly to cell kill at low doses (*i.e.*, a low α/β ratio). This principle is reflected in the differential sensitization seen in the 3 cell lines studied here, and suggests that the efficacy of these and other radiation modifiers can be predicted in part on the basis of the *in vitro* α/β ratios, provided they are measured *at low dose*, and provided that the mode of action of the sensitizer is understood (with respect to its effect on α and β). It also suggests that tumours with a large shoulder (large β component), which would normally be the most resistant to treatment with a fractionated regime, would be the most effectively sensitized by radiosensitizers that are mechanistically similar to etanidazole or RB6145. We acknowledge that other factors such as drug uptake, enzyme profiles, and GSH levels within the cell will also contribute to the sensitizer efficacy, however these results clearly demonstrate a link between the importance of β in terms of cell kill at low dose, and the efficacy of these drugs.

3.3.3 Sensitization is Dose-Dependent

The results with etanidazole showed that hypoxic cell sensitization is primarily due to a change in the β-component, and that those cell lines with the largest relative β-contributions to cell kill (smallest α/β ratio) under hypoxic conditions alone were most

effectively sensitized. With RB6145 sensitization results primarily from a change in the

α-component, and that modification was most effective in cell lines where this parameter

initially contributed little to cell kill. Thus both of these drugs preferentially sensitize cell

lines with a low α/β ratio, but through different modifications of the shape of the dose

response curve. This results in a dramatically different dose dependence for the efficacy

of these two agents. The dose dependence of both radiosensitizers is dependent on the

parameter modification after treatment, and on changes in the degree of substructure in

the resulting survival response.

3.3.3.1 Parameter Modification

The suggestion that treatment with etanidazole or RB6145 predominantly

modifies one of the parameters in the LQ model has the consequence that the efficacy of

these drugs will be dose-dependent. It can be shown that the sensitizer enhancement ratio

for cell lines, whose dose response can be characterized by a LQ function, will vary as a

sigmoid function of dose from an initial value of α_s/α_h to a final value at high dose of

$(\beta_s/\beta_h)^{1/2}$ (s and h denote irradiation under hypoxic conditions with and without sensitizer

present, respectively) (Palcic 1984). The SER will be independent of dose only if these

ratios are equal. The α/β ratio determined from the low dose fit parameters, or the

relative contribution of either of these parameters to cell kill at low dose, will also

determine the dose or survival level at which the transition from the initial SER of α_s/α_h

to the final value of $(\beta_s/\beta_h)^{1/2}$ is made. This is because at doses below α/β, the αd term

dominates cell kill, whereas at doses above α/β, the βd^2 term dominates. The results with

HT-29 cells treated with etanidazole (figure 3-30, table 3-5), show that the SER at low dose is somewhat reduced (only noticeable for 0.5 mM etanidazole) but rises quickly to a stable value at a relatively high survival (or low dose value). This rapid change occurs because of the small α/β ratio, with the β parameter becoming responsible for the majority of cell kill by a dose of 2-3 Gy. In contrast, in DU145 cells (figure 3-31, table 3-6), which also exhibit a lower SER at low doses for etanidazole (reflecting selective modification of β), the change is much more gradual, and extends to a somewhat higher dose. This is because this cell line has a high α/β ratio, and thus the β parameter is less responsible for cell kill at low dose. These results show that in cell lines with a high α/β ratio, sensitization will not only be reduced, but it will also be more dose-dependent. This dose dependence will further reduce the effectiveness of etanidazole when it is used in conjunction with the low daily doses of fractionated radiotherapy. The dose dependence is intermediate for HT-144 cells that have an intermediate α/β value (see tables 3-1, 3-2, and 3-3).

A similar situation applies to the observed dose dependence of the oxygen enhancement ratio (OER) for the three cell lines. A clear reduction at low dose is observed in DU145 and HT-144 cell lines that have correspondingly larger α/β ratios. HT-29 cells are a possible exception, where the OER followed a more complex response. In this cell line the OER was fairly constant over the first log of cell kill, rose slowly at higher doses, and also *rose* at very low doses (fig. 3-30). It is likely that the rise in OER at high dose is related more to changes in the extent of response substructure in the aerobic and hypoxic responses (see 3.3.2), than to parameter modification, since the

predicted sigmoidal function is not observed. The rise in OER at very low dose is largely influenced by an apparent hypersensitive initial low dose region in the aerobic response (see first data point in fig. 3-7). The radiation response at very low doses is the subject of investigation in chapter 4, but on the basis of these data in chapter 3, one cannot conclude that this apparent rise is real.

Sensitization produced by RB6145 resulted primarily from a change in the α-component, and was most effective in HT-29 cells that have a very small α/β ratio. Under conditions where there is a selective modification of α, one would expect a much larger dose dependence as compared to sensitization through selective modification of β. Because α is very small initially, the ratio of the α value after sensitizer treatment to the α value under hypoxic conditions alone, is large. This results in a correspondingly large initial SER value, and since the α/β ratio after treatment is also much larger, the rate of change in the SER from α_s/α_h to $(\beta_s/\beta_h)^{1/2}$ is much more gradual. This is particularly evident in figure 3-30, which shows a gradual change from the initially high value to the lower value after treatment with 80 μM, and an even slower change after treatment with 150 μM . This figure also shows that because of this gradual change, for RB6145 there is no single value for the SER that can describe sensitization with RB6145 in HT-29 cells. At low, clinically relevant doses, treatment with 80 μM and 150 μM RB6145 results in extremely good sensitization with SER values at 80% survival of 3.27 and 6.55, which are gradually reduced to values of approximately 1.69 and 2.32 respectively.

In contrast to etanidazole, the results with DU145 and HT-144 cells treated with RB6145 show a reduced dose dependence as compared to HT-29 cells. This could

indicate that the sensitization results from an additive increase in α, rather than a multiplicative increase. If this were the case, the percentage change in α would be expected to be much smaller in those cell lines that have larger α values to begin with. This would result in a smaller initial SER value (α_s/α_h), and an even slower change to the final $(\beta_s/\beta_h)^{1/2}$ value.

3.3.3.2 Substructure Dependence

The dose dependence of these radiosensitizers will also be influenced by the degree of substructure present in the survival curve. Because of this substructure, the predicted sigmoidal change in the SER will hold only at doses where the low dose fit parameters apply. At higher doses, there is an apparent increase in radioresistance due to selective killing of the most sensitive cells, and if this response substructure is altered by treatment with the sensitizer, then it will contribute to the dose dependence. This would occur, for example, if the radiosensitizer were more effective with one particular subpopulation of cells, perhaps in one phase of the cell cycle. There is some evidence to suggest that this may be the case for certain cell lines. In DU145 cells, there was very little observable substructure under either aerobic or hypoxic conditions alone (see figs. 3-9 and 3-13). However, after treatment with 0.5, 2, or 5 mM etanidazole (see figs. 3-10, 3-11, and 3-12) or with 80 μM or 150 μM RB6145, substructure was easily observable, and fits to low and high dose ranges gave markedly different results (see table 3-2). This suggests that either a subpopulation within the heterogeneous, asynchronously growing cell population is preferentially sensitized, or that one subpopulation is particularly

resistant to treatment. Regardless of the mechanism involved, this will influence the dose dependence of the SER values, particularly at high dose or low survival levels.

The dose dependence of the OER(a gradual rise with increasing dose) observed in HT-29 cells (see fig. 3-30), suggests that oxygen may also act selectively on different subpopulations of cells. This would imply that the OER is not the same for all subpopulations of cells, and suggests, for example, that the OER may be different in different phases of the cell cycle. Such a dependence has been observed in CHO cells measured using a similar cell sorting assay (Freyer *et al.* 1991) and in human T-1 cells using a conventional survival assay (Blakely *et al.* 1988).

3.3.3.3 Comparison With Other Data

Previous investigations into the dose dependence of sensitization by etanidazole have indicated mixed results. A recent study in V79 and CHO cells reported a reduced SER at low doses for high concentrations of etanidazole (2-3 mM), but an increased SER at low doses (below 1 Gy) for *low* concentrations of etanidazole (0.1-1.0 mM) (Skov and MacPhail 1994, Skov *et al.* 1994). Although the present results show no significant evidence of an increased SER at low dose, the SER has not been evaluated at such low etanidazole concentrations or at as low doses of radiation. Other studies have indicated both reduced SERs (Skarsgard *et al.* 1986 - measured using the cell sorting assay), and no change (Shibamoto *et al.* 1992 - measured using the micronucleus assay) at low doses of radiation. Although these authors used different methods to evaluate the SER at low dose, the cell lines investigated also exhibited important differences. Skarsgard *et al.* used V79 cells that have a small shoulder, while Shibamoto *et al.* used EMT6 cells which

they describe as having a large shoulder, and thus the different results are consistent with the etanidazole dose dependence observed in the three cell lines studied here; cell lines with the largest α/β ratios (small shoulders) exhibited the greatest dose dependence. Reduced SER values at low dose in V79 cells have also been reported for misonidazole (Palcic et al. 1984b, Watts et al. 1986) and pimonidazole (Skarsgard et al. 1986), and these results are again consistent with the relatively large α/β ratio of this cell line. In a fractionated irradiation schedule with artificially hypoxic tumours, a relatively high value for the SER of etanidazole, 1.6, was found for the RIF-1 tumour (Brown and Yu 1984). This value was similar to the single, high dose value of 1.8 reported in that study, and thus also represents no significant reduction at low dose, consistent with this tumour exhibiting a small α/β ratio or large shoulder (Zeman et al. 1990). On the basis of our results in the three human tumour lines studied, the discrepancies in dose-dependence of SER values reported in the literature may be explained on the basis of cell line dependence, which results from the differences in the α and β parameters as determined at low doses.

A similar situation applies to the dose dependence of the sensitizing effects of oxygen. Our results with the three cell lines suggest that hypoxic cell sensitization with oxygen results in a somewhat selective increase in the β parameter, and thus results in a reduced oxygen enhancement ratio (OER) at low doses. This is particularly evident in HT-144 and DU145 cells that have larger α-contributions to cell kill than for HT-29 cells. This is similar to several other studies that have previously indicated a reduced oxygen enhancement ratio (OER) at low doses (Littbrand and Revesz 1969, Revesz et al. 1975,

Palcic *et al.* 1984a, Palcic and Skarsgard 1984, Skarsgard and Harrison 1991) in V79 and CHO rodent cells. However there have been other reports that indicated no reduction in OER, measured in EMT6 and B14FAF cells (Phillips *et al.* 1975). The EMT6 and B14FAF cells in that report exhibited large shoulders on the radiation survival curves, and thus would be characterized by a small α/β ratio. These apparently contradictory results are again associated with a cell-line-specific dose dependence, which can be predicted on the basis of the α and β parameters. The radiation dose dependence is only observed in the cell lines with larger α/β ratios, where the α component is sensitized to a smaller degree, but dominates cell-kill out to a higher dose (given by α/β).

3.3.3.4 Mechanistic Differences Between Etanidazole and RB6145

The search for an effective hypoxic cell radiosensitizer has historically been aimed at developing one that can closely mimic the effects of oxygen. The results with etanidazole show that the pattern of sensitization is similar to that observed with oxygen (see the dose dependence in figs. 3-30, 3-31, and 3-32), though the sensitization with etanidazole is somewhat more selective for the β parameter in the LQ model. Since sensitization with this drug had a much smaller effect on the α parameter, it was less effective in cell lines in which this parameter contributed significantly to cell kill. The results with RB6145, on the other hand, demonstrate a mechanism of action significantly different from that of etanidazole or oxygen. Treatment with this sensitizer produced a large enhancement of the α parameter in cell lines that were most effectively sensitized, and had a substantially different dose dependence.

In an effort to further our understanding of the basis for the intrinsic radiosensitivity of mammalian cells, many mathematical models have been proposed, however the LQ model has arguably gained the widest acceptance for describing the radiation survival response in a broad range of mammalian cell studies. One interpretation of the LQ model proposes that the α parameter is associated with cell kill arising from single-hit events (proportional to dose), while the β parameter is associated with cell kill arising from two-hit, or damage interaction events (proportional to dose squared) (Chadwick and Leenhouts 1973). If such a hypothesis is adopted, then one could interpret the sensitization observed with etanidazole as an increase in the number of two-hit events. Thus one would expect a corresponding increase in the number of sublesions that interact to form the lethal lesions attributable to the β parameter. This could result, for example, through interaction of etanidazole with transient, reversible lesions such that they become sublesions capable of interacting with other sublesions to produce lethal damage. This mechanism of sensitization would be expected to work best in cell lines where this pathway for sublethal damage production is functional and predominant.

Since sensitization with RB6145 results in an increase in both α and β, interpretation with this model suggests that RB6145 can create a spectrum of 'upgraded' lesions by interacting either with transient reversible lesions (to increase the number of sublesions), or directly with radiation-induced sublesions (to create additional lethal, single-hit events). The results with HT-29 cells show that the hypoxic cells surviving pretreatment for 1 hour are initially more sensitive than fully aerobic cells (compare

aerobic and hypoxic with 150 μM RB6145 responses in figure 3-27). This implies that these cells are sensitized beyond the chemical capability of oxygen, and further suggests that there may be an interaction between drug-induced and radiation-induced damage. In HT-29 cells, in which substantial toxicity is produced by pretreatment with RB6145 (40% and 73% of cells are killed by 80 μM and 150 μM RB6145, respectively), it is likely that a substantial amount of sub-lethal damage is produced as part of this toxicity. Interaction between this sublethal damage and radiation-induced sublesions could then produce additional (apparent) single-hit events and a corresponding increase in the α parameter. In other words, some of the damage that would normally be a part of two-hit events is converted to single-hit events by interaction with the damage produced by RB6145. In DU145 cells, where most of the damage results from the single-hit component under hypoxic conditions alone, this damage interaction would not be expected to result in a large increase in this component of cell-kill, consistent with what is observed. In addition, treatment with RB6145 produced very little toxicity (10-25%) in this cell line, and thus presumably there was less potential for damage interaction. This analysis could also explain why, at high doses the sensitization resulting after treatment with 80 μM RB6145 in HT-144 cells is somewhat larger than that in HT-29 cells. Because the absolute value of the β component is larger in HT-144 cells than in HT-29 cells, there is presumably more sublethal damage to interact with the damage produced by RB6145. In addition, treatment of HT-144 cells with this concentration of drug produced the highest level of toxicity (80-85%) of the three cell lines investigated.

Another interpretation of shouldered survival curves that can also be accommodated by the LQ model is one that assumes that the curvature in the response is the result of a dose-dependent reduction in the fraction of radiation-induced lesions that are repaired. There are several lines of evidence that suggest that the initial level of damage induced in cell lines of different intrinsic sensitivity for a given experimental condition is roughly the same, and that the differences in observed survival are due to different repair capabilities (Ward 1990). Assuming this hypothesis is true, then the average number of lesions introduced per cell in any cell line for a given experimental condition can be described by a linear function in dose:

$$induced\ lesions\ /\ cell = a_l d \qquad\qquad \text{Equation 3-8}$$

These lesions are subsequently acted upon by biological repair mechanisms, such that only a fraction of the original lesions remains after a given dose. According to probability theory, the average number of lethal lesions at a given dose is equal to -ln(S), and since the radiation response is well characterized by a LQ function, the number of remaining lethal lesions that define this response can be characterized by the following equation:

$$lethal\ lesions\ /\ cell = \alpha d + \beta d^2 \qquad\qquad \text{Equation 3-9}$$

The number of induced lesions that are not repaired can then be determined as a function of dose by taking the ratio of these two equations:

$$fraction\ of\ lesions\ not\ repaired = \frac{\alpha d + \beta d^2}{a_l d} = \frac{\alpha}{a_l} + \frac{\beta}{a_l} d = c_1 + c_2 d \qquad \text{Equation 3-10}$$

This interpretation of the model implies that the constants c_1 and c_2, which are proportional to the measured α and β values, respectively, are both related to the repairability of the induced lesions. In this hypothesis, the c_1 value is equal to the initial (low dose) fraction of irreparable lesions, while the c_2 value is equal to the rate of increase in the fraction of irreparable lesions as a function of dose. Interestingly, equation 3-10 scaled by the factor a, is identical to the -ln(S)/d plots shown in the results section for the different cell lines. Interpretation of the model in this fashion implies that cell lines with small α values are those which, at low doses, are able to repair a large fraction of the induced lesions. They would thus be characterized by a small c_1 value, and in the extreme case where the initial slope of the survival curve is zero, the c_1 value would also be zero, and all lesions induced at low dose would be repairable. Cell survival curves that are characterized by a large β value imply that the c_2 value is large, and thus there would be a large increase in the fraction of unrepaired lesions with increasing dose. In the extreme case where the β parameter was equal to zero, and thus survival curve completely exponential, the c_2 parameter would also be zero, and there would be no dose dependence for the fraction of unrepaired lesions. This could occur both in a cell line with a small α value (small c_1 value and a high level of repair) and in one with a large α value (large c_1 value and a low level of repair). It should be pointed out that the increase in the fraction of unrepaired lesions characterized by c_2 (or β), could result either from repair saturation, or from an increased complexity of lesion that is created at higher dose.

If this interpretation is applied to the results with the cell lines studied here, HT-29 cells that have a small α value, and small α/β ratio, would have a small c_1 value and

thus only a small number of irreparable lesions. Most of the cell kill in this cell line would thus result from a comparatively large c_2 value such that at higher dose an increasing fraction of lesions is irreparable. DU145 cells, which are characterized by a more exponential response, would have a higher proportion of irreparable lesions, but exhibit only a small increase in the fraction of unrepaired lesions as a function of dose. In terms of the implications for sensitization, this model suggests somewhat different conclusions regarding the two hypoxic sensitizers RB6145 and etanidazole. Treatment with either sensitizer might increase the initial number of lesions ($a_i d$), but since this affects α and β equally, selective modification of either α or β implies that the repair constants c_1 and c_2 would also be selectively modified. Sensitization with etanidazole predominantly modifies the β parameter, and thus according to this model, the drug increases the relative *yield* of unrepaired lesions as a function of dose. This could be due in part to an increased number of lethal lesions (*i.e.*, repair saturation), since the number of induced lesions (*ad*) would also be expected to increase. Sensitization with RB6145 resulted in a selective increase in the α component, and thus this model would suggest that at low dose the fraction of irreparable lesions rises after treatment with this drug. This reduction in repairability of lesions would be consistent with the DNA binding ability of this drug, which could presumably interfere with DNA repair enzymes. If this were the case, then one would expect the largest effect in cell lines where there is initially a large fraction of repairable lesions (*e.g.*, HT-29 cells) and in those cell lines in which the drug is most effective in its binding ability.

4

HYPERSENSITIVITY AT LOW DOSES IN

HUMAN TUMOUR CELLS

4.1 Introduction

In chapter 3 it was shown that the low dose radiation response played an important role in determining both the absolute efficacy of different radiosensitizers and the dependence on radiation dose, of that efficacy, in different human tumour cell lines. This finding adds further weight to the argument that the shape of the low dose response, as well as the absolute value of the intrinsic radiosensitivity, will be important determinants of clinical outcome. In order to understand the mechanisms by which radiation causes cell inactivation, clearly one must understand the dose-response relationship for this agent. Since the earliest use of the colony forming assay for measurement of the *in vitro* survival curve (Puck and Marcus 1956), investigators have measured the responses of a large number of different cell lines exhibiting a wide range in sensitivity. Attempts to interpret these responses through the application of mathematical models had until recently, focused on the description of the radiation response at high doses (*e.g.*, the terminal slope on the radiation survival curve). This is because it is much more difficult to measure the radiation response at low doses due to the statistical uncertainty present in radiation survival data. Due to the nature of this assay, where one measures survival to assess lethality, the relative uncertainty is greatest at low doses of radiation, where the radiation effect is small.

The effects of low doses of radiation are important for several reasons. There is widespread concern in the general public in regard to the risks of low-level background radiation. The greatest risk that these low level exposures pose is that of carcinogenesis. However, it is difficult, if not impossible, to perform conclusive studies to determine the

relative risk of cancer induction after exposure to very low doses of radiation. This is due to both the long latent period associated with cancer induction, and the extremely small excess risk of cancer which small doses confer. As a result, the current low-dose risk estimates evaluated by various national and international committees and regulatory groups (including the International Commission on Radiological Protection - ICRP (1991), the United Nations Scientific Committee on the Biological Effects of Atomic Radiation - UNSCEAR (1988) and the Committee on the Biological Effects of Ionizing Radiation - BEIR V report (1990)) rely heavily upon extrapolation of data obtained from larger radiation exposures. These data have come from a variety of nuclear accidents, medical exposures, and occupational exposures, but the largest and most reliable data are those from the continued lifespan study (LSS) of the Japanese atomic bomb survivors (Shimizu *et al.* 1989, 1990, Mabuchi *et al.* 1994, Preston *et al.* 1994, Ron *et al.* 1994, Thompson *et al.* 1994). Although there are some studies of cancer incidence at much lower doses, the results are rather inconclusive, and in review the BEIR V committee, for example, concluded that they were generally not useful for determination of risk estimates.

Extrapolation from higher dose data is dependent upon the choice of a theoretical (or empirical) model, and assumes that the mechanisms responsible for the effects of radiation are well understood. Clearly this is not the case, and thus there is a need to measure the effects of radiation at the lowest possible dose in order to infer with the best accuracy, the effects of low level radiation exposure on the general public.

The radiation effects at very low doses are also important because an understanding of the low dose response might reveal mechanisms to explain the very different radiosensitivity patterns that are observed between different human cell lines at clinically relevant doses. The work of Malaise and colleagues (Fertil and Malaise 1981, 1985, Fertil *et al.* 1984, Malaise *et al.* 1987) which showed that the variability among different human tumour cell lines at low dose correlated with the diverse clinical outcomes of different tumours, along with that of Skarsgard and colleagues which identified an extremely wide range in α and β values when survival was *measured* rather than extrapolated, at clinically relevant doses, emphasizes the importance of understanding the mechanisms that lead to low dose radiation effects. This understanding should lead to improved treatment strategies for tumour control in the clinic.

Until recently, it has been technically difficult to measure cell survival after irradiation with doses in the range 0-1 Gy, and thus little is known about the response of different cells in this important dose region. This is because measurement of cell survival at low doses of radiation is complicated by the presence of random errors in counting, plating and dilution associated with standard clonogenic assays (Boag 1975, Bedford and Griggs 1975, Durand 1986). Two methods have been used extensively to improve upon this resolution, the Dynamic Microscope Image Processing Scanner (DMIPS) microscopic assay which recognizes and counts cells individually (Palcic *et al.* 1983, 1984a, 1984b, Palcic and Skarsgard 1984, Skarsgard *et al.* 1986, Palcic and Jaggi 1986, Marples and Joiner 1993, Lambin *et al.* 1993), and the cell sorting assay, optimized in this laboratory (Durand 1984a, 1986, Skarsgard *et al.* 1986, 1991, 1992, 1993, 1994a,

1995, Skarsgard and Harrison 1991, Skwarchuk *et al.* 1993, Wouters and Skarsgard 1994, Wouters *et al.* 1995). The cell sorting assay allows one to count and plate an accurately known number of cells, thereby changing the survival distribution from Poisson to binomial, and also reduces the random error associated with dilution and plating. This assay also retains the ability to make multiple measurements of survival involving a large number of cells over a large range of radiation doses. With this ability, data averaging can be used to remove much of the other random error associated with survival measurement. Data averaging is the only way to reduce the error associated with the random distribution of the radiation event itself, and this becomes particularly important at low doses where the initial damage level is small, and hence the variance comparatively large. This assay was sufficiently precise to identify substructure associated with cell-cycle subpopulations of different radiosensitivity, at clinically relevant doses (Skarsgard *et al.* 1991, 1992, 1993, 1994a, 1995, Skwarchuk *et al.* 1993), and was used in chapter 3 to assess the efficacy of hypoxic radiosensitizers at low doses of radiation.

Using the microscopic assay, several authors have recently reported another form of substructure in the radiation response curve at doses below 1 Gy. Marples and Joiner (1993) showed that the response at very low doses may be significantly different from that which would be predicted by back extrapolation of the linear quadratic (LQ) model. They measured cell survival with the DMIPS assay in V79 cells at doses significantly below 1 Gy and found that very low single doses of radiation were more effective than predicted by the LQ model, inferring that these cells exhibit a region of low dose

hypersensitivity followed by an increase in radioresistance (Marples and Joiner 1993). This phenomenon has since been measured in several human cell lines using the same assay (Lambin *et al.* 1993, 1994a, 1994b, Singh *et al.* 1994), and has also been implicated for the survival of cells irradiated in vivo (Joiner and Johns 1988). Marples and Joiner have suggested that this effect may be due to a radiation-induced repair mechanism that offers protection at higher doses of radiation. This proposal is similar to one offered by Calkins *et al.* (1989) to explain an unusual low dose response measured using a conventional cell survival assay.

The purpose of this chapter is to determine the very low dose response of several human tumour cell lines in order to identify possible mechanisms that may be responsible for their differences in intrinsic radiosensitivity at higher doses. To do this, the cell sorting assay has been adapted to measure survival at doses as low as 0.05 Gy. Three human tumour cell lines were chosen for low dose radiosensitivity measurements. The extreme level of precision required for measurement at low doses demands that the cell lines under investigation possess certain qualities. First, high plating efficiencies are desirable to limit the statistical variation due to this factor alone. Secondly, the ability to score colonies with accuracy is also important. These two requirements were met with the two radioresistant cell lines, HT-29 and DU145, which were previously investigated in chapter 3. These two are also well-suited for investigation of mechanistic differences because they represent cell lines that have similar high dose sensitivity, but very different shape, and as we have seen, this had important implications for the use and evaluation of hypoxic cell radiosensitizers. The sensitive cell line, HT-144, which was used in chapter

3, has a low plating efficiency (~25%) and forms colonies that are more difficult to score accurately. For this reason, the cell line A549 (lung adenocarcinoma) was chosen for investigation instead. This is an interesting cell line that has an intermediate sensitivity, a high plating efficiency, and forms easily scorable colonies. The dose range was limited to a maximum value of 4 Gy in order to minimize the influence of substructure observed in the response of these cell lines resulting from cell-cycle associated subpopulations of cells of different radiosensitivity. As illustrated previously in chapter 3, the radiation response above approximately 4 Gy (aerobic data) is more resistant than would be predicted from the low dose data due, most likely, to selection of resistant cells in the heterogeneous population.

4.2 Results

4.2.1 Radiation Survival At Very Low Dose

The measurement of cell survival following very low radiation doses, where only a small percentage of cells are killed, requires an assay with high precision and high accuracy. The cell sorting assay, which proved useful in identifying the fine substructure in the radiation response at clinical doses, was adopted to investigate the very low dose response in human tumour cell lines. The first series of experiments was carried out using a protocol identical to that used for irradiation of cells under aerobic conditions (see 2.2.1.1), where cells were trypsinized, irradiated in a stirred suspension at 37°C, placed on ice, and then sorted and plated. Figure 4-1 shows the first attempt at obtaining high precision radiation survival data at very low doses for the HT-29 cell line. Although the first two data points in the response shown in the right frame indicate a possible hypersensitive response, the results are ambiguous.

4.2.1.1 DU145 Human Prostate Carcinoma Cells

4.2.1.1.1 Postsort Protocol

In order to improve upon the precision of these data, a number of refinements to the assay were made. One of these was the elimination of the low temperature incubation of cells following irradiation. Incubation of cells at temperatures significantly below 37°C disrupts their progression through the cell cycle, and since repair of radiation damage can occur without cell cycle progression (Elkind *et al.* 1965) incubation at low temperature may alter the absolute amount of repair that is possible in growing cells.
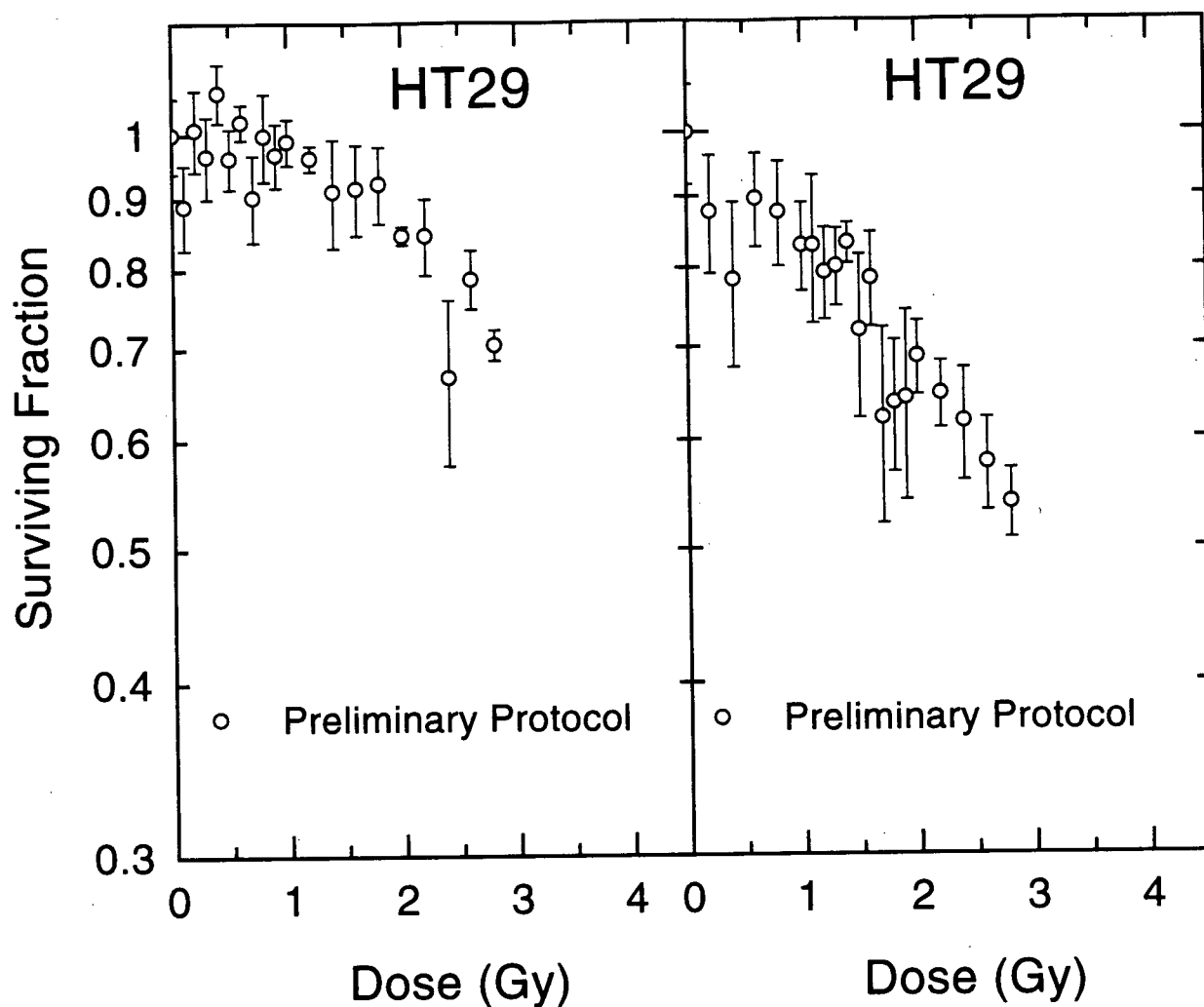
Figure 4-1 Preliminary Low-Dose Radiation Survival Experiment
Cell survival data of asynchronous HT-29 human colon carcinoma cells irradiated with low doses of X-rays. Survival was measured using the cell sorting assay in its original form (see 2.2.1.1) with irradiation taking place at 37°C in suspension. Prior to cell sorting and plating, irradiated cell samples were placed on ice. The data shown in each frame are the results from a single dose response measurement with each point representing the average from six individual Petri dishes. Error bars are the standard error in the mean.

To eliminate these effects, and to ensure consistent treatment of all irradiated cells, optimal growth conditions were maintained throughout the experimental procedure. Thus, following irradiation at 37°C, cells were immediately placed in a 37°C water bath and shaken in a rotary fashion at 200 RPM to prevent cell clumping. Cells were maintained in this condition until cell sorting was initiated. Because irradiation took place over a shorter period of time (approximately 15-20 minutes), than that required for sorting all samples (approximately 1 hour), some cell samples remained in the shaker bath for a longer period of time than others. However, care was taken to ensure that all samples received this treatment for at least 10 minutes, and most of the very low dose samples (0-1 Gy) were incubated for similar periods of time. This procedure was termed the postsort protocol because cell sorting took place following irradiation.

The postsort protocol was used to measure 8 complete radiation survival responses in DU145 cells. For each of these 8 survival responses, the clonogenic fraction was measured at 18-20 dose points over the dose range 0.05-4 Gy. At each of these dose points, two suspension samples were drawn from the irradiation vessel and from each, 3 aliquots of cells were sorted (appropriate numbers to produce 400-600 colonies) and then plated with growth medium and feeder cells into 100 mm Petri dishes. Thus the survival at each dose point in this data set from 8 cumulative responses is the average of approximately 48 Petri dishes producing a total of approximately 24, 000 colonies. This extensive data averaging was required to reduce the statistical error in the assay to an acceptable level for measurement of survival at very low doses where the radiation effect (cell killing) is small. Figure 4-2 is a scatter plot of this data set that shows the surviving

fraction calculated from each of the individual Petri dishes at each dose point (*i.e.,* 48

measurements/dose point). Although the degree of variability observed in this plot at first

glance, appears quite large, one must consider that the survival values plotted are within

the first log of cell kill. Although the variability is larger than that which can be attrib-

uted to binomial statistics alone (see detailed analysis of HT-29 data in section 4.2.2), if

one plots these individual measurements on a more typical survival scale extending over

4 logs of cell inactivation (see fig.4-3), the variability is comparatively small.

The average radiation survival response and the standard error in the mean

calculated from the 8 survival responses measured in DU145 cells using the postsort

protocol, are plotted in figure 4-4. The data in this figure show an initial hypersensitive

region below 0.5 Gy, followed by an increase in radioresistance, and at doses above 1 Gy

a relatively resistant response that is more typical of this cell line. To compare directly,

the measured radiation response at very low doses, to that which would be predicted by

extrapolation of a fit of the data beyond this region, the survival data from 1-4 Gy have

been fitted with the LQ model (equation 3-4). The best fit to this region of data is shown

as the solid line in figure 4-4, and the best-fit α and β values are given in table 4-1 (see

page 162). Above approximately 0.6 Gy there is a good fit to the data, but at doses below

this value there is a significant reduction in survival levels in comparison to the predicted

(extrapolated) values. This deviation can be more effectively visualized if the data are

replotted in the form -ln(S)/d versus dose, which represents the relative effectiveness per

unit dose of the radiation at each dose point. As previously explained, if the data

followed the response of a LQ function, then one would observe a straight line with a

Figure 4-2 DU145 Postsort High Survival Scatter Plot

Individual survival measurements calculated from single Petri dishes for DU145 human prostate carcinoma cells after exposure to low doses of X-rays. The data shown in this figure comprises 8 survival responses and a total of 48 measurements at each dose point, determined using the postsort cell sorting assay. The survival for each Petri dish was determined by dividing the measured plating efficiency in the Petri dish by the average of the zero dose plating efficiencies from the appropriate survival response curve.

Figure 4-3 DU145 Postsort 'Typical' Survival Scatter Plot
Data are the same as those in figure 4-2, but plotted on a more 'typical' survival response scale. This scale, which is the same as those used to plot aerobic data for this cell line in chapter 3 (see fig. 3-13), shows that the scatter observed in these individual measurements is relatively small.

slope equal to the β parameter, and a y-intercept equal to the α parameter. Figure 4-5 shows that at doses above 0.6 Gy the data can be well described by the LQ fit. However, below this dose the relative effectiveness of the radiation increases dramatically as the dose approaches 0 Gy, corresponding to the initial steep slope in the radiation response in figure 4-4. The relative effectiveness is at a minimum at a dose of approximately 0.6 Gy, corresponding to the 'flattest' region of the survival response.

Although the precision obtained using this assay was comparatively very good, some reservations remained which could not be answered using this protocol. One of these involved the fact that because of the scatter in the data, the initial hypersensitivity could not be observed in each of the 8 individual survival responses, it became clear only in the averaged data. A second question involved the effects of the assay itself, specifically the fact that cells were sorted following irradiation, and at different times post-irradiation. This meant that the cells being sorted were not all in the same initial state, leaving open possibilities for error. One possibility is that the cell sorter might select somewhat different populations of cells after different doses of radiation. This selection bias could also occur if some of the irradiated cells were lost (due to cell-lysis or other damage) before they could be sorted. Presumably these cells would be the most heavily damaged, and thus elimination of these cells would artificially increase the measured survival. Both of these errors would be influenced by the dose of radiation given, and possibly the time at which cell samples were sorted following irradiation. Although these types of errors would normally be considered small, at very low dose where the radiation effect is also small, they could significantly influence the measured survival response.

Figure 4-4 DU145 Low Dose Survival I - Postsort Protocol
Cell survival data of asynchronous DU145 human prostate carcinoma cells irradiated with low doses of X-rays. Survival was measured using the postsort cell sorting assay with irradiation taking place at 37°C in suspension prior to cell sorting. The mean data are the average of 48 measurements from 8 individual survival responses, and error bars are the standard error in the mean. The solid line represents the best fit of the LQ model, $S=\exp(-\alpha d-\beta d^2)$, to the data above 1Gy.

Figure 4-5 DU145 Low Dose Survival II - Postsort Protocol
The DU145 low dose data obtained using the postsort protocol and shown figure 4-4 are replotted in terms of the relative effectiveness per unit dose, -ln(S)/d. The data at low dose show an increased effectiveness as compared to that which is predicted by the LQ fit of the data above 1 Gy.

4.2.1.1.2 Presort Protocol

In attempt to address these problems, a new experimental procedure was adopted termed the presort protocol. In this procedure, a stirred cell suspension at 37°C was used as a source of cells from which to sort samples prior to irradiation. Samples were sorted from this stock suspension into 5 ml test tubes, which were subsequently irradiated in a 37°C phantom and then plated for colony formation. This considerably reduced the variability in cell handling during and among different experiments. All cell samples were irradiated and plated in approximately a 5-6 minute period after being sorted. In addition all samples consisted of cells that were sorted while they were in the same initial state, before irradiation.

Four additional low dose survival responses were measured for DU145 cells over the dose range 0.05-4 Gy, using the presort protocol, and in figure 4-6 a 'scatter' plot of all measurements from individual Petri dishes is shown. Thus in this figure, at each dose point, 24 measurements of survival have been plotted. In comparison to figure 4-2, one can observe a dramatic decrease in the variability of this data, which most likely results from the increase in consistency among the handling of the cell samples. This figure also reveals what can be interpreted as a region of initial hypersensitivity at doses below approximately 0.6 Gy. Figure 4-7 shows these same data plotted on the more typical scale of 4 logs of inactivation. On this scale the degree of variability is seen to be very small.
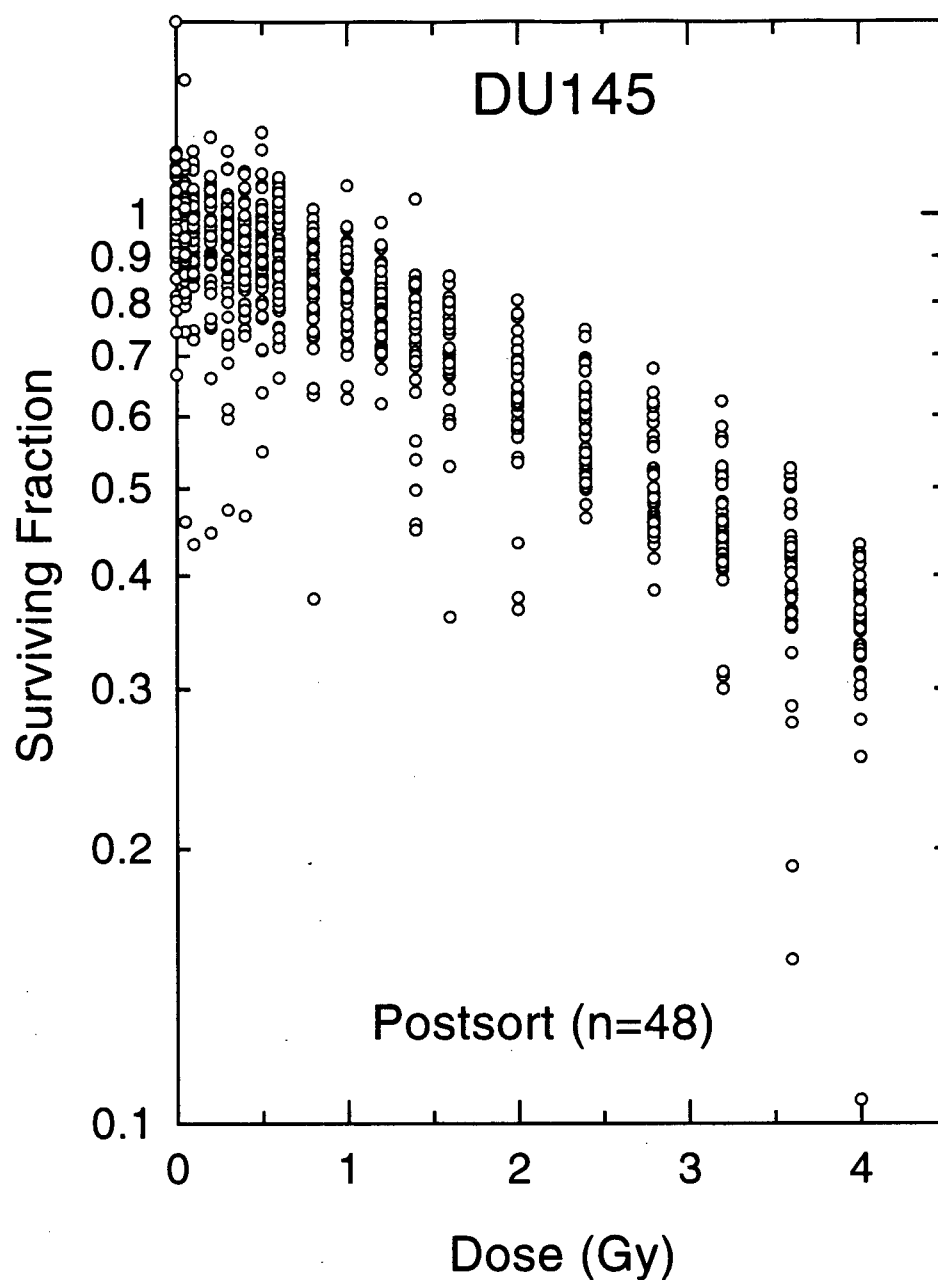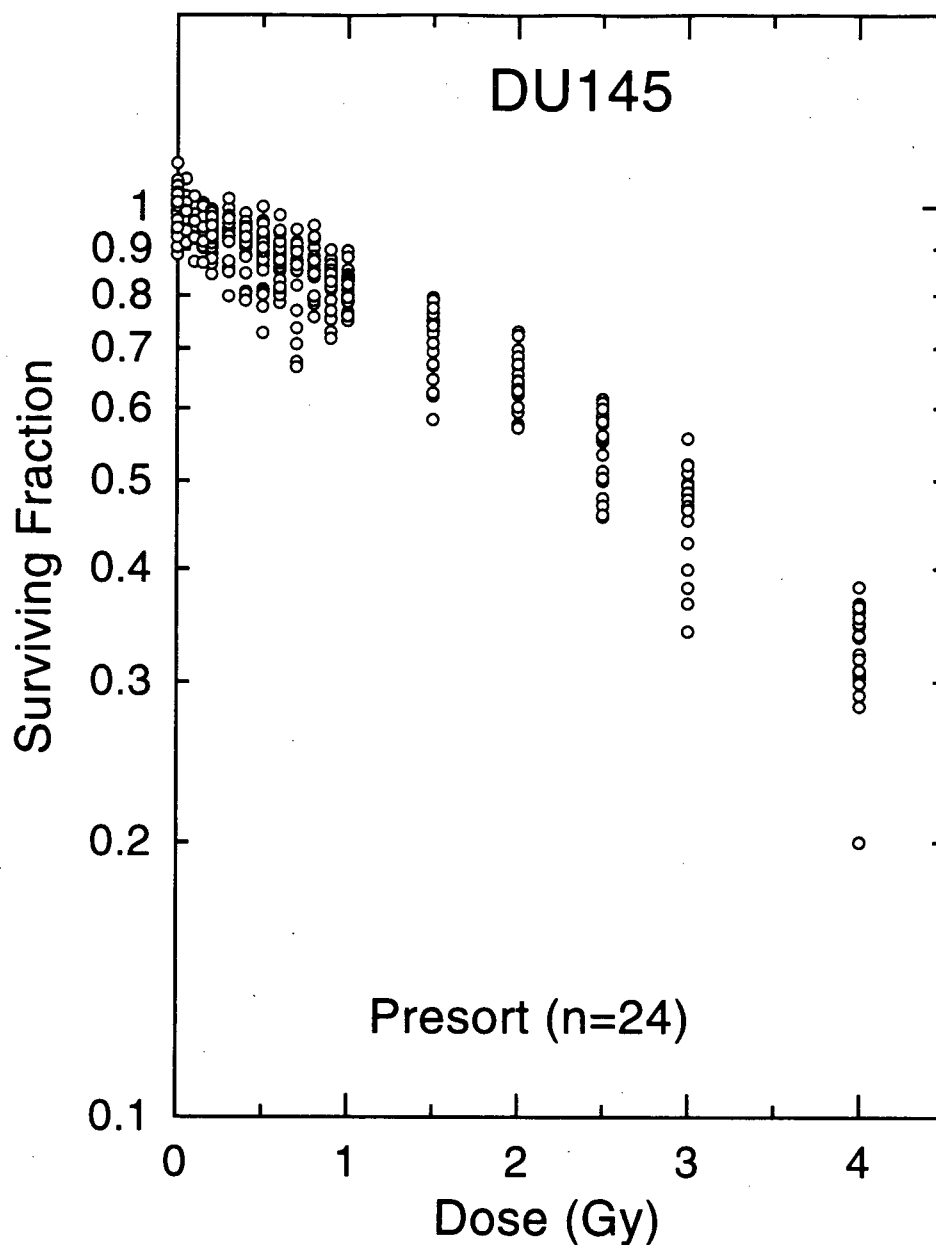
Figure 4-6 Presort High Survival Scatter Plot
Individual survival measurements calculated from single Petri dishes for DU145 human prostate carcinoma cells after exposure to low doses of X-rays. The data shown in this figure comprise 4 survival responses for a total of 24 measurements at each dose point, determined using the presort cell sorting assay. The survival for each Petri dish was determined by dividing the measured plating efficiency in the Petri dish by the average of the zero dose plating efficiencies from the appropriate survival response curve.
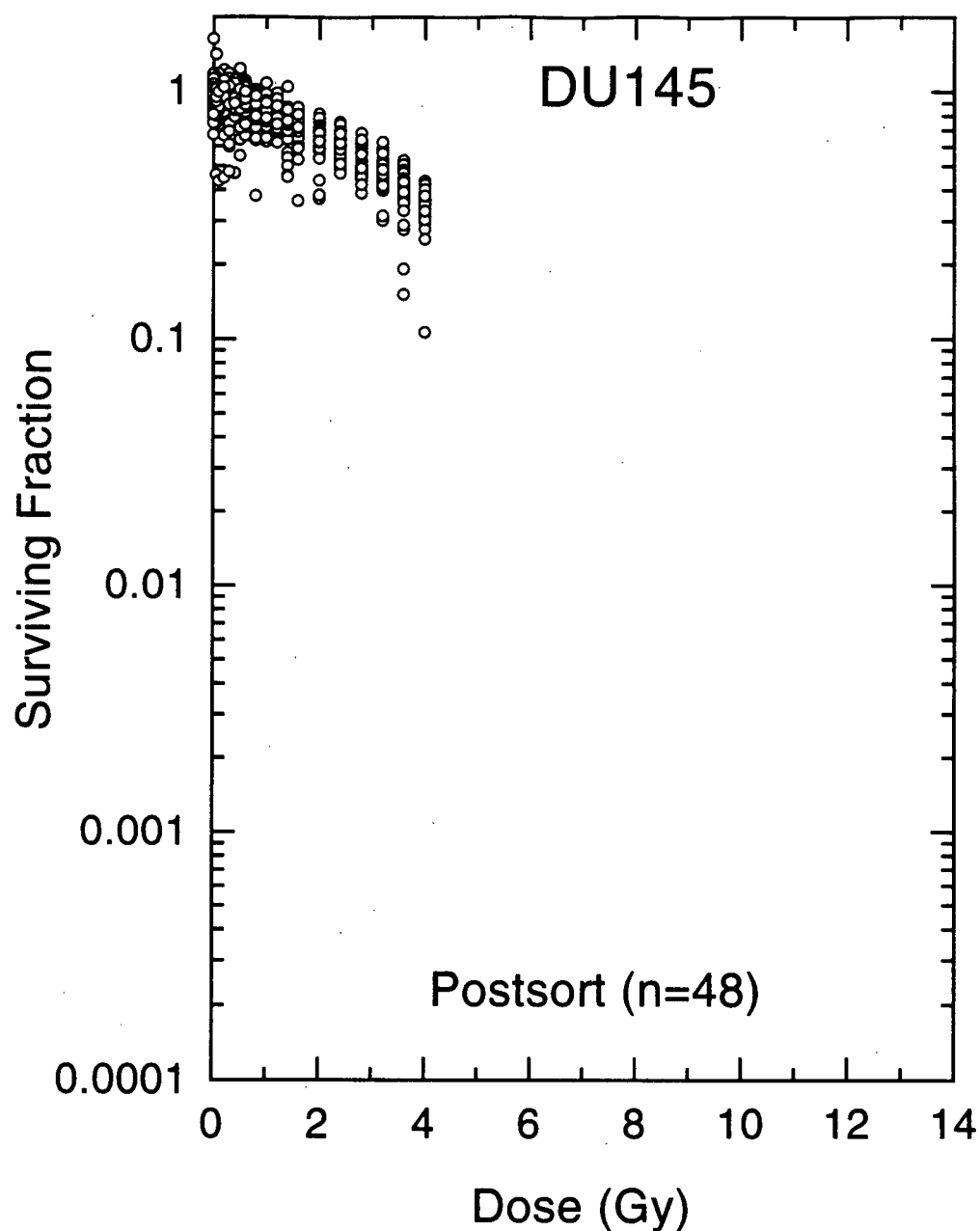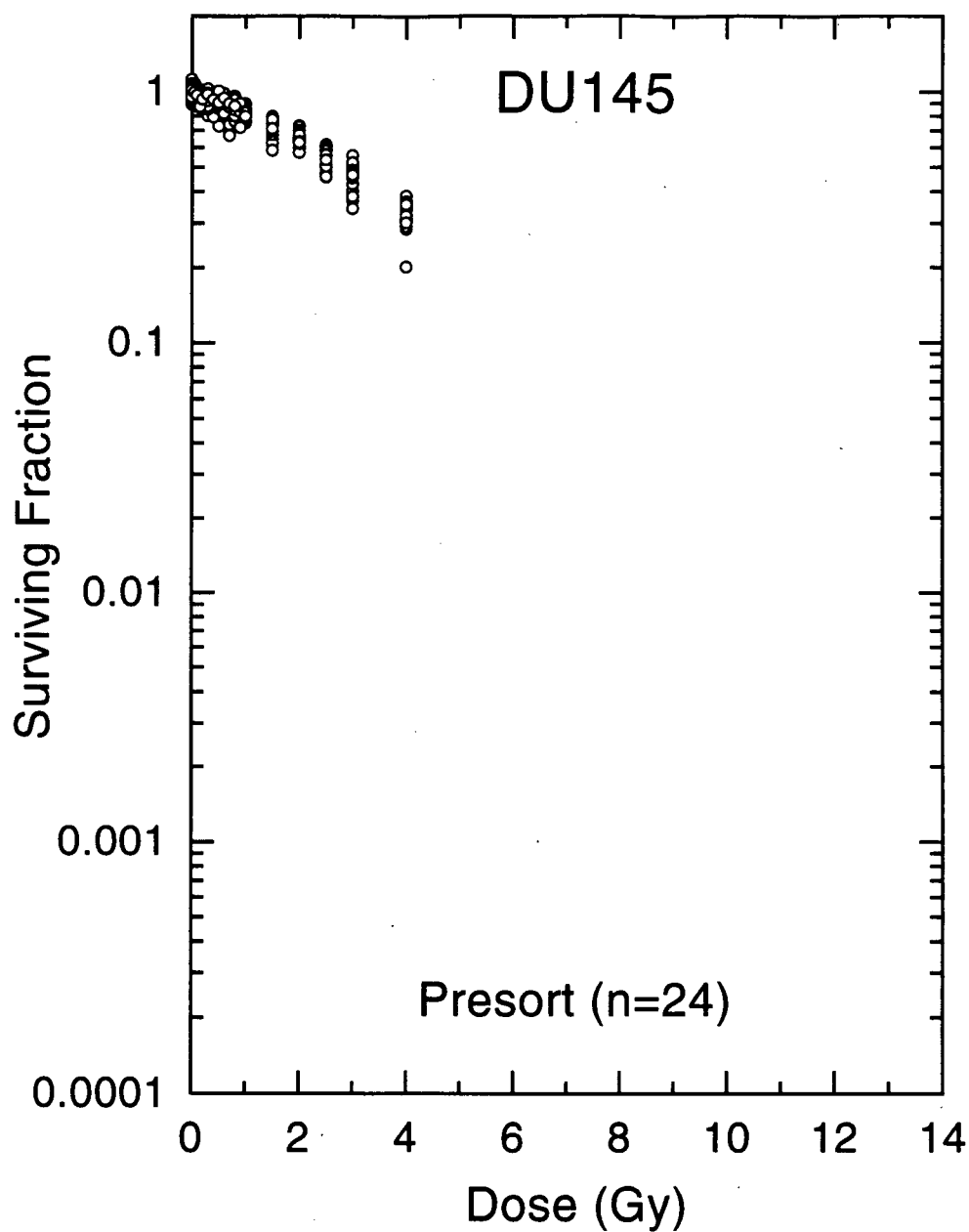
Figure 4-7 Presort 'Typical' Survival Scatter Plot
Data are the same as those in figure 4-6, but plotted on a more 'typical' survival response scale. This scale, which is the same as those used to plot aerobic data for this cell line in chapter 3 (see fig. 3-13), shows that the scatter observed in these individual measurements is considerably smaller than that obtained using the postsort protocol (fig. 4-3).

The average data and standard error in the mean determined from the four presort survival responses determined for DU145 cells are plotted in figure 4-8, and the corresponding effect per unit dose (-ln(S)/d) plot for this data set is shown in figure 4-9. Once again, the data above 1 Gy have been fitted with the LQ model (solid line in figures 4-8 and 4-9) to allow a comparison of the predicted values of survival versus the measured values (best-fit parameter values are given in table 4-1). Clearly these data exhibit a region of low dose hypersensitivity that is very similar to the average data obtained with the postsort protocol show in figure 4-4. However, because the variability in the data at each dose point has been reduced, the significance of this hypersensitivity is greater.

4.2.1.1.3 Average DU145 Data

To allow a direct comparison of these two sets of data, they have been plotted together in figure 4-10. This figure illustrates very good agreement between the two sets of data over the entire dose range, and suggests that neither of the two protocols introduces any systematic error that significantly influences the measured survival. However it is clear from these data, and from the corresponding scatter plots that the random error associated with measurement of survival using the presort protocol is much smaller than that associated with the postsort protocol. The plotted error bars which represent the standard error in the *mean*, are considerably smaller in the presort data set despite the fact that only half as many measurements were made with this protocol as compared to the postsort protocol (24 versus 48 at each dose point).
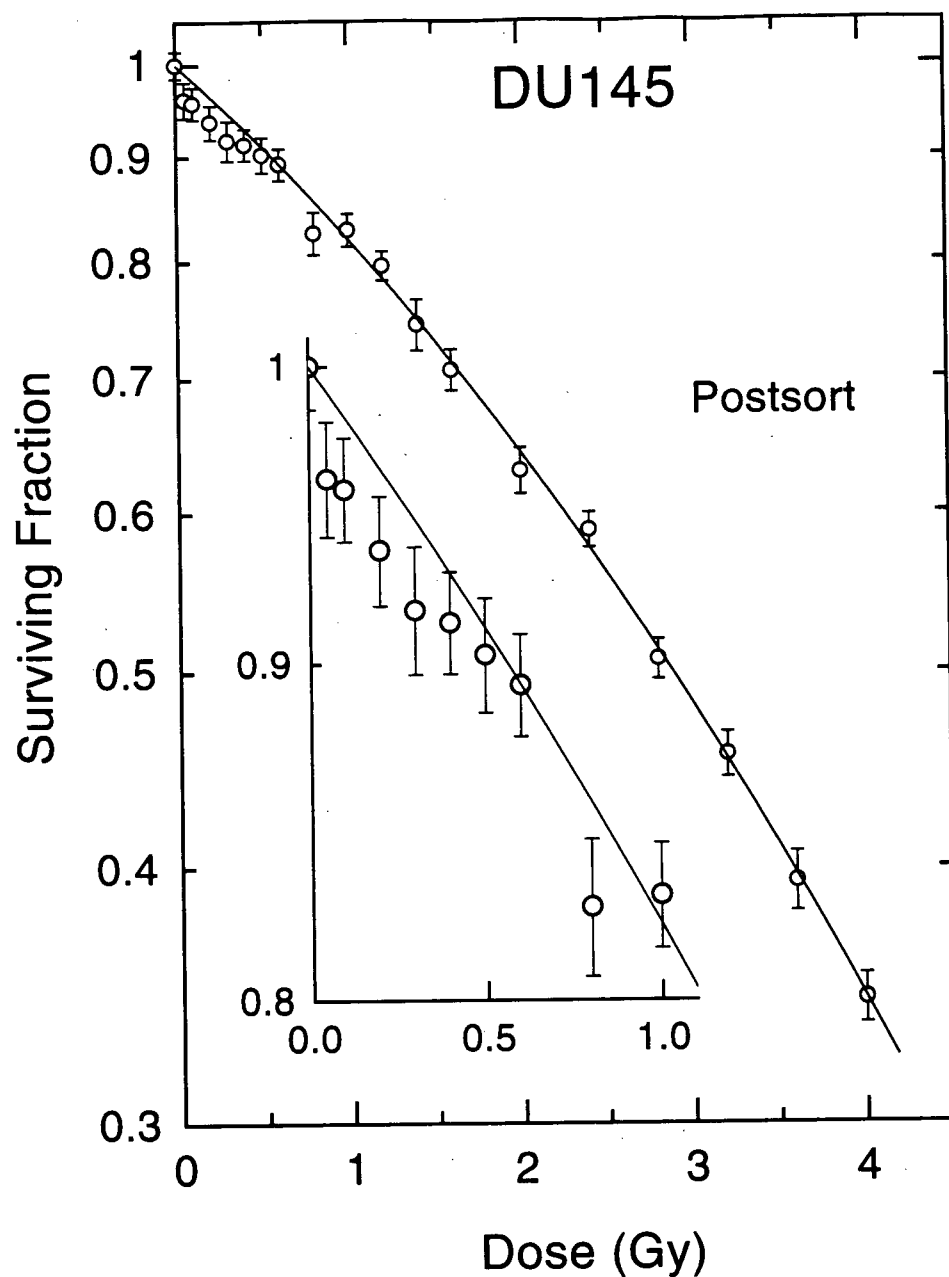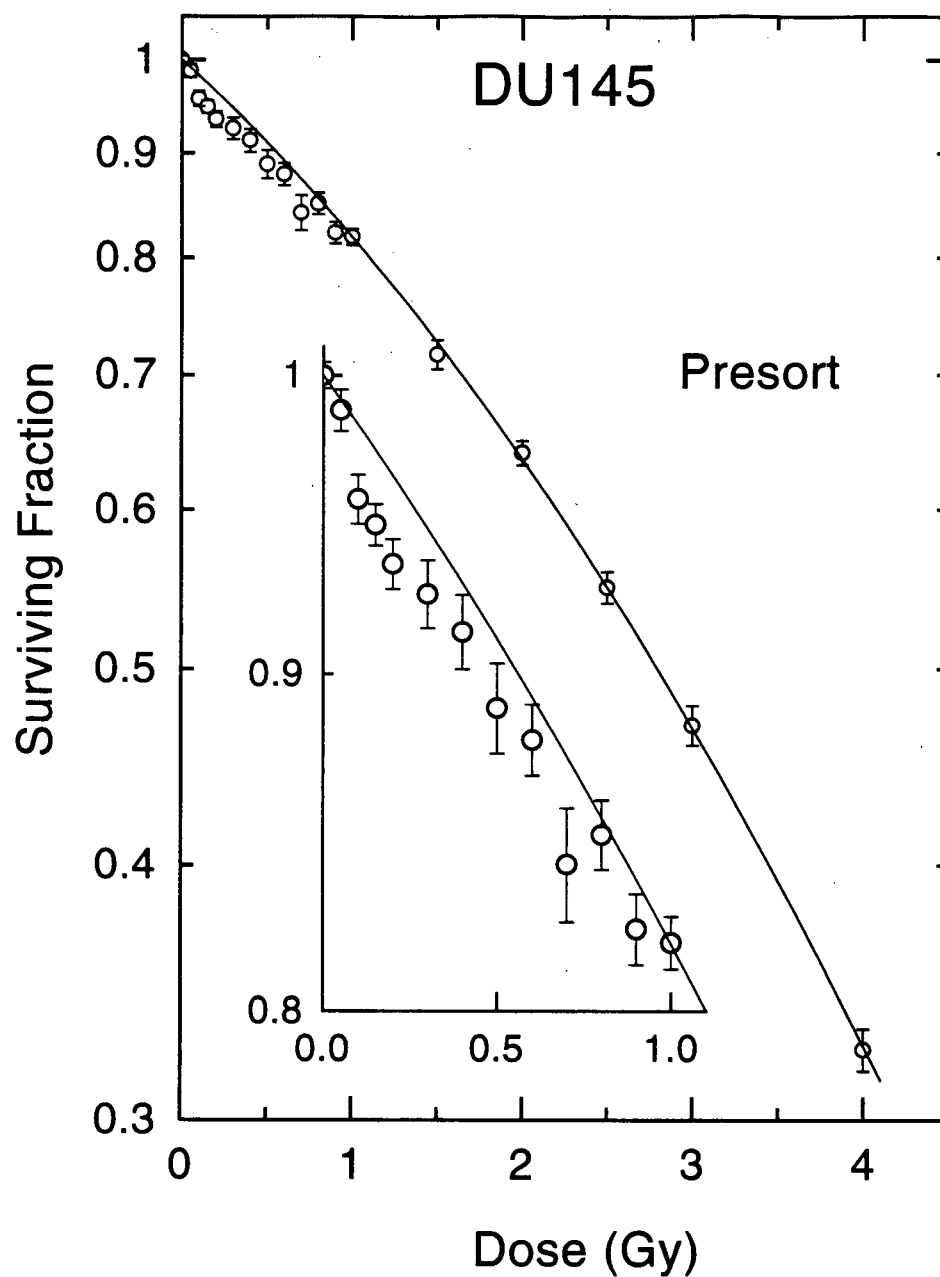
Figure 4-8 DU145 Low Dose Survival I - Presort Protocol

Cell survival data of asynchronous DU145 human prostate carcinoma cells irradiated with low doses of X-rays. Survival was measured using the presort cell sorting assay with irradiation taking place in a 37°C phantom following cell sorting. The mean data are the average of 24 measurements from 4 individual survival responses, and error bars are the standard error in the mean. The solid line represents the best fit of the LQ model, $S=\exp(-\alpha d-\beta d^2)$, to the data above 1Gy.
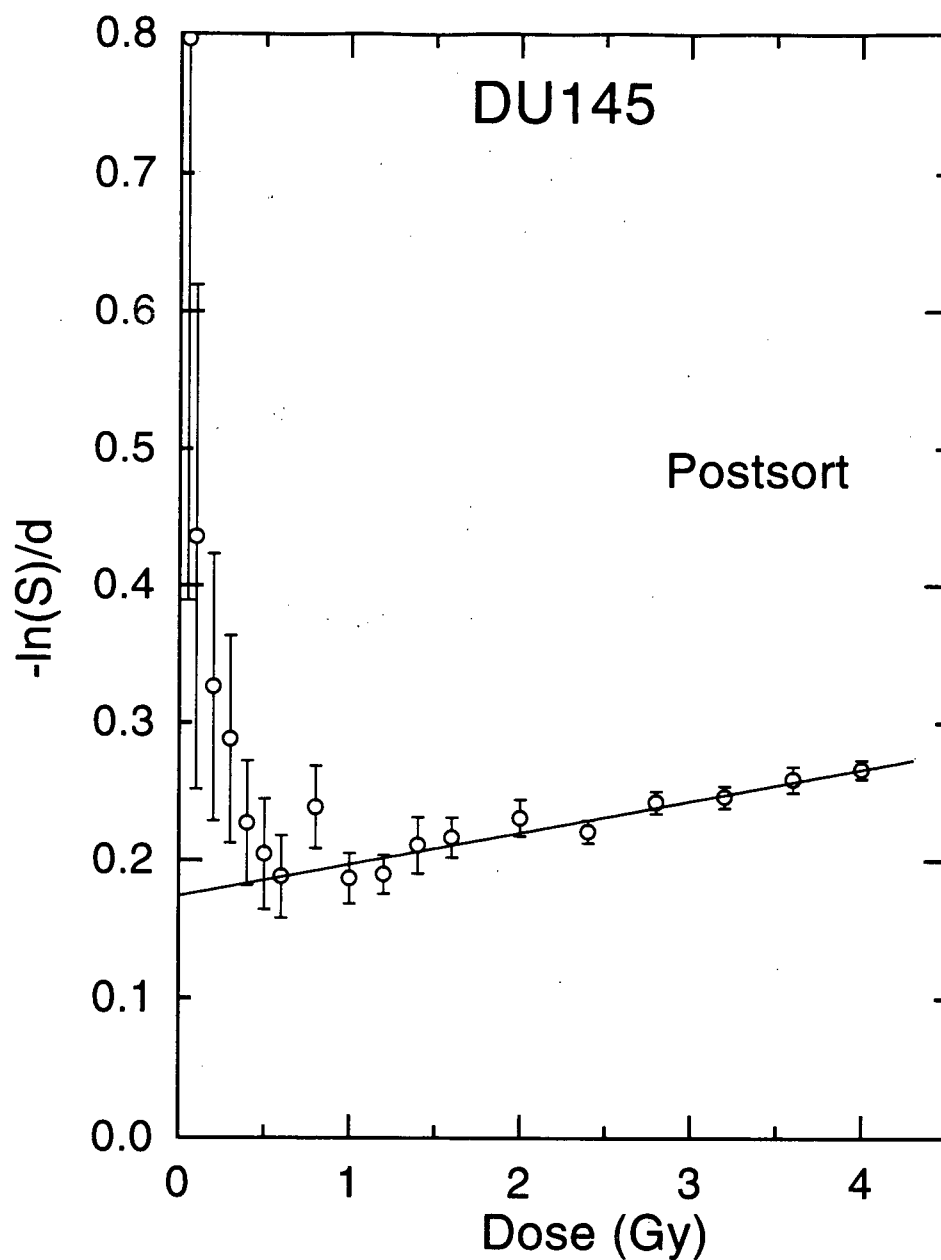
Figure 4-9 DU145 Low Dose Survival II - Presort Protocol

The DU145 low dose data obtained using the presort protocol and shown figure 4-8 are replotted in terms of the relative effectiveness per unit dose, -ln(S)/d. The data at low dose show an increased effectiveness as compared to that which is predicted by the LQ fit of the data above 1 Gy.

The lack of any significant differences in survival between the two protocols suggested the two data sets could be averaged together to further reduce the statistical error inherent to the clonogenic assay. Figures 4-11 and 4-12 show the resulting data set (the average of 12 survival responses), which has been used subsequently for all further analysis. The solid line in this fit represents the LQ fit of the data above 1 Gy, and illustrates the clear overestimation of cell survival at low doses (best-fit parameter values are given in table 4-1). The corresponding -ln(S)/d plot in figure 4-12 also visually demonstrates the increased effectiveness of radiation doses below 0.6 Gy.

4.2.1.2 HT-29 Human Colon Carcinoma Cells

The low dose radiation response was also investigated in HT-29 cells. This cell line demonstrates similar high dose sensitivity to DU145 cells, but has a different shape, exhibiting a much larger shoulder and correspondingly higher survival at low (clinical) doses. Figure 4-13 shows the average low dose radiation response calculated from a total of 15 survival responses for this cell line. Similar to the analysis for DU145 cells, the data above 1 Gy have been fitted with the LQ model to allow a comparison of the predicted values for survival to those that were measured. The HT-29 average data in figure 4-13 show a significant reduction in the measured survival as compared to the linear-quadratic predicted values (solid line) for all 10 dose points measured below 0.8 Gy, but above 1 Gy data are well characterized by the LQ fit. These data have also been plotted in terms of the relative effectiveness of the radiation per unit dose (-ln(S)/d) in figure 4-14. This plot, perhaps more clearly, demonstrates the deviation between measured and predicted values based on the LQ fit. The relative effectiveness of the
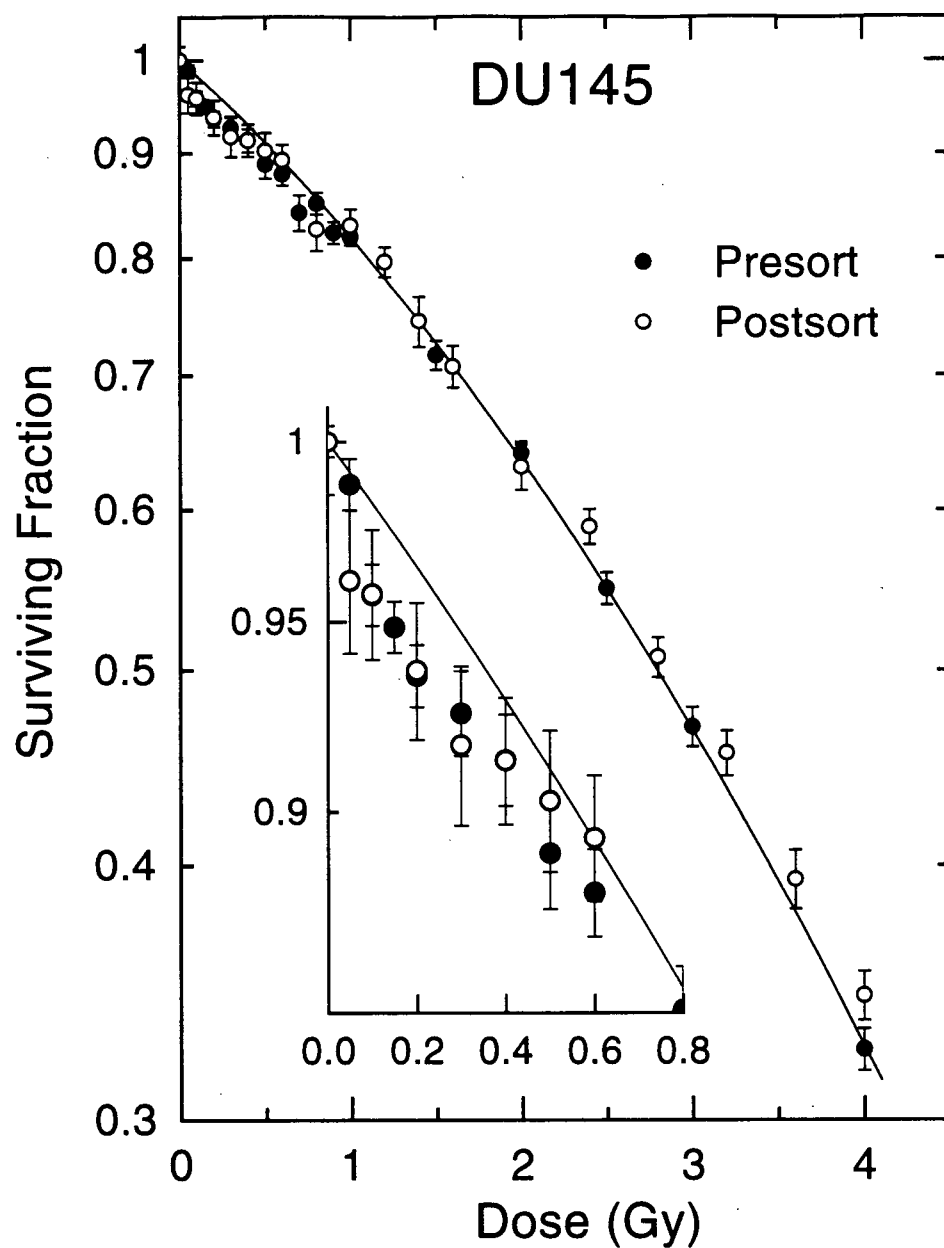
Figure 4-10 DU145 Low Dose Survival - Presort and Postsort Protocol
Comparison of the low dose data for DU145 cells obtained using either the postsort (solid circles) or presort (open circles) cell sorting assays. The data obtained using both methods are in very good agreement over the entire dose range (0-4 Gy).
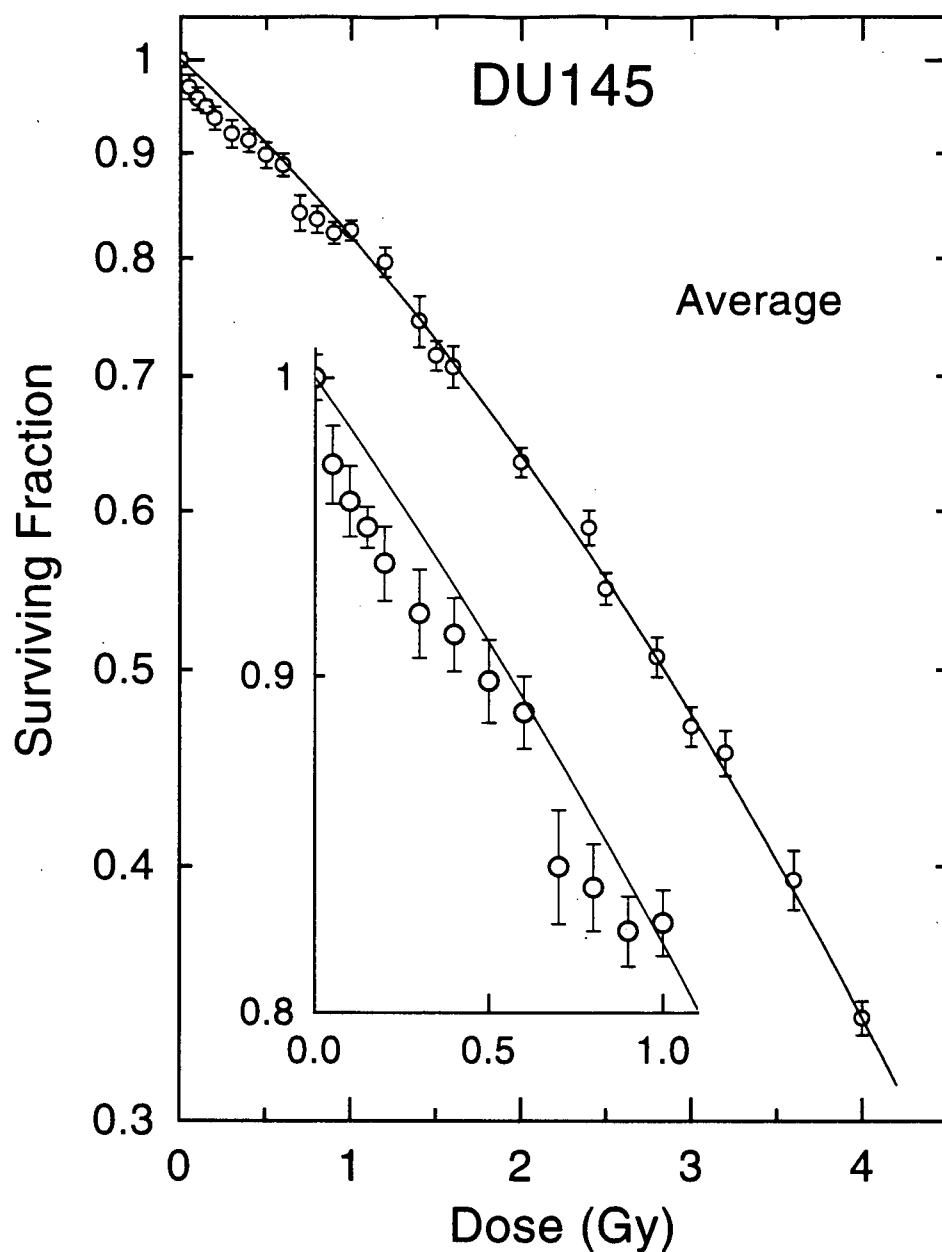
Figure 4-11 DU145 Average Low Dose Survival I
Cell survival data of asynchronous DU145 human prostate carcinoma cells irradiated with low doses of X-rays. To improve the statistical accuracy of this data set, the mean survival from the 8 responses measured using the postsort protocol (fig. 4-4), and the 4 measured using the presort protocol (fig. 4-8) have been pooled. The mean data are thus the average of 72 measurements from 12 individual survival responses, and error bars are the standard error in the mean. The solid line represents the best fit of the LQ model, $S=exp(-\alpha d-\beta d^2)$, to the data above 1Gy.
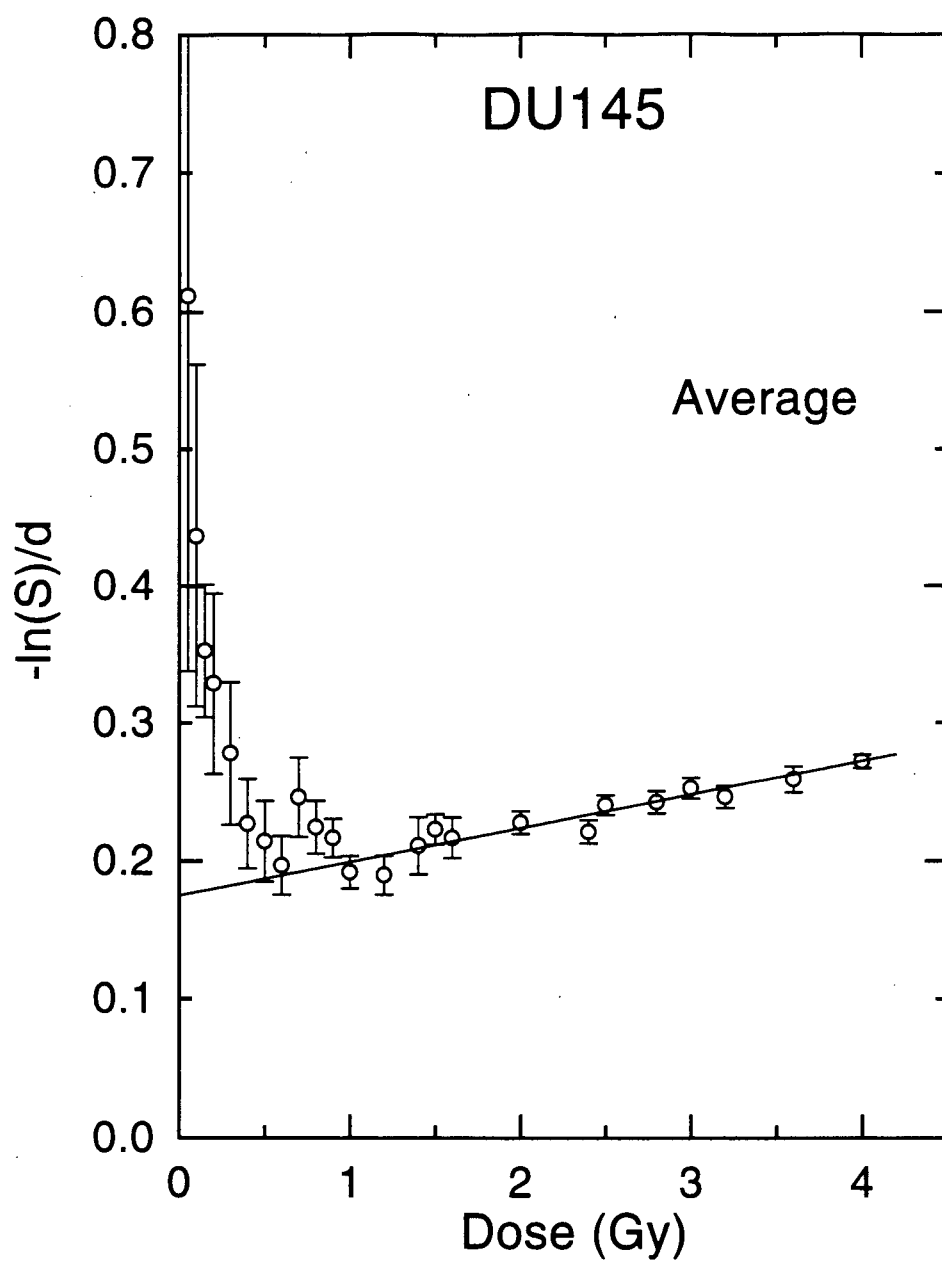
Figure 4-12 DU145 Average Low Dose Survival II
The average DU145 low dose data obtained using the presort and postsort protocols and shown figure 4-11 are replotted in terms of the relative effectiveness per unit dose, -ln(S)/d. The data at low dose show an increased effectiveness as compared to that which is predicted by the LQ fit of the data above 1 Gy.

radiation approaches a maximum as the dose approaches zero. This plot also clearly shows that the radiation effect for an incremental dose is a minimum at doses of approximately 0.8 Gy, contrary to what is predicted by the LQ model. In comparison to the DU145 cell line, the initial slope of the HT-29 radiation survival response (y-intercept in figure 4-14) is somewhat smaller, however the decrease in effectiveness per unit dose with increasing dose (below 1 Gy) persists to a higher dose before rejoining the fit to the LQ model. This is reflected in the smaller α value determined from fits of the data above 1 Gy (see table 4-1).

4.2.1.3 A549 Human Lung Carcinoma

Both HT-29 and DU145 cells are considered radiation resistant cell lines. In order to determine whether the observed low dose hypersensitivity was somehow related to the absolute intrinsic radiation sensitivity, the low dose response was investigated in the more radiosensitive cell line A549. The average low dose response determined from 8 A549 survival responses is plotted in figure 4-15, and the corresponding -ln(S)/d plot is shown in figure 4-16. The survival data above 1 Gy have again been characterized with the LQ model, and the resulting best fit is shown as the solid line in these figures (best-fit parameters are given in table 4-1). This data set also suggests a region of low dose hypersensitivity, however both the dose range of hypersensitivity and deviation from predicted values, are smaller. In this cell line the four dose points measured below 0.25 Gy illustrate a clear increased effectiveness as compared to the fitted line, while doses from 0.3 Gy to 3 Gy are reasonably well characterized by the fit (it could be argued that hypersensitivity exists to a dose as high as 1Gy). The region of hypersensitivity does show
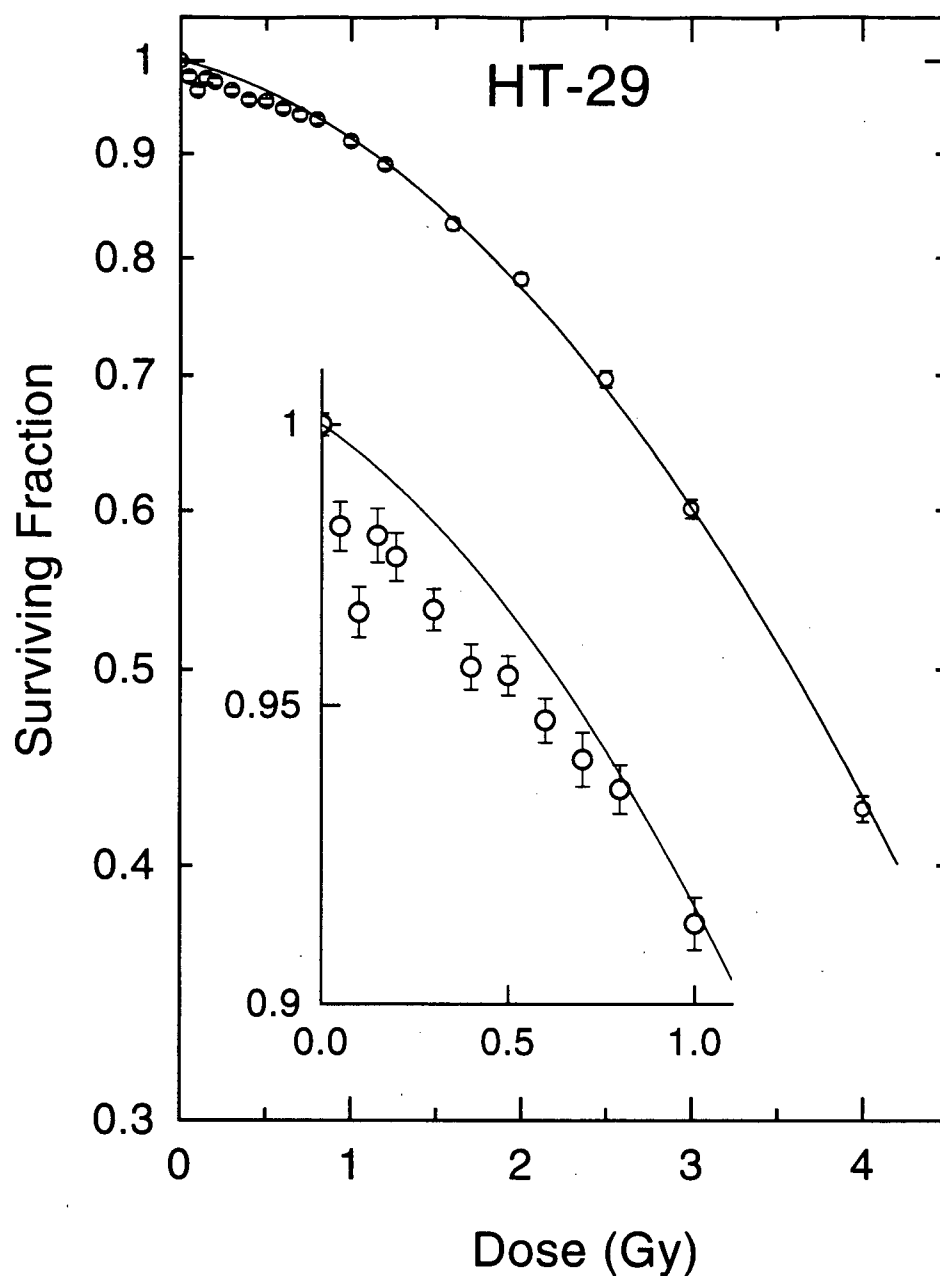
Figure 4-13 HT-29 Average Low Dose Survival I
Cell survival data of asynchronous HT-29 human colon carcinoma cells irradiated with low doses of X-rays. Survival was measured using the presort cell sorting assay with irradiation taking place in a 37°C phantom following cell sorting. The mean data are the average of 90 measurements from 15 individual survival responses, and error bars are the standard error in the mean. The solid line represents the best fit of the LQ model, $S=\exp(-\alpha d-\beta d^2)$, to the data above 1Gy.
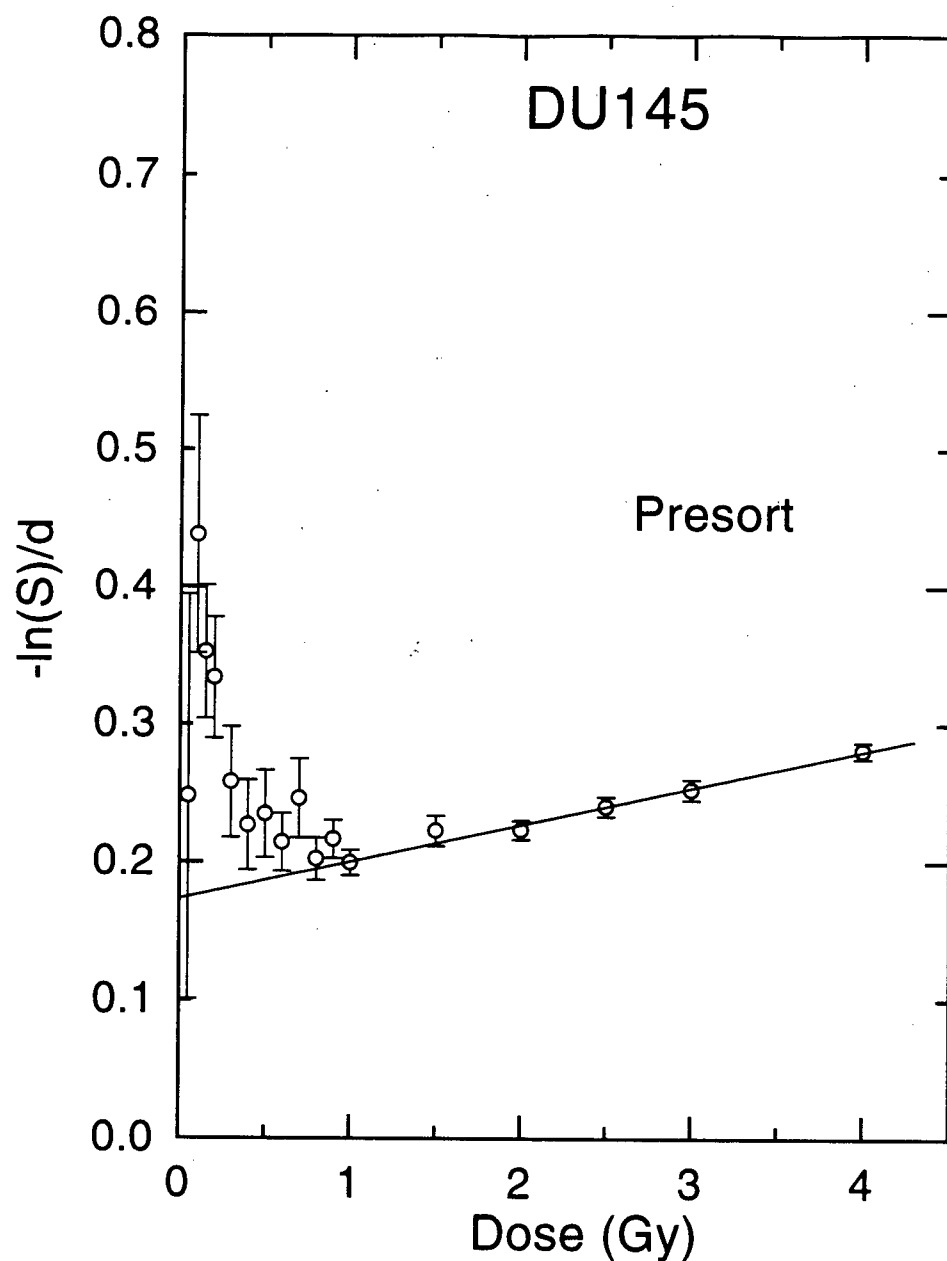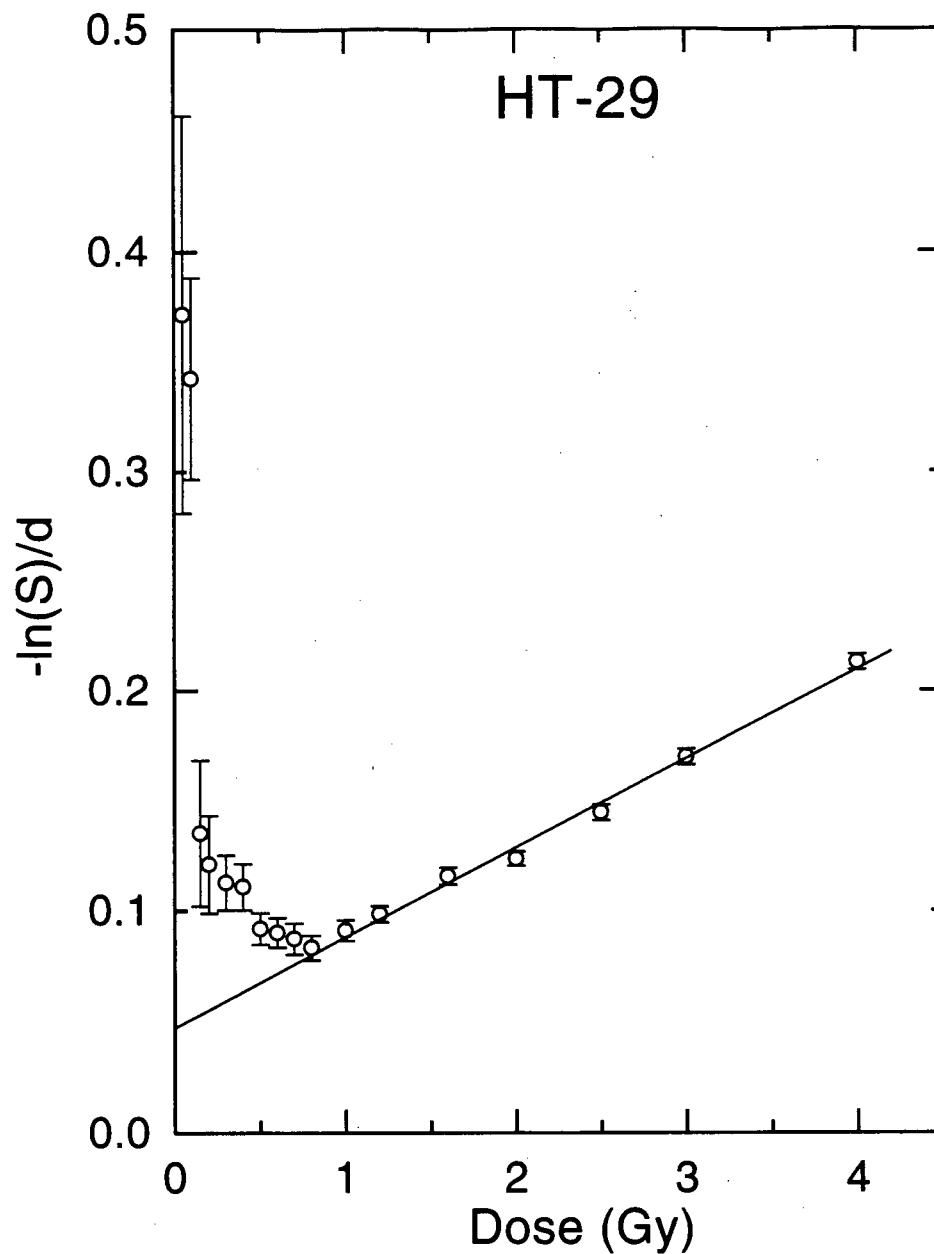
Figure 4-14 HT-29 Average Low Dose Survival II

The HT-29 low dose data obtained using the presort protocol and shown figure 4-13 are replotted in terms of the relative effectiveness per unit dose, -ln(S)/d. The data at low dose show an increased effectiveness as compared to that which is predicted by the LQ fit of the data above 1 Gy.
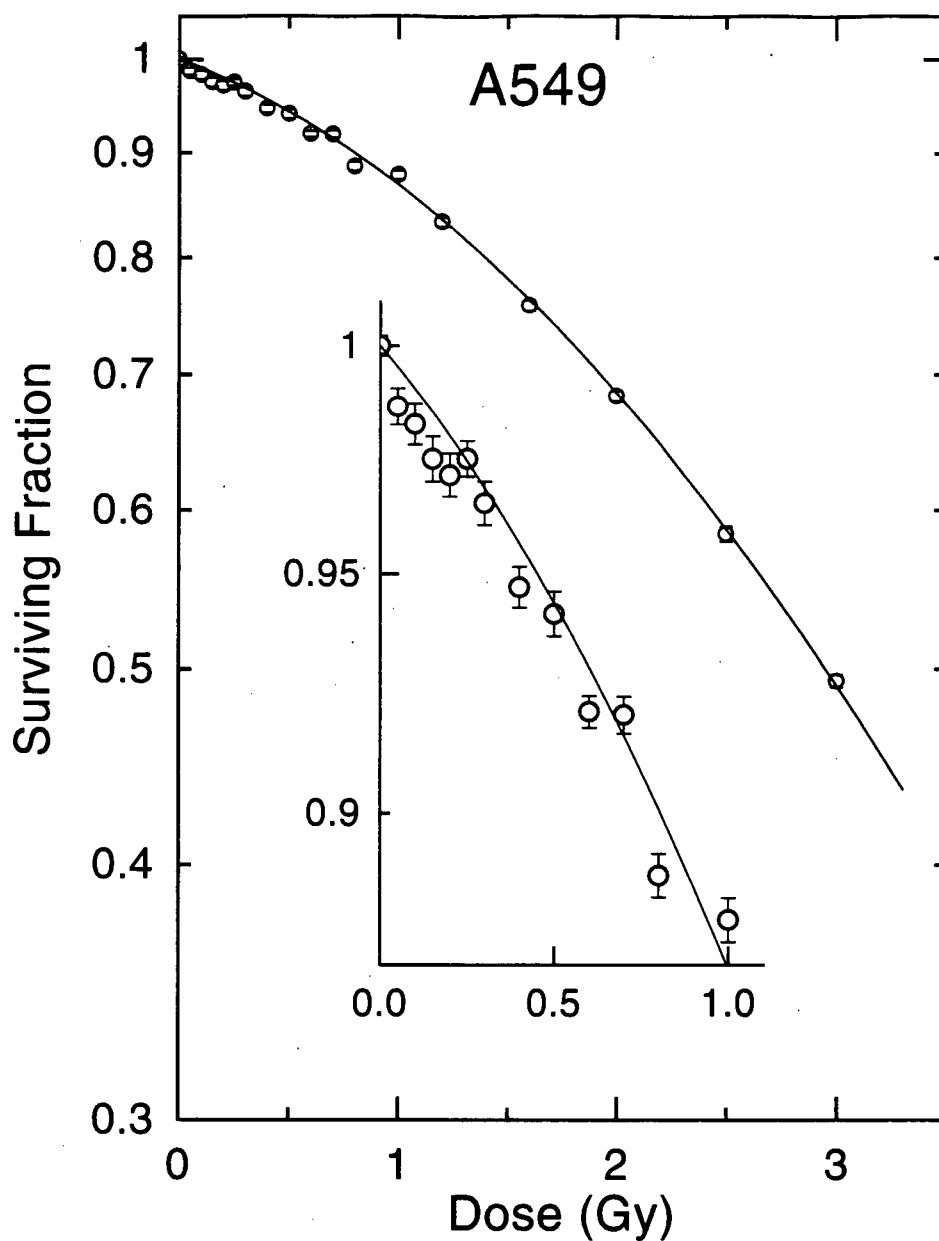
Figure 4-15 A549 Average Low Dose Survival I
Cell survival data of asynchronous A549 human lung adenocarcinoma cells irradiated with low doses of X-rays. Survival was measured using the presort cell sorting assay with irradiation taking place in a 37°C phantom following cell sorting. The mean data are the average of 24 measurements from 4 individual survival responses, and error bars are the standard error in the mean. The solid line represents the best fit of the LQ model, $S=\exp(-\alpha d-\beta d^2)$, to the data above 1Gy.
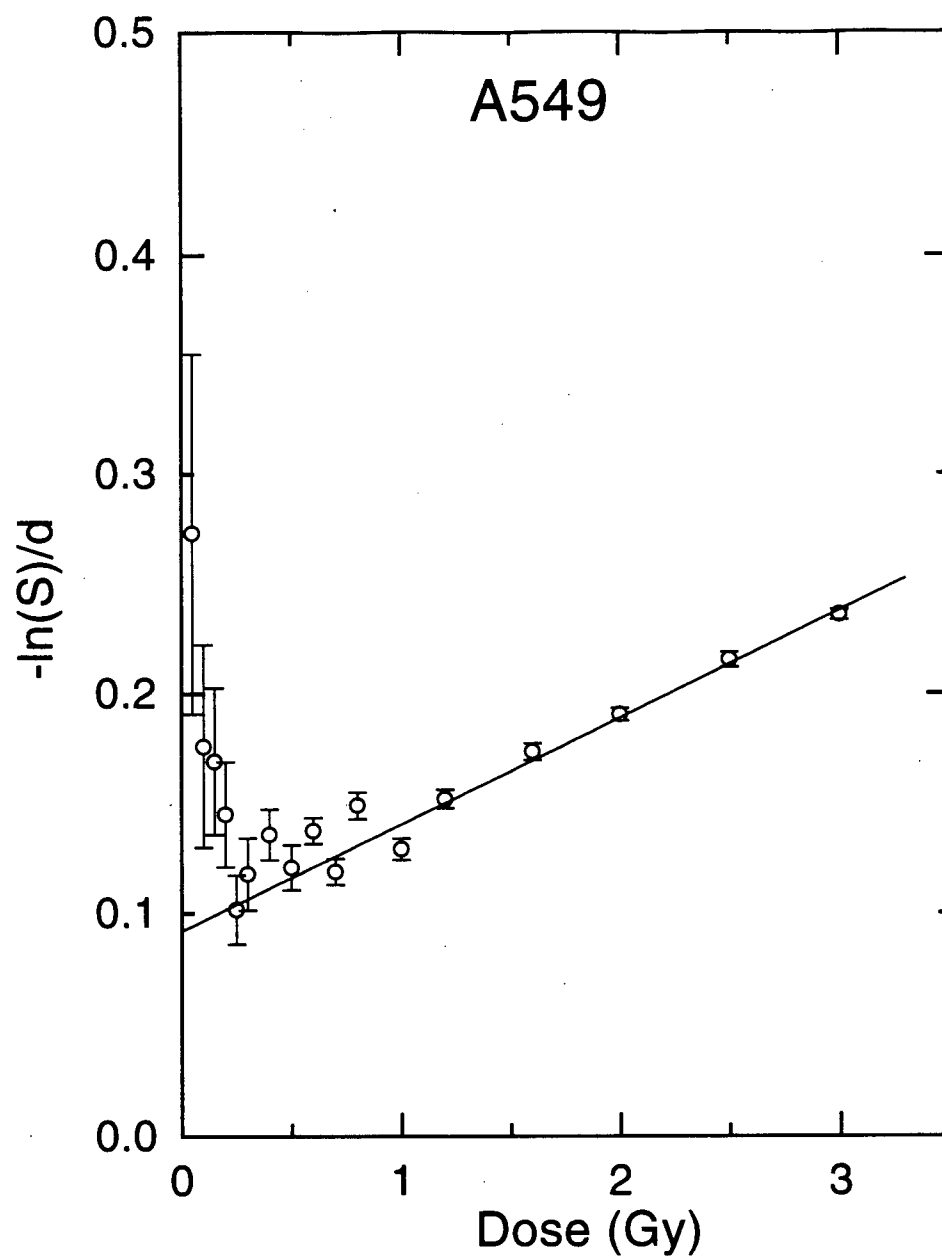
Figure 4-16 A549 Average Low Dose Survival II

The A549 low dose data obtained using the presort protocol and shown figure 4-15 are replotted in terms of the relative effectiveness per unit dose, -ln(S)/d. The data at low dose show some evidence of an increased effectiveness as compared to that which is predicted by the LQ fit of the data above 1 Gy, although to a smaller degree than either DU145 (fig 4-12) or HT-29 (fig 4-14).

the same characteristics as that observed in HT-29 and DU145 cells, with the effectiveness approaching a maximum as the dose approaches zero. For this cell line the minimum relative effectiveness is reached at a dose of 0.3 Gy (see figure 4-16).

Table 4-1 Best-Fit Parameters in the Linear Quadratic (LQ) Model.
For each data set the LQ model was fit to the data above 1Gy. Values in parenthesis are the upper and lower 95% confidence limits in the quoted values.

Data Set	α (Gy^{-1})	β (Gy^{-2})
DU145 (8 postsort responses)	.170 (.160-.180)	.0243 (.0213-.0273)
DU145 (4 presort responses)	.174 (.166-.182)	.0267 (.0237-.0297)
DU145 (average of 12 responses)	.175 (.170-.179)	.0243 (.0227-.0259)
HT-29 (15 presort responses)	.0473 (.0445-.0501)	.0406 (.0395-.0418)
A549 (8 presort responses)	.0918 (.0891-.0945)	.0486 (.0474-.0498)

4.2.2 Statistical Analysis of Survival Data

In order to evaluate the statistical significance of the observed low dose hypersensitivity, an investigation into the error associated with these survival measurements has been made using HT-29 cells as an example. The uncertainty associated with the average survival value at each dose point arises from statistical uncertainty inherent to the assay itself, as well as to biological variation from one experiment to another. Statistical analysis of the HT-29 data set allows a delineation of these two types of errors, because of the large number of survival responses that have

been measured in HT-29 cells from both low dose studies and from other experiments for which low dose responses served as controls. Thus more measurements of survival have been made for this cell line than for any other (averaged data comprise a total of 15 survival responses). These measurements have been made over a considerable period of time, with different lots of serum, and with different trypsinization protocols. Small variations in overall sensitivity from one time period to another were observed, and although the data from each of these periods showed similar evidence of a low dose hypersensitive region, the biological variation over time had the effect of increasing the overall variance not associated with simple random error. It also had the effect of 'smoothing' the substructure at very low doses. One method that has been devised for allowing comparison of such sets of data is based on the premise that the radiosensitivity modification can be approximated by a simple dose-modification throughout the entire dose range. For each data set, a quantity termed the mean inactivation dose ($\overline{D}$) is calculated, and then each data set normalized by the average of the mean inactivation doses from each data set. The mean inactivation dose is defined as the surviving fraction integrated over dose, and is thus equal to the area under the survival response (Fertil *et al.* 1984):

$$\overline{D} = \int_0^\infty S \cdot \partial d \qquad\qquad \text{Equation 4-1}$$

The 15 survival responses measured for the HT-29 cell line have been grouped into four time periods for which serum lots and trypsinization protocols were the same, and for which the overall radiation sensitivity was similar. The mean inactivation dose

for each of these groups (table 4-2) was calculated by fitting each data set with the LQ model, and then integrating the resulting function over dose. The average of the mean inactivation doses (3.96) was used to normalize the dose values in each group, producing four new data sets with somewhat different dose values. Each of the four new sets of data have been plotted together in figure 4-17. Although these data can no longer be averaged together, the composite plot illustrates a far more consistent pattern of hypersensitivity below 0.75 Gy, followed by an increased radioresistance, than would be observed among the unnormalized groups. This is despite the fact that the normalization factor for each group is determined almost independent of the response in the hypersensitive region (this region does not contribute significantly to the overall area under the survival curve). This suggests that the hypersensitivity at very low doses is a more consistent phenomenon than one would perceive simply by plotting the unnormalized data sets together. The normalized data contain many points below 0.25 Gy which demonstrate a consistent hypersensitive response in this dose range, followed by a dose region (0.25-0.75 Gy) where the survival remains essentially constant. This pattern of hypersensitivity is also illustrated in terms of the relative effectiveness per unit dose plotted in figure 4-18.

Table 4-2 Mean Inactivation Dose for HT-29 Cells
The HT-29 data set was grouped into 4 subsets and the data above 1 Gy fitted with the LQ model. The parameters from this fit were then used to determine the mean inactivation dose for that particular subset.

Data Set	α (Gy^{-1})	β (Gy^{-2})	$\overline{D}$ (Gy)
HT-29 Data Set 1 (8 responses)	.0505	.0377	3.96
HT-29 Data Set 2 (3 responses)	.0722	.0471	3.42
HT-29 Data Set 3 (2 responses)	.0671	.0349	3.92
HT-29 Data Set 4 (2 responses)	.0320	.0312	4.54
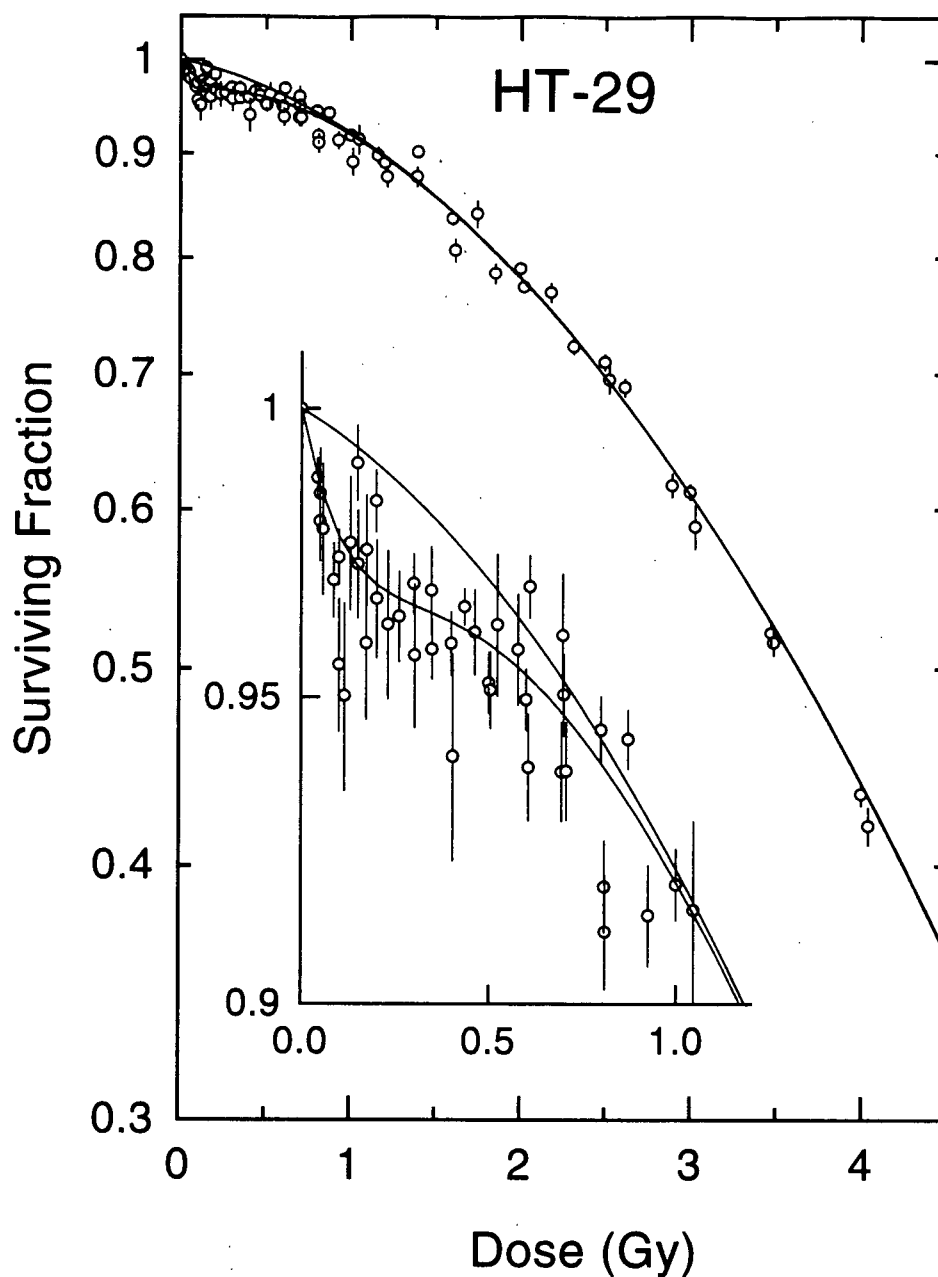
Figure 4-17 HT-29 Normalized Low Dose Survival I
The data set for HT-29 cells was subdivided into 4 time period subsets for which the trypsinization protocol, serum lots and overall sensitivity were similar. The mean inactivation dose was then determined for each subset, and the average of these values used to 'normalize' the radiation response for each of the 4 subsets. These 4 normalized responses are shown together, and exhibit a consistent pattern of low dose hypersensitivity followed by an increase in radioresistance.
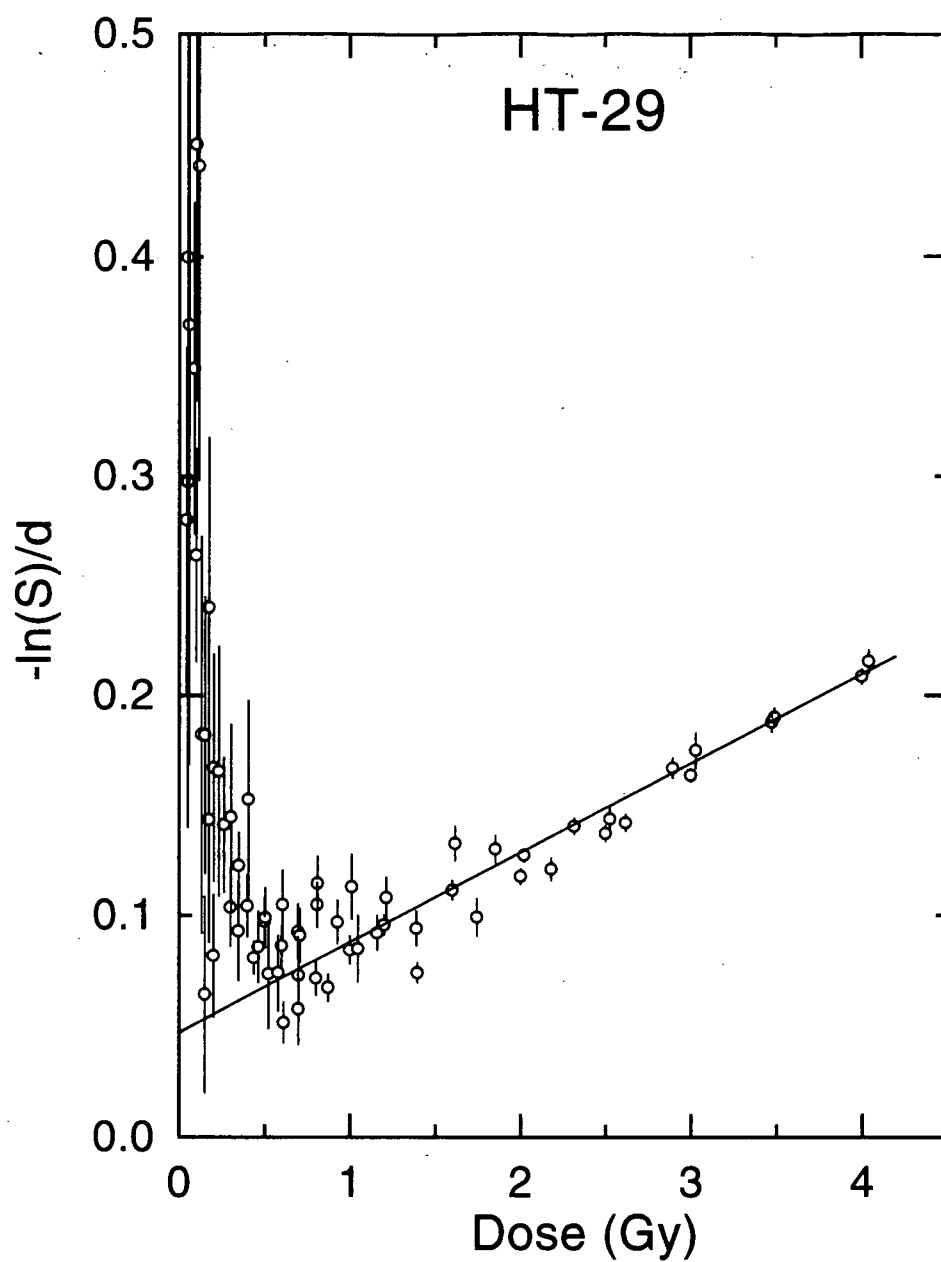
Figure 4-18 HT-29 Normalized Low Dose Survival II

The HT-29 normalized low dose data shown figure 4-17 are replotted in terms of the relative effectiveness per unit dose, -ln(S)/d. The data at low dose show a clear pattern of increased effectiveness as compared to that which is predicted by the LQ fit of the data above 1 Gy.

To determine the magnitude and source of random errors associated with the counting statistics and the cell sorting assay itself, an analysis was made for one subset of the total data set, which comprises a set of four survival responses obtained on the same day. Figures 4-19 and 4-20 show the 4 individual survival responses and the scatter plot of all individual survival measurements respectively for this set of data. The data did not exhibit any significant biological variation from one response to another and thus proved useful for this type of analysis. For each of the four survival responses, each survival point is the average of 24 Petri dishes, or roughly 12000 colonies. At zero dose extra controls bring the total to 72 Petri dishes, or roughly 36000 colonies.

Table 4-3 contains calculated values obtained from these measurements for the mean plating efficiency, the associated standard deviation, and the percentage error in the mean plating efficiency, represented by this standard deviation (the methods used in these error calculations are outlined in appendix 8.1). Also tabulated, is the expected error resulting from binomial counting statistics based on the number of cells tested per Petri dish and the probability of survival. Finally the residual error not accounted for by the binomial statistics, is also tabulated. This error represents all other random errors in the experiment. Values are tabulated for both the error associated with a single measurement (*i.e.*, one Petri dish), and for the mean value (here the average of 24 measurements). A more detailed description of these errors follows in the discussion.
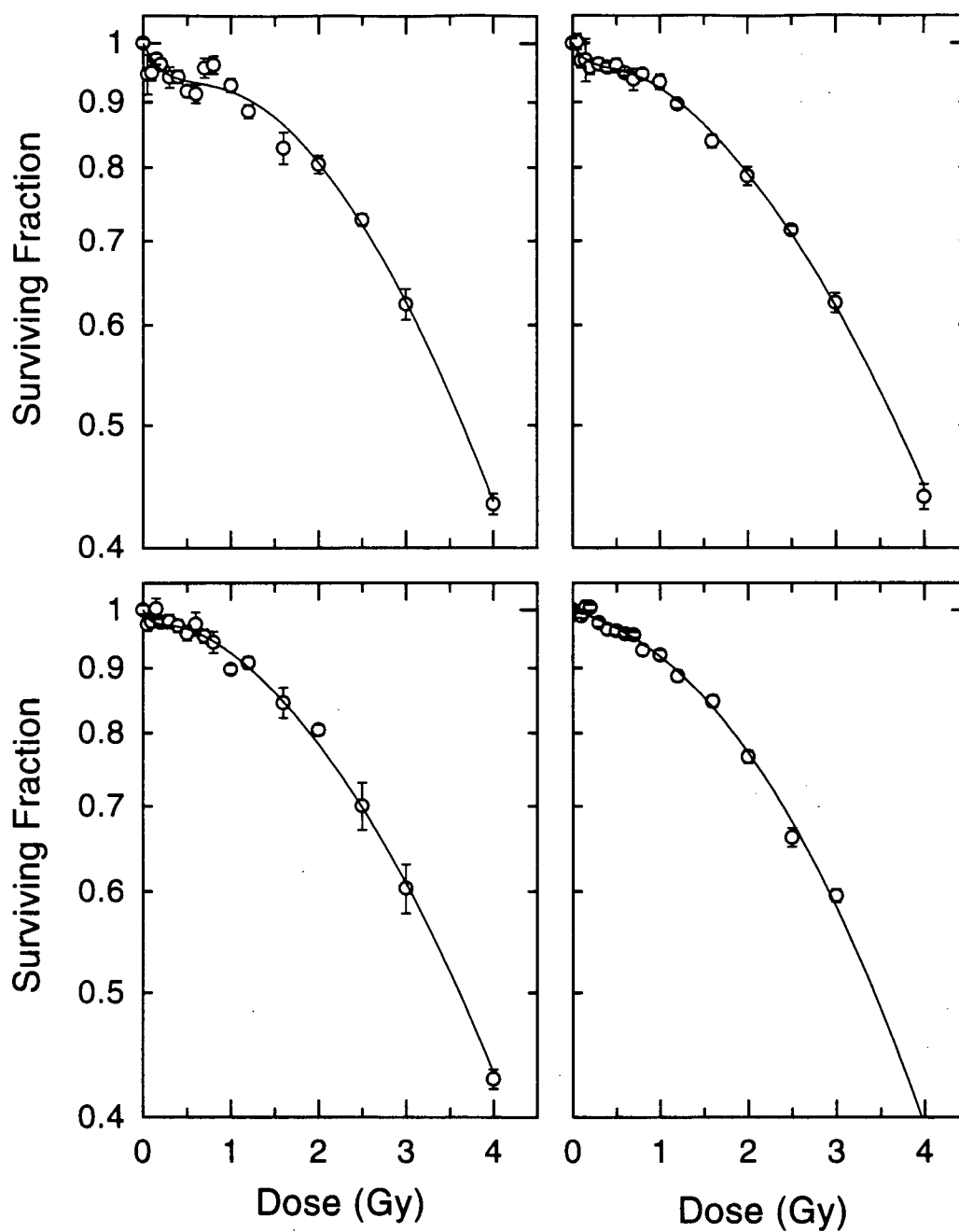
Figure 4-19 Individual HT-29 Survival

Survival data obtained from asynchronous HT-29 cells in response to low doses of X-rays obtained on one experiment day. Each frame shows an individual radiation response curve obtained using the presort cell sorting assay, with each data point representing the average of 6 measurements. Error bars are the standard error in the mean. These four responses have been used to identify the magnitude and source of uncertainty in the presort cell sorting assay.
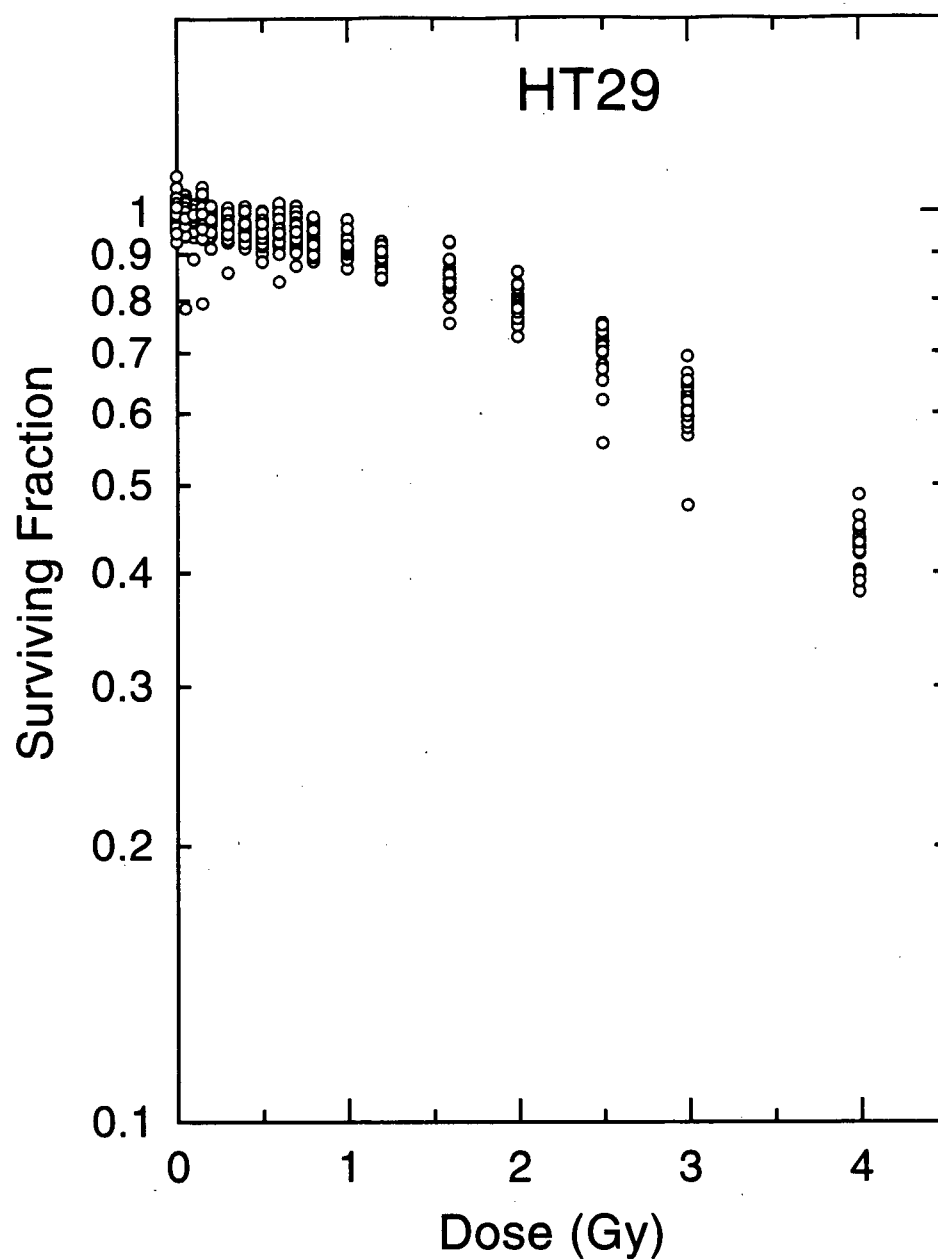
Figure 4-20 HT-29 Scatter Plot

Individual survival measurements calculated from single Petri dishes for four HT-29 survival responses obtained on one day and shown in figure 4-19. The data shown in this figure comprise 4 survival responses for a total of 24 measurements at each dose point, determined using the presort cell sorting assay. The survival for each Petri dish was determined by dividing the measured plating efficiency in the Petri dish by the average of the zero dose plating efficiencies from the appropriate survival response curve.

Table 4-3 HT-29 Statistical Error Analysis
The measured uncertainty in the average plating efficiency was determined from 4 survival curves obtained on one day. This error was subdivided into that which could be attributed to binomial statistics inherent to the assay, and to that attributed to all other random errors. Data from one day were chosen to minimize the biological variation between responses.

Measured Values			% error(measured)		% error(binomial)		% error(other)	
Dose	Mean	SD(σ_M)	(σ_M/PE)		(σ_B/PE)		(σ_O/PE)	
(Gy)	P.E.	(n=24)	(1 dish)	(mean)	(1 dish)	(mean)	(1 dish)	(mean)
0.000	0.834	0.027	3.18%	0.65%	1.92%	0.39%	2.54%	0.52%
0.050	0.816	0.046	5.64%	1.15%	2.02%	0.41%	5.27%	1.08%
0.100	0.810	0.028	3.41%	0.70%	2.05%	0.42%	2.72%	0.56%
0.150	0.823	0.045	5.52%	1.13%	1.98%	0.40%	5.16%	1.05%
0.200	0.814	0.025	3.10%	0.63%	2.03%	0.42%	2.34%	0.48%
0.300	0.805	0.030	3.76%	0.77%	2.08%	0.43%	3.13%	0.64%
0.400	0.800	0.024	3.01%	0.61%	2.11%	0.43%	2.15%	0.44%
0.500	0.792	0.031	3.96%	0.81%	2.15%	0.44%	3.32%	0.68%
0.600	0.791	0.035	4.37%	0.89%	2.16%	0.44%	3.80%	0.78%
0.700	0.793	0.027	3.39%	0.69%	2.14%	0.44%	2.63%	0.54%
0.800	0.788	0.027	3.47%	0.71%	2.17%	0.44%	2.71%	0.55%
1.000	0.767	0.026	3.38%	0.69%	2.27%	0.46%	2.50%	0.51%
1.200	0.746	0.022	2.94%	0.60%	2.38%	0.49%	1.73%	0.35%
1.600	0.700	0.036	5.12%	1.04%	2.58%	0.53%	4.42%	0.90%
2.000	0.659	0.024	3.62%	0.74%	2.75%	0.56%	2.36%	0.48%
2.500	0.585	0.038	6.47%	1.32%	3.04%	0.62%	5.71%	1.17%
3.000	0.511	0.036	7.01%	1.43%	3.30%	0.67%	6.19%	1.26%
4.000	0.356	0.021	5.95%	1.21%	3.78%	0.77%	4.59%	0.94%

See appendix 8.1 for a discussion of error calculations.

4.2.3 Modeling the Low Dose Radiation Response

The data for these three cell lines have also been fitted with a series of equations designed to model the observed low dose substructure. Specifically, the data have been fitted with a two-population linear quadratic (TPLQ) model, and with two induced resistance models.

4.2.3.1 Two-population Model

The TPLQ model assumes that the substructure observed at very low doses arises from a situation similar to that which causes substructure at clinical doses (see chapter 3), namely that the observed response is a composite of more than one population of cells. This hypothesis proposes that the cell population contains a small radiosensitive population (f) and a large resistant population, each with a characteristic radiosensitivity:

$$S = fe^{-\alpha_r D} + (1 - f)e^{-\alpha_r D - \beta D^2}$$

Equation 4-2

Fits of the survival data for DU145, HT-29, and A549 cells with this equation are shown as the solid lines in figures 4-21, 4-22, and 4-23. As indicated in table 4-4, the best-fit value for the parameter describing the sensitive population, α_s, was extremely large for all three cell lines (in DU145 cells this value increased without bound) implying that if the response is the result of two populations, the small population must be extremely radiosensitive. However, because the parameter (α_s) is determined from limited data (the hypersensitive region extends to only about 0.5 Gy), the error in this value is quite large. For this reason the lower 95% confidence limit in this parameter has been used for calculating the fits shown in figures 4-21 to 4-23. Also plotted in each figure (dashed line

near axis) is the response of the sensitive population alone (again using the lower 95%

confidence limit for α_s, *i.e.*, the most resistant probable value), demonstrating the extreme

sensitivity of this hypothetical population even at its minimum acceptable

radiosensitivity.

The choice of the model to represent the sensitive population, in this case a single

hit, single target model characterized by α_s, is somewhat arbitrary but perhaps justified

given the small amount of data in the low dose region and the required extreme sensitivity

of this population. The simple exponential response provides the maximum sensitivity at

low dose, and assumes the least about the response at higher doses. A LQ model can

also be used to describe the response for this population, but it results in a large

correlation between the two parameters α and β. For this population the data simply

require a high degree of cell kill at very low dose, and the single hit, single target equation

is adequate for describing this condition. The dominant resistant population is

characterized by a LQ equation with the parameters α_r and β. The values of the fitted

parameters in the TPLQ model for all cell lines are given in table 4-4.

Table 4-4 Best-Fit Values for the Parameters in the Two-population (TPLQ) Model
The TPLQ model (equation 4-2) was fitted to the mean survival data for each cell line using a non-linear χ^2 minimization routine. Values in parentheses are the upper and lower 95% confidence limits in the quoted values, except for the α_s parameter for which the upper limit increased without bound. The relative goodness of fit is shown by the χ^2/n values (n is the number of dose points), and the RMS values allow a comparison of the goodness of fits between cell lines where the relative errors are not necessarily the same.

Data Set	Dose Range	f (%)	α_s (Gy^{-1})	α_r (Gy^{-1})	β (Gy^{-2})	χ^2/n	R.M.S.
HT-29	(0-4 Gy)	2.23 (2.01-2.47)	40 (16.5-?)	.0233 (.0209-.0259)	.0458 (.0447-.0470)	0.756	0.0046
DU145	(0-4 Gy)	2.04 (1.78-3.41)	* (13.6-?)	.157 (.154-.164)	.0273 (.0261-.0295)	0.679	0.0133
A549	(0-3 Gy)	1.96 (1.65-2.26)	12 (3.5-?)	.0699 (.0675-.0724)	.0539 (.0528-.0551)	2.01	0.0069

* For DU145 cells, no best-fit value for α_s is quoted because this parameter was limited only by the acceptable level of convergence of the fit.

Figure 4-21 DU145 Two-Population Fit
The average low dose data set for DU145 cells (12 survival responses) is shown along with the best fit (solid line) of the TPLQ model (equation 4-2). The best fit in this case was determined using the lower 95% confidence limit in the sensitive parameter, α_s (see text). The radiation response of the hypothesized small sensitive population alone, characterized by α_s in the TPLQ model, is also plotted using the lower 95% confidence limit in this parameter (dashed line near axis).
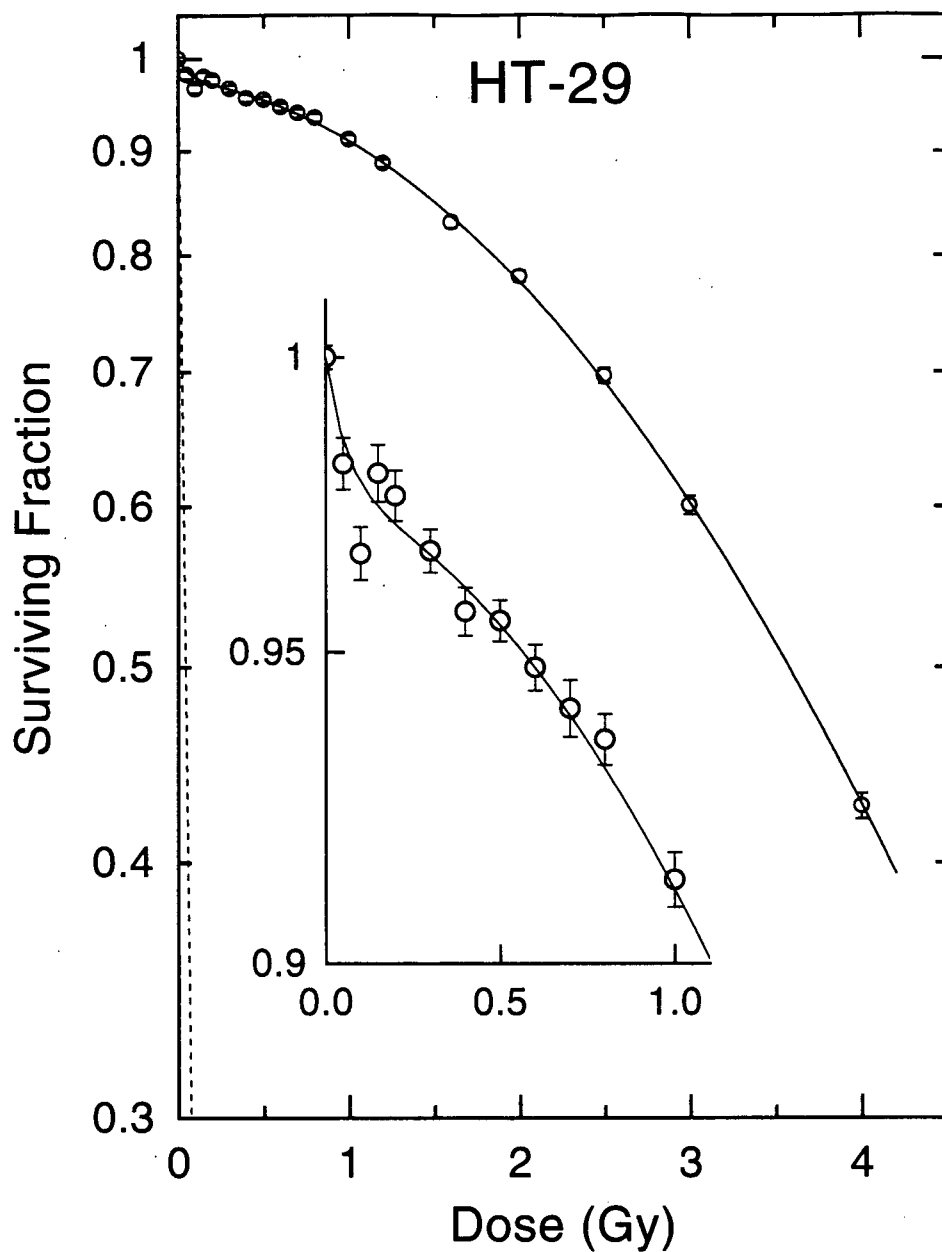
Figure 4-22 HT-29 Two-Population Fit
The average low dose data set for HT-29 cells (15 survival responses) is shown along with the best fit (solid line) of the TPLQ model (equation 4-2). The best fit in this case was determined using the lower 95% confidence limit in the sensitive parameter, α_s (see text). The radiation response of the hypothesized small sensitive population alone, characterized by α_s in the TPLQ model, is also plotted using the lower 95% confidence limit in this parameter (dashed line near axis).
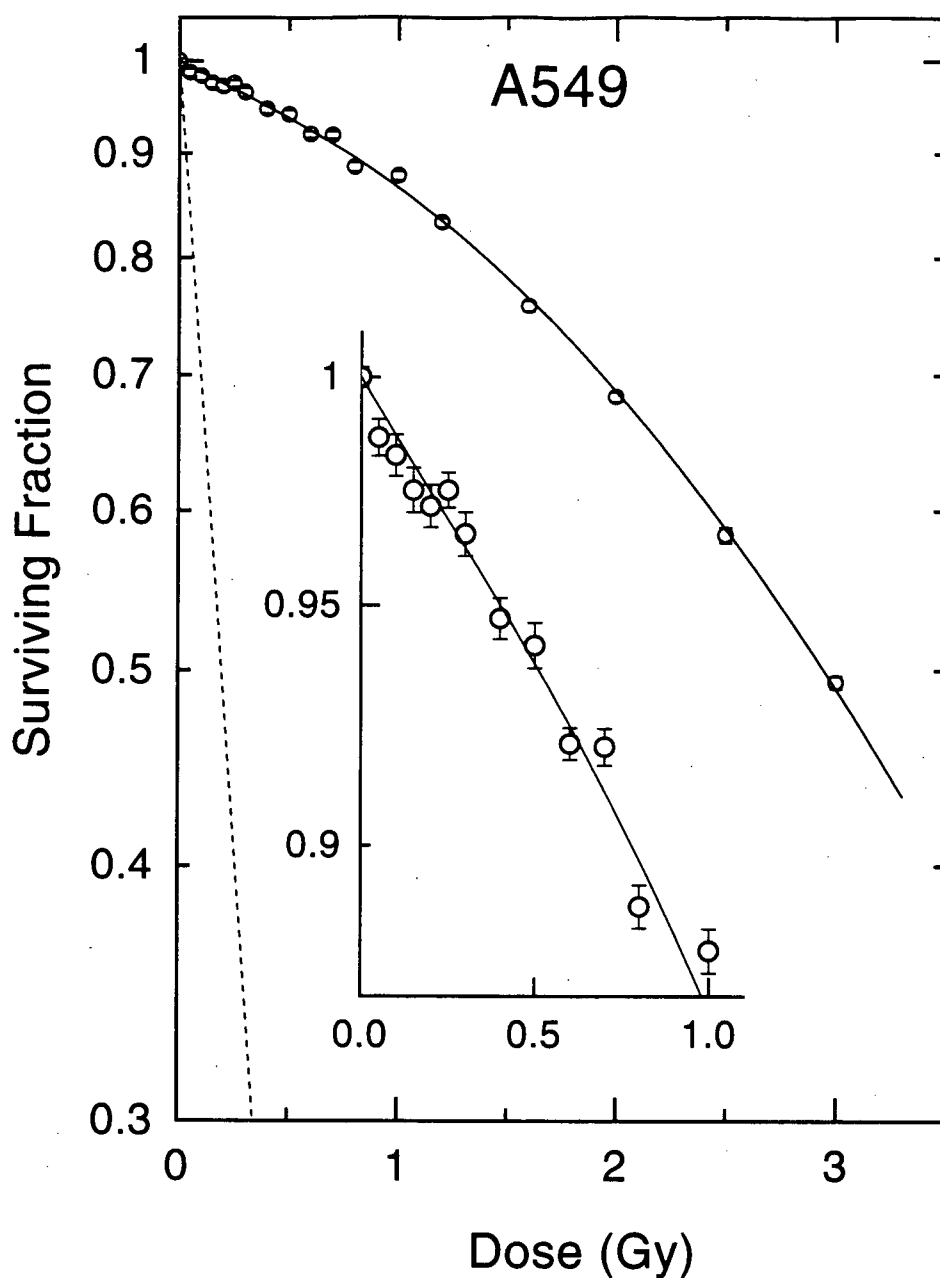
Figure 4-23 A549 Two-Population Fit
The average low dose data set for A549 cells (8 survival responses) is shown along with the best fit (solid line) of the TPLQ model (equation 4-2). The best fit in this case was determined using the lower 95% confidence limit in the sensitive parameter, α_s (see text). The radiation response of the hypothesized small sensitive population alone, characterized by α_s in the TPLQ model, is also plotted using the lower 95% confidence limit in this parameter (dashed line near axis).

4.2.3.2 Variable-α Induced Radioresistance

The variable-α induced radioresistance model was also used to fit the low dose response. This model, which is an extension of the LQ model, was originally suggested by Joiner and Johns (Joiner and Johns 1988), and is represented by the equation:

$$S = e^{-\alpha(d)d - \beta d^2}$$

Equation 4-3

where $\alpha(d) = \alpha_r - (\alpha_r - \alpha_s)e^{-d/d_c}$. This model is fundamentally different from the two-population model because it assumes that the *entire* cell population is initially radiosensitive, and becomes resistant as a continuous function of dose. The induction of resistance is characterized by an exponential decrease in the α value from a larger initial value of α_s to a final value, α_r. The best fits of the survival data for DU145, HT-29, and A549 are shown as solid lines in figures 4-24, 4-25, and 4-26, and parameter values are given in table IV.

Table 4-5 Best-Fit Values for the Parameters in the Variable-α Induced Radioresistance Model
The variable-α induced radioresistance model (equation 4-3) was fit to the mean survival data for each cell line using a non-linear χ^2 minimization routine. Values in parentheses are the upper and lower 95% confidence limits in the quoted values. The relative goodness of fit is shown by the χ^2/n values (n is the number of dose points), and the RMS values allow a comparison of the goodness of fits between cell lines where the relative errors are not necessarily the same.

Data Set	d_c (Gy)	α_s (Gy^{-1})	α_r (Gy^{-1})	β (Gy^{-2})	χ^2/n	R.M.S.
HT-29	.206	.322	.0467	.0408	1.25	0.0065
	(.180-.230)	(.271-.372)	(.0441-.0492)	(.0397-.0419)		
DU145	.184	.604	.180	.0226	0.546	0.0128
	(.131-.236)	(.454-.755)	(.175-.184)	(.0211-.0242)		
A549	.080	.404	.0983	.0460	1.63	0.0059
	(.048-.108)	(.225-.585)	(.0958-.0101)	(.0448-.0471)		

Figure 4-24 DU145 Variable-α Fit
The average low dose data set for DU145 cells (12 survival responses) is shown along with the best fit (solid line) of the variable-α model (equation 4-3).
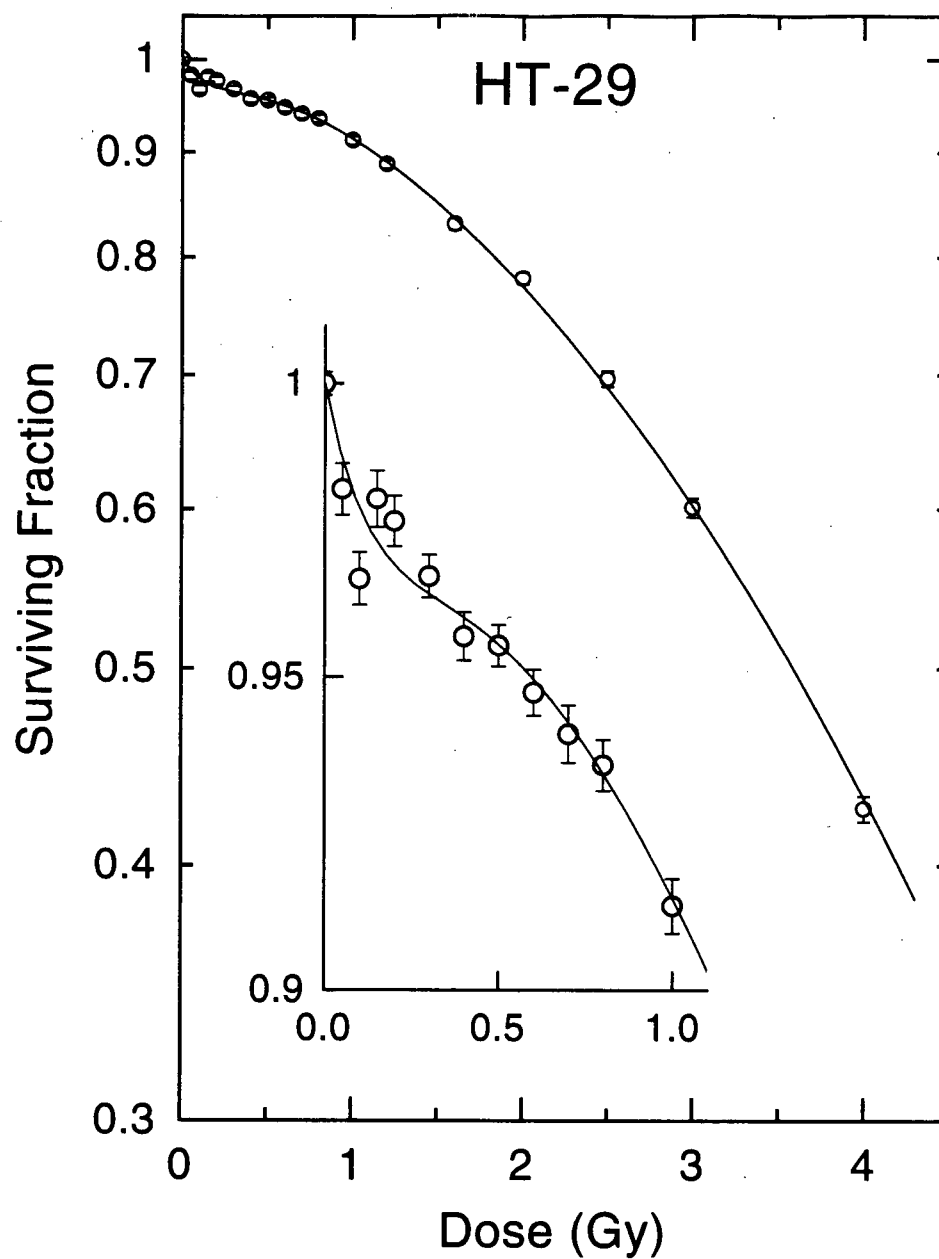
Figure 4-25 HT-29 Variable-α Fit
The average low dose data set for HT-29 cells (15 survival responses) is shown along with the best fit (solid line) of the variable-α model (equation 4-3).

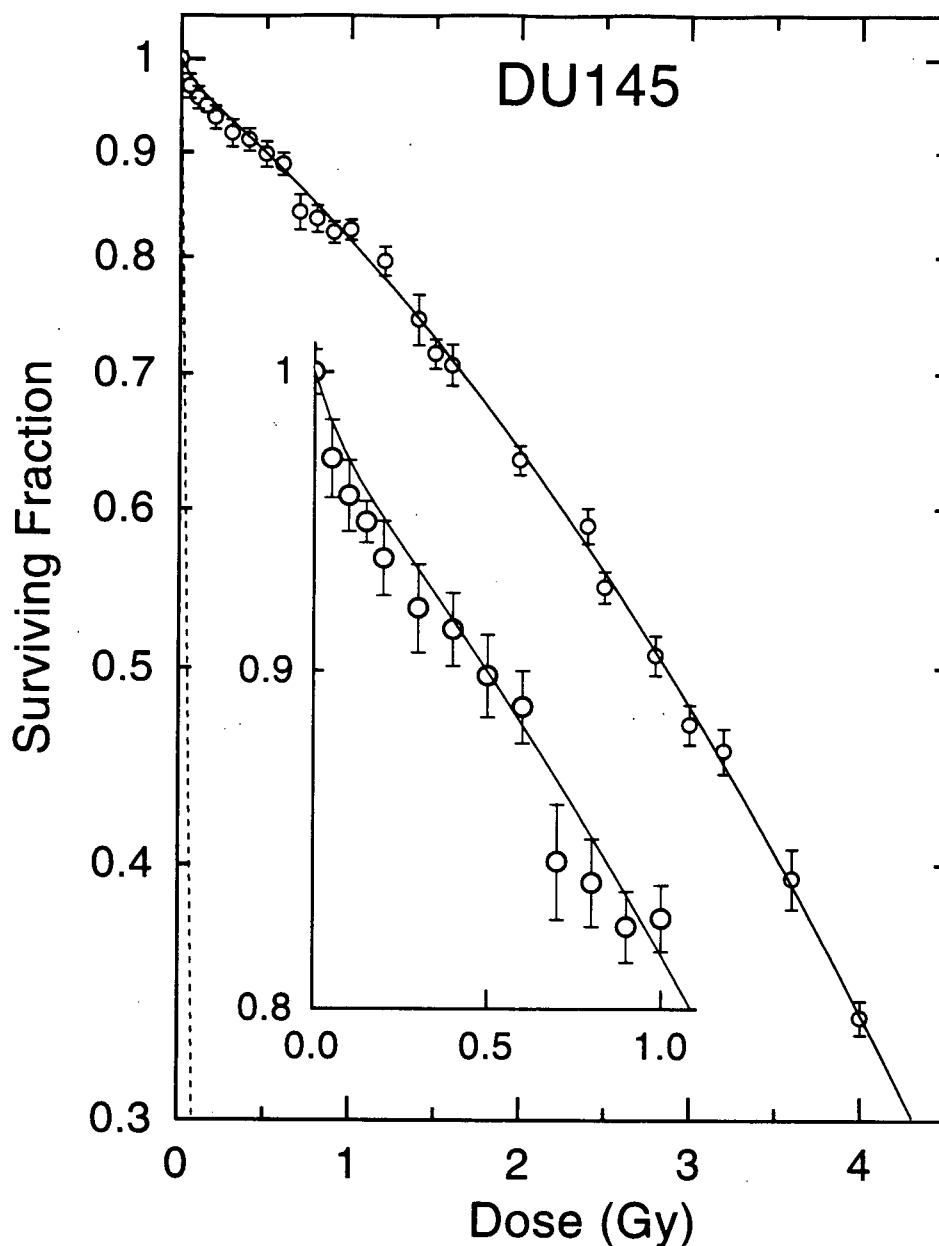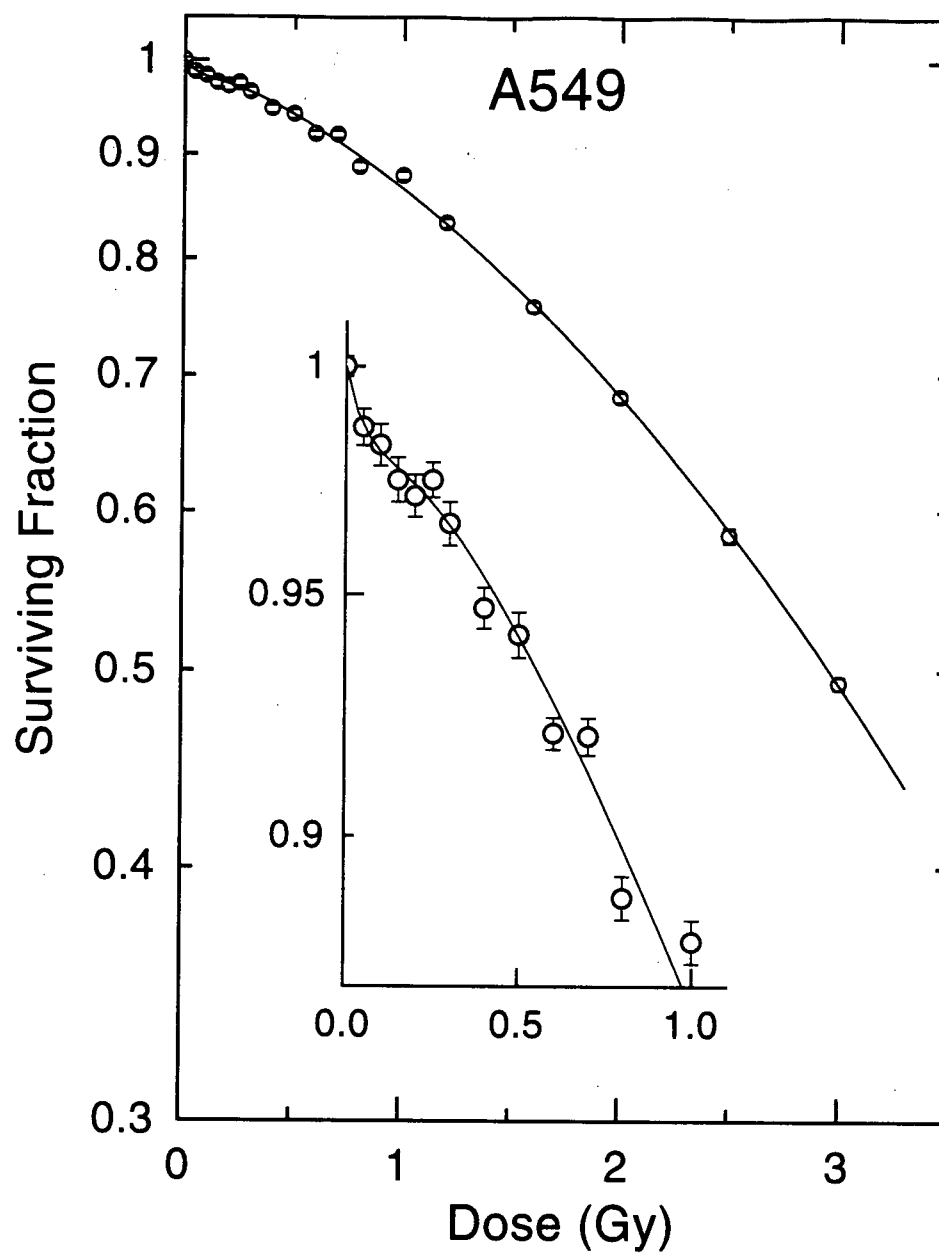**Figure 4-26 A549 Variable-α Fit**
The average low dose data set for A549 cells (8 survival responses) is shown along with the best fit (solid line) of the variable-α model (equation 4-3).

4.2.3.3 Accumulated Damage Induced Radioresistance

The variable-α model assumes a continuous decrease in the radiosensitivity of the cell population over the initial dose range. A second possible explanation for the observed low dose hypersensitivity that is also based on the induction of a radioresistance mechanism is one that hypothesizes that the cells can exist in either a radiosensitive or a radioresistant state. This model could apply, for example, to the two states in which a cell exists before and after the induction of a hypothetical repair mechanism. These two states could also reflect a differential ability to respond to radiation insult by the active form of cell death known as apoptosis. Here the resistant state conferred by radiation damage would be that where the ability to induce this form of cell death is compromised. This second induced radioresistance function is termed the accumulated damage induced radioresistance (ADIR) model (Wouters and Skarsgard 1994). It is the hypothesis of this model that the cells are all initially sensitive, and that they are 'triggered' to become radioresistant only after sustaining some critical damage level. Thus the population contains a sensitive and a resistant subpopulation at each dose level, each with a characteristic radiosensitivity. The proportions of each subpopulation change as a function of dose, and are defined by a critical damage level using the Poisson distribution. The ADIR model can be described by the following equation:

$$S = fe^{-\alpha_r D} + (1 - f)e^{-\alpha_r D - \beta D^2} \qquad \text{Equation 4-4}$$

where
$$f = \sum_{n=0}^{c-1} \frac{(ad)^n e^{-ad}}{n!} \qquad \text{Equation 4-5}$$

This model assumes that there is an average number, a, of damage events per gray, and that cells must sustain a critical number, c, of these events before a protective mechanism is induced and the cells move to the radioresistant state. The rate of the transition from the sensitive to the resistant state (*i.e.*, the dose range over which this occurs) is governed by the rate at which damage is sustained (the a parameter in the ADIR model), while the critical number, c, determines the actual dose at which the transition will occur. Figure 4-27 shows examples of how these parameters influence the dose at which, and the rate at which the transition occurs.

For reasons similar to those outlined for the two-population model, sensitive and resistant populations are characterized by a single hit-single target model and a linear quadratic model respectively. Fits to the data using this model were made under two separate conditions. In the first, the average number of events per Gy, a, was fixed at 20, such that the bulk of the cell population remains in the sensitive, untriggered state until a significant level of damage is sustained (see figure 4-27). This number is similar to estimates of the number of double strand breaks (DSBs) induced per Gy of radiation (Iliakis *et al.* 1991). If the hypothesis is made that the accumulation of a critical number of DSBs can trigger the induction of resistance, then fits with the model should provide estimates of the number, c, of DSBs required to induce radioresistance, as well as best-fit values for the parameters describing both the sensitive (untriggered) and resistant (triggered) populations. Fits of the DU145, HT-29, and A549 data with the ADIR model for this condition are shown as solid lines in figures 4-28, 4-29, and 4-30, and the parameters for each are given in table 4-6. It is interesting to compare the c values for the
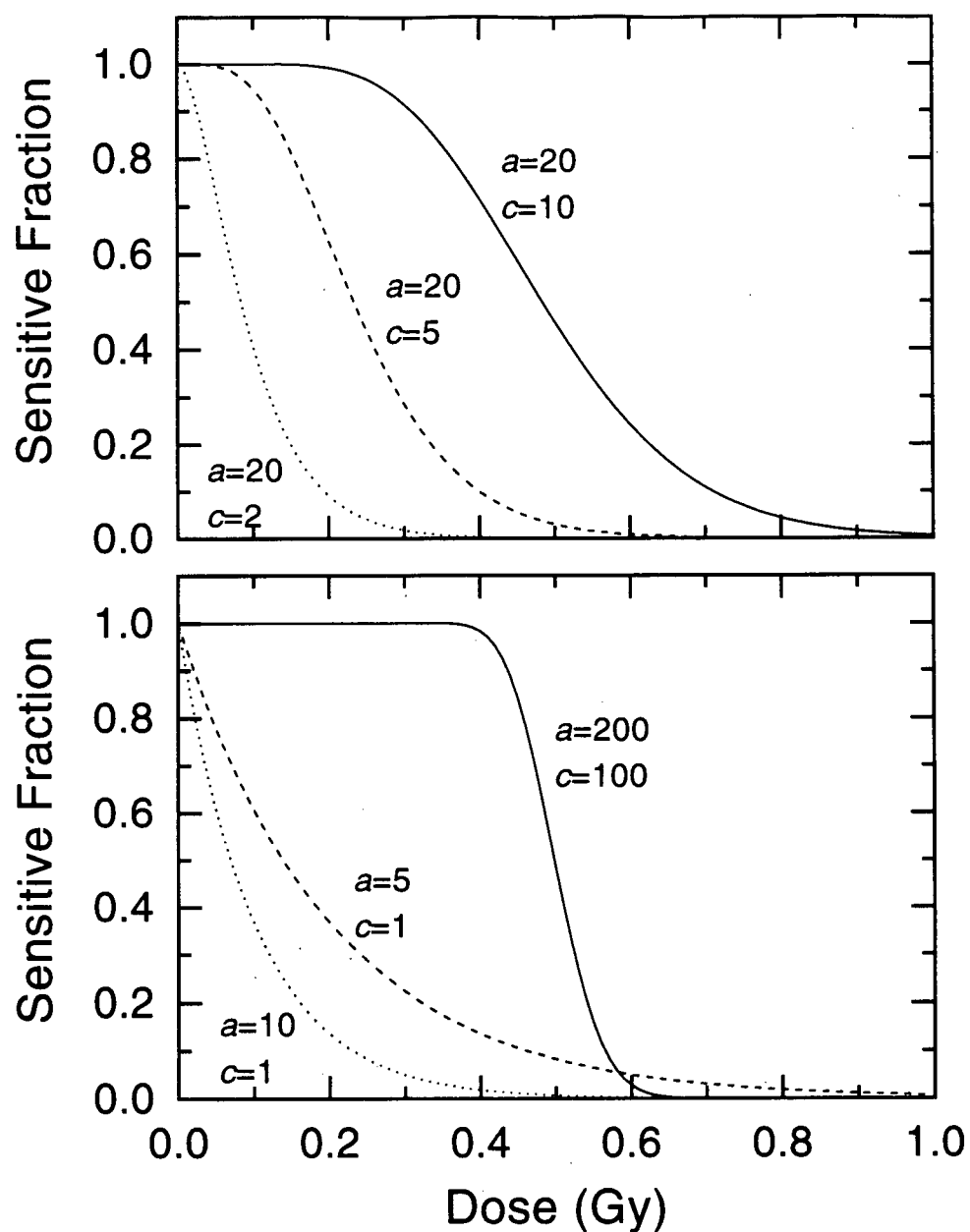
Figure 4-27 ADIR Model State Transitions

Rate of transition from the sensitive to the resistant state as predicted by the ADIR model. The remaining sensitive fraction is shown as a function of dose, and is determined using a Poisson relation (equation 4-5). The upper frame shows three plots using a fixed value for the average number of events produced per gray, a, equal to 20, and different values for c, the critical number of events required to induce radioresistance. The lower frame shows three additional plots for different a and c values. Note the rapid change that is exhibited when the a value is large (a=200, lower frame).

different cell lines. For HT-29 and DU-145, which exhibit extended regions of hypersensitivity, the model predicts values for c of 9 and 6 respectively as the number of DSBs required to induce radioresistance. For A549 cells, which showed the smallest hypersensitive region, the value of c was only 2. These fits also predict a more modest initial radiosensitivity for the untriggered population than does the variable-α model.

In the second application of the ADIR model, the data were fitted assuming that there is only one critical event that must occur for induction of radioresistance, and that the cell lines have different susceptibilities to this event. Thus the c value was fixed at 1, and the a value was allowed to be determined along with the other parameters. In this situation the change from the initial sensitive state to the resistant state begins immediately, and proceeds at a rate dependent on the value of a (see fig. 4-27). Fits under this condition are shown as dashed lines in figures 4-28, 4-29 and 4-30, and the parameters are given in table 4-7. This scenario predicts slightly more sensitive initial populations, and a more continuous change from the sensitive to the resistant population. It also suggests that HT-29 and DU145 cell lines are less susceptible than A549 to the induction of the critical event required for increased radioresistance.

Table 4-6 Best-Fit Values for the Parameters in the ADIR Model (I)

The accumulated damage induced radioresistance (ADIR) model (equation 4-4) was fit to the mean survival data for each cell line using a non-linear χ^2 minimization routine. Values in parentheses are the upper and lower 95% confidence limits in the quoted values. The relative goodness of fit is shown by the χ^2/n values (n is the number of dose points), and the RMS values allow a comparison of the goodness of fits between cell lines where the relative errors are not necessarily the same. In this application of the model, a , the average number of events produced per gray, was fixed at 20, and c, the critical number required to induce resistance, determined along with other best-fit parameters.

Data Set	α_s (Gy^{-1})	α_r (Gy^{-1})	β (Gy^{-2})	c	a	χ^2/n	R.M.S.
DU145	.388	.183	.0215	6	20	.647	0.014
	(.312-.466)	(.179-.188)	(.0199-.0231)				
HT-29	.140	.0492	.0399	9	20	2.17	0.008
	(.126-.160)	(.0466-.0519)	(.0388-.0411)				
A549	.334	.0987	.0458	2	20	1.64	0.006
	(.197-.473)	(.0963-.101)	(.0446-.0470)				

Table 4-7 Best-Fit Values for the Parameters in ADIR Model (II)

Similar results as in table 4-6, but in this application of the ADIR model, c, the critical number of events required to induce resistance, was fixed at 1, and the best-fit value for a, the average number of events produced per gray, determined along with other best-fit parameters.

Data Set	α_s (Gy^{-1})	α_r (Gy^{-1})	β (Gy^{-2})	c	a	χ^2/n	R.M.S.
DU145	.585	.179	.0228	1	5	0.513	0.013
	(.441-.732)	(.175-.184)	(.0212-0244)				
HT-29	.345	.0480	.0404	1	5	1.27	0.007
	(.290-.402)	(.0454-.0505)	(.0392-.0415)				
A549	.396	.0982	.0460	1	12	1.63	0.006
	(.224-.572)	(.0958-.101)	(.0449-.0472)				

Figure 4-28 DU145 ADIR Fit

The average low dose data set for DU145 cells (12 survival responses) is shown along with the best fits with the accumulated damage induced radioresistance (ADIR) model (equation 4-5) under two separate conditions. The solid line shows the best fit of the model using a fixed value for a, the average number of events produced per gray, equal to 20. The dashed line shows the best fit using a fixed value for c, the number of critical events required to induce radioresistance, equal to 1.
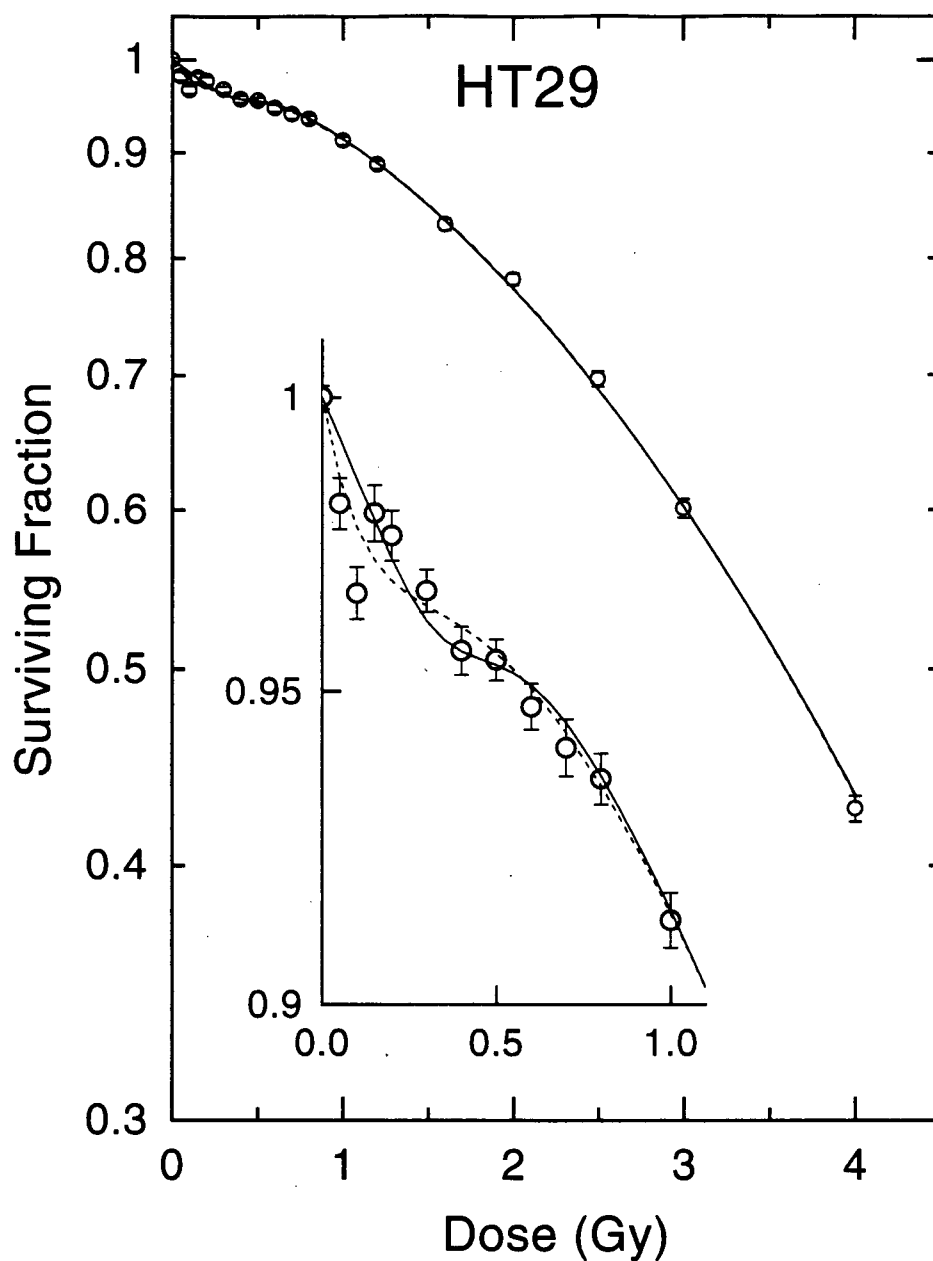
Figure 4-29 HT-29 ADIR Fit

The average low dose data set for HT-29 cells (15 survival responses) is shown along with the best fits with the accumulated damage induced radioresistance (ADIR) model (equation 4-5) under two separate conditions. The solid line shows the best fit of the model using a fixed value for a, the average number of events produced per gray, equal to 20. The dashed line shows the best fit using a fixed value for c, the number of critical events required to induce radioresistance, equal to 1.
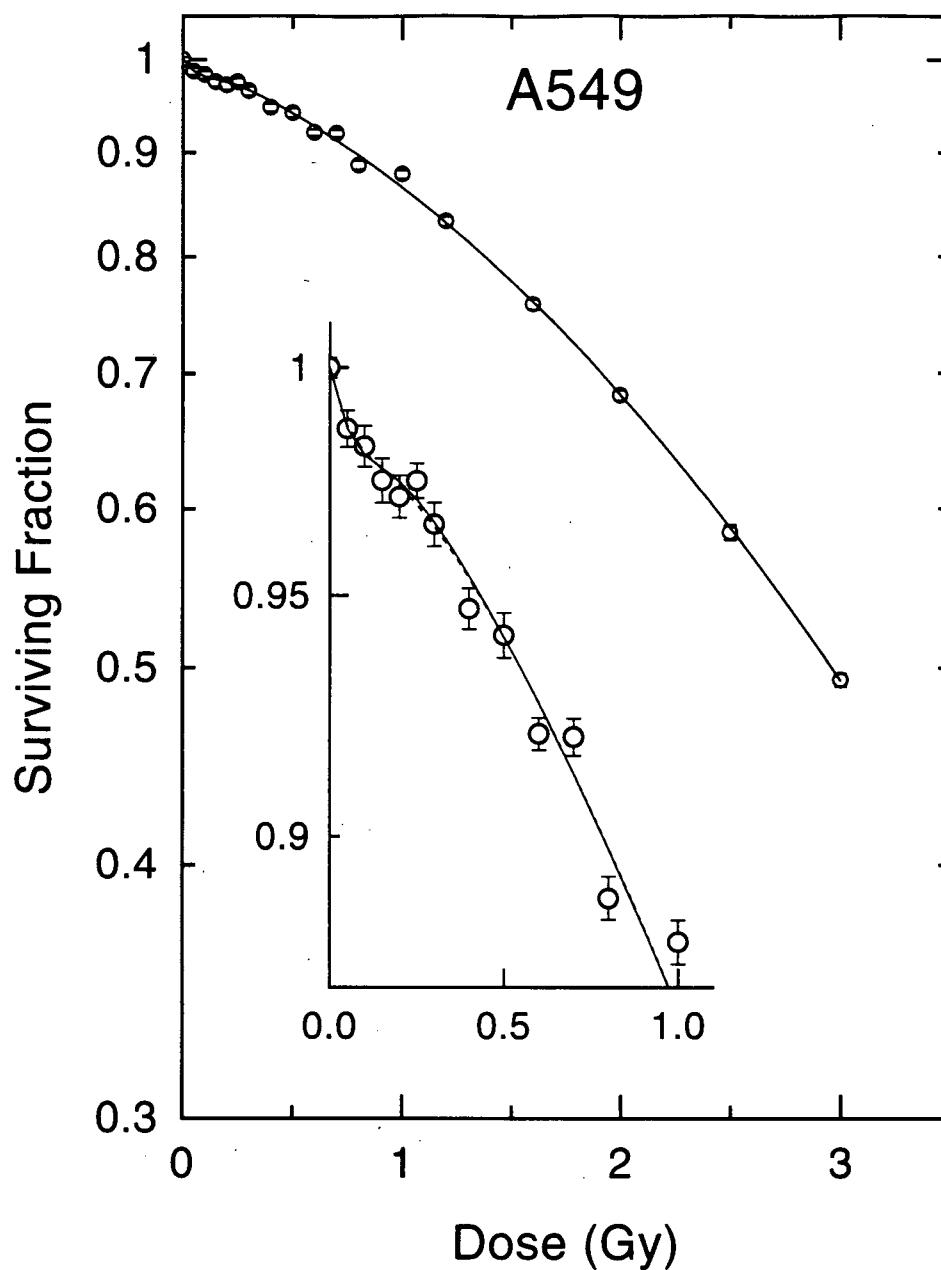
Figure 4-30 A549 ADIR Fit

The average low dose data set for A549 cells (8 survival responses) is shown along with the best fits with the accumulated damage induced radioresistance (ADIR) model (equation 4-5) under two separate conditions. The solid line shows the best fit of the model using a fixed value for a, the average number of events produced per gray, equal to 20. The dashed line shows the best fit using a fixed value for c, the number of critical events required to induce radioresistance, equal to 1.

4.2.4 Priming Dose Studies

The observation of a hypersensitive region at very low doses, followed by an increase in radioresistance in these three cell lines, suggested a possible relationship to the phenomenon known as the adaptive response (Olivieri *et al.* 1984). The adaptive response hypothesizes the induction of a repair mechanism after a small priming dose that allows the cells to better withstand a challenge dose of radiation given several hours following the priming dose. A series of experiments was carried out with HT-29 cells to determine whether irradiation with a small priming dose would result in a more radioresistant response measured 4-6 hours later, consistent with this phenomenon.

4.2.4.1 Monolayer Priming

The first sets of experiments were carried out using a protocol in which cells were primed with a dose of 0.3 Gy while still growing as monolayers in the tissue culture flask. Six hours following this 'monolayer priming', the cells were harvested, and a complete low dose survival response measured for an additional dose of 0-4 Gy using the presort protocol. Figure 4-31 shows the average of 2 primed and 2 unprimed radiation survival responses obtained on one experiment day. In this figure, the survival of the primed cell population is that for exposure to the second dose of irradiation only. Thus the survival for each of the primed cell populations was calculated from the measured plating efficiency after the second dose, divided by the measured plating efficiency of cells that had been primed, but received no second dose. The primed plating efficiency was measured at the same time as the initiation of the presort protocol for irradiation with the second dose,

since cells remained as monolayers during the 6 hour interval after the priming dose.

Figure 4-31 shows that the HT-29 unprimed response exhibited hypersensitivity at doses below 0.5 Gy, similar to that observed previously for this cell line (see figs. 4-13 and 4-17), while the primed cell population shows no evidence of low dose hypersensitivity to the second dose given. However, contrary to the hypothesis of the adaptive response, no protection from higher doses was observed in the primed cell population. The data suggest that the cell population surviving the priming dose is some-what more sensitive, rather than more resistant, as compared to the original unprimed population.

4.2.4.2 Suspension Priming

The unexpected results of the previous study using the monolayer priming method led to the development of a new protocol for priming experiments. Since the response to the second dose was, if anything, more sensitive than the unprimed population response, it would be interesting to compare the survival as a function of the *total dose* (including the priming dose) delivered to the cells. However, since the previous protocol did not allow for measurement of the plating efficiency of the cells *prior* to the priming dose, the zero dose plating efficiency was not known, and the survival as a function of *total dose* could not be calculated. Although unprimed control responses were measured at the same time, the zero dose plating efficiency measured for each of these responses varied somewhat, presumably due to subtle differences in cell handling (the cells for each response were grown in a separate tissue culture flask). Thus, one could not assume a normalizing value for the zero dose plating efficiency. To overcome this problem a protocol was developed in which cells could be primed and incubated in suspension

Figure 4-31 HT-29 Monolayer Primed Cell Response To Challenge Doses
Data are the average of 2 unprimed (open circles) and 2 primed (solid circles) HT-29 survival responses
obtained using the presort protocol. For the primed response, culture flasks were removed from the
incubator and irradiated with 0.3 Gy. Flasks were then incubated an additional 6 hours prior to
measurement of the dose response. Survival of the primed population is to the second dose of irradiation,
and thus is normalized to the plating efficiency of the primed cells. The unprimed response is fitted with the
variable-α model (equation 4-3 - solid line) and the primed response fitted with the LQ model (equation 3-4
- dashed line).

culture, allowing for measurement of the plating efficiency immediately before and after the priming dose. Preliminary measurements were made to ensure cells would remain in exponential growth phase during the extended period (up to 7 hours) in spinner culture. For this purpose, cell populations were harvested and loaded into two water-jacketed irradiation vessels. In one of these vessels, cell populations were first incubated for 30 minutes with 10 μM BrdU to label the fraction of cells synthesizing DNA during that time period. Samples were taken from each vessel every 30-60 minutes for up to 10 hours after initiation of spinner culture, and analyzed for DNA content or DNA and BrdU content. Figure 4-32 shows the DNA histograms determined by flow cytometry for the entire cell population, and for the labeled cohort (the original S-phase fraction) sampled at different time points after irradiation. No measurable change was observed in the DNA histograms obtained from either vessel during this time period. In addition, the originally labeled S-phase cells were observed to continue to move through the cell cycle.

For the 'suspension' priming experiments, sufficient numbers of HT-29 cells were harvested for measurement of four complete survival responses. The cell population was divided equally into 4 irradiation vessels, such that 2 primed and 2 unprimed survival responses could be individually assessed in one experiment. The 0.3 Gy priming dose was delivered to cell populations in suspension, and measurements of plating efficiency were made immediately before and after this dose using the cell sorting assay. Following the priming dose, cells remained in suspension culture for an additional 4 hours, and were then assayed for survival after a second dose of 0 to 4 Gy using the presort cell sorting assay.
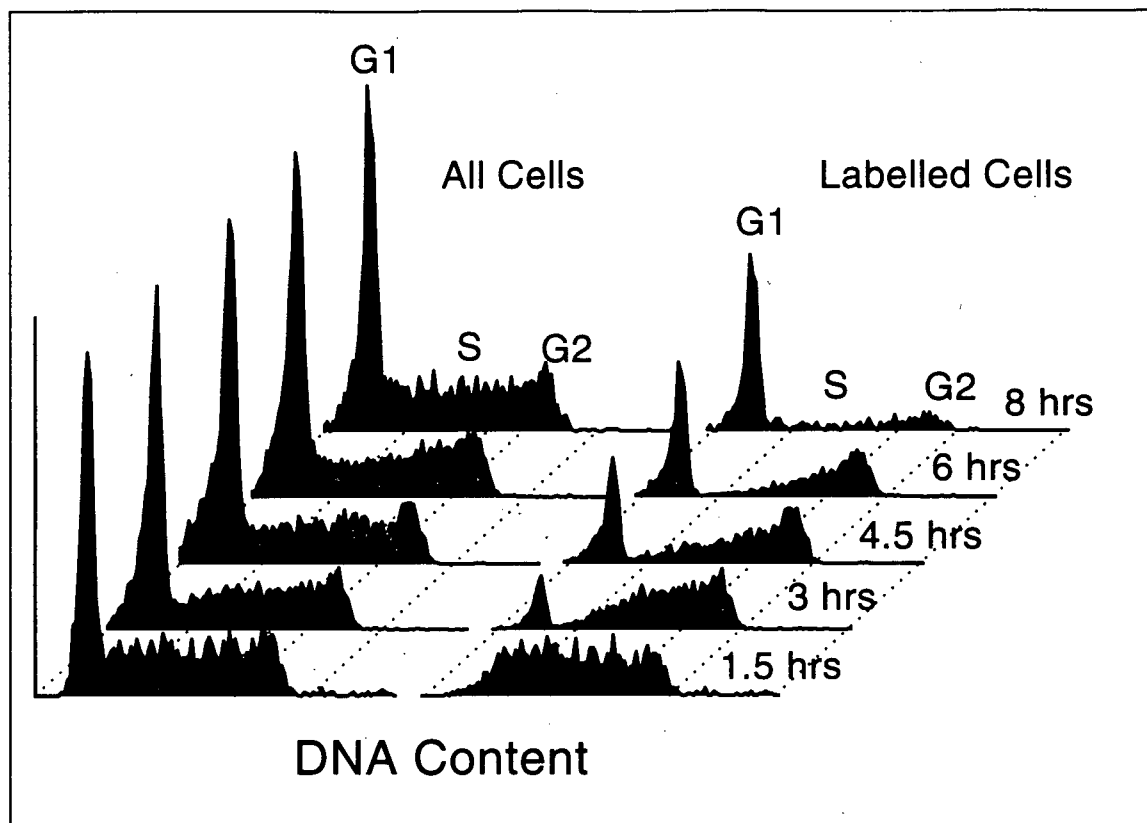
Figure 4-32 DNA Profiles of Cells in Suspension Culture

Histograms show the DNA distribution of HT-29 asynchronous cell populations incubated in suspension culture for different periods of time (left frame). Also shown are the DNA distributions of the original S-phase fraction of cells as a function of time in suspension culture (right frame). The DNA profiles of this labeled cohort were determined by labeling S-phase cells with 10 µM BrdU for 30 minutes prior to initiation of suspension culture. These data show that HT-29 cells continued to proliferate for at least 8 hours in suspension culture.

Control populations were treated identically, but were mock irradiated. Figure 4-33 shows that there was no significant change in the zero dose plating efficiency as a function of time in the irradiation vessel for up to 5 hours in suspension culture.

The radiation survival response calculated from the average of two of these experiments (the average of a total of 4 survival responses for each of the primed and unprimed data) are shown in figure 4-34. The data are also plotted in terms of the effectiveness per unit dose (-ln(S)/d), in figure 4-35. In both of these figures, the survival of the primed cells has been plotted as the response to the challenge dose only (in the same manner as figure 4-31), and thus were normalized by the plating efficiency of the primed cells measured after the four hour incubation period. These data demonstrate a response similar to that seen previously with the monolayer priming protocol, with the primed cells exhibiting a slightly more sensitive response at higher doses as compared to the unprimed cells. There is also a complete absence, in both of these experiments, of any low dose hypersensitivity in the primed cells, though it is clearly demonstrated in the unprimed cell population. The data at low dose suggest a small increase in survival over the first 0.1 Gy, although the increase is not statistically significant. The difference in response at low dose of the primed and unprimed cells is dramatically illustrated in figure 4-35 with the unprimed cells showing the typical increase in effectiveness at doses less than 0.5 Gy, while the primed cells exhibit a much reduced effectiveness, below that predicted from a LQ fit to the data above 1 Gy. The points below zero on this graph are those which show an increase in survival above that of the cells that received only the priming dose(see fig 4-34). For these data points the calculated survival is greater than 1.
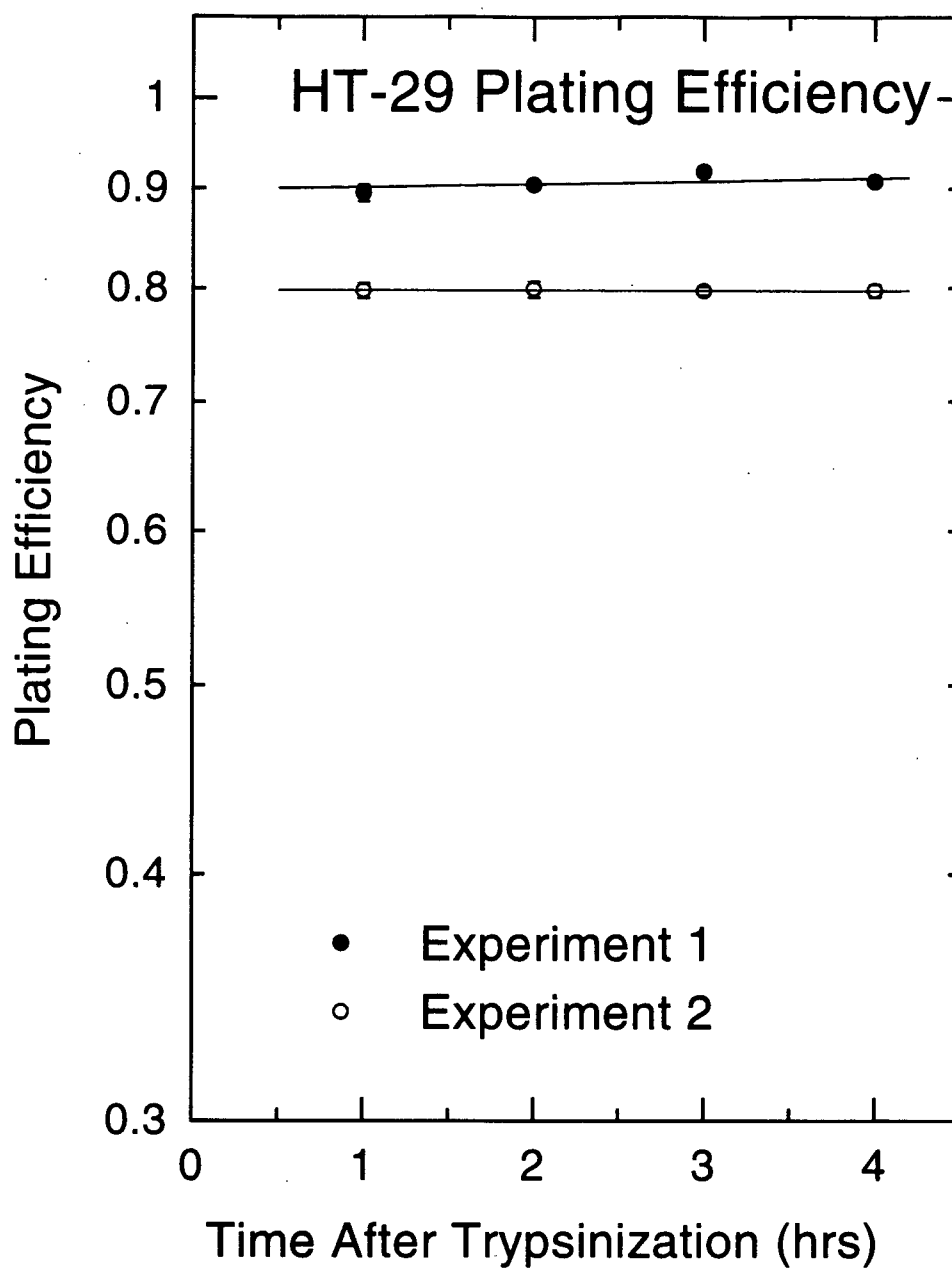
Figure 4-33 Plating Efficiency in Suspension Culture
The zero dose plating efficiency of HT-29 cells is shown as a function of time in suspension culture. Data are from two separate experiments.
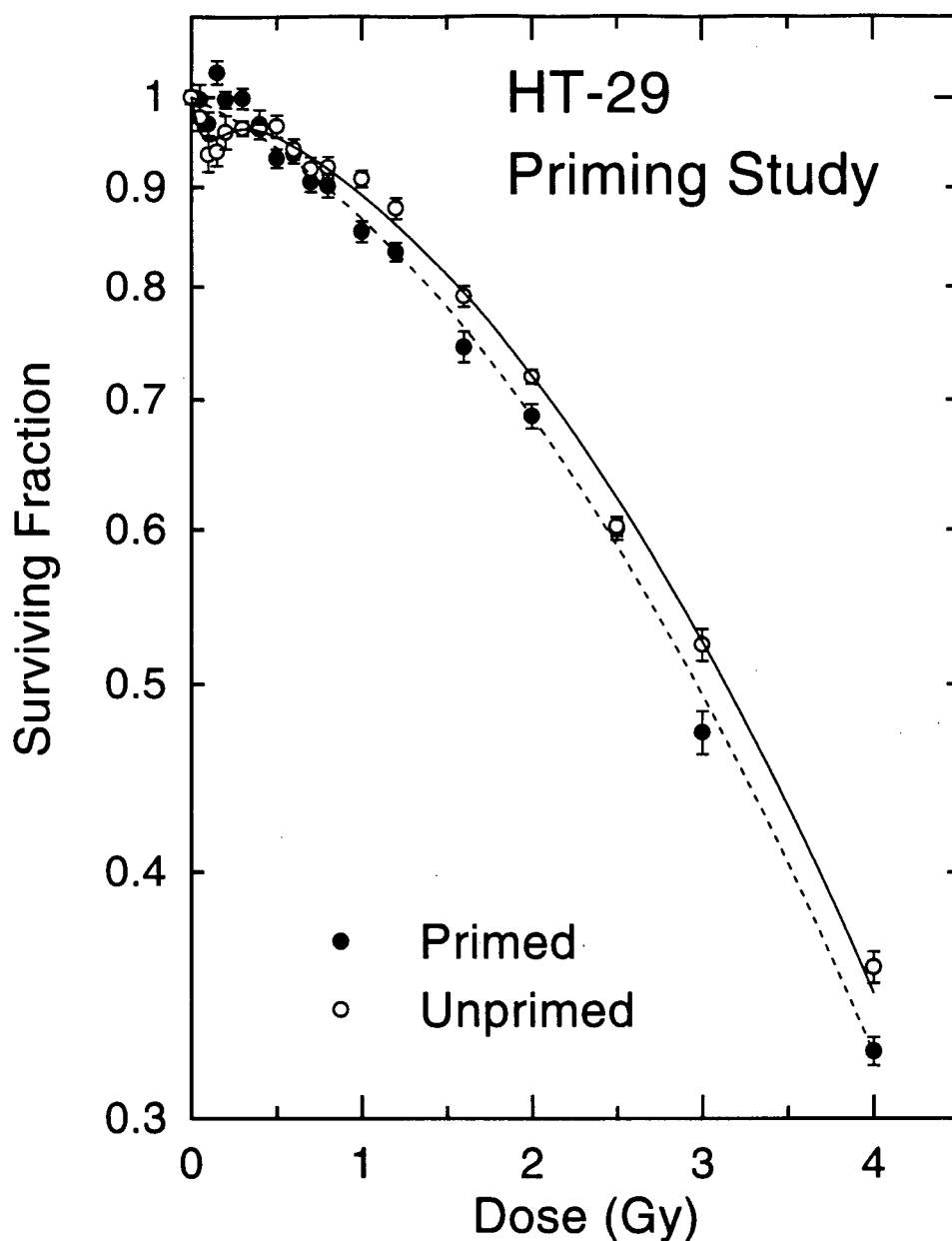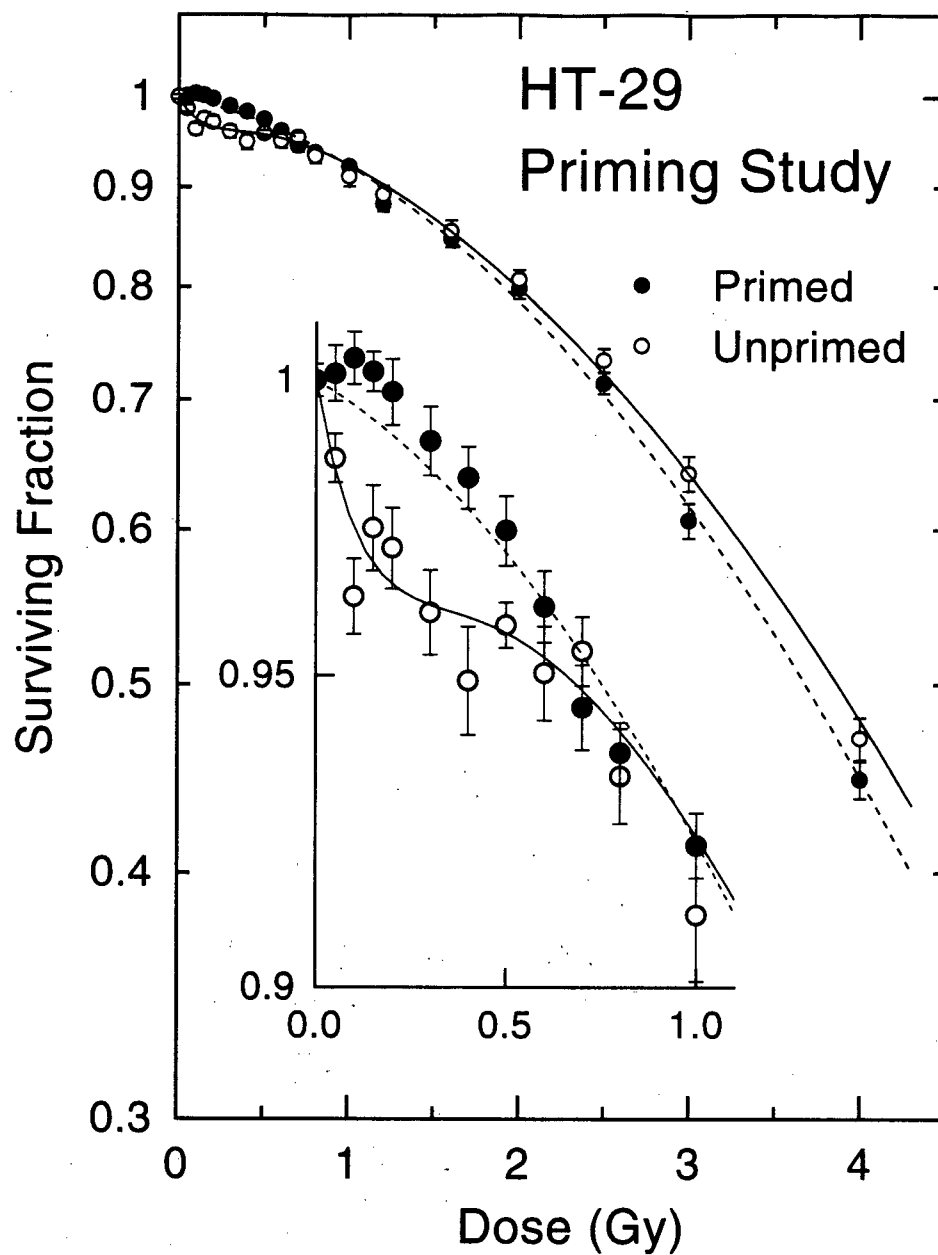
Figure 4-34 Suspension Primed Cell Response to the Challenge Dose I
Data are the average of 4 unprimed (open circles) and 4 primed (solid circles) HT-29 survival responses obtained using the presort protocol. Primed responses received 0.3 Gy while in suspension culture, 4 hours prior to measurement of the dose response. Survival of the primed population is to the second dose of irradiation, and thus is normalized to the plating efficiency of the primed cells. The unprimed response is fitted with the variable-α model (equation 4-3 - solid line) and the primed response fitted with the LQ model (equation 3-4 - dashed line).
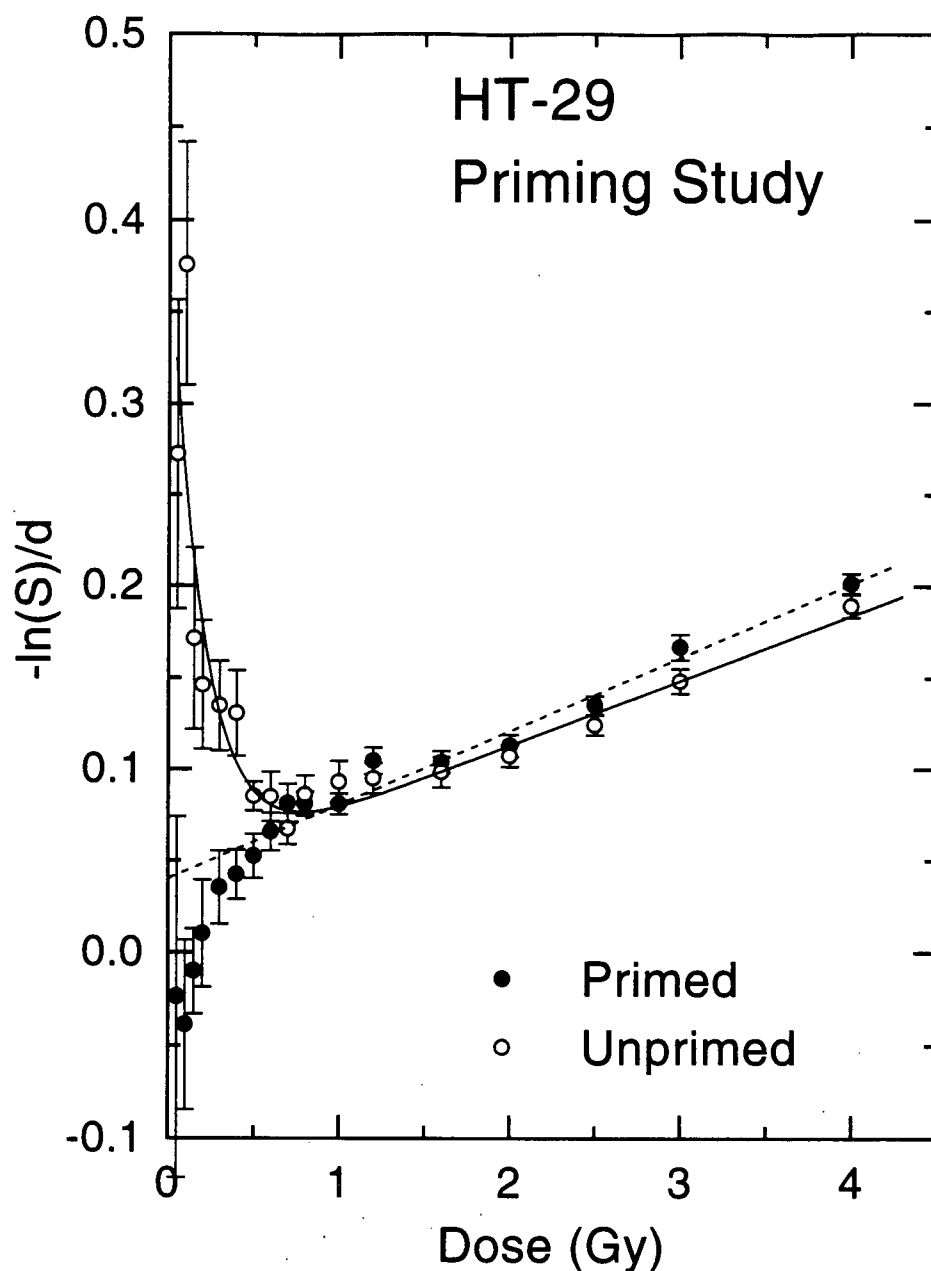
Figure 4-35 Suspension Primed Cell Response to the Challenge Dose II
The HT-29 suspension priming data shown in figure 4-34 are replotted in terms of the relative effectiveness per unit dose, -ln(S)/d. The data at low dose show a clear distinction between the response of the primed (solid circles) and unprimed (open circles) responses. The unprimed response exhibits an increased effectiveness (hypersensitivity) at low doses, while the primed response exhibits a reduced effectiveness as compared to that which is predicted by a LQ fit to the data.

Utilization of this protocol also allows one to plot the survival as a function of total dose. In figures 4-36 and 4-37 the primed data have been replotted as a function of the total dose delivered (*i.e.*, including the priming dose), and were thus normalized by the zero dose plating efficiency measured immediately prior to the priming dose. Although this value was measured 4 hours prior to initiation of irradiation with the challenge doses, as shown previously (see figure 4-33), no significant change in the zero-dose plating efficiency was observed over this time period. Figures 4-36 and 4-37 show that plotted in this manner, the primed and unprimed radiation responses above 1 Gy are indistinguishable. This suggests that there was little or no repair of the sublethal damage produced by the priming dose during the 4 hour incubation period. Instead, the primed cells respond as though the total dose received was delivered at once, as opposed to two doses separated by 4 hours. Figure 4-38 shows that this finding cannot be explained by a change in plating efficiency of the primed cells over the 4 hour period between doses. This figure shows that the plating efficiency determined immediately after the priming dose is identical to that determined 4 hours later. Figure 4-37 suggests that at doses below 1 Gy, there is some protection offered by the protraction of the two doses, with the primed cells exhibiting a more resistant response over the dose range 0.3-0.8 Gy.

4.2.5 Synchronous Low Dose Response

To investigate further, the mechanisms responsible for the observed low dose hypersensitivity, the radiation response was measured in a population of tightly synchronized HT-29 cells. This approach was taken to reduce the effect of cell-cycle specific subpopulations of cells with different intrinsic radiosensitivity, on the
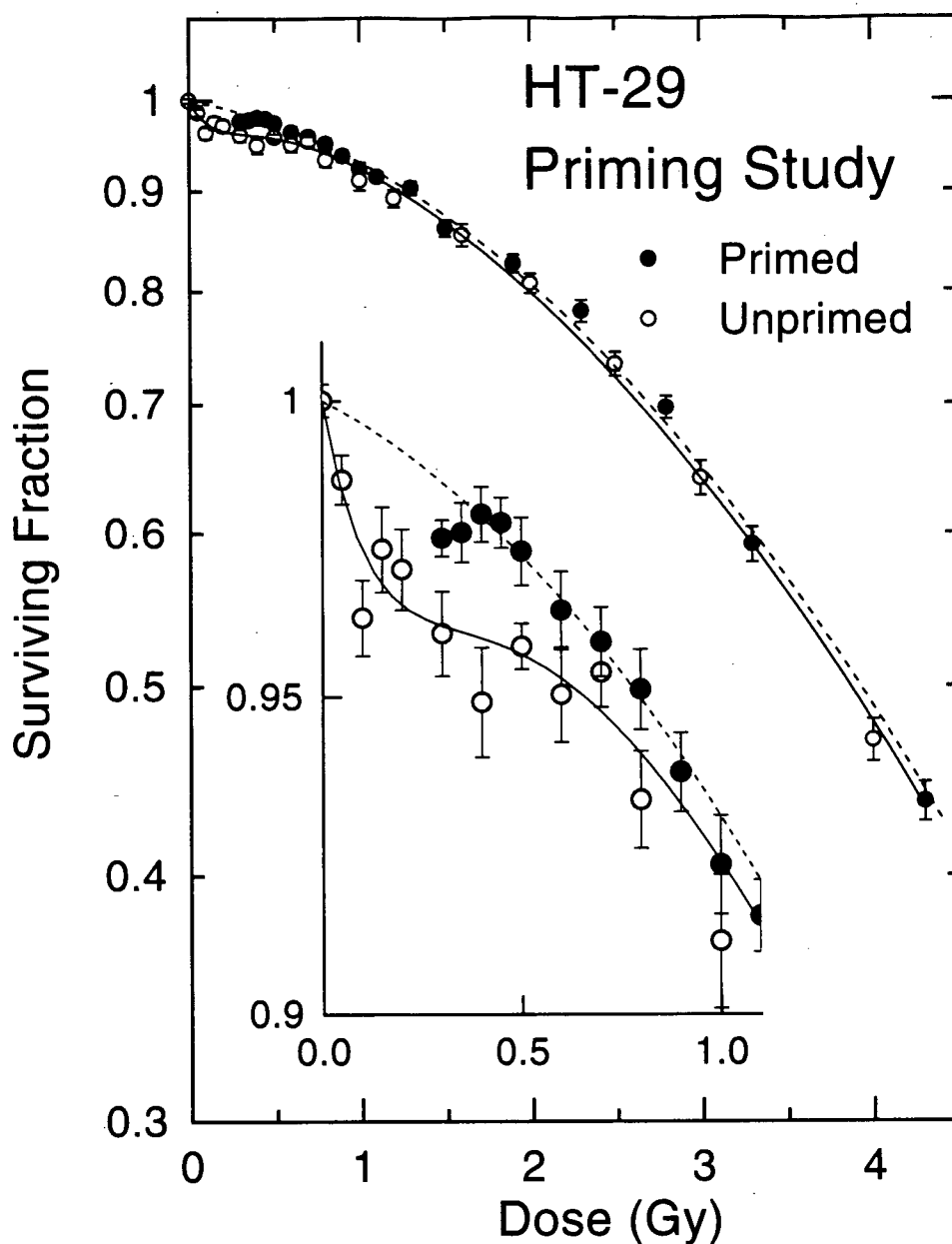
Figure 4-36 Suspension Primed Cell Response to the Total Dose I
Data are the average of 4 unprimed (open circles) and 4 primed (solid circles) HT-29 survival responses obtained using the presort protocol. Primed responses received 0.3 Gy while in suspension culture, 4 hours prior to measurement of the dose response. Survival of the primed population is plotted as a function of the total dose, and thus is normalized to the zero dose plating efficiency determined prior to the priming dose. The unprimed response is fitted with the variable-α model (equation 4-3 - solid line) and the primed response fitted with the LQ model (equation 3-4 - dashed line).
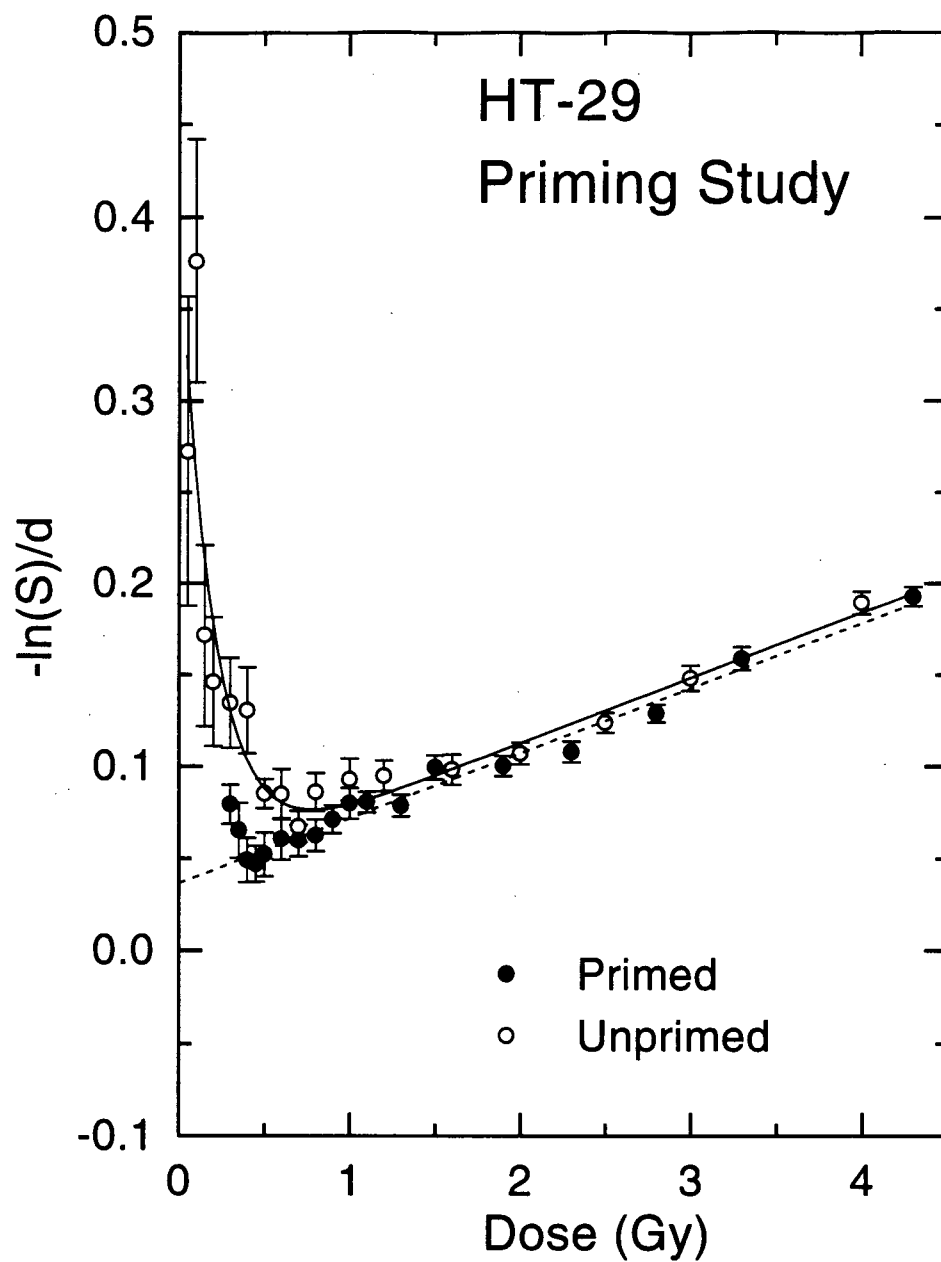
Figure 4-37 Suspension Primed Cell Split Dose Response II

The HT-29 suspension priming data shown in figure 4-36 are replotted in terms of the relative effectiveness per unit dose, -ln(S)/d. The unprimed and primed cells exhibit similar responses, except for very low doses in the primed response where there is a somewhat reduced effectiveness as compared to the unprimed data.
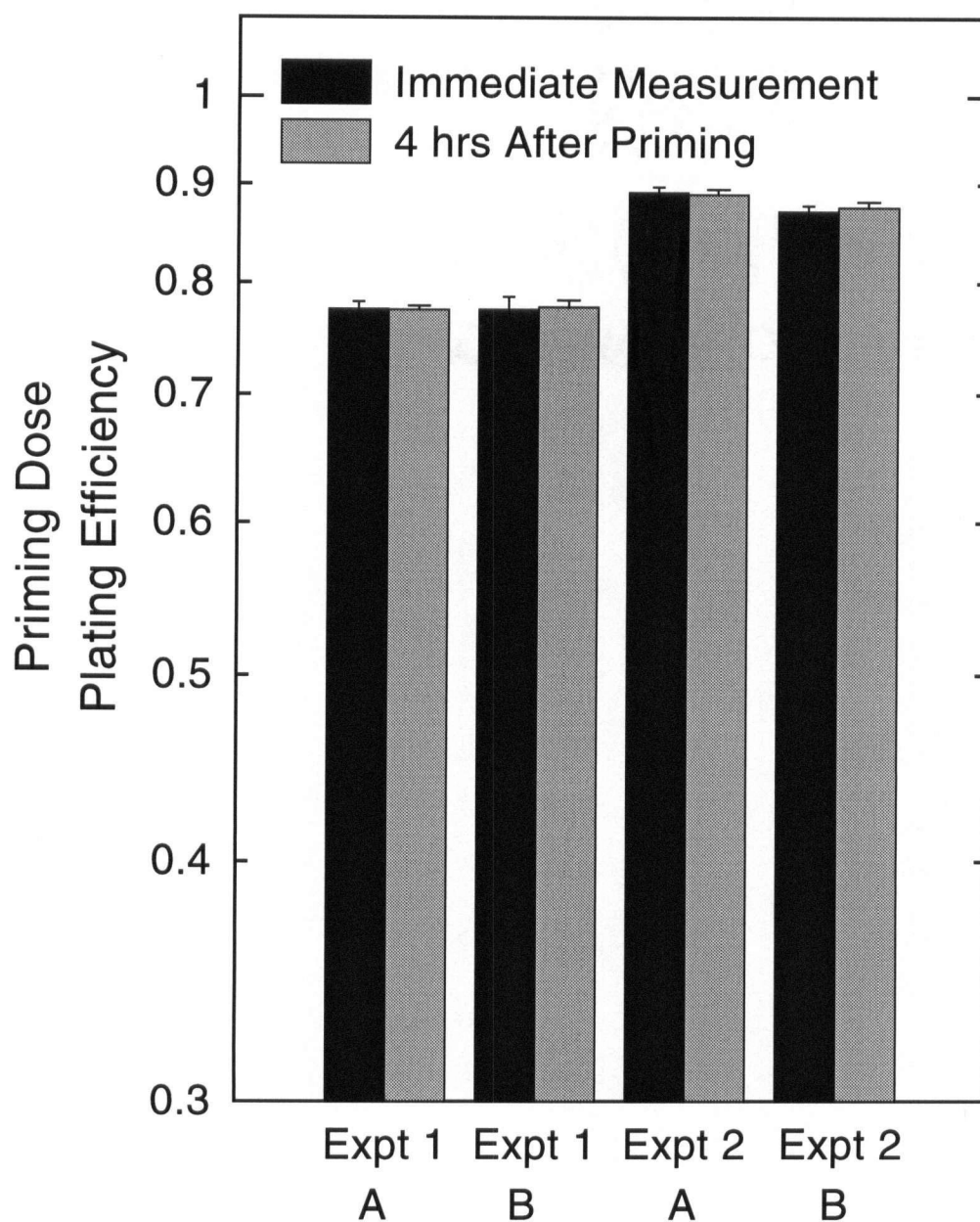
Figure 4-38 Priming Dose Plating Efficiency
The plating efficiency of HT-29 cells in suspension culture following a 0.3 Gy dose is shown measured either immediately following the dose (solid bars) or 4 hours later (gray bars). Results from 4 individual survival responses in 2 separate experiments are shown.

substructure observed at low doses of radiation. HT-29 cells were synchronized by forcing them to growth arrest in plateau phase (G0 phase of the cell cycle). To evaluate the best method for plateau phase synchronization, HT-29 cells were seeded at high density in tissue culture flasks, such that monolayers reached 100% confluency (complete coverage of the growth surface) in 2-3 days. On day 3, the cell monolayers were fed with growth medium containing serum levels of 10%, 5%, 1%, 0.1%, or were not fed at all. This procedure continued daily for an additional 4 days, at which time cells were harvested and analyzed for DNA content. Figure 4-39 shows the resulting DNA histograms of the cell populations for each of the monolayers, as well as the DNA profile of an exponentially growing control population of HT-29 cells. This figure demonstrates that the most homogeneous population of cells was the one that was not fed during the 8 day period. In all other populations, regardless of whether they were fed with medium, or medium with any percentage of serum, there was a small fraction of cells that remained in exponential growth, even though most of the cells were arrested in G1/G0. This is evident both from the peak at the G2 DNA content, and from the measurable numbers of cells with S-phase DNA content. In the unfed population, a small G2 phase population was evident (~4%), however no measurable proliferative fraction was observed.

The radiation survival response of plateau-phase (G0) cultures of HT-29 cells obtained by the optimal synchronization method described above was measured using the presort protocol. The mean data determined from the average of six such responses, along with the standard error in the mean, are plotted in figures 4-40 and 4-41. Similar to

DNA Content
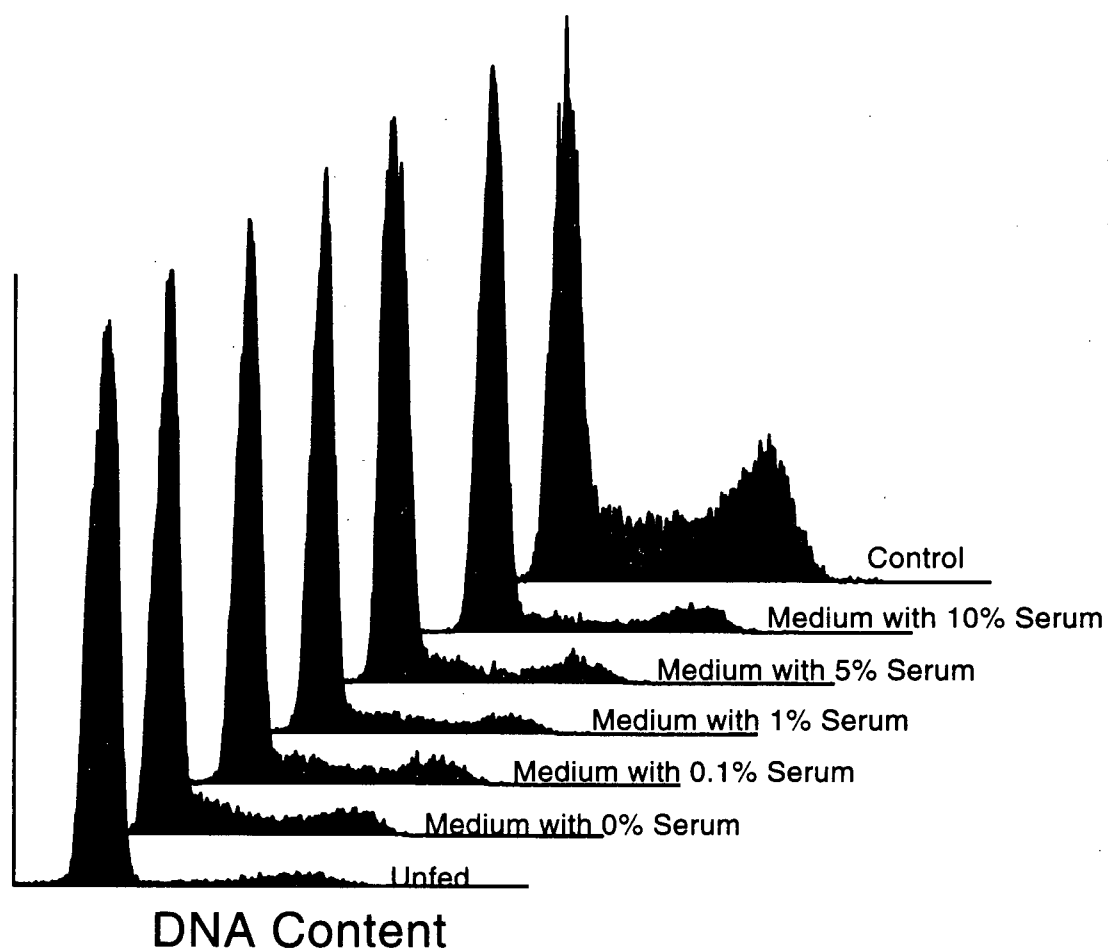
Figure 4-39 Induction of Plateau-Phase in HT-29 Cells

DNA histograms of confluent cultures of HT-29 cells grown under different conditions. Cells were seeded at high density such that confluency was reached within 3 days. Cultures were then fed with medium with different amounts of serum, or not fed at all. 8 days after seeding, cells were harvested and analyzed for DNA content. The DNA distribution in an exponentially growing population is shown as a control.

the results with asynchronously growing cells, this data set also exhibits a complex response at doses below 1 Gy. The response of these cells is initially hypersensitive (first 2-3 dose points) followed by a rapid increase in radioresistance over the dose range 0.1-0.3 Gy. At this dose, the measured surviving fraction is not significantly different from that at zero dose. Beyond this point the cell kill increases in the manner that would be expected based on a LQ fit of the data. The suggestion that there is an increase in the measured surviving fraction with an increase in dose cannot be explained on the basis of subpopulations of cells, and suggests that the observed response is the result of a radiation-induced resistance that increases the capacity of cells to survive this treatment. The DNA profiles for each of the six plateau phase responses are shown in figure 4-42.
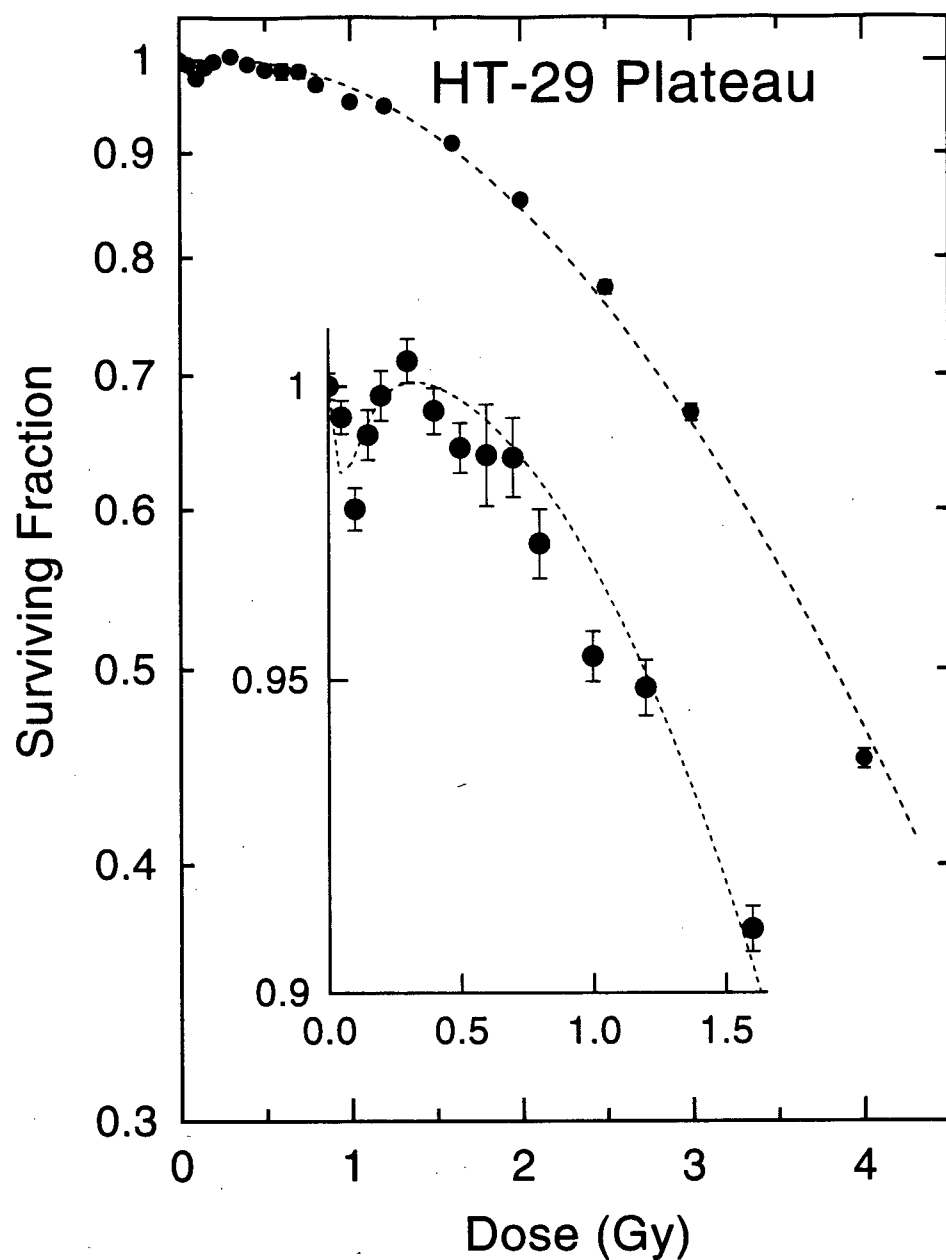
Figure 4-40 Low Dose Radiation Response of Plateau-Phase HT-29 Cells I
Cell survival data of synchronous HT-29 cells irradiated with low doses of X-rays. Survival was measured using the presort cell sorting assay with irradiation taking place in a 37°C phantom following cell sorting. Cells were synchronized in the plateau/G_0 phase of the cell cycle by a combination of high cell density, and nutrient deprivation (no reduction in the zero dose plating efficiency was observed). The mean data are the average of 36 measurements from 6 individual survival responses, and error bars are the standard error in the mean. The dashed line represents the best fit of the variable-α model (equation 4-3) to the data.
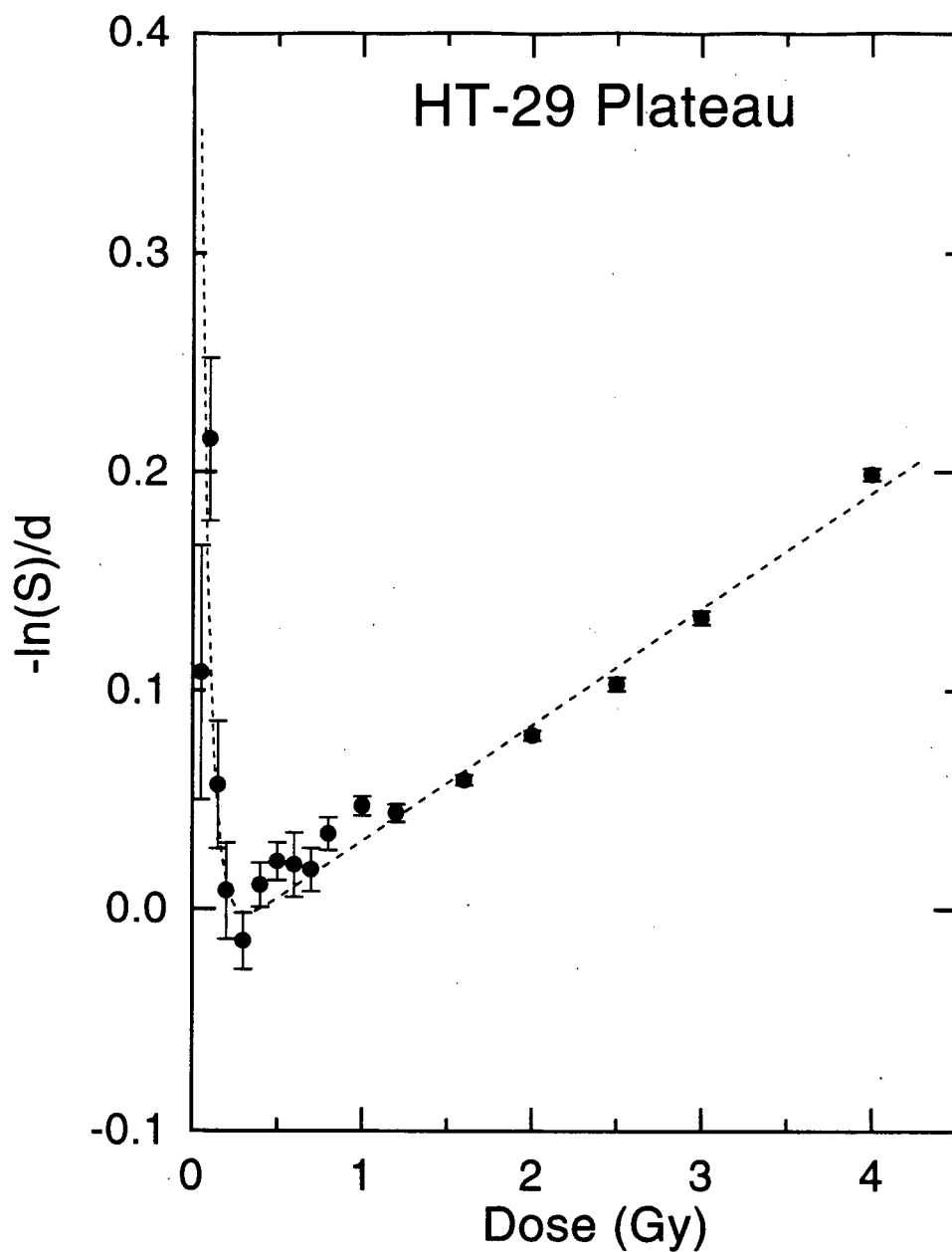
Figure 4-41 Low Dose Radiation Response of Plateau-Phase HT-29 Cells II
The HT-29 synchronous low dose survival data shown figure in 4-40 are replotted in terms of the relative effectiveness per unit dose, -ln(S)/d. The first three data points at low dose exhibit an increased effectiveness per unit dose as compared to that which would be expected by a LQ fit of the data above 1 Gy.

DNA Content
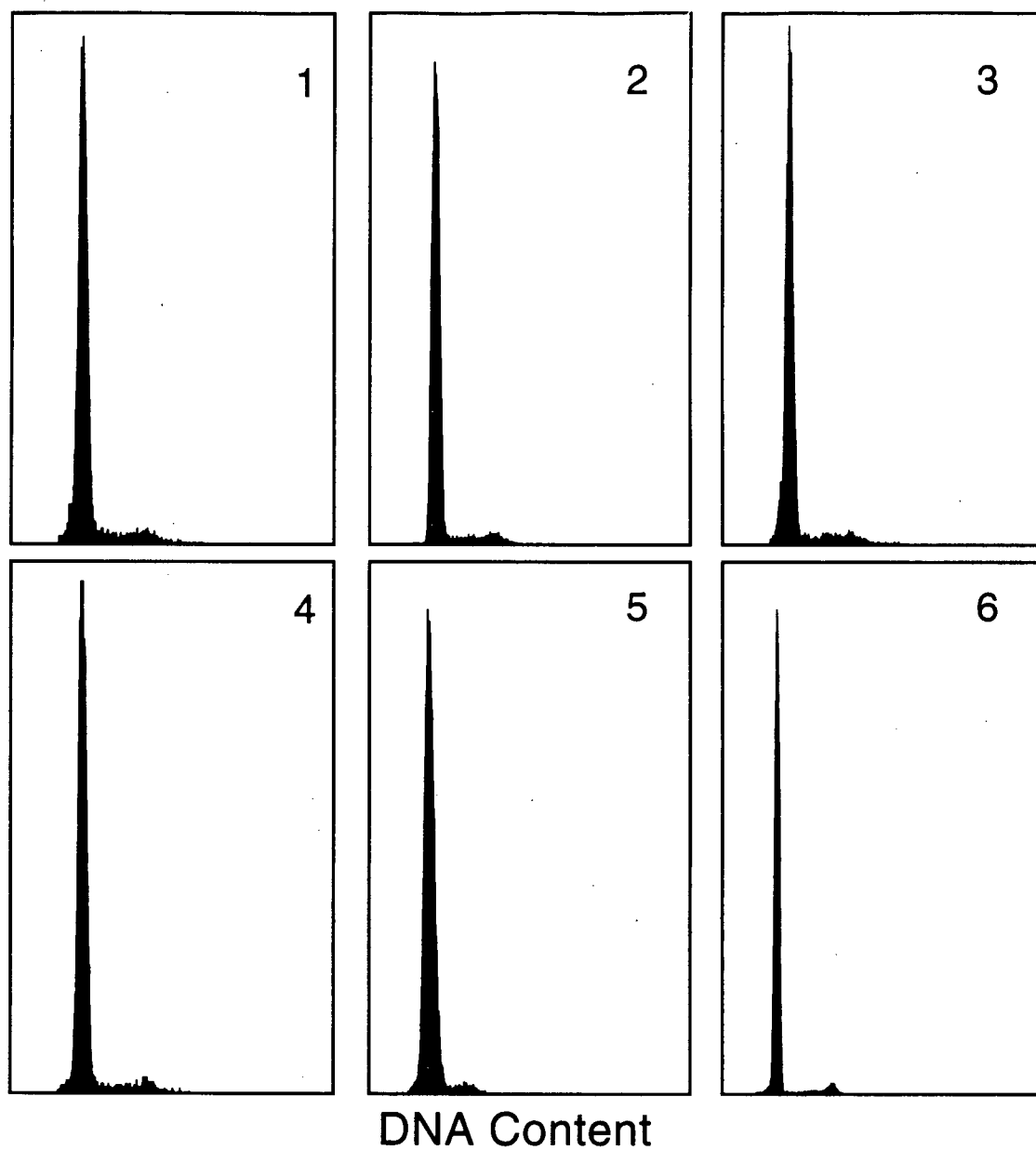
Figure 4-42 HT-29 Plateau-Phase DNA Histograms
DNA histograms from each of the six HT-29 synchronous cell populations for which survival after low doses of radiation were measured. Cell populations were synchronized in the G0/G1 phase of the cell cycle through a combination of high cell density and nutrient deprivation.

4.3   Discussion

The radiation response of DU145 cells was first measured using the postsort cell

sorting assay. Eight survival responses were measured, and when the data were averaged,

a region of low dose hypersensitivity below 1 Gy was observed (see fig. 4-4) (Wouters

and Skarsgard 1994). However, in this data set the existence of this hypersensitivity

could not be confirmed in each individually measured survival response; it became clear

only in the averaged data. Subsequently, a new experimental procedure, termed the

presort protocol, was adopted, and an additional four survival responses measured for this

cell line. The presort data confirmed the existence of low dose hypersensitivity measured

with the postsort protocol, and in this latter data set, a clear indication of the

hypersensitivity was seen in each of the four individual survival responses (data not

shown). Data for DU145 cells obtained using the presort protocol had significantly less

variability than data obtained with the postsort protocol, as observed in the scatter plots of

figures 4-2 and 4-6. Examination of the error bars in the mean data for each of these two

data sets (fig. 4-10) shows that the relative error in the mean data was significantly lower

for the presort than for the postsort protocol even though twice as many measurements

were made in the latter protocol (48 versus 24 measurements at each dose point). The

increase in precision with the presort assay is most likely due, in large part, to the

reduction in time required for sorting, irradiation, and plating. This sequence was very

regulated, and generally could be performed within approximately 7 minutes. In addition,

all cells were sorted under the same starting conditions, eliminating the possibility of cell

loss or cell selection prior to sorting. However, despite differences in the variability of

the presort and postsort data, the average values for survival determined by both methods are in very good agreement over the entire dose range (fig. 4-10).

The application of the presort assay to two additional cell lines, HT-29 and A549, revealed similar low dose substructure. A clear indication of hypersensitivity at low doses is evident in comparison to the predicted response obtained from a LQ fit of the data above 1 Gy. In both of these additional cell lines a LQ fit which accurately characterized the data above 1 Gy, significantly overestimated the measured survival below approximately 0.5 Gy. The hypersensitive response was different in each of the three cell lines, with HT-29 and DU145 cells exhibiting extended regions of hypersensitivity, followed by a large increase in radiation resistance. This increase is reflected in the overall greater radioresistance of these cell lines at higher doses as compared to A549 cells, for which an increase in radiation resistance is observed at a lower dose and to a smaller extent, resulting in a more sensitive overall response.

4.3.1 Possible Explanations for the Observed Low Dose Hypersensitivity

4.3.1.1 Is It Real?

One possible explanation for the substructure below 1 Gy in these responses, is that the observed reduction in survival at low doses is simply a statistically random one, resulting from limited sampling statistics at low doses. Measurement of a reduction in survival of the order of 0-5% at low doses is severely hampered by statistical variation, in addition to other random errors in counting, plating, and dilution that are associated with the clonogenic assay (Boag 1975). The cell sorting assay improves on the conventional

plating technique by counting accurately the number of cells to be plated, thereby reducing the plating variation from a Poisson to a binomial distribution, which has a statistical advantage at high plating efficiencies or low radiation dose. At lower plating efficiencies the variance approaches that of a Poisson distribution. To examine this possibility, an attempt was made to isolate the error that arises from application of the assay itself. For this purpose, a set of data consisting of four survival responses measured on one day was chosen. This selection eliminated, as much as possible, the biological variation that is observed from one experiment day to another. From this data set, the relative error in the measured plating efficiency was calculated, and is shown in table 4-3. Column 4 of this table shows that the measured relative errors calculated for each Petri dish from the standard deviation in this data set are between 3-7% of the measured plating efficiency. This error represents the variation from one measurement to another based on counting approximately 500 colonies per Petri dish, and is not sensitive to variations in overall sensitivity from one experiment day to another, observed in some cell lines. For the average of all 24 measurements (4 survival responses) the error is reduced to 0.6-1.4% of the mean value (column 5). The source of this error is subdivided into two elements. The first is the contribution due solely to counting statistics, resulting from limited sampling of data, and is not influenced by any biological variation or experimental error. This error (column 6) ranges from approximately 1.9% at 0 Gy (P.E.= 83.4%) to 3.8% at 4 Gy (P.E.= 35.6%) in terms of the variation from one dish to another, and the relative error in the mean is reduced to a range of 0.4-0.77%. The residual error in the data, represented by the difference between the measured error and

the binomial error, is due to biological and other experimental variance. Table 4-3 also lists these values, which range from 1.7% to 6.2% from plate to plate (column 8) and 0.35% to 1.26% for the relative error in the mean (column 9). A total of 8-15 survival responses has been measured for each of the cell lines under study here, thus reducing this error even further. The residual experimental variance is kept small by careful attention to maintaining identical experimental conditions in all experiments, but for all cell lines still contributes more to the measured error than the binomial error. This analysis shows that the gain in accuracy through the combination of the cell sorting assay and data averaging has reduced the error in the mean values to sufficiently small values as to discount the suggestion that the observed phenomenon is a random, statistical one. This is reflected in all three cell lines (figures 4-11, 4-13, and 4-15) where data points within the hypersensitivity region, including the range in S dictated by the measured standard error, fall below the LQ prediction. This is despite the fact that these data contain error that is attributable to an experiment-to-experiment biological variation, rather than just the errors that are demonstrated in table 4-3. In addition, the mean data show a consistent trend for HT-29, DU145 and A549 cells, and are not simply scattered about the LQ response as would be expected from unknown random errors. Further support for the concept of a genuine hypersensitive low dose region comes from the fact that evidence of this phenomenon was observable in all individual presort survival responses for these cell lines; the mean data were not influenced significantly by just one or two responses (data not shown).

Because these measurements were made over many months, small variations in

the overall sensitivity were occasionally found. In a standard clonogenic assay over 3-4 logs of cell kill, these variations would be considered quite small. However, with the precision in these data, plotted over only a single log of cell kill, the effect is significant. This variation may be, in part, due to different experimental conditions including medium and serum changes, and trypsinization protocols. However, despite these changes in radiosensitivity, the hypersensitive low dose region was always present. In general, averaging data with these slightly different responses had the effect of smoothing out the transition from the sensitive to resistant region, especially in the HT-29 data for which 15 survival responses were averaged. When the data for HT-29 cells were first normalized by the average mean inactivation dose (see results section 4.2.2), more consistent responses were obtained. These responses are shown together in figure 4-17, and they exhibit an even more pronounced substructure at very low dose. The radiation responses are consistently hypersensitive at doses below 0.25 Gy, followed by an increase in radioresistance that results in a very flat response over the dose range 0.25-0.75 Gy.

4.3.1.2 A Sensitive Subpopulation?

A second possible explanation for the observed low dose hypersensitivity is the presence of a small subpopulation of sensitive cells, perhaps in some specific phase of the cell cycle, which is preferentially killed at low doses. This is analogous to the substructure observed at higher, clinical doses, as shown in the radiation responses in chapter 3, and which has been previously identified in mammalian survival responses and attributed to cell-cycle variations in radiosensitivity (Skarsgard *et al.* 1991, 1992, 1993, 1994a, 1995, Skwarchuk *et al.* 1993). This substructure revealed the emergence of a

more resistant subpopulation at doses of approximately 3-4 Gy (under aerobic conditions), and has been shown to be present in the same cell lines under investigation here (Skarsgard *et al.* 1995, chapter 3). In order to illustrate these 2 forms of substructure in one plot, the aerobic survival data for DU145 cells measured for the studies reported in chapter 3 (fig. 3-13), together with the low dose data presented in this chapter (figure 4-11) are shown in -ln(S)/d form in figure 4-43. The emergence of a more resistant population at a dose of 4-6 Gy results in a LQ fit of the high (or entire) dose region that underestimates the true survival in the low dose region (Skarsgard *et al.* 1991, 1992, 1993, 1994a, 1995, Skwarchuk *et al.* 1993). This apparent paradox results simply from fitting high dose data in which sensitive (G1 and G2) cells have been selectively killed. Separate fitting of the low dose DU145 data (0-4 Gy) from chapter 3 (see table 3-1), and from other earlier studies (Skarsgard *et al.* 1995), yields α and β values that are similar to those which describe the 1-4 Gy data presented in this chapter, that is, excluding the hypersensitive region. For 2 of the 3 cell lines, DU145 and A549, differences in parameter values between this work and previous data (Skarsgard *et al.* 1995) may reflect a drift in the response characteristics of the cell lines during the considerable time over which the 2 studies were carried out, and/or slight differences in experimental technique. Because the first data point in the earlier data was at a dose of 0.4 Gy, or greater, it would not have been possible to observe the low dose hypersensitivity that is observed in these very low dose studies. However, many of the responses shown in chapter 3, such as the average aerobic HT-29 response (fig. 3-7, and fig. 4-43), do show an increased effectiveness for the first data point (0.4 Gy) consistent with the hypersensitivity observed here.
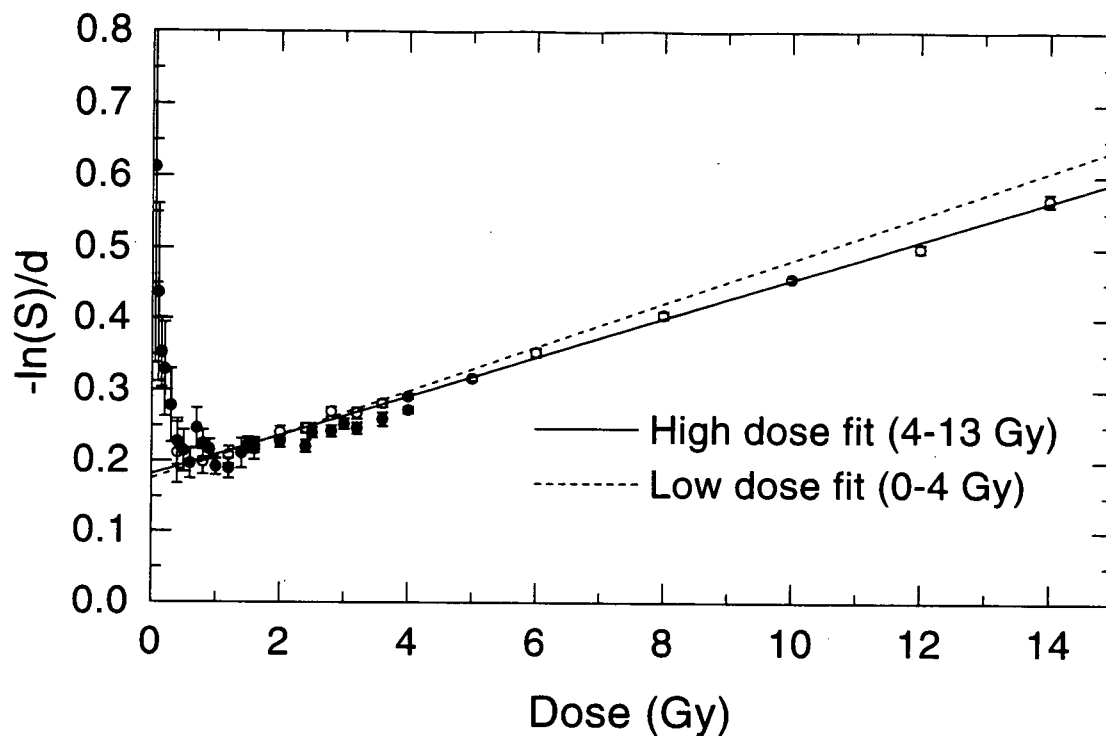
Figure 4-43 Two Forms of Substructure
Survival data for DU145 cells are the average of 12 low dose responses (fig. 4-11) and 4 full dose responses (chapter 3 fig. 3-13) and are replotted together in the -lnS/d form. This plot illustrates two forms of substructure in the radiation response curve. Emergence of a resistant population (reduced effectiveness) is evident at doses above ~6 Gy due to cell-cycle associated subpopulations. At very low doses, the second form of substructure is manifested as a hypersensitivity, or increased effectiveness per unit dose. The solid and dashed lines are fits of the high and low dose regions of the data from figure 3-13, respectively.

Thus the hypothesis that a small subpopulation is the basis of the low dose hypersensitivity would imply a second order of substructure in a dose range below that previously investigated with the cell-sorter assay (chapter 3). This hypothesis was tested by fitting the data with a two-population model (the TPLQ model), a method that has previously been shown to provide excellent fits to multiphasic survival responses (Skarsgard *et al.* 1994a). As expected, modeling the response provided very good fits to the data, indicated by the small χ^2 and RMS values in table 4-4. However, these fits require the sensitive fraction, f, to have an extremely high radiation sensitivity, resulting in very large values for α_s. In DU145 cells, this value was limited only by the required goodness of fit, and thus for this cell line, only the lower 95% confidence limit in the value of α_s is quoted. The extreme sensitivity for this small population is required because the initial slope for the entire cell population, hypothesized as containing two subpopulations with different sensitivity, is not equal to the initial response of this sensitive subpopulation, but rather is the composite response of the two populations. Adequate fits require (i) that the sensitive population constitute only ~2% of the total population, and (ii) that α_r be very much smaller than α_s. As a consequence, the sensitivity of the small population must be sufficiently large as to increase the overall initial slope to a value that is consistent with the data, such that nearly all of the sensitive cells are killed by a dose of 0.10-0.3 Gy. Because the estimate for α_s is made from a limited range of data, all analysis has been carried out using a conservative estimate for this parameter (the lower 95% confidence limit). For illustration purposes the survival response of this population is plotted alone (dotted line near the y-axis in figs. 4-21, 4-22,

and 4-23). Even the lower 95% limit on these parameters results in a subpopulation that is *initially* 50 to 700 times more sensitive than the initial response of the remainder of the population. If one considers *best-fit* values, the ratio of the α values would be several times larger than this. The fitted sensitivity of this subpopulation is even several times greater than DNA repair-deficient XRS mutants, or human A-T cell lines (Taylor *et al.* 1975, Jeggo and Kemp 1983, Deschavanne *et al.* 1986, Thacker 1994). It seems unlikely that there would be a subpopulation as sensitive as this, given (i) that observed cell-cycle variations in sensitivity have not exceeded a factor of approximately 10 (Sinclair 1972), and (ii) if there were a cell-cycle specific population with this sensitivity one would expect continuous low dose rate irradiation to be much more effective than it is, because cells would be eliminated as they moved through this exquisitely sensitive phase.

A further argument against the proposal of a cell-cycle specific subpopulation of sensitive cells is revealed by the results of the plateau-phase HT-29 cells. These cells, despite the fact that they contain ~95% G0/G1 cells, also exhibit an initial hypersensitive response followed by a rapid increase in radioresistance (fig. 4-40). Assuming the hypothetical sensitive population (normally ~2% of the total population) is reduced by a factor similar to the reduction in the number of cells in the S and G2 phases of the cell cycle upon induction of plateau phase, then one should not have observed any low dose hypersensitivity. On the other hand, if synchronizing the cells in plateau phase had the effect of selectively enriching this hypothetical population, one would have expected to have observed a substantial increase in the low dose radiosensitivity as compared to the heterogeneous cell population. Furthermore, the two-population model is unable to

accommodate the *increase* in survival with increasing dose that is suggested in this plateau phase response; this model will always result in a continuous decrease in survival with increasing dose.

In comparison with the data for asynchronous populations, the low dose response of synchronous HT-29 plateau-phase cells is considerably different. These cells exhibit a similar initial hypersensitivity, however the increase in radioresistance occurs at a lower dose, and to a greater degree as compared to the heterogeneous population. This suggests that there may be cell-cycle related differences in the low dose hypersensitivity pattern, similar to the already identified cell-cycle related differences in radiosensitivity at higher doses (Terasima and Tolmach 1961, Sinclair and Morton 1966, Sinclair 1972, Skwarchuk *et al.* 1993). However, these differences cannot explain low dose hypersensitivity (in both plateau-phase and heterogeneous populations) as simply a cell-cycle effect.

The results with the priming dose studies are also not consistent with the two-population hypothesis. If the cell population initially contained a subpopulation that was sensitive enough to be effectively killed by the priming dose (as the fitting results suggest), then one would expect that the measured response (without the 2% sensitive fraction) to be that much more resistant than the unprimed population (containing the hypothetical sensitive subpopulation) at *all* dose points. The data presented in figures 4-34 and 4-36 show that the primed cells (0.3 Gy) exhibit no low dose hypersensitivity and are thus more radioresistant as compared to the unprimed cells in this dose region. However, at higher doses these cells are somewhat more sensitive as compared to the unprimed cell population, contrary to the results predicted by this hypothesis. One

possible explanation that could be offered for this lack of increased resistance at higher doses is that the sensitive subpopulation was cell-cycle related; if this were the case, then it would be reasonable to assume that during the 4-6 hour period following the priming dose, a new sensitive subpopulation would be created as cells progressed through the cell cycle. However, since the response showed no evidence of low dose hypersensitivity, this explanation is also implausible (consistent with the plateau-phase results).

Although the existence of a radiosensitive subpopulation cannot be ruled out completely, the modeling results in conjunction with the asynchronous and priming data suggest strongly that this cannot be the sole explanation for the observed low dose hypersensitivity.

4.3.1.3 Induced Radioresistance?

The third possibility explored is the induction of a radioprotective mechanism in the cell following a small dose of radiation. This possibility has been tested by modeling the data with two induced radioresistance models. These models assume that the entire population is initially hypersensitive, and that it becomes resistant as a function of dose. The variable-α model assumes that the cellular sensitivity evolves from a sensitive to a resistant state as a continuous function of dose. This model provided excellent fits to the data for all three cell lines exhibiting low dose hypersensitivity, as illustrated by the goodness of fit values in table 4-5, and the solid lines in figures 4-24, 4-25, and 4-26. This model is characterized by an α value that decreases exponentially as a function of dose from α_s to α_r. The α_r value is thus the same as the α value in a LQ fit to the data above 1 Gy. Interestingly, if we adopt the repair interpretation of the LQ model that was

suggested in chapter 3, this equation can be derived by simply adding a repair induction parameter. In this interpretation, a LQ response results after partial repair of damage that accumulates as a linear function of dose. The fraction of lesions that are not repaired is a linear function of dose, and is given by equation 3-10. In this equation the parameter c_1 represents the initial fraction of unrepaired lesions, and thus the fraction of lesions that are initially repaired is $1-c_1$. The variable-α model is equivalent to adding an exponential term to this value, such that the fraction of potentially repairable lesions rises from zero to $1-c_1$ as an exponential function of dose over the initial dose region. The fraction of initially repairable lesions can then be redefined as:

$$initially\ repairable\ fraction = (1 - c_1)(1 - e^{-d/d_c}) = 1 - c_1 - e^{-d/d_c} + c_1 e^{-d/d_c} \qquad \text{Equation 4-6}$$

The fraction of lesions that are not repaired as a function of dose then becomes:

$$1 - (1 - c_1 - e^{-d/d_c} + c_1 e^{-d/d_c}) + c_2 d = c_1 - (c_1 - 1)e^{-d/d_c} + c_2 d \qquad \text{Equation 4-7}$$

And the corresponding average number of lethal lesions per cell (from equations 3-8 and 4-7) is given by:

$$a_1 d \cdot (fraction\ not\ repaired) = \left[\alpha - (\alpha - a_1)e^{-d/d_c}\right]d + \beta d^2 \qquad \text{Equation 4-8}$$

Then if one defines $a_f=\alpha_s$, and $\alpha=\alpha_r$, the survival response is given by:

$$S = exp\left[-\left(\alpha_r - (\alpha_r - \alpha_s)e^{-d/d_c}\right)d - \beta d^2\right] \qquad \text{Equation 4-9}$$

which is the same expression as the variable-α model. Interpretation of the LQ model in terms of this repair hypothesis is thus consistent with no repair of the lesions that lead to cell death in the initial dose region. This leads to the observed low dose hypersensitivity,

but as damage is sustained, the number of repairable lesions increases exponentially to the value expected on the basis of the LQ response that is observed above 1 Gy.

The ADIR model differs from the variable-α model, in that it assumes that at any dose there exist two populations of cells, one in which the hypothetical induced radioresistance has been triggered and one in which it has not. These populations are defined as those which have received levels of damage above and below some critical damage threshold. Damage is assumed to occur as a linear function of dose, and the two populations are calculated on the basis of a Poisson distribution of damage. Reasonably good fits were obtained with the average damage level fixed at 20 events per gray, although the RMS values were slightly larger than for the variable-α model. Best fits with this model were found with the value of c (the critical number of events required to induce resistance) fixed at 1, resulting in RMS and χ^2 values similar to those for the variable-α model. The prediction of a value of $c=1$ suggests that there is one critical event that is required to induce resistance, and that the different cell lines have different susceptibilities to this event, as indicated by the different values of a (in this model, the average number of events per Gy) shown in table 4-6. The ADIR model predicts that the triggering event cannot be a very common one. Although adequate fits could be obtained assuming 20 events/Gy, similar to the values quoted for the number of DSBs induced per gray (Iliakis et al. 1991), if we assume that the triggering event is a much more common occurrence, such as a single strand break, good fits are not possible. The high yield of such an event results in a very rapid transition of the cell population from the sensitive to the resistant state (see fig. 4-27), which in turn produces a very discontinuous survival

versus dose function that does not produce adequate fits to the data. Similar to the results obtained with the TPLQ model, both the ADIR and variable-α models predict an initial hypersensitive response. However this initial sensitivity of the whole cell population is much less extreme than the sensitivity predicted for the sensitive population in the TPLQ model. For all three cell lines the initial sensitivities correspond to values that are well within the range of sensitivities reported for mammalian cells (Deacon *et al.* 1984, Fertil and Malaise 1985, Deschavanne *et al.* 1986, Malaise *et al.* 1987). Also in contrast to the TPLQ model, both of these induced radioresistance models were able to characterize an increase in survival over the dose range 0.15-0.3 Gy, which is suggested in the plateau-phase results with HT-29 cells (see fig. 4-40).

The good fits exhibited by these models are perhaps not surprising given the number of parameters involved. In general, models with a large number of parameters will normally provide good fits, but at a cost of large correlations between parameters in the model. However, for both the ADIR and variable-α models, fits yielded α and β values for the induced population (resistant response) which agree with each other, and with the values from the simple LQ fit for doses above 1 Gy (tables 4-1, 4-5, 4-6, and 4-7). This indicates that these parameters are not sensitive to the initial response of the cells and thus do not have a large correlation with the other parameters in the model. This allows more confidence in the low dose fitted parameters, and in the goodness of fit statistics. Taken together, the fitting results suggest that the observed hypersensitivity followed by an increase in radioresistance is most likely due to a changing intrinsic radiosensitivity of the cell over the initial low dose region. This result is consistent with

several recent reports using a different clonogenic assay that recognizes and counts cells microscopically, followed by revisitation for colony scoring. Hypersensitive responses were observed in both V79 cells (Marples and Joiner 1993), and in human tumour cell lines (Lambin *et al.* 1993, 1994a, 1994b, Singh *et al.* 1994). These authors have also argued that the observed low dose hypersensitivity is due to a changing radiosensitivity of the whole cell population, rather than to a subpopulation of sensitive cells, and have attributed the increased radioresistance to a radiation-induced repair mechanism. Lambin has previously reported low dose hypersensitivity in one of the same cell lines (HT-29) under investigation here (Lambin *et al.* 1993). Although they reported a slightly larger initial sensitivity, a similar amount of induced resistance was seen, with a relatively flat region (constant response) over the dose range 0.3-0.6 Gy. Multiphasic survival responses with initial low dose hypersensitivity have also been demonstrated with insect cell lines, a result that was also attributed to an induction of radioresistance with increasing dose (Koval 1984). Evidence for radiation-induced protective responses in mammalian cells is also available from a variety of other studies using different endpoints, including chromosome aberrations (Olivieri *et al.* 1984, Wolff *et al.* 1988, Wolff 1992, Seong *et al.* 1995), micronuclei (Azzam *et al.* 1994), mutation studies (Crompton *et al.* 1990), and *in vivo* low dose fractionation studies (Joiner and Johns 1988) (for a review, see Joiner 1994). Recently, evidence of hypersensitivity to doses below 1 Gy that could not be explained on the basis of a sensitive subpopulation of cells, was reported for normal uroepithelium using a postirradiation proliferation assay (Mothersill *et al.* 1995).

4.3.2 Possible Mechanisms For an Increase in Radioresistance

4.3.2.1 The Adaptive Response

The proposal of a radiation-induced increase in radioresistance suggests a possible relationship to a number of studies that have been carried out largely in human lymphocytes, that report the presence of a so-called adaptive response (Olivieri *et al.* 1984, Wolff *et al.* 1988, Shadley 1994). In these studies, a small priming dose protected lymphocytes from radiation-induced chromosome damage 4-6 hours later. These authors have attributed this protection to the induction of a repair mechanism that has the capacity to protect cells against further damage. Marples and Joiner have also conducted priming studies in V79 cells for which they previously reported low dose hypersensitivity in response to single doses (Marples and Joiner 1995). In this study, cells were damaged either with small doses of radiation, or with hydrogen peroxide, several hours before measurement of the radiation response curve. Although these measurements were made only at very low doses (below ~1 Gy), the data showed that the primed cells did not exhibit low dose hypersensitivity following the incubation period. They suggested that this is likely due to an induction of radioresistance over the time period between priming and irradiation. Marples and Joiner suggested that this result provided evidence that the two phenomena are related, and proposed that radiation-induced mechanisms can operate in two ways, either protecting cells primed with a small dose, from damage due to a second challenge dose (termed the adaptive response), or by influencing the response of cells to single doses (Joiner 1994, Marples and Joiner 1995,). However, it should be noted that there are significant differences between the adaptive response and the single

dose induced response. Because the latter is the response to single doses, it is not sensitive to redistribution of cells in the cell-cycle, cell loss over the adaptation period, or changes in factors affecting initial DNA damage (*e.g.*, sulfhydryl levels). The induction of a radioprotective response to single doses cannot protect against initial radiation damage, it can only alter the processing of that damage.

The priming results reported in this chapter are consistent with the data of Marples and Joiner, but offer a different explanation for this phenomenon. Consistent with their findings in V79 cells, irradiation of HT-29 cells 4 hours following a 0.3 Gy priming dose resulted in no hypersensitivity to the second dose of radiation (figs. 3-31, 3-33). However, contrary to the adaptive response, there was no protection offered at higher doses of radiation. The response beyond 1 Gy was, if anything, somewhat more sensitive as compared to the unprimed population (figs. 3-31, 3-33, 3-34). If one compares the survival as a function of the *total* dose received, the primed and unprimed cells responded nearly identically (beyond 1 Gy) as though they had received the total dose at the same time point (figs. 3-36, 3-37). Thus, there appears to have been no protection afforded by the 0.3 Gy priming dose (*i.e.*, no adaptive response) in these cells, at least with respect to damage at total doses greater than 1 Gy. However, this is consistent with the hypothesis that the damage induced by doses below 0.5 Gy is not recognized, or not repaired, and thus results in a radiosensitive phenotype in this dose region. In other words, the constitutive repair mechanisms that operate at doses above 1 Gy in this cell line are either inactive, or less efficient below 0.5 Gy. This results in the observed lack of repair of any sublethal damage during the 4 hour period between doses.

However, the data in figure 3-36 suggest that the split dose treatment can provide a small level of protection against doses just beyond the 0.3 Gy priming dose. This suggests that the threshold or triggering dose that is required to induce the resistant phenotype can be reduced by a split dose treatment, that is , if it is delivered in 2 fractions. These priming studies thus indicate little or no correlation between the adaptive response and induced radioresistance, suggesting that the mechanisms responsible for these two phenomena may be entirely different.

4.3.2.2 An Alteration in Damage Processing

The proposal that, even for single doses, there is an increase in radioresistance over the initial part of the dose response, suggests that there is an alteration in the processing of radiation damage in this dose range. In this hypothesis, cells either do not repair damage as efficiently, or alternatively they may, for example, initiate programmed cell death to a greater degree in response to initial low doses as compared to higher doses beyond the hypersensitive region. There is accumulating molecular evidence that rather than responding passively to radiation, cells monitor and process damage through complex pathways. It is well established that at least two checkpoints exist which relate to DNA damage, one at the G1-S transition, and one at the G2-M transition. These presumably allow time for repair of radiation damage before critical events such as DNA replication or mitotic cell division takes place. Induction of cell-cycle checkpoints following irradiation has recently been shown to be a direct, active response to damage within the cell, rather than simply an inability to replicate damaged DNA (Kuerbitz *et al.* 1992). In particular, many of the molecular events controlling the G1/S checkpoint have

been elucidated. Cells with DNA damage accumulate p53 protein (Kuerbitz *et al.* 1992), resulting in the induction of separate pathways that lead to apoptosis and/or arrest at the G1/S checkpoint (Lowe *et al.* 1993, Guillouf *et al.* 1995), mediated through the induction of many cell-cycle control genes including *GADD45* (Kastan *et al.* 1992) and *WAF-1/CIP1/SDI1* (Xiong *et al.* 1993, Serrano *et al.* 1993). Mutations in the p53 gene have been implicated in the failure of cells to arrest in G1 following irradiation (Kastan *et al.* 1991, Kuerbitz *et al.* 1992), or failure to induce apoptosis (Clarke *et al.* 1993, Lowe *et al.* 1993). Studies have also found a relationship between mutant p53 and an increase in radiation resistance (O'Connor *et al.* 1993, Lee and Bernstein 1993, McIlwrath *et al.* 1994, Little 1994). Less is known about the molecular events at the G2 checkpoint, although it has been shown that the length of the delay induced by radiation, and the relative radioresistance, can be increased by transfection with oncogenes (McKenna *et al.* 1991, Su and Little 1993, Maity *et al.* 1994). Regulation of other genes involved in apoptotic and signal transduction pathways such as *NF-kB* (Prasad *et al.* 1994), *bcl-2, bcl-xl* (Chen *et al.* 1995), protein kinase C (*PKC*) (Woloschak *et al.* 1990) and other genes specific to radiation (Boothman *et al.* 1989), has been shown to be modulated by radiation, and this is likely able to influence the cellular response to damage. In particular, the transcription factor *NF-kB* (Prasad *et al.* 1994), and the immediate early response genes *c-fos, c-jun, c-myc, and c-ras*, are preferentially induced at doses around 0.25-0.5 Gy (Prasad *et al.* 1995), similar to the dose at which induced radioresistance is observed in our studies. Prasad *et.al.* (1995) showed that these low doses of radiation resulted in multiple gene activation from different signal transduction pathways. These

important cell-cycle, signal transduction, and apoptosis-associated genes are modulated by irradiation to different extents at different dose levels, and likely result in altering the inherent radiation sensitivity at different dose levels.

These results suggest that the repair of radiation damage is not simply a static process carried out by constitutively expressed proteins, but rather is a complicated process involving induced gene products, cell-cycle interruptions, and the induction of programmed cell death pathways. Further evidence for the importance of DNA damage processing pathways comes from investigations with A-T cell lines which suggest that the extreme radiosensitivity of these lines may be due in part to a defect in the processing of DNA damage resulting from impaired signal transduction pathways (Thacker 1994, Lavin *et al.* 1994, Meyn 1995). Recently the gene implicated in the A-T disorder has been cloned (designated *ATM*) (Savitsky *et al.* 1995). This gene product has homology to PI-3 kinase that is involved in signal transduction and cell-cycle control (Savitsky *et al.* 1995). Recently, the Damage Surveillance Network model has been suggested to explain the A-T phenotype (Meyn 1995). This model proposes that in the normal phenotype, DNA damage triggers the induction of a signal transduction network, which results in the activation of genes that act to arrest cell progression around the cell cycle, while at the same time inhibiting or down-regulating apoptosis and activating DNA repair. In this model, the ATM gene plays a critical role in the activation of this signal transduction network. The mutation in A-T individuals could thus lead to an inability to inhibit apoptosis (leading to radiation sensitivity), and an inability to arrest the cell cycle (Meyn *et al.* 1994, Meyn 1995). This molecular understanding of the response of cells to

damage allows for the possibility that the processing of damage could be different at different dose levels, and also that induced radioresistance could be a reflection of defective cell-cycle control or programmed cell death pathways, rather than a novel induced repair mechanism. Thus, induction of radioresistance can be hypothesized as resulting from an alteration in damage processing, due to either an increase in repair of radiation damage, or a down-regulation of programmed cell death. An increase in 'repair' might result from an increase in damage recognition, an increase in time available for repair, an increase in the fidelity of repair, or an increase in the amount of repair enzymes available to carry out repair. In addition to the outlined cell-cycle and apoptotic effects, increased damage recognition could also result from an alteration in chromatin structure within the cell. Radiation damage within cells produces chromatin breaks which lead to DNA unwinding and corresponding alterations in chromatin structure, and it has been hypothesized that DNA conformation is an important determinant of cell radiosensitivity (Olive 1992, McMillan and Peacock 1994). Modulation of this chromatin structure by low doses of radiation might in turn modify the processing of DNA damage within that structure following irradiation.

These multiple pathways for processing damage also suggest explanations for radiosensitivity differences observed between the different cell lines. Many of the important tumour suppressor genes and oncogenes involved in cell-cycle regulation are mutated in human cancer cells. In particular, p53 is mutated in both HT-29 and DU145 cells (Rodrigues *et al.* 1990, Isaacs *et al.* 1991, Li *et al.* 1995), both of which show extended ranges of hypersensitivity in relation to A549, which is reported to have wild

type p53 (Lehman *et al.* 1991). It is likely that many other important regulatory genes are mutated in these cells, which could result in differences in damage processing. It is interesting that in DU145, HT-29, and A549 cell lines, it is not the initial very low dose radiosensitivity that differs widely, but rather the final intrinsic radiosensitivity. The initial sensitivity, described by the parameter α_s in either of the induced resistance models, is in close agreement for these cell lines considering the confidence limits (tables 4-5, 4-6, and 4-7). However, the radiosensitivity of all cell lines at higher doses is remarkably different, suggesting that the classically defined intrinsic radiosensitivity may be due in part to the degree of induced radioresistance that occurs.

5

RBE MEASUREMENTS ON THE 70 MEV PROTON BEAM AT TRIUMF USING V79 CELLS

5.1 Introduction

The rationale for the use of particle radiations as an alternative to X-rays for the treatment of cancer is a direct result of the physical nature of these particles. There are two distinct advantages that can be realized with different particle beams, the basis of which can be ascribed to the nature by which the energy of these particles is deposited within biological material.

5.1.1 Relative Biological Effectiveness

5.1.1.1 RBE and LET

The relative biological effectiveness (RBE) of a given type of radiation is generally defined in terms of the ratio of the doses of the conventional and novel radiations that produce equivalent biological effect. Photon beams (X- or γ-rays) are used as the standard for historical reasons. If a dose d_x of X-rays and a dose d_p of some particle beam were found to produce equivalent biological effect, then the RBE equals d_x/d_p for that particle beam *and* for the biological endpoint used. The RBE is important from a clinical standpoint; appropriate use of RBE values allows new radiation modalities to be delivered using doses that produce biological effects equivalent to standard therapy protocols for which the risks of complication are understood. However, RBE must not be regarded as a single-valued parameter, with a characteristic value for each type of radiation. Instead, it has been shown to depend on biological endpoint and on dose, and failure to recognize this can have serious consequences. This was demonstrated by the detrimental late effects observed after the first use of neutrons in which many patients

were severely overdosed (Stone 1959). It was the RBE for acute (early) effects that was used to plan those first clinical tests of neutrons and while the resulting acute effects produced were about as expected, late effects were much more severe. This led to the realization that the RBE for the late effects of neutrons was significantly larger than the RBE for acute effects. High LET radiation has RBE values greater than 1.0, which can in large part be explained by the nature of the microscopic distribution of energy along the path of charged particles. High LET radiations, by definition, deposit large amounts of energy within small volumes. This creates an increase in the relative amounts of complex or clustered damage, which is hypothesized to be more difficult to repair, and thus important for mammalian cell inactivation (Goodhead 1980, 1989, Ward 1988). As a result, the efficiency of cell inactivation (and thus the RBE) increases with increasing LET, at least up to a point. The RBE for most charged particles increases beyond an LET of approximately 10 keV/μm to a maximum at approximately 100 keV/μm, and then begins to decline (Deering and Rice 1962, Barendsen and Walter 1964, Skarsgard *et al.* 1967, Blakely *et al.* 1979). The decline is most likely due to an 'overkill' effect, where the increase in energy deposition within a small volume cannot contribute to any increased cell killing effect. Thus an increase in LET in this range will lead to a reduced efficiency of cell killing, increasing the dose without increasing the amount of cell kill.

5.1.1.2 RBE, OER, and the Cell Cycle

The increased efficiency of cell killing with high LET radiation has important implications for many radiobiological phenomena. Near the point of maximum RBE, the survival response should be dictated simply by the probability that a particle will traverse

a cell nucleus, and thus should be characterized by a single-hit, single target mode of inactivation (equation 1-3). This results in a change in the shape of the cell survival curve, as compared to that found after irradiation with photons, and thus further complicates the notion of RBE. Because the shape of the curve changes with increasing LET (it tends towards a simple exponential), the RBE at high LET values becomes a strong function of dose. It is largest at low doses, where the X-ray response exhibits a shoulder, and becomes steadily smaller with increasing dose. At high doses, or low survival levels, the dose dependence is generally much smaller. This has obvious implications for fractionated radiotherapy protocols where radiation doses are given in small daily increments.

The increased effectiveness of high LET radiation also influences the oxygen enhancement ratio (OER). Hornsey and Silini (1963) showed that irradiation of mouse ascites tumours with neutrons (created by bombarding a thick beryllium target with 16 MeV deuterons) under hypoxic and oxic conditions resulted in an OER for cell survival of 1.8 as compared to an OER of 3.1 determined for X-rays. A similar finding was reported by Fowler *et al.* (1963), providing a stimulus for the renewed use of neutrons at Hammersmith Hospital in London. It was expected that the reduced OER of neutrons should lead to therapeutic gains in tumours containing hypoxic cells. This time, initiation of this modality involved considerable research into the RBE of neutrons, the results of which indicated a dependence on dose (related to the shape of the response) and on the tissue or tumour irradiated (for reviews see Field and Hornsey 1975, Field 1976). Skin has been the most widely studied normal tissue with respect to the effects of neutrons.

Results in human, pig, rat, and mouse show consistent RBE responses, with elevated values at low doses/fraction (Field and Hornsey 1975). Detailed RBE measurements for fractionated doses of pions at TRIUMF in mouse, pig and human skin have also indicated a close correspondence (Skarsgard *et al.* 1980, Goodman *et al.* 1982, Douglas 1983, Douglas *et al.* 1986, Chaplin *et al.* 1987).

High LET radiation also reduces the cell-cycle associated changes in radiosensitivity. In general, the magnitude of the changes in radiosensitivity are reduced for radiations of increased LET (Skarsgard *et al.* 1966, Withers *et al.* 1974, Bird and Burki 1975). In some cell lines the shape of the relative response as a function of cell-cycle position is also altered at high LET, with G2 cells becoming as radioresistant as late S phase cells (Skarsgard *et al.*, private communication). The reduced cell-cycle changes in radiosensitivity are a function of LET, and follow the same general trend as the reduction in OER and increase in RBE with increasing LET (Barendsen *et al.* 1966, Chapman 1980). This adds a further possible advantage for the use of high LET radiation in the clinic, reducing the variability that can result from redistribution of tumour cells within the cell cycle following irradiation.

5.1.2 Dose Distributions of Heavy Charged Particles

The second distinct advantage of particle irradiation is the superior dose distribution that can be realized. Wilson (1946) first suggested the use of fast protons on the basis of their superior dose distribution quality. This advantage is due exclusively to the physical characteristics of energy deposition by heavy charged particles. For such particles, the range within tissue is a well-defined quantity, and since the LET reaches a

maximum near the end of each particle's path, most of the dose is deposited near the end of the track. This results in the characteristic Bragg peak of heavy charged particles. Generally, the width of this peak is quite small, and thus a spread out Bragg peak (SOBP), useful for treatment of tumours, is created by placing a rotating wheel of variable thickness in front of the beam. This scans the position of the peak forwards and back, and the wheel can be constructed to produce a flat physical depth-dose profile (Larsson 1961). However, for high LET particles, production of such a profile results in an increasing effectiveness of the radiation as a function of depth because the proportion of dose that is attributable to the low energy, attenuated particles increases with depth. At the distal edge of the SOBP, 100% of the dose is deposited by the low energy particles, and thus will have a RBE equivalent to that in the Bragg peak alone. An increasing RBE with depth in such beams has been documented for heavy ions and pions (*e.g.*, Blakely *et al.* 1979, Skarsgard *et al.* 1982) and thus the physical depth-dose profiles are shaped to compensate for this increase, such that the biologically equivalent dose is uniform across the width of the SOBP.

5.1.3 Protons and RBE

Protons are perhaps the most desirable of all particles in terms of their dose distribution qualities. With the advent of high quality imaging systems, including computed tomography (CT) and nuclear magnetic resonance imaging (MRI), it has become easier to define the appropriate treatment volume with a high degree of accuracy. This ability lends itself then to the use of particles for which the dose distribution is very

accurate, such that an increase in dose to the tumour can be afforded without a corresponding increase to normal tissue.

High energy proton beams that have significant penetrating ability in tissue are of relatively low LET, and thus their RBE is considered to be small, close to that of X-rays. The RBE-LET relationship for protons follows the same general shape as other charged particles, but reaches a peak at a somewhat lower LET (~30 keV/μm) (Folkard *et al.* 1989, Belli *et al.* 1989). These low energy, short range protons have significantly higher RBE values (Belli *et al.* 1989, 1991, 1993, 1994, Folkard *et al.* 1989), but have a very short range in tissue. Protons of energy in the range of 3 to 1 MeV, have LET values of approximately 10 to 30 keV/μm and a range of approximately 160 to 25μm (Belli *et al.* 1994). Irradiation of V79 cells with protons in this energy range resulted in RBE values for survival of ~1.5 to 3, evaluated at a dose of 2 Gy (Belli *et al.* 1994).

Early laboratory studies of the biological effectiveness of therapy related proton beams, using both *in vivo* and *in vitro* systems, have reported RBE values ranging from 0.6 to 1.8 (reviewed by Raju 1980, 1995). However, a number of these early studies using range-modulated proton beams reported RBE values in the range 1.0 to 1.2 (Tepper *et al.* 1977, Hall *et al.* 1978, Raju *et al.* 1978a) consistent with more recent measurements on high energy, range-modulated proton beams (Urano *et al.* 1980, 1984, Tsunemoto *et al.* 1985, Rosengren *et al.* 1991, Blomquist *et al.* 1993, Robertson *et al.* 1994). In most centres which are using proton beams clinically, the RBE is assumed to be 1.1 (*e.g.*, Munzenrider *et al.* 1989) though in some, a value of 1.0 is used (Tsunemoto *et al.* 1985).

Because of the lower RBE found for protons, it is generally assumed that there is no significant depth dependence for the RBE, and early measurements did not detect any such effect (Raju *et al.* 1978b). However, in view of the fact that the low energy protons have significantly elevated RBE values, and since the SOBP contains, at different depths, different amounts of dose attributable to low energy protons, the proton RBE *should* increase with depth in the stopping peak. The significance of this effect is unknown and at present no compensation is made for this potential rise in RBE. This is probably due to the lack of sufficiently precise techniques for measurement of survival. A recent study has suggested that an increase in RBE with depth in a proton SOBP is resolvable, although the data contained large uncertainties, and the results were not statistically significant (Blomquist *et al.* 1993).

Another question concerning the RBE of protons is whether or not one should consider this value to be tumour or tissue specific. Recent reports have suggested that the RBE of neutrons measured *in vitro* can be very cell-line-specific (Britten *et al.* 1992, Warenius *et al.* 1994). The RBE of the neutron beam from the Clatterbridge Cyclotron (62.5 MeV [p→Be$^+$]) for cell inactivation ranged from 1.5 to more than 3 in a wide range of different human tumour cell lines. This wide range in values results primarily from differences in the photon survival response, which shows much greater cell-line dependence than the neutron survival response, particularly at low dose. The very different shapes of the survival curves of human tumour cells after photon irradiation suggests that the range in RBE values may also be highly dependent on the dose, or level of survival, chosen for comparison. Those cell lines with a large shoulder would most

likely show a larger increase in RBE at low doses for a higher LET radiation that produces a more linear survival curve. For a cell line with a small shoulder, the dose dependence would be expected to be minimal. In view of the fact that the cell-cycle dependence of the radiosensitivity is also affected, the level of cell-cycle associated substructure might also be expected to change. Thus, the true RBE at low doses in different cell lines may be even more different than indicated by measurements made at high dose only. The cell line and dose dependence of the proton RBE is largely unknown, and measurements to date have insufficient precision at low dose to allow confident estimates of RBE at such doses.

The purpose of this chapter is to determine the RBE for the 70 MeV proton beam at TRIUMF. Measurement of the proton RBE using the cell sorting assay in combination with the sliced-gel technique, developed for earlier pion beam studies (Skarsgard *et al.* 1974, 1982, 1983), has allowed measurements of the dose and depth dependence of this value. In view of the fact that there may be a large cell line dependence for both the absolute value and dose dependence of the RBE, a widely studied cell line, Chinese hamster V79 cells, was chosen for evaluation of this parameter.

5.2 Results

A series of experiments were carried out to determine the radiation survival response of V79-WNRE cells both to ^{60}Co irradiation, and to irradiation with the 70 MeV spread out Bragg Peak (SOBP) at TRIUMF. It was important to determine the effectiveness of the beam as a function of both dose and depth within the stopping peak. This required accurate and reproducible positioning of cell samples along the beam axis, and for this purpose, the sliced-gel technique of Skarsgard *et al.* (1974, 1982, 1983) was adopted. This technique involved placing the cells in a liquid gelatin solution at 37°C, loading this suspension into special plastic irradiation tubes, and then solidifying the gel by reducing the temperature to 0°C. Cells could then be irradiated while in this solid support matrix, the tube collinear with the beam axis. After irradiation, the gel was extruded and sliced at 2 mm intervals and cell survival was determined in each slice. This allowed measurement of cell inactivation and hence biological effectiveness of the proton beam as a function of depth in the proton stopping peak.

A total of 3 large experiments were performed. The first of these experiments served partially as a test of the ability of this assay to determine, with good precision, the biological effectiveness of the 70 MeV proton beam. In order to determine with good accuracy the response of V79-WNRE cells to different proton doses as a function of depth within the stopping peak, it was necessary to carry out large, long experiments. This required the cells being exposed to gelatin at low temperatures for extended periods of time. This first experiment also served as a test of the cells to withstand this protocol, and to ensure that the radiation response was not modified by this treatment.

A more detailed analysis of the cell survival response to the 70 MeV SOBP was carried out in two repeated experiments. These two experiments used a different gel preparation (which was dialyzed for 2 weeks as compared to 1 week for the first experiment) and a new set of physical peak-shaping devices (range modulator and collimator). These two experiments were conducted within a 1 month period.

5.2.1 Physical Dose

Figures 5-1(a) and 5-1(b) show the axial and transverse physical dose profiles, respectively, of the 70 MeV range-modulated proton beam at TRIUMF that was used in the first experiment in these studies. Figures 5-2(a) and 5-2(b) show similar data for the proton stopping peak used in both of the second two experiments. In both cases, range modulation of the Bragg peak resulted in a uniform dose distribution over the depth range of interest. In the first experiment, a uniform dose distribution ($\pm 1\%$) within the SOBP extended from a depth of 14-30 mm (fig. 5-1(a)), while in the second experiment, a uniform dose distribution extended from 8-30 mm (fig. 5-2(a)), allowing for more measurements of survival as a function of depth. The apparent non-zero dose beyond 33 mm in figure 5-2(a) results from a leakage current in the detector, and is not real (Dr. Gabe Lam, personal communication). No such leakage was present in the detector used for the absolute dose calibration (see section 2.3.3). Scattering and collimation of the beam resulted in a transverse dose profile with a physical width of approximately 25 mm and 20 mm, for the 1st and 2nd experiments respectively, providing a uniform dose distribution across the diameter of each gel tube.
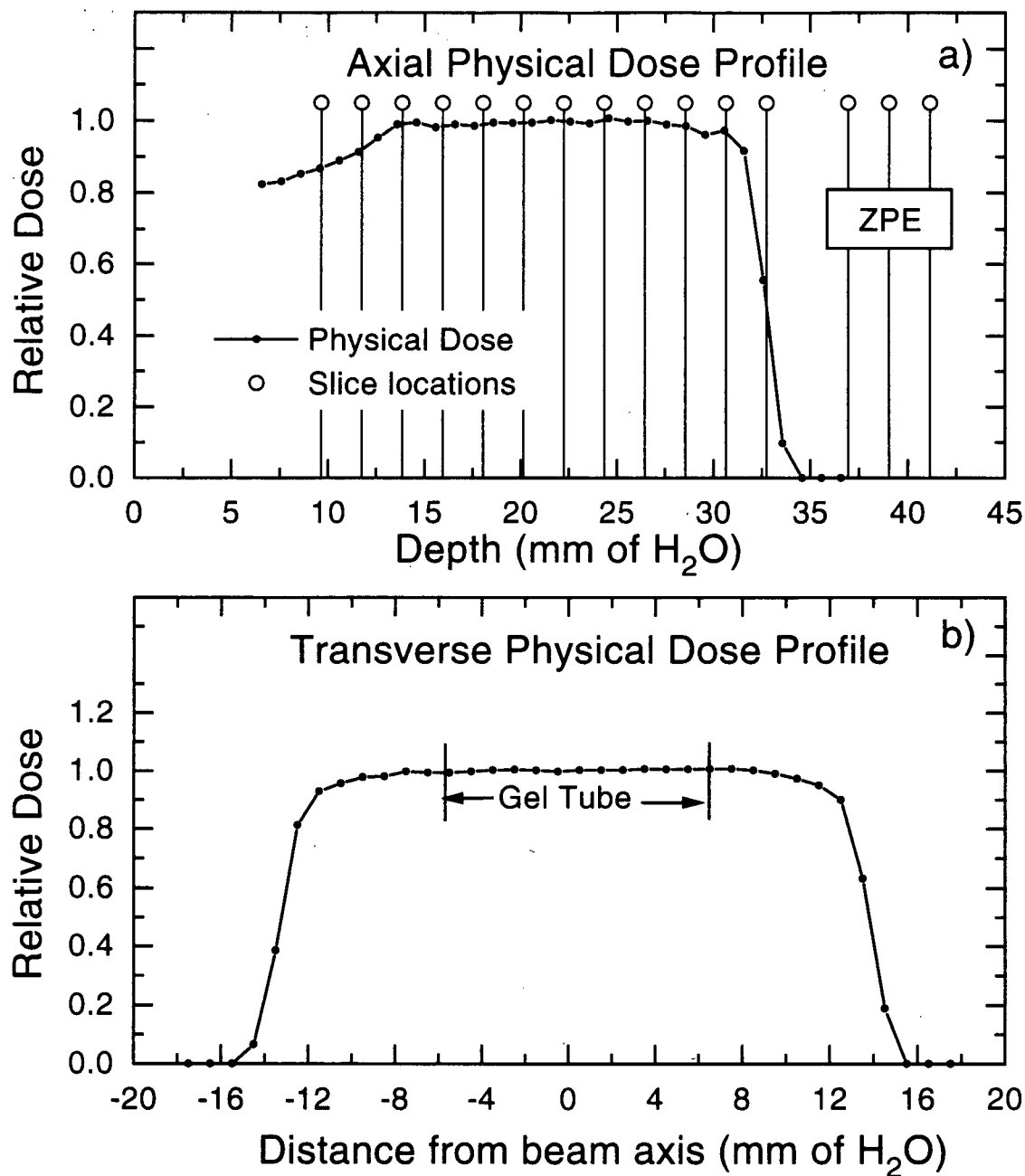
Figure 5-1 Physical Dose Profiles I
The physical dose along the axis of the range modulated 70 MeV proton beam at TRIUMF used for the first experiment, as a function of depth in water (panel a). The Bragg peak was spread out to create a flat stopping peak of approximately 2 cm width using a rotating wheel with sectors of different thickness. Also plotted (vertical lines) is the centre location of each 2 mm gel slice from which survival was measured. The peak has been divided into the proximal and distal regions. Three slices at the end of the tube were used as controls to calculate the zero dose plating efficiency for each tube (ZPE). Panel (b): the transverse physical dose profile. The position of the gel tube is also shown.
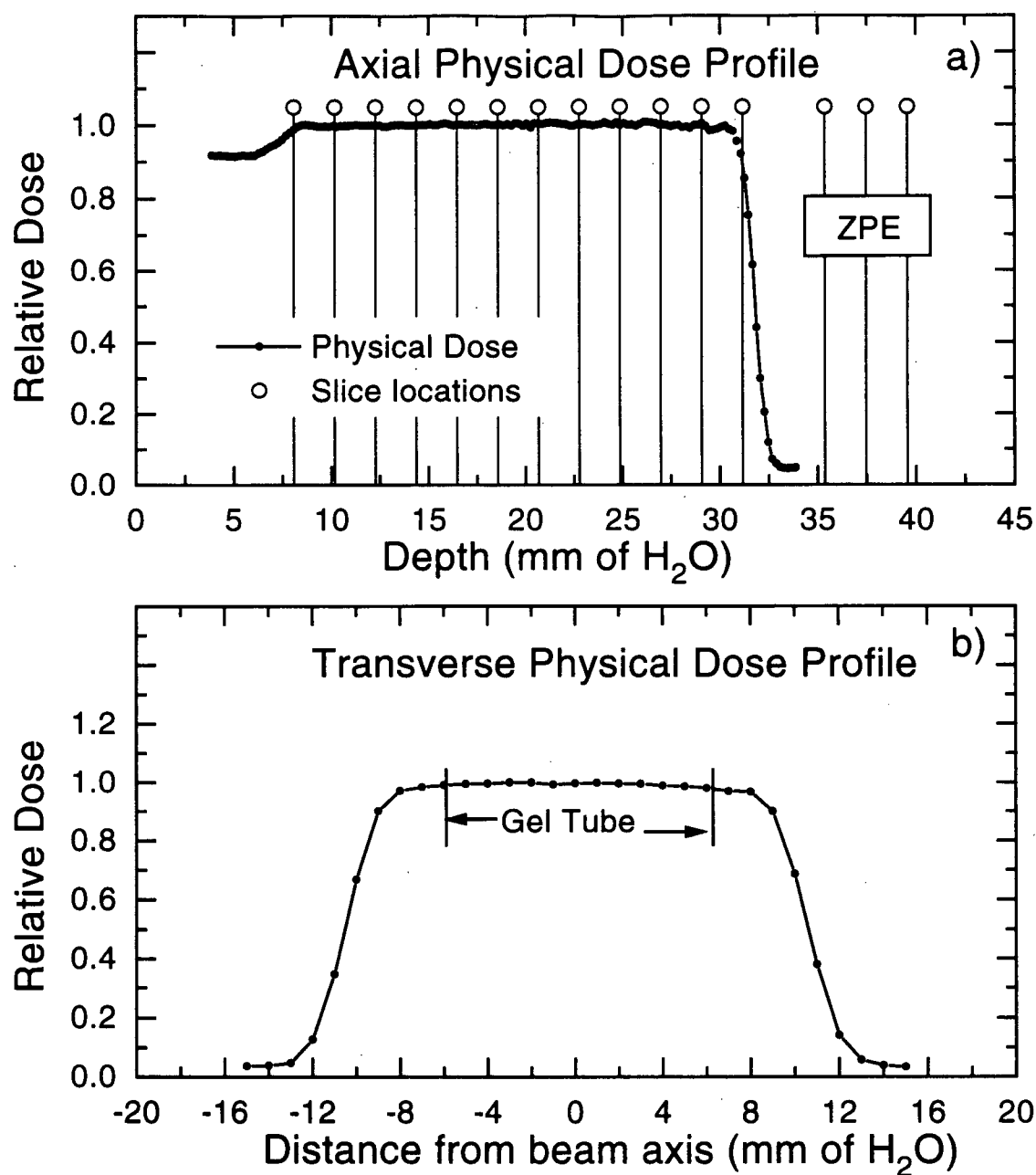
Figure 5-2 Physical Dose Profiles II
The physical dose along the axis of the range modulated 70 MeV proton beam at TRIUMF used for two additional experiments, as a function of depth in water (panel a). The Bragg peak was spread out to create a flat stopping peak of approximately 2 cm width using a rotating wheel with sectors of different thickness. Also plotted (vertical lines) is the centre location of each 2 mm gel slice from which survival was measured. The peak has been divided into the proximal and distal regions. Three slices at the end of the tube were used as controls to calculate the zero dose plating efficiency in each tube (ZPE). Panel (b): the transverse physical dose profile. The position of the gel tube is also shown.

A separate gel tube was placed on the beam axis and irradiated for each prescribed dose point. The gel was extruded and sliced at 2 mm intervals, and each slice assayed for survival using the cell sorting assay. The vertical lines in figures 5-1(a) and 5-2(a) indicate the centre position for each of these slices throughout and beyond the spread out Bragg peak (SOBP). The positions of these slices have been converted to their water equivalent depth. This value can be found by adding the thickness of the entrance window to the phantom tank, the thickness of the cap on the gel tube, and the depth within the gel, all converted to water equivalent depths. For example the water equivalent depth of the 4th slice in experiment 2 would be calculated as follows:

$$Depth = d_w \frac{\rho_w}{\rho_{H_2O}} + d_c \frac{\rho_c}{\rho_{H_2O}} + d_{dgel} \frac{\rho_{gel}}{\rho_{H_2O}} + (2n-1) \frac{\rho_{gel}}{\rho_{H_2O}}$$

$$= 3.11mm \left(\frac{1.15 g/cm^3}{1.0 g/cm^3} \right) + 2.1mm \left(\frac{1.14 g/cm^3}{1.0 g/cm^3} \right) + 1.0mm \left(\frac{1.05 g/cm^3}{1.0 g/cm^3} \right) + (7mm) \left(\frac{1.05 g/cm^3}{1.0 g/cm^3} \right)$$

$$= 14.37mm$$

Here d_w is the window thickness of the phantom, d_c is the gel tube cap thickness, d_{dgel} is the thickness of discarded gel, and n is the gel slice number. The value *(2n-1)* gives the centre position of the *nth* slice. The stopping power for protons, of these various components is taken to be proportional to the density ρ_w, ρ_c, ρ_{gel}, ρ_{H_2O} for the window, cap, gel and water, respectively.

5.2.2 Plating Efficiency

The three slices beyond the SOBP received zero dose, and served as individual plating efficiency controls for each gel tube. This allowed one to control for any effects

of differential toxicity related to the individual treatment of each gel tube. The length of each of these experiments required that the cells remain in the gel matrix for different and extended periods at low temperature (up to 19 hrs). Figure 5-3 shows the combined effects of exposure to the gel solution, and holding at $0^{\circ}C$ on the zero dose plating efficiency for each of the three experiments. Although there is a trend towards increased toxicity at later time points, the average plating efficiency remained comparable to standard sorting experiments with this cell line during which there is no exposure to gelatin, no slicing, and no prolonged storage at $0^{\circ}C$ (an average of 74% and 66% for the latter two experiments compared to 85% in the standard experiment (Skwarchuk *et al.* 1993)). The somewhat lower and more variable plating efficiency in the first experiment (average plating efficiency=52%) is likely due to the fact that the gelatin used for this experiment was dialyzed for only 1 week, as opposed to the standard 2 week procedure.

5.2.3 Individual Experiments

5.2.3.1 Proton Survival Response

The proton radiation responses measured in each of the 3 experiments are plotted in figures 5-4, 5-5, and 5-6. These plots show the average measured survival for V79-WNRE cells in each individual gel slice, plotted as a function of the water equivalent depth within the 70 MeV proton SOBP. Each line represents the survival profile for a single proton tube, irradiated with the designated physical dose. Survival was assayed in 16 gel tubes for the first experiment, and in 19 gel tubes for the second two experiments, rep-resenting proton doses of 0.5 to 10.0 Gy. Due to limitations in cell numbers available
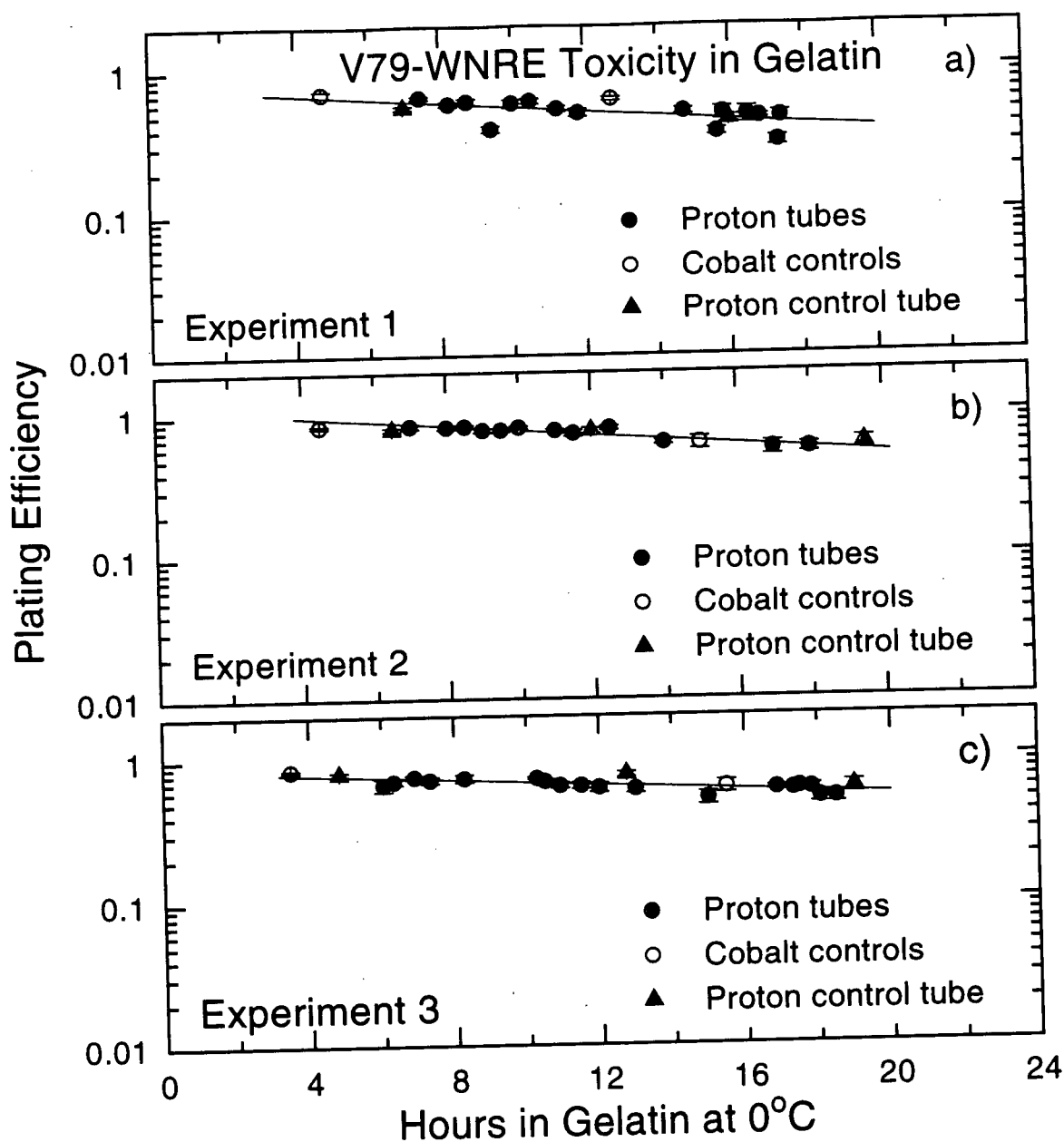
Figure 5-3 W79-WNRE Toxicity in Gelatin
The plating efficiency of V79-WNRE cells as a function of time at 0°C in gelatin-containing medium. Plating efficiency was calculated from a portion of each proton tube that received no dose. One gel tube that received no irradiation (Proton Control) was sampled at various times during each experiment. Also shown are the plating efficiencies for ^{60}Co control samples. The data plotted are from a) experiment 1, (b) experiment 2, and c) experiment 3. The average plating efficiencies (52% in a, 74% in b, and 66% in c) compare well with plating efficiencies under standard experimental conditions (85%).

for sorting, survival within each *individual* slice could only be measured up to a dose of 8.0 Gy. For these slices, the average survival plotted in figures 5-4, 5-5, and 5-6 was calculated from the average of two or three repeats, each producing approximately 300-500 colonies. In the first experiment only (fig. 5-4), available sorting time prohibited measurement of survival for each individual slice in the 7 Gy and 8 Gy irradiated samples, and thus a reduced number of data points were obtained for these doses. Each of the three experiments revealed a small but consistent reduction in cell survival with increasing depth, despite the constant physical dose, this differential becoming more noticeable at higher doses where the radiation effect is larger. Of particular interest is the last slice within the SOBP (at 30.6 mm depth in experiment 1 and 29.1 mm depth in experiments 2 and 3) which exhibits a significantly greater effect as compared to the other slices in the SOBP. This reduced survival results from an increased biological effectiveness, since the physical dose to this slice is, if anything, below the prescribed dose (see figures 5-1(a) and 5-2(a)). The slice beyond this distal edge of the beam (at 32.7 mm depth in experiment 1 and 31.2 mm depth in experiments 2 and 3) received a reduced and non-uniform physical dose and thus exhibited a higher survival. This point also served as a check on the positioning of the gel tube within the measured physical depth profile of the beam.

For doses above 8 Gy, sufficient numbers of cells were not available for cell sorting to provide adequate numbers of colonies from a single 2 mm slice. In experiment 1, conventional plating was used to establish the survival for these doses, the results of which are also plotted in figure 5-4. For experiments 2 and 3, gel slices within the SOBP
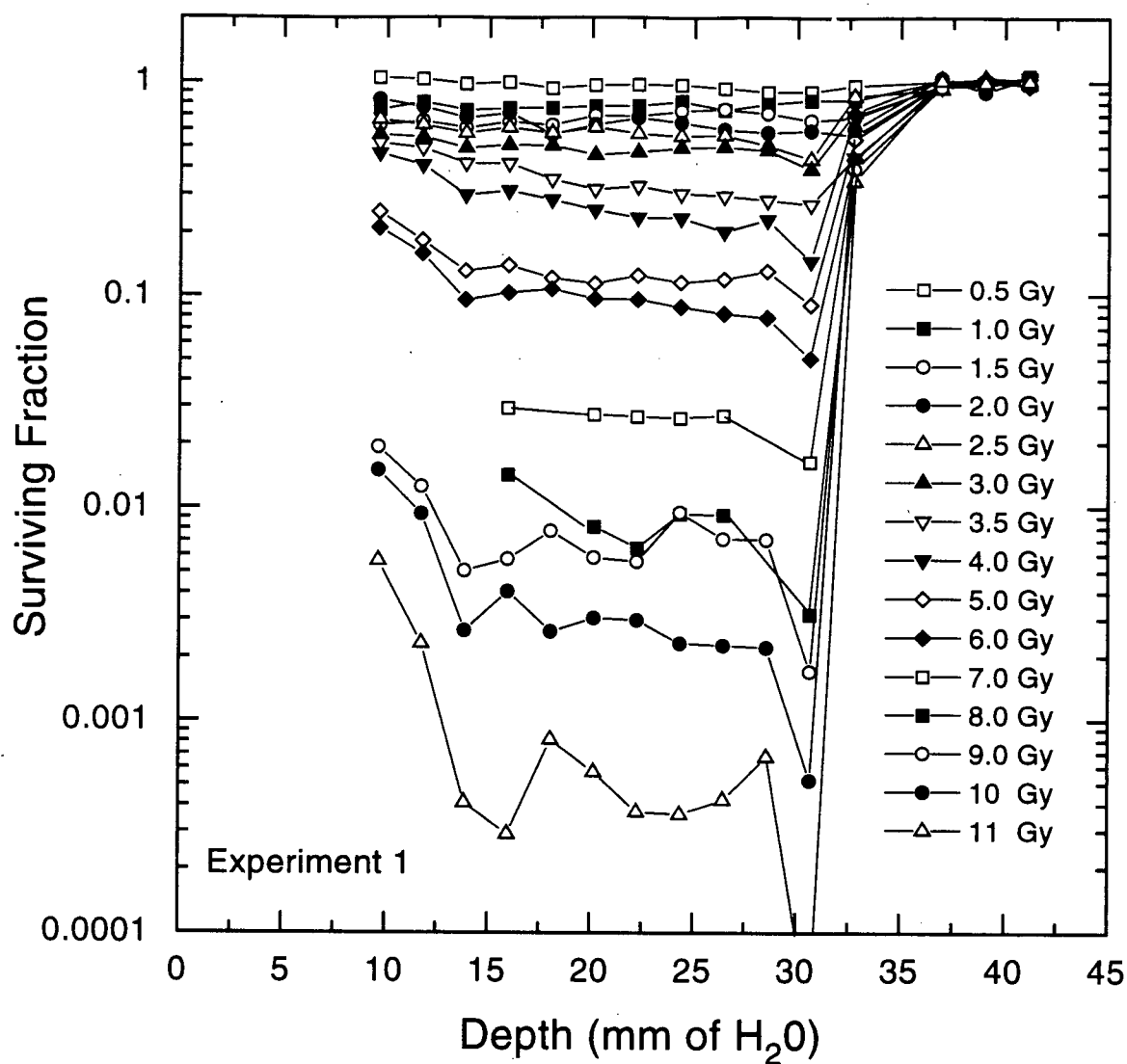
Figure 5-4 V79-WNRE 70 MeV Proton Response-Experiment 1
The surviving fraction of V79-WNRE cells as a function of depth along the axis of the 70 MeV proton beam spread out Bragg peak (SOBP) at TRIUMF for experiment 1. Cells were irradiated with protons in ~2°C gelatin-containing medium. Each line represents the survival profile for a different gel tube, which received the indicated peak dose (see legend). Survival was determined in 2 mm gel slices throughout and beyond the range of the peak. The depth in gel has been converted to the water equivalent depth. The three last slices received no dose, and were used as plating efficiency controls.
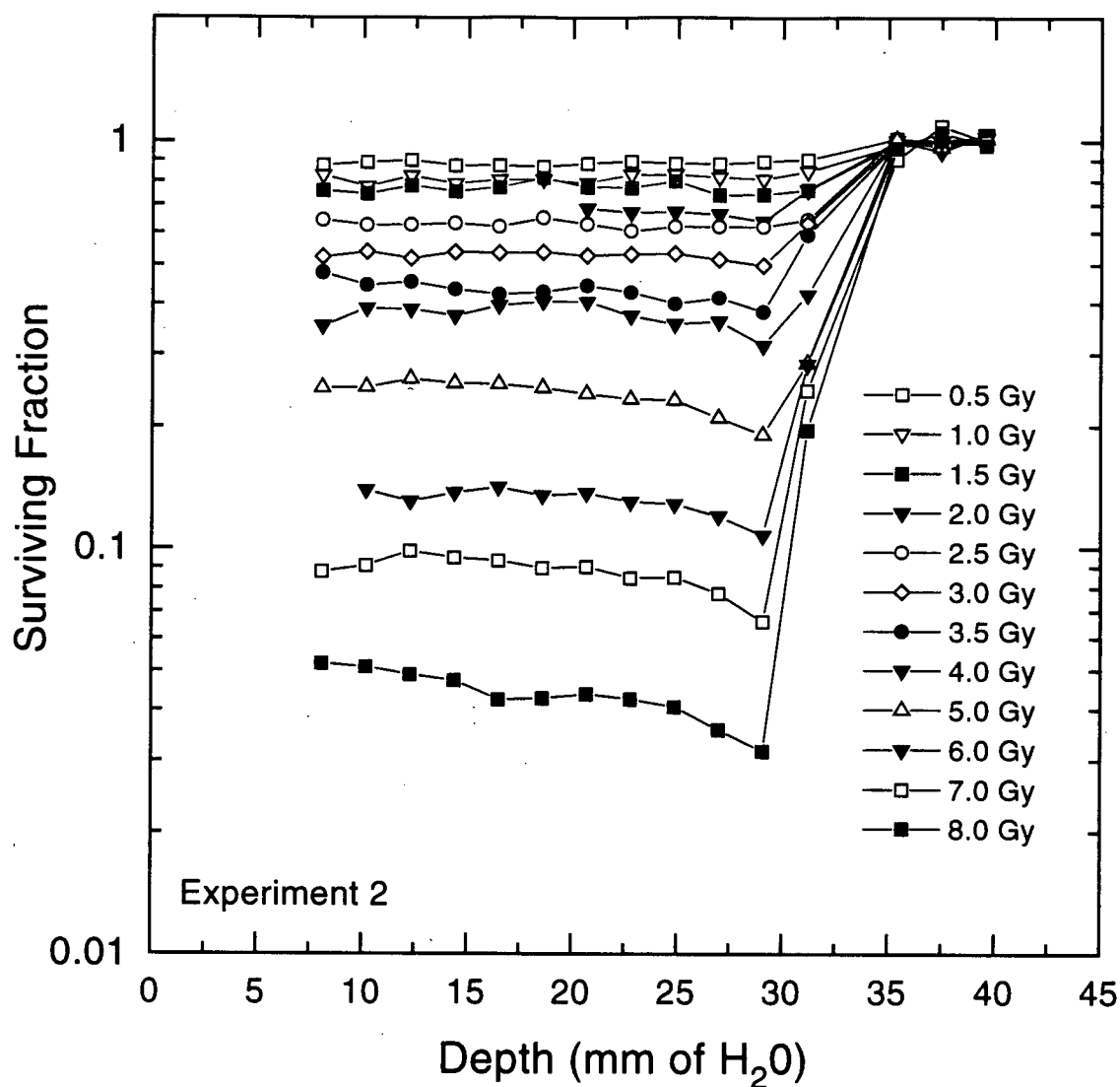
Figure 5-5 V79-WNRE 70 MeV Proton Response-Experiment 2
The surviving fraction of V79-WNRE cells as a function of depth along the axis of the 70 MeV proton beam spread out Bragg peak (SOBP) at TRIUMF for experiment 2. Cells were irradiated with protons in ~2°C gelatin-containing medium. Each line represents the survival profile for a different gel tube, which received the indicated peak dose (see legend). Survival was determined in 2 mm gel slices throughout and beyond the range of the peak. The depth in gel has been converted to the water equivalent depth. The three last slices received no dose, and were used as plating efficiency controls.
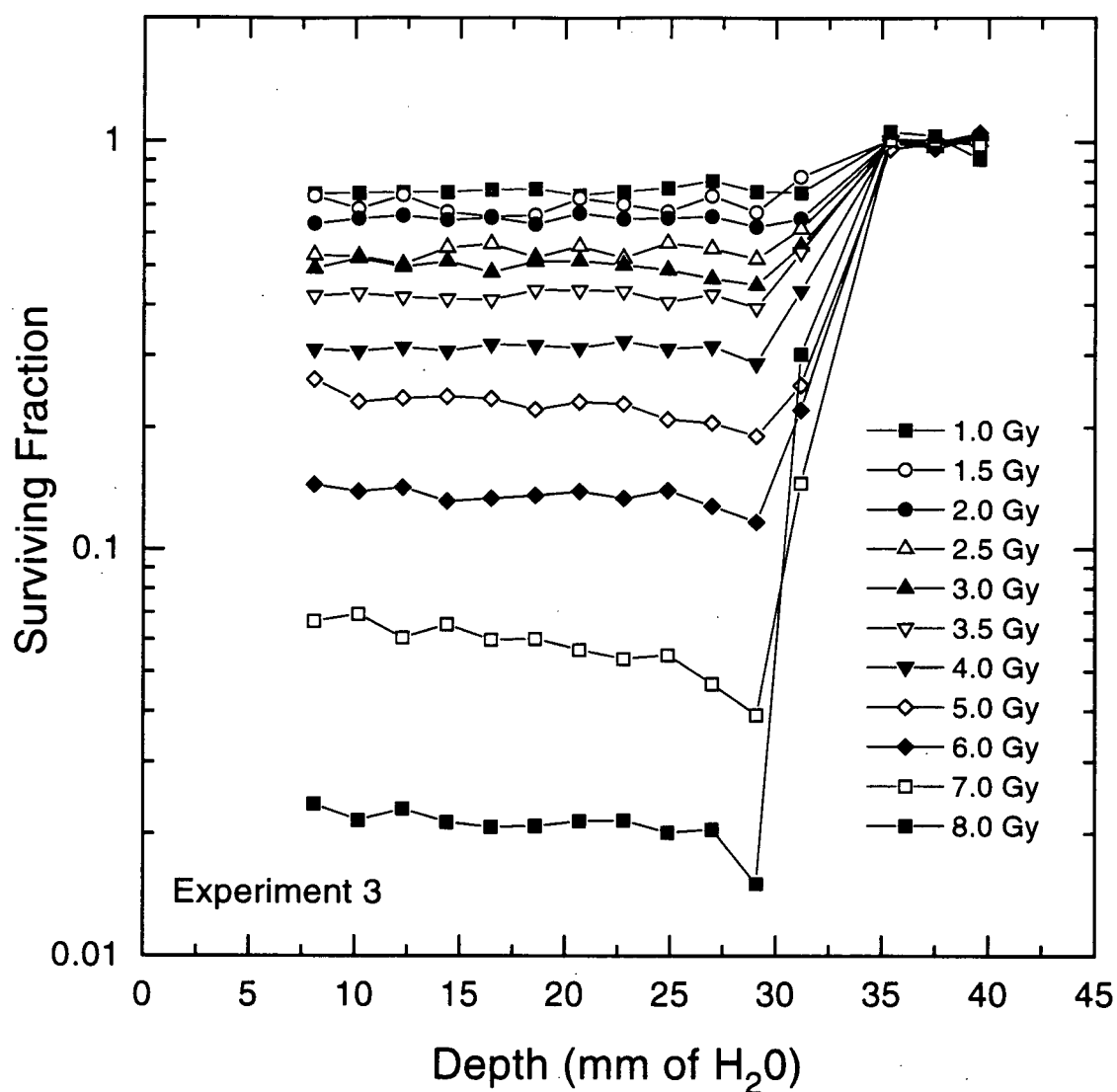
Figure 5-6 V79-WNRE Proton Response-Experiment 3
The surviving fraction of V79-WNRE cells as a function of depth along the axis of the 70 MeV proton beam spread out Bragg peak (SOBP) at TRIUMF for experiment 3. Cells were irradiated with protons in ~2°C gelatin-containing medium. Each line represents the survival profile for a different gel tube, which received the indicated peak dose (see legend). Survival was determined in 2 mm gel slices throughout and beyond the range of the peak. The depth in gel has been converted to the water equivalent depth. The three last slices received no dose, and were used as plating efficiency controls.

were pooled to provide sufficient numbers of cells for analysis using the cell sorting assay, and thus at 9, 10 and 11 Gy, only average survival values throughout the SOBP (excluding the last slice at the distal edge which showed significantly increased cell kill) were determined.

For each of the 3 experiments, survival versus dose profiles have been constructed from the data in figures 5-4, 5-5, and 5-6. While one could plot complete dose response curves (S vs. d) for each of the 11 different depths (gel slices) within the SOBP for which survival was measured, the statistical uncertainty in the response for each depth would be comparatively large. To reduce this uncertainty, the data within the SOBP have been pooled. The average survival of all the data within the SOBP, excluding the distal edge which showed a significantly increased effect (*i.e.,* slices 3-10 representing a depth of 12.8-29.6 mm for experiment 1, and the first 10 slices representing a depth of 7-28 mm for experiments 2 and 3), are plotted as a function of proton dose in figures 5-7, 5-8, and 5-9. In these plots, each dose point thus comprises the average of approximately 21 (experiment 1) or 30 (experiments 2 and 3) measurements of cell survival. The data have been replotted in terms of effect per unit dose (-ln(S)/d) for each of the 3 experiments in figures 5-7(b), 5-8(b), and 5-9(b). These responses show that, except for the data at low doses, the radiation response can be well characterized by a LQ fit (a straight line on this plot - see 3.2.2.1 page 64). Thus, each response has been fitted with the LQ model (solid lines in figures 5-7, 5-8 and 5-9). The best-fit parameters for each fit are given in table 5-1.

Table 5-1 Best-Fit Parameters in the LQ model for Fits of the Proton SOBP Survival Responses
For each data set the LQ model (equation 3-4) was fit to the data throughout the entire dose range. Uncertainty values are 95% confidence limits in the quoted parameter values. The average data set was produced by pooling experiments 2 and 3 (see 5.2.4).

Proton SOBP Data Set	α (Gy^{-1})	β (Gy^{-2})
Experiment 1	.121±.005	.0529 ±.001
Experiment 2	.136±.008	.0298±.001
Experiment 3	.137±.011	.0390±.002
Average Data	.136±.010	.0333±.001
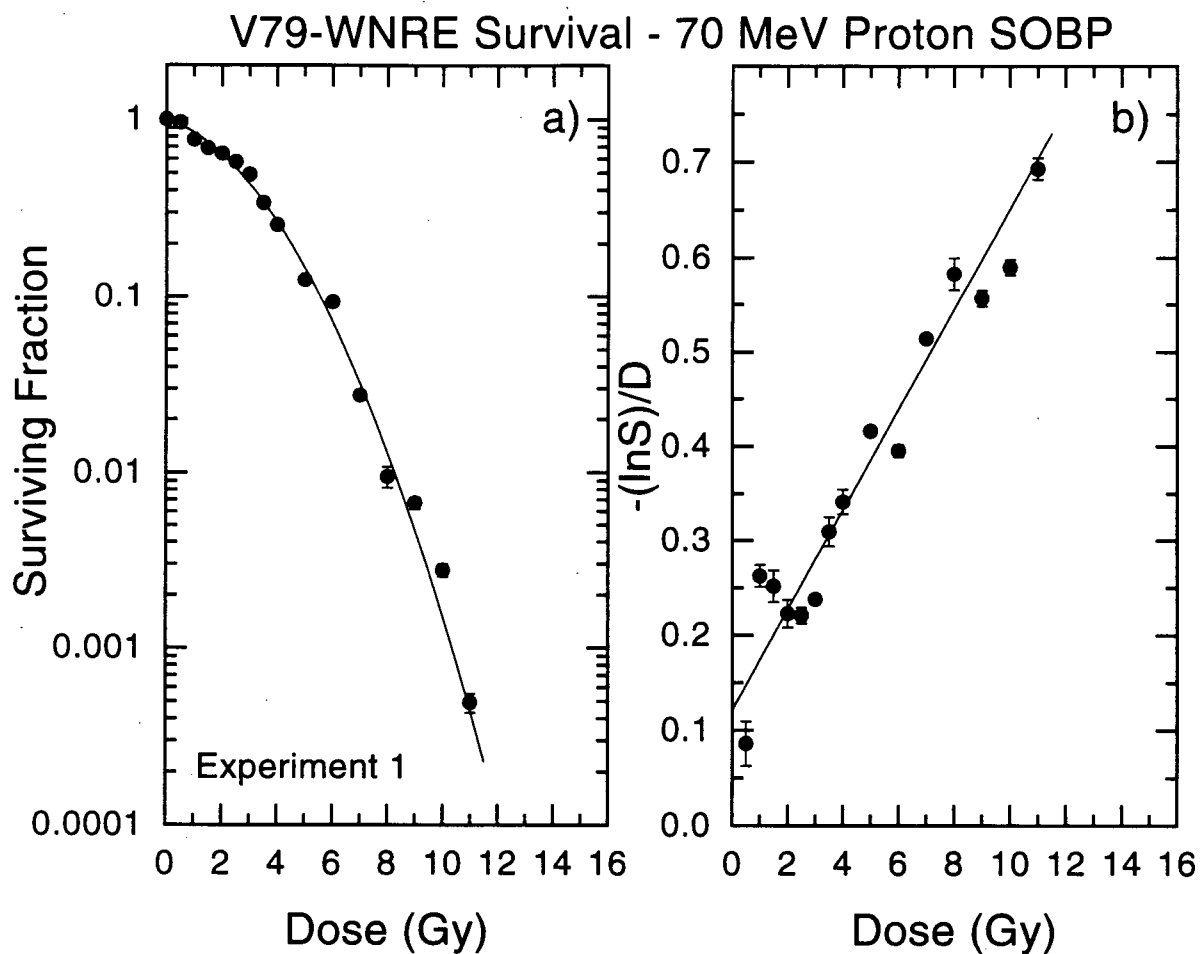
Figure 5-7 V79-WNRE 70 MeV Proton SOBP Radiation Response-Experiment 1
The average survival of V79-WNRE cells within the SOBP (*i.e.*, slices 3-10, depth 12.8-29.6 mm) of the 70 MeV proton beam as a function of proton dose for experiment 1(left frame). Error bars are the standard deviation determined from all measurements within the SOBP. The data are also shown in the form, -(lnS)/d, as a function of dose (right frame). The solid line is the best fit of the LQ model, $S=\exp(-\alpha d-\beta d^2)$, to all of the survival data.

V79-WNRE Survival - 70 MeV Proton SOBP

Figure 5-8 V79-WNRE 70 MeV Proton SOBP Radiation Response-Experiment 2
The average survival of V79-WNRE cells within the SOBP (*i.e.*, slices 1-10, depths 7-28 mm) of the 70 MeV proton beam as a function of proton dose for experiment 1(left frame). Error bars are the standard deviation determined from all measurements within the SOBP. The data are also shown in the form, -(lnS)/d, as a function of dose (right frame). The solid line is the best fit of the LQ model, $S=\exp(-\alpha d-\beta d^2)$, to all of the survival data.

V79-WNRE Survival - 70 MeV Proton SOBP

Figure 5-9 V79-WNRE 70 MeV Proton SOBP Radiation Response-Experiment 3
The average survival of V79-WNRE cells within the SOBP (*i.e.*, slices 1-10, depths 7-28 mm) of the 70 MeV proton beam as a function of proton dose for experiment 1(left frame). Error bars are the standard deviation determined from all measurements within the SOBP. The data are also shown in the form, $-(\ln S)/d$, as a function of dose (right frame). The solid line is the best fit of the LQ model, $S=\exp(-\alpha d-\beta d^2)$, to all of the survival data.

5.2.3.2 Cobalt Survival Response

For comparison with the proton response results, concurrent measurements of survival after irradiation with ^{60}Co γ-rays were made. For each of the 3 experiments, the ^{60}Co radiation response was measured in cells from the same starting population used for proton irradiation, and was conducted under comparable experimental conditions. Two complete survival responses, irradiated at different times, were measured during each experiment. For each of these responses, survival was measured in two repeats (each producing 300-600 colonies) for each of two samples at 16 different dose points over the range 0-14 Gy. Figures 5-10(a), 5-11(a), and 5-12(a) show the *average* of the two ^{60}Co responses for each of the first, second, and third experiments, respectively.

The survival data are also plotted in figures 5-10(b), 5-11(b), and 5-12(b) in terms of effect per unit dose $(-\ln(S)/D)$. Analysis of these plots shows clearly that the radiation response of V79-WNRE cells to ^{60}Co gamma rays cannot be well characterized by a single LQ function (on this plot a straight line). The data suggest the presence of substructure analogous to that observed in cells irradiated with 250 kVp X-rays and attributed to the presence of subpopulations of cells with different, cell-cycle associated, radiation sensitivity (chapter 3, Skarsgard *et al.* 1991, 1992, 1993, 1994a, 1995, Skwarchuk *et al.* 1993). This substructure results from an emerging resistant subpopulation of cells at higher doses as sensitive cells within the population are selectively killed, and correspondingly results in a misfit of the LQ equation when it is applied to the complete response. In order to characterize accurately the radiation response of asynchronously growing cells that exhibit this response substructure, the

survival data can be modeled by separate LQ fits to the low and high dose regions (Skarsgard *et al.* 1991, 1992, 1993, 1994a, 1995, Skwarchuk *et al.* 1993), similar to the analysis carried out in chapter 3. This strategy was used to characterize the ^{60}Co data shown in figures 5-10, 5-11 and 5-12. In each of these figures, the data at low and high doses have been fitted separately with the LQ model, and best-fit values are given in table 5-2.

Examination of figures 5-7(b) to 5-12(b) indicate some clear differences between the proton and ^{60}Co radiation responses: the putative subpopulation substructure, which is clearly evident in the ^{60}Co response, seems less evident in the proton response, although this may be due, in part, to the fact that the proton measurements were not carried to as high a dose. Accurate characterization of the cobalt data requires separate fits to the low and high dose data, but the proton radiation response is reasonably well fit with a single LQ function, at least for doses greater than ~2 Gy. Also, the first 2-3 data points in the proton response show evidence of an increased effectiveness, or hypersensitivity, when compared to the remainder of the data. This is similar to the low dose hypersensitivity observed in HT-29, DU-145, and A549 cells after X-irradiation, reported on in chapter 4 (see figs. 4-11, 4-13, and 4-15). However the hypersensitivity observed with proton irradiation extends to a somewhat higher dose and lower survival as compared to the human tumour cell studies with X-rays.
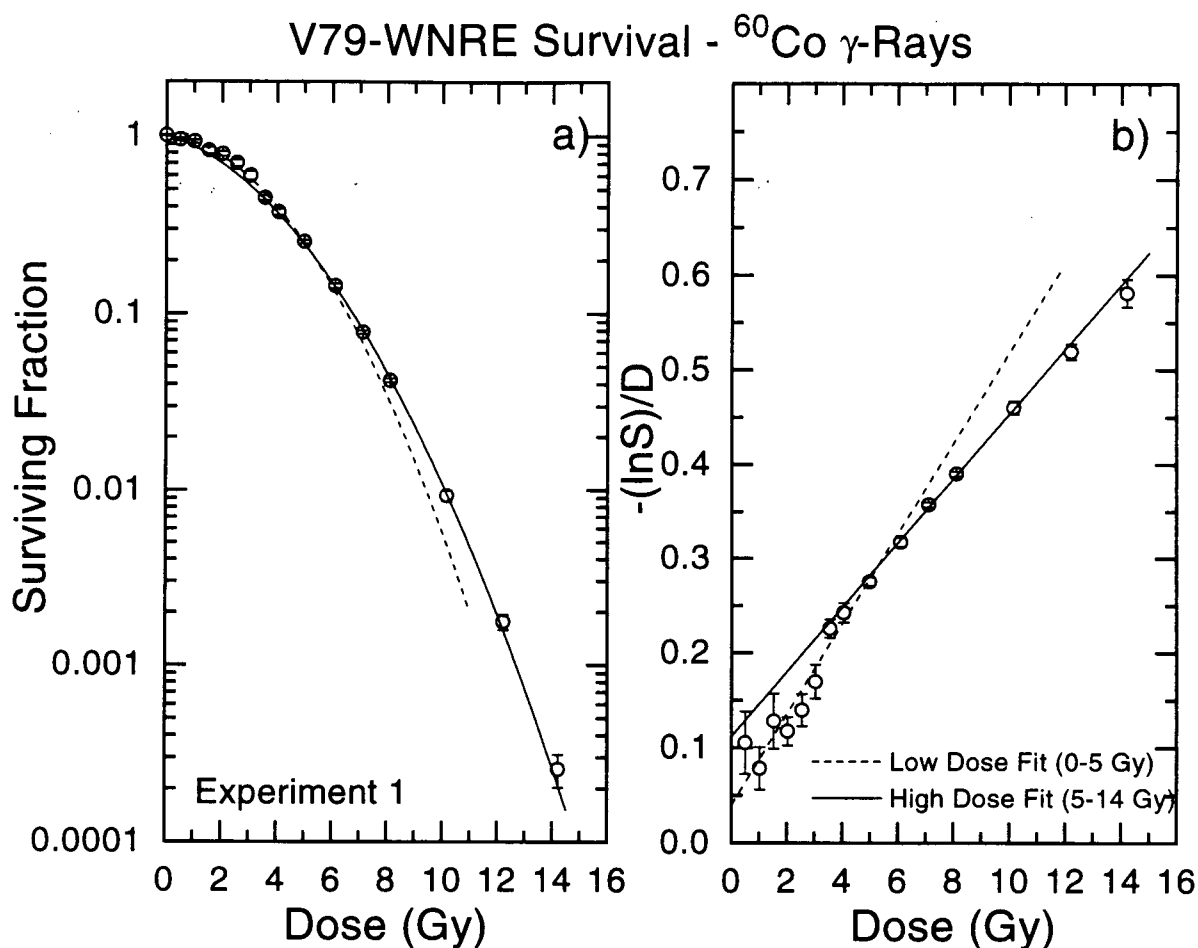
Figure 5-10 V79-WNRE ^{60}Co Radiation Response-Experiment 1
The mean survival of V79-WNRE cells as a function of ^{60}Co dose (left frame) for experiment 1. Cells were irradiated at 0°C in gelatin-containing medium. Data are the average of 2 survival curves, and error bars are the standard deviation in the data at each dose point. The data are also shown in the form, -(lnS)/d, as a function of dose (right frame). This plot illustrates response substructure resulting from cell-cycle variations in radiosensitivity analogous to that observed in chapter 3. The survival data have been fitted in the low and high dose ranges with the LQ model (equation 3-4).

V79-WNRE Survival - ^{60}Co γ-Rays
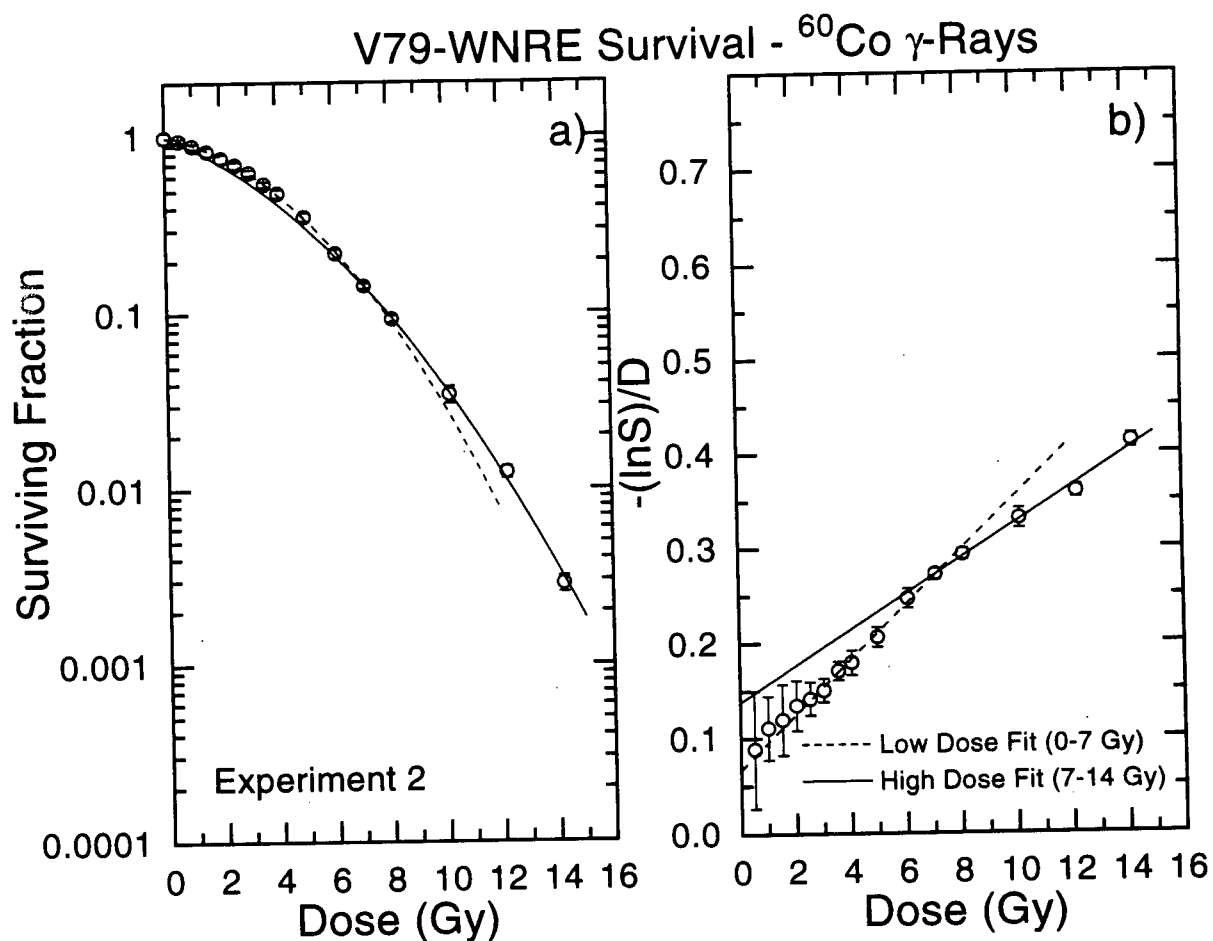
Figure 5-11 V79-WNRE ^{60}Co Radiation Response-Experiment 2
The mean survival of V79-WNRE cells as a function of ^{60}Co dose (left frame) for experiment 2. Cells were irradiated at 0°C in gelatin-containing medium. Data are the average of 2 survival curves, and error bars are the standard deviation in the data at each dose point. The data are also shown in the form, -(lnS)/d, as a function of dose (right frame). This plot illustrates response substructure resulting from cell-cycle variations in radiosensitivity analogous to that observed in chapter 3. The survival data have been fitted in the low and high dose ranges with the LQ model (equation 3-4).

V79-WNRE Survival - ^{60}Co γ-Rays

a)

b)

Figure 5-12 V79-WNRE ^{60}Co Radiation Response-Experiment 3
The mean survival of V79-WNRE cells as a function of ^{60}Co dose (left frame) for experiment 3. Cells were irradiated at 0°C in gelatin-containing medium. Data are the average of 2 survival curves, and error bars are the standard deviation in the data at each dose point. The data are also shown in the form, -(lnS)/d, as a function of dose (right frame). This plot illustrates response substructure resulting from cell-cycle variations in radiosensitivity analogous to that observed in chapter 3. The survival data have been fitted in the low and high dose ranges with the LQ model (equation 3-4).

Table 5-2 Best-Fit Parameters in the LQ model for Fits of the ^{60}Co Survival Responses

Due to the presence of cell-cycle associated substructure, for each data set the LQ model (equation 3-4) was fit to the ^{60}Co survival data in the low and high dose ranges separately. The dose that delineates the boundary between the low and high dose regions was determined by fitting the data at low dose to an increasing dose range until a point was reached for which significantly different values for α and β were found. Uncertainty values are 95% confidence limits in the quoted parameter values. The average data set was produced by pooling experiments 2 and 3 (see 5.2.4).

^{60}Co Data Set	α (Gy^{-1})	β (Gy^{-2})
Experiment 1 Low Dose Range (0-5 Gy) High Dose Range (5-14 Gy)	 .040±.013 .111±.008	 .048 ±.003 .034±.001
Experiment 2 Low Dose Range (0-7 Gy) High Dose Range (7-14 Gy)	 .067±.011 .138±.011	 .029 ±.002 .019±.001
Experiment 3 Low Dose Range (0-5 Gy) High Dose Range (5-14 Gy)	 .036±.017 .111±.015	 .041 ±.005 .025±.002
Average Data Low Dose Range (0-5 Gy) High Dose Range (5-14 Gy)	 .054±.015 .115±.013	 .034 ±.004 .023±.002

5.2.3.3 Proton RBE

The relative biological effectiveness of the proton SOBP can be found by taking the ratio of X-ray dose to proton dose required to achieve the same level of biological effect, similar to the manner in which the SER was determined in chapter 3 (equation 3-6). The effects of higher LET radiation are not simply dose-modifying, and thus the RBE value is dependent on the level of effect that is chosen. For this reason, the RBE value for the average SOBP has been determined as a function of survival. To facilitate calculations of RBE at different survival levels, it is desirable to characterize the entire dose response with one equation, and thus the ^{60}Co radiation response data have also been fitted with the two population model (equation 3-7). Fitting with this equation provided

good fits to the radiation responses measured in chapter 3 (see figs. 3-27, 3-28 and 3-29), and has been shown to also provide accurate characterization of the radiation survival response for this same cell line following irradiation with 250 kVp X-rays (Skarsgard *et al.* 1994a). Although fitting with this equation leads to non-unique solutions (see 3.2.4, Skarsgard *et al.* 1994a), for the purposes of determining the RBE, this equation is useful since it accurately characterizes the survival response throughout the entire dose range. The best-fit parameters in the two-population model for fits of the ^{60}Co response in each experiment are given in table 5-3.

Table 5-3 Best-Fit Parameters in the Two-Population Model for Fits of the ^{60}Co Survival Responses
Due to the presence of cell-cycle associated substructure, for each data set the two population model (equation 3-6) was fit to the ^{60}Co survival data for the entire dose range. In this model a fraction (f) of the cell population is characterized by the parameters α_s and β_s, while the remainder of the population $(1-f)$ is characterized by α_r and β_r. Unique solutions with this model were not possible, however this fit was able to characterize the measured survival throughout the entire dose range, and was used for determining the RBE as a function of dose. The average data set was produced by pooling experiments 2 and 3 (see 5.2.4).

^{60}Co Data Set	f (%)	α_s (Gy^{-1})	β_s (Gy^{-2})	α_r (Gy^{-1})	β_r (Gy^{-2})
Experiment 1	44.1	.0206	.0731	.0423	.0353
Experiment 2	62.4	.0877	.0200	.0130	.0504
Experiment 3	88.0	.0976	.0277	0.0	.0606
Average Data	80.5	.0518	.0373	.0406	.0178

The ^{60}Co and proton average SOBP radiation response data for each experiment have been plotted together in the lower frames of figures 5-13, 5-14, and 5-15. The proton and ^{60}Co data are shown with the best fits to the LQ and the two population model respectively. The 95% confidence limits in each of these fits are also shown. The RBE value has been calculated from these fits at different levels of survival, and is plotted as a
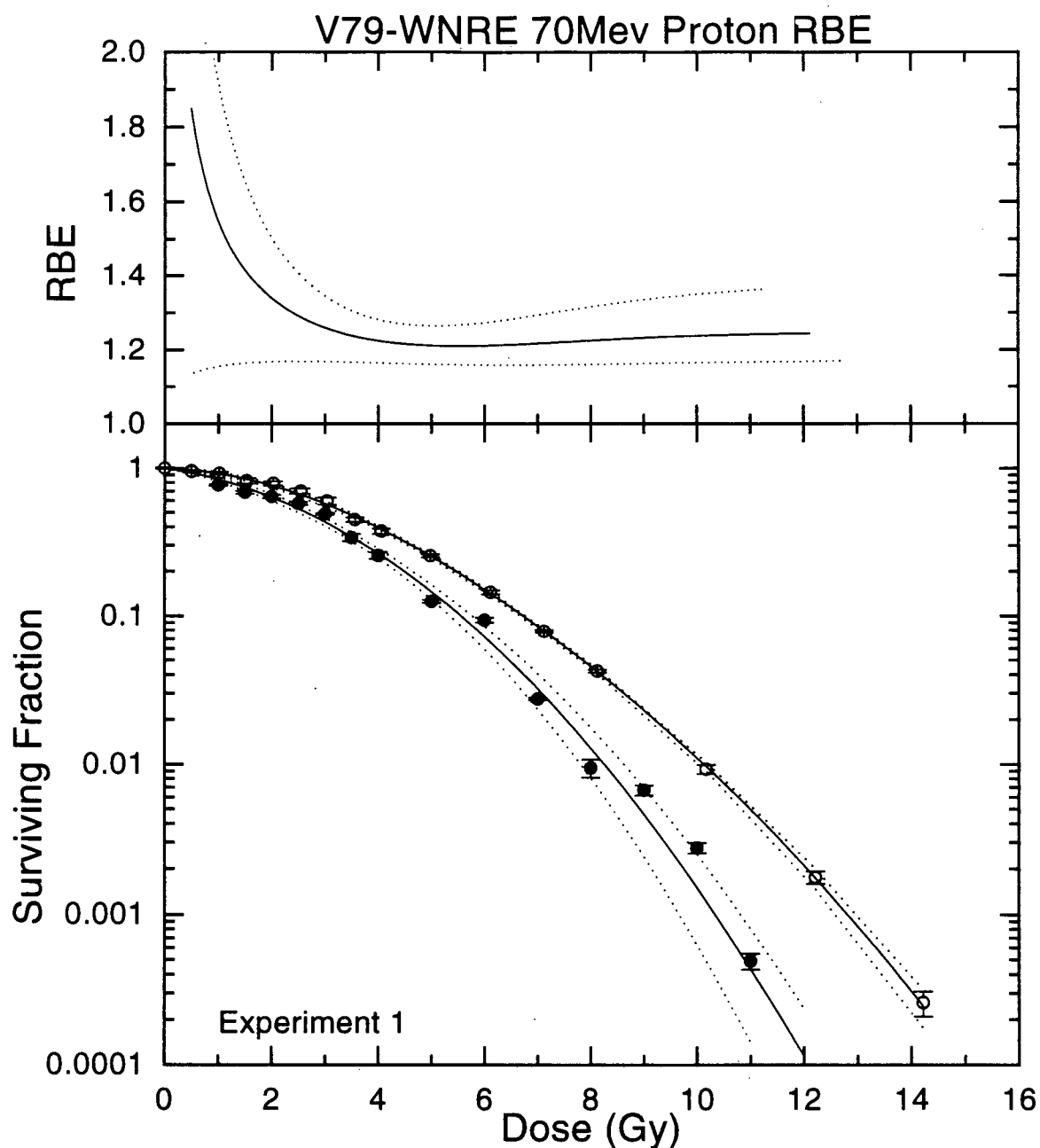
Figure 5-13 RBE of the Proton Average SOBP-Experiment 1

The average radiation response of V79-WNRE cells within the SOBP of the 70 MeV proton beam at TRIUMF is shown with the average response to ^{60}Co irradiation for experiment 1 (solid lines, lower frame). Dashed lines are upper and lower 95% confidence limits in the fitted functions: the two population model (equation 3-6) for the ^{60}Co response and the LQ model (equation 3-4) for the proton SOBP response. The average proton RBE within the SOBP is shown as a function of proton dose in the upper frame. The RBE was determined from the fitted functions shown in the lower frame. Dashed lines are the upper and lower 95% confidence limits in the RBE as determined from the confidence limits in the fitted functions.
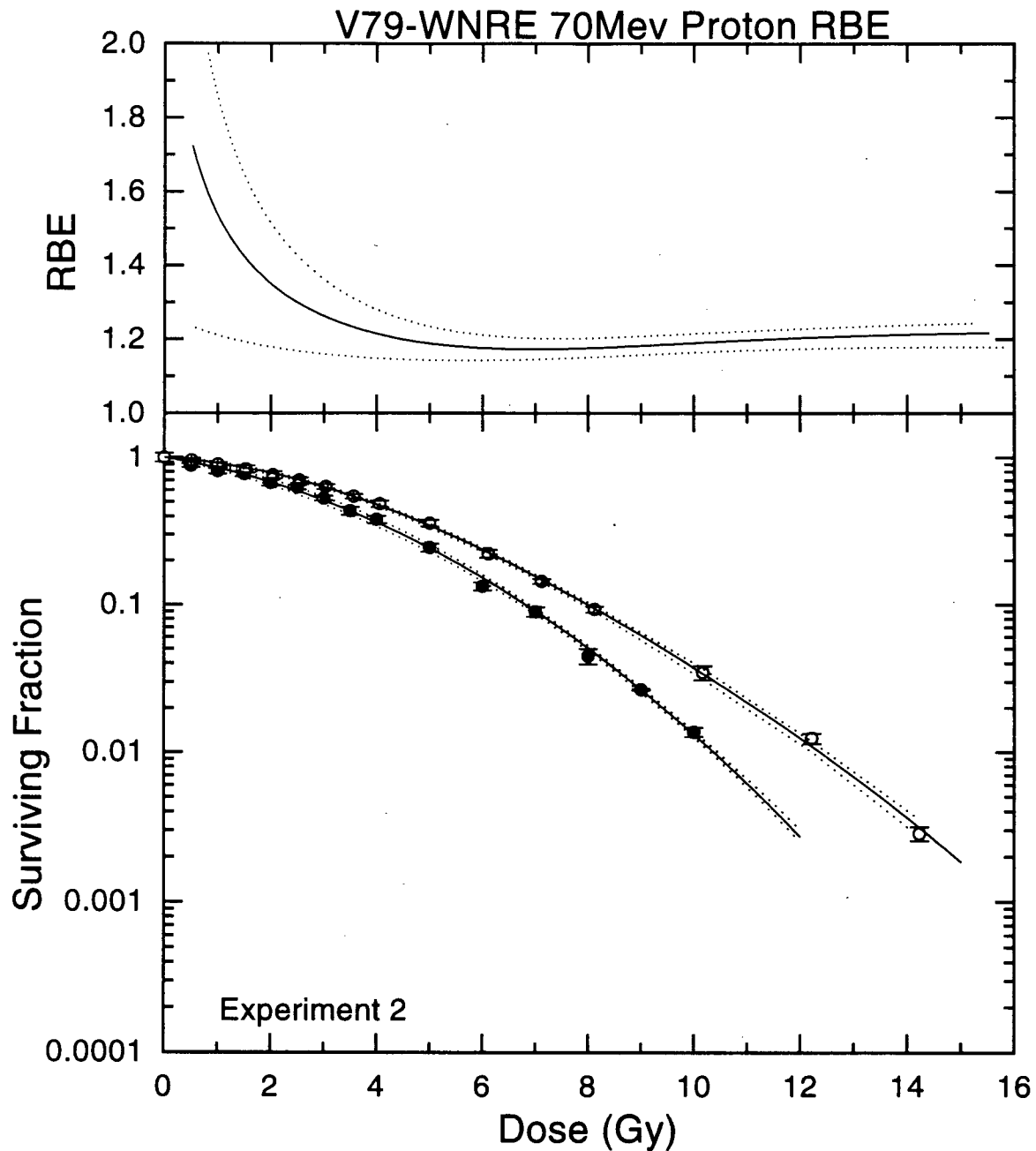
Figure 5-14 RBE of the Proton Average SOBP-Experiment 2
The average radiation response of V79-WNRE cells within the SOBP of the 70 MeV proton beam at TRIUMF is shown with the average response to ^{60}Co irradiation for experiment 2 (solid lines, lower frame). Dashed lines are upper and lower 95 % confidence limits in the fitted functions: the two population model (equation 3-6) for the ^{60}Co response and the LQ model (equation 3-4) for the proton SOBP response. The average proton RBE within the SOBP is shown as a function of proton dose in the upper frame. The RBE was determined from the fitted functions shown in the lower frame. Dashed lines are the upper and lower 95% confidence limits in the RBE as determined from the confidence limits in the fitted functions.
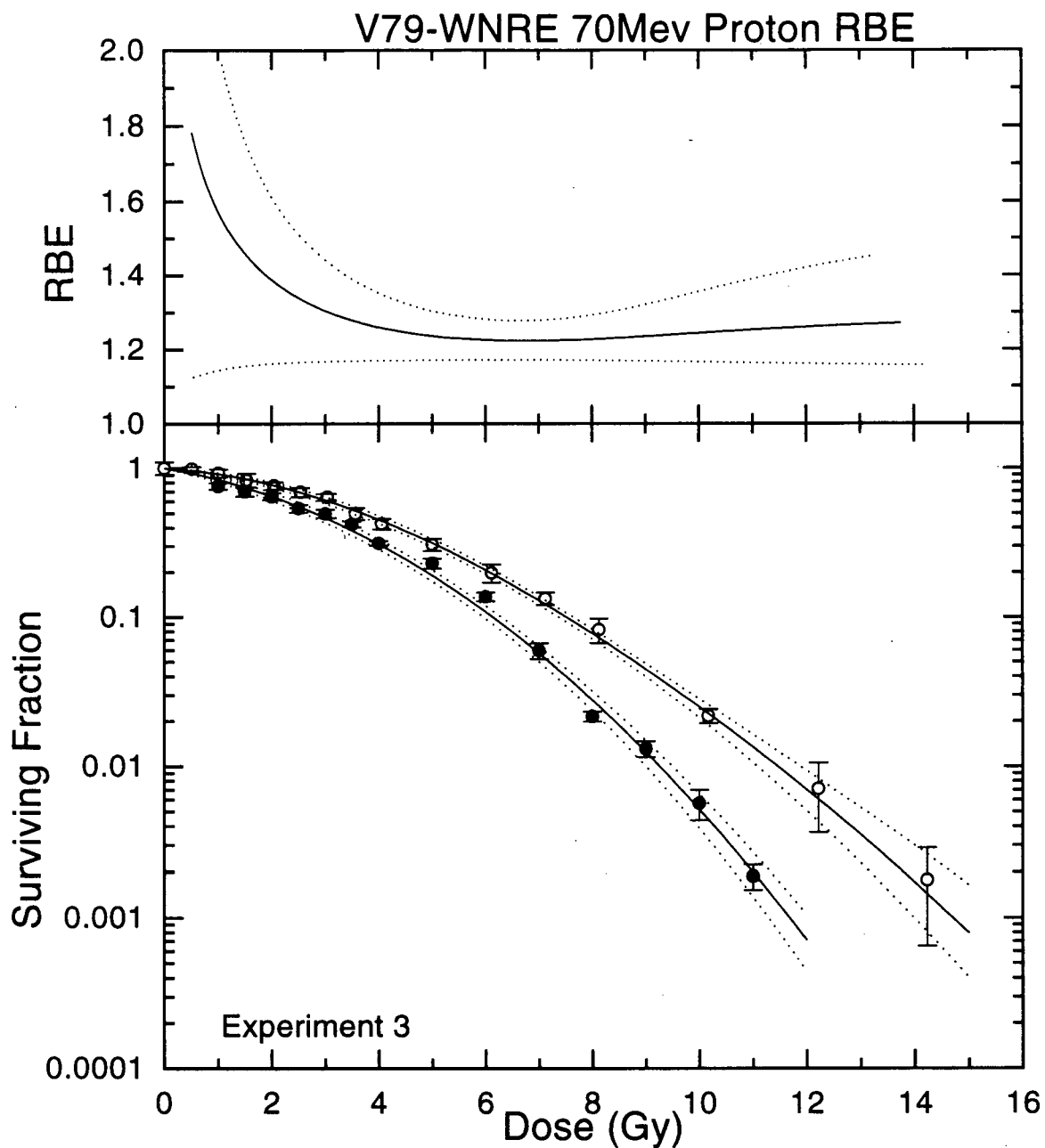
Figure 5-15 RBE of the Proton Average SOBP-Experiment 3
The average radiation response of V79-WNRE cells within the SOBP of the 70 MeV proton beam at TRIUMF is shown with the average response to ^{60}Co irradiation for experiment 3 (solid lines, lower frame). Dashed lines are upper and lower 95 % confidence limits in the fitted functions: the two population model (equation 3-6) for the ^{60}Co response and the LQ model (equation 3-4) for the proton SOBP response. The average proton RBE within the SOBP is shown as a function of proton dose in the upper frame. The RBE was determined from the fitted functions shown in the lower frame. Dashed lines are the upper and lower 95% confidence limits in the RBE as determined from the confidence limits in the fitted functions.

function of proton dose in the top frames of figures 5-13, 5-14, and 5-15, along with the 95% confidence limits in the RBE determined from the corresponding confidence limits in the fitted survival responses. The absolute values of the RBE and its dependence on dose are remarkably similar of for the 3 experiments. It exhibits a large dose dependence, rising significantly below doses of 4 Gy.

5.2.4 Average Data

To decrease the statistical uncertainty in the measurements of RBE both as a function of dose and of depth, the data for experiments 2 and 3 were pooled. These two experiments used the same physical dose profile, the same gel batch, and were conducted within a 1 month period. Although the absolute sensitivity of these cells was different in the two experiments (compare figures 5-5 and 5-6 and figures 5-11 and 5-12), the change in sensitivity was similar in both the ^{60}Co and proton responses, such that the RBE value was essentially the same.

5.2.4.1 Survival Data

The averaged ^{60}Co radiation response, and the best fits of the data within the low and high dose regions with the LQ model, are plotted in figure 5-16 (see table 5-2 for best-fit parameter values). These averaged data exhibit substructure analogous to that shown in the individual experiments. The radiation response for the averaged proton data within the SOBP (first 10 slices representing a depth of 7-28 mm), and the best fit of the LQ equation to these data, are plotted in figure 5-17 (see table 5-1 for best-fit parameter values).
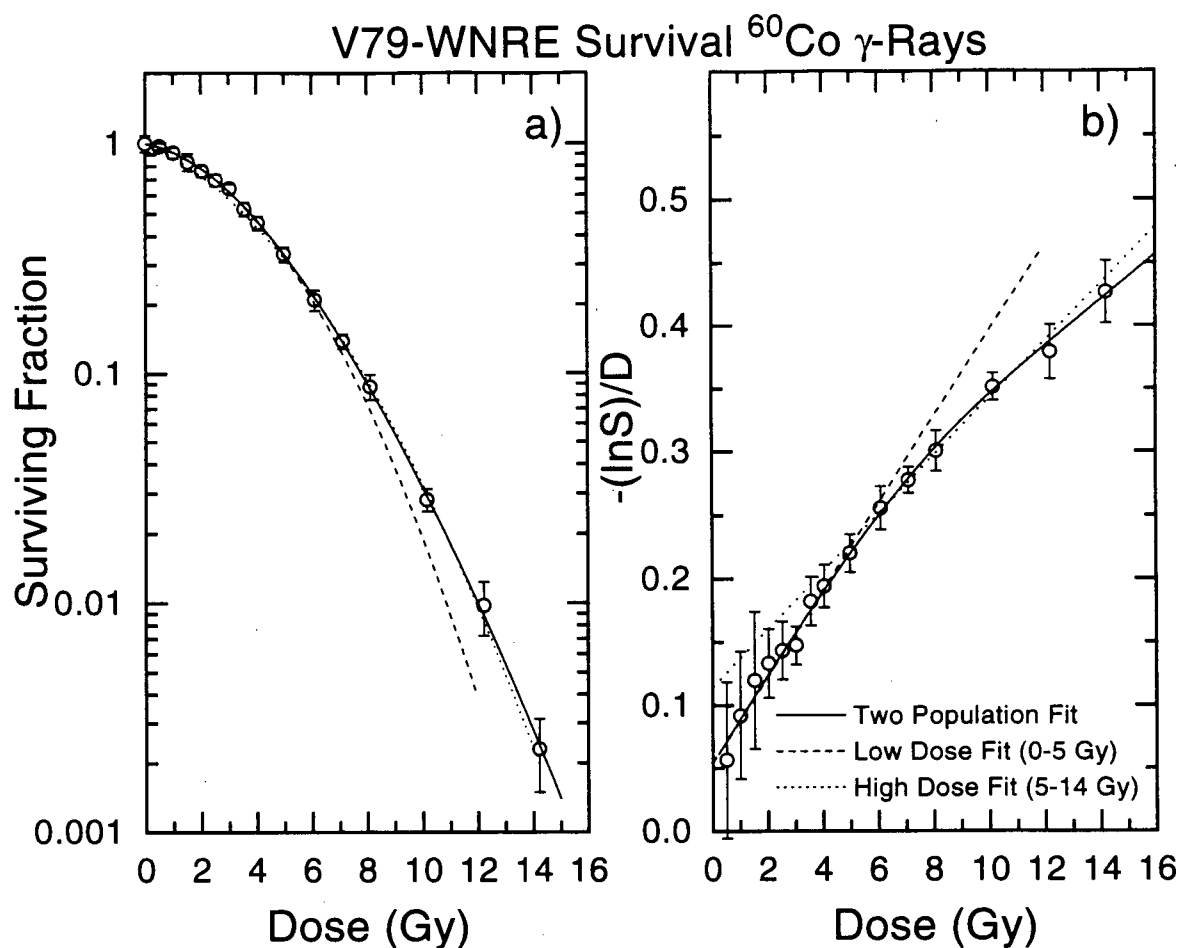
Figure 5-16 V79-WNRE [60]Co Radiation Response-Averaged data
The mean survival of V79-WNRE cells as a function of ^{60}Co dose (left frame) for the average of experiments 2 and 3. Data are the average of 4 survival curves, and error bars are the standard deviation in the data at each dose point. The data are also shown in the form, -(lnS)/d, as a function of dose (right frame). This plot illustrates substructure resulting from cell-cycle variations in radiosensitivity, analogous to that observed in chapter 3. The survival data have been fitted in the low and high dose ranges with the LQ model, equation 3-4 (dashed and dotted lines, respectively) and for the full dose range with the two population model, equation 3-7 (solid line).
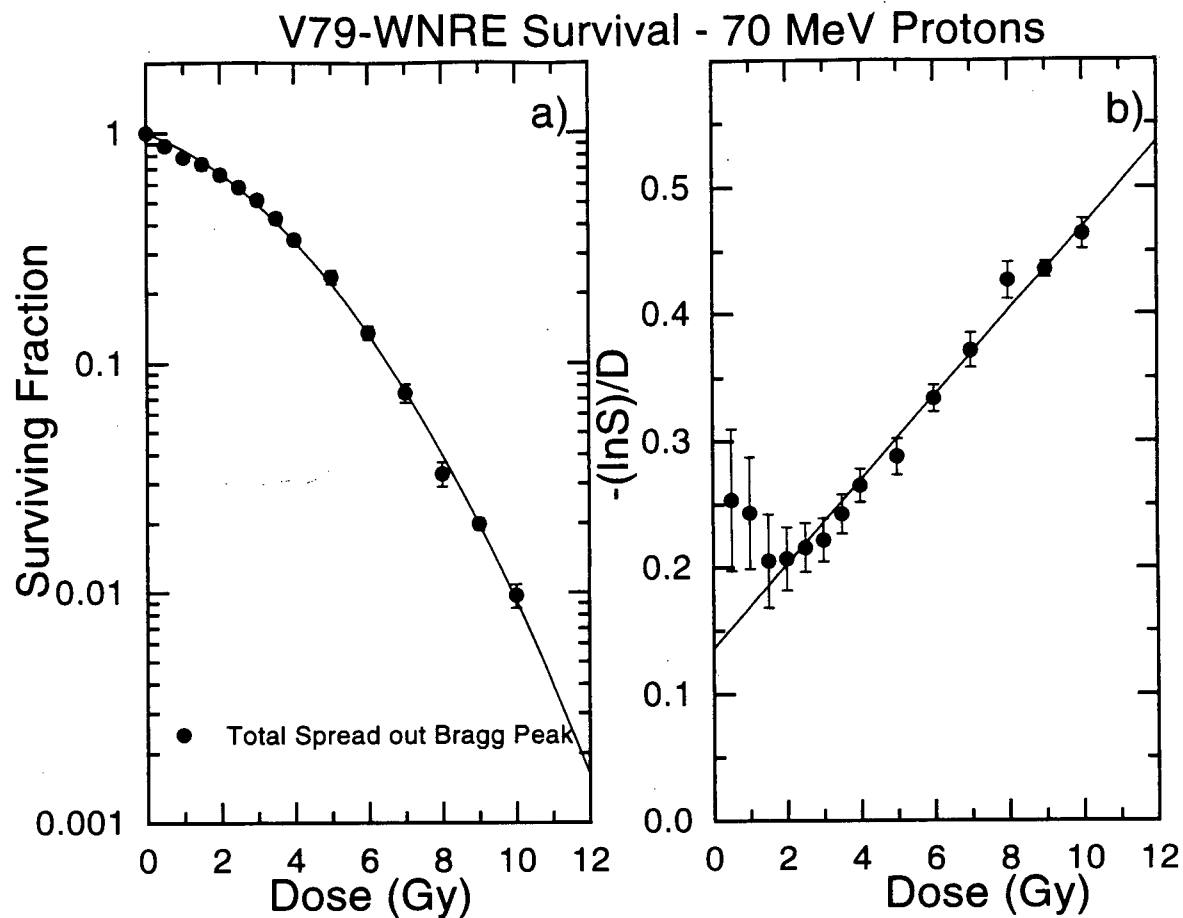
Figure 5-17 V79-WNRE Proton SOBP Radiation Response-Averaged data
The mean survival of V79-WNRE cells within the SOBP (*i.e.,* slices 1-10, depths 7-28 mm) of the 70 MeV proton beam as a function of proton dose for the average of experiments 2 and 3(left frame). Error bars are the standard deviation determined from all measurements within the SOBP. The data are also shown in the form, -(lnS)/d, as a function of dose (right frame). The solid line is the best fit of the LQ model, S=exp(-αd-βd^2), to all of the survival data.

To determine the depth dependence of the measured radiation response to protons, the SOBP was first further subdivided into the proximal (slices 1-5 representing a depth of ~7-17.5 mm) and distal (slices 6-10 representing a depth of ~17.5-28 mm) regions, and average survival values calculated within these regions. The average survival response within each of these two regions, as well as the survival response derived for the last slice at the distal edge of the stopping distribution (~28-30 mm), were calculated and are plotted in figure 5-18. These data have also been fitted with a single LQ equation, and the α and β parameters are given in table 5-4. The survival response in the proximal region is more resistant than the distal region, and both are substantially more resistant than the response at the distal edge. The data in this figure reflect the generally consistent decrease in survival with increasing depth observed in figures 5-5 and 5-6.

Table 5-4 Best-Fit Parameters in the LQ Model for Fits of the Proton Data in Regions of the SOBP
Data from experiments 2 and 3 were pooled, and the average survival response within the SOBP determined. The regions of the SOBP were subdivided into the proximal (first 5 slices), distal (next 5 slices) and distal edge (last slice in the SOBP) regions. The data within each of these regions was fitted with the LQ model (equation 3-4). Uncertainty values are 95% confidence limits in the quoted parameter values.

Proton SOBP Data Set	α (Gy^{-1})	β (Gy^{-2})
Proximal (slices 1-5)	.135±.012	.0327 ±.002
Distal (slices 6-10)	.137±.012	.0349±.002
Distal Edge (slice 11)	.141±.011	.0397±.002
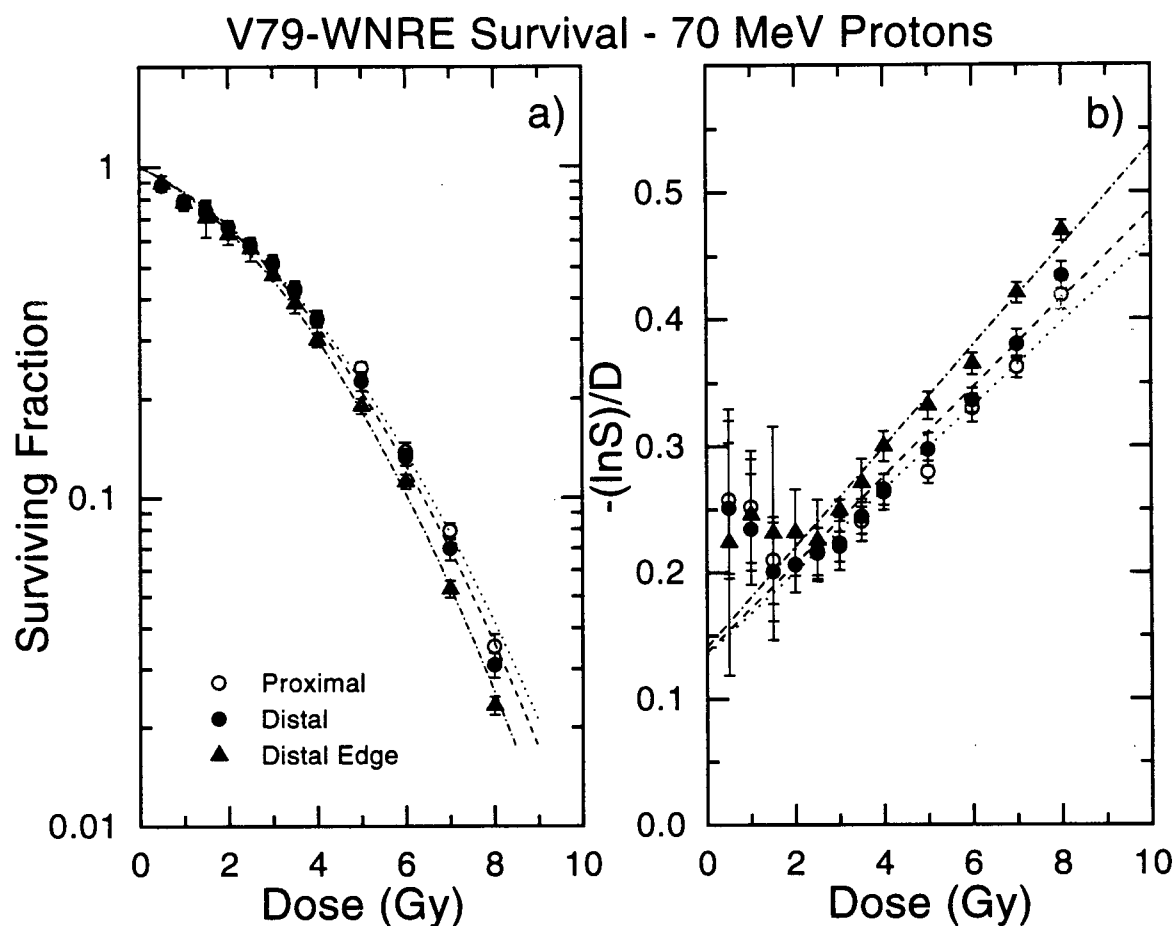
Figure 5-18 V79-WNRE Proton Regional Radiation Response-Averaged Data
The radiation response within different regions of the SOBP is shown as a function of dose (left frame). Data from experiments 2 and 3 were pooled, and the average survival response within the SOBP determined. The regions of the SOBP were subdivided into the proximal (first 5 slices), distal (next 5 slices) and distal edge (last slice in the SOBP) regions. Dashed lines are the best fit of the LQ model to the data in each of these regions. The data are also shown in the form, -(lnS)/d, as a function of dose (right frame).

5.2.4.2 Proton RBE

The average radiation survival responses of V79-WNRE cells to the proton SOBP and to ^{60}Co gamma rays, have been replotted together in figure 5-19. The proton response is characterized by the best fit of the LQ model (*i.e.*, the same as in figure 5-17) and the ^{60}Co response is characterized with the two-population model to facilitate calculations of RBE (see table 5-3 for best-fit parameter values). Also plotted are the 95% confidence limits in the best-fit lines for each of the two responses. Figure 5-19 shows clearly that, in terms of survival, the biological effect of the 70 MeV proton beam is considerably greater than that of ^{60}Co gamma rays.

5.2.4.2.1 Dose-Dependence of the RBE

Using the data shown in figure 5-19, the RBE was calculated at different levels of survival in the same manner as for the individual experiments, and in figure 5-20 this value is plotted as a function of both proton dose (fig. 5-20(a)) and surviving fraction (fig. 5-20(b)). Also plotted are the 95% confidence regions for the RBE as derived from the confidence regions shown in figure 5-19. These plots illustrate a dose dependence of the RBE value throughout the SOBP of the proton beam. The average RBE for the total SOBP rises rapidly below 4 Gy, and at a dose of 1 Gy is approximately 1.56. Above 5 Gy, the RBE stabilizes at approximately 1.21. The confidence limits in this plot represent both the experimental uncertainty in the measured RBE *and* the variation in RBE with depth. This is because the RBE shown is calculated from the data throughout theSOBP, which we have seen (figs. 5-5, 5-6, and 5-18) increases with increasing depth.

V79-WNRE Survival
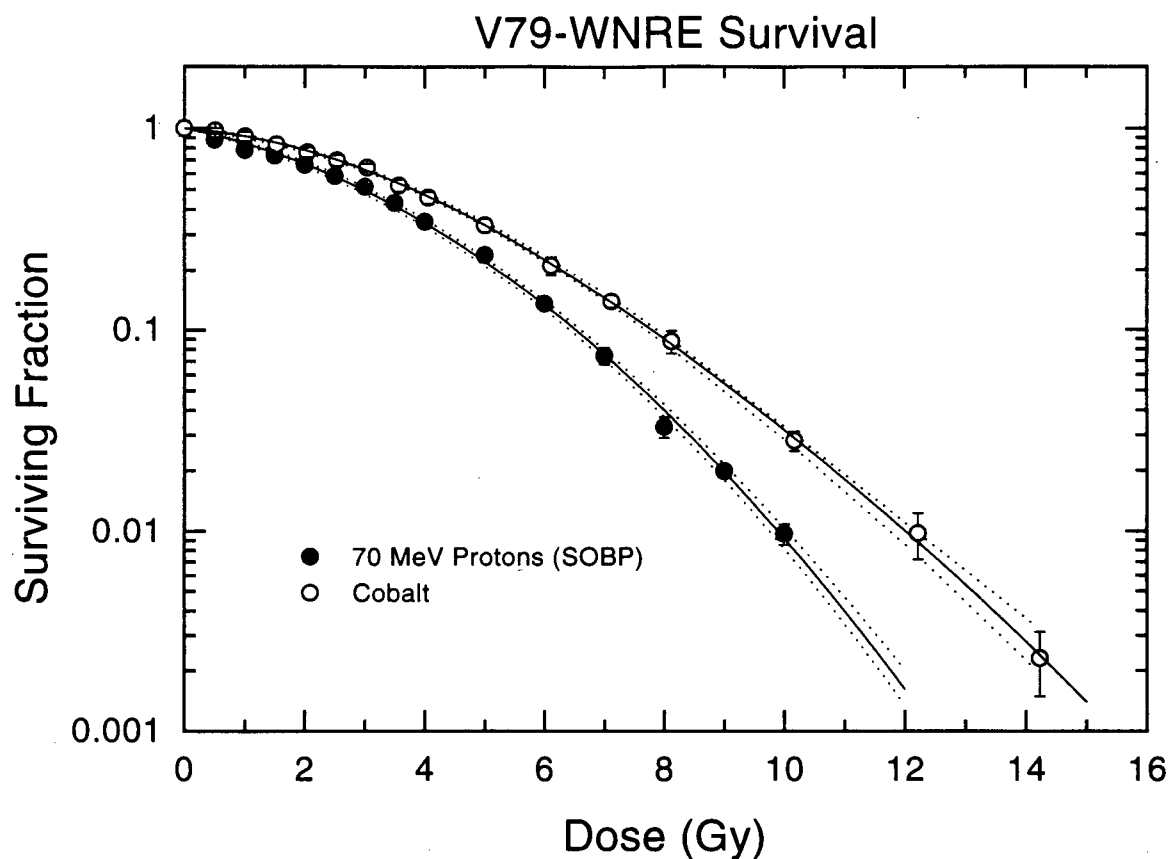
Figure 5-19 Comparison of the Proton Average SOBP and ^{60}Co Responses
The average radiation response of V79-WNRE cells within the SOBP (7-28 mm) of the 70 MeV proton beam at TRIUMF is shown with the average response to ^{60}Co irradiation for the average of experiments 2 and 3. Dashed lines are upper and lower 95 % confidence limits in the fitted functions: the two population model (equation 3-6) for the ^{60}Co response and the LQ model (equation 3-4) for the proton SOBP response.

As a test of the reproducibility of these measurements, we have also plotted in the inset of figure 5-20, the RBE derived from results of the first experiment (shown previously in figure 5-13), together with the RBE results for the averaged data. These data show very good consistency despite the fact that the previous data were measured using a different modulator wheel and a larger collimator, resulting in a somewhat different physical dose profile (see fig. 5-1).

5.2.4.2.2 Depth-Dependence of the RBE

To illustrate the depth dependence of the RBE, fits of the data shown in figure 5-18 were used to determine the RBE in the distal and proximal regions of the SOBP, as well as the distal edge (~28-30 mm) of the stopping distribution. Figure 5-21 shows the RBE values for each of these regions plotted as a function of proton dose. These plots exhibit a dose dependence similar to that observed for the total SOBP, but they also demonstrate the depth dependence of the RBE. The RBEs for the proximal and distal regions of the stopping distribution are slightly lower and higher than the average (total), respectively. The distal edge RBE is considerably larger, approximately 1.3 at doses above 5 Gy. As a further test of the depth dependence, survival curves were generated from data at each *individual slice* and fitted with a LQ function. RBE values were then derived at survival levels of 80%, 50% and 3% (representing proton doses of approx. 1.2 Gy, 3 Gy and 8 Gy) for each of these survival responses at different depths, and the results are plotted in figure 5-22. These data exhibit additional scatter resulting from a reduction in the amount of data available for averaging, but illustrate a consistent increase in RBE with depth at all 3 survival levels.
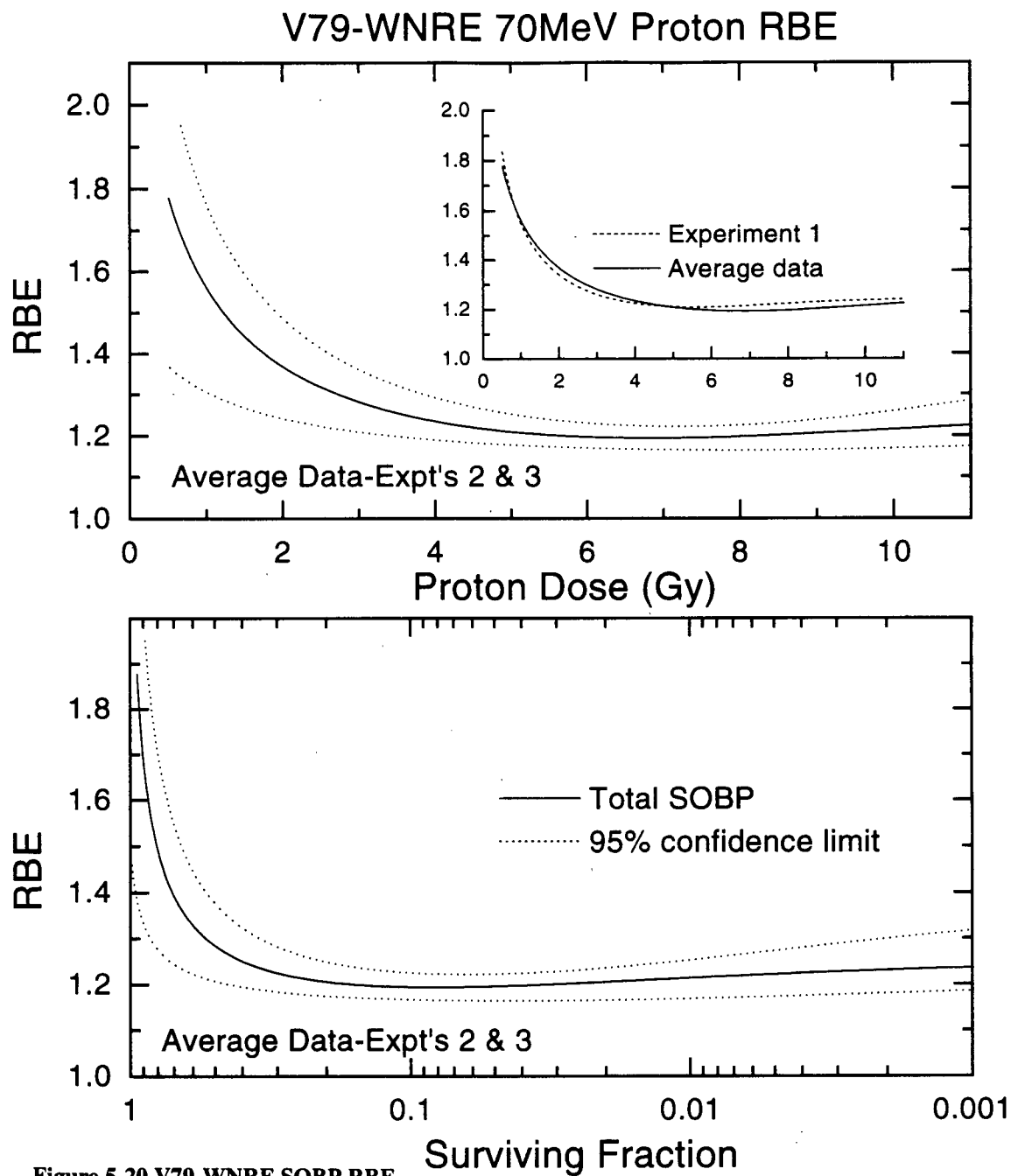
Figure 5-20 V79-WNRE SOBP RBE

The average proton RBE within the SOBP is shown as a function of proton dose (upper frame) and survival (lower frame). The RBE was determined from the fitted functions shown in figure 5-19 (experiments 2 and 3). Dashed lines are the upper and lower 95% confidence limits in the RBE as determined from the confidence limits in the fitted survival functions. Also shown (inset of upper frame) is the RBE from this average data with the average SOBP RBE determined from the first experiment, which was obtained using a somewhat different physical dose profile.

V79-WNRE RBE for 70 MeV Protons
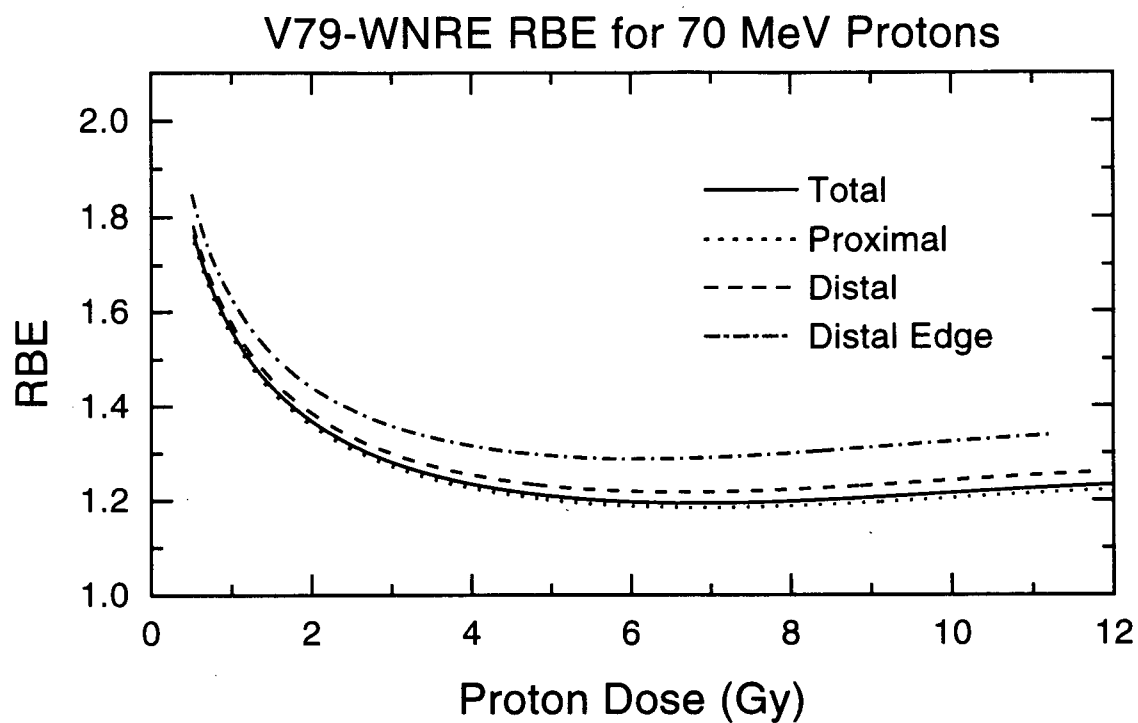
Figure 5-21 V79-WNRE Regional RBE Values

The proton RBE at different depths within the SOBP are shown as a function of proton dose. The RBE was determined from fits to survival data in the proximal, distal, and distal edge regions of the SOBP. These data illustrate that the RBE increases with increasing depth, and is largest at the distal edge of the stopping distribution. These data also illustrate a consistent dose dependence in all regions of the SOBP.

In figure 5-22 an attempt has also been made to correlate the observed depth dependence of the RBE with the depth dependence of the dose-averaged linear energy transfer (LET_d). The LET_d distribution for the physical dose profile used in the two latter experiments was determined at TRIUMF using a Monte-Carlo simulation (Dr. Uwe Oelfke personal communication), and is plotted in figure 5-22(b). This plot demonstrates a depth dependence that is consistent with the depth dependence observed for the RBE. For reference, the dose profile of the SOBP, and the centre position of each slice location are also plotted in figure 5-22c).

RBE Depth Dependence
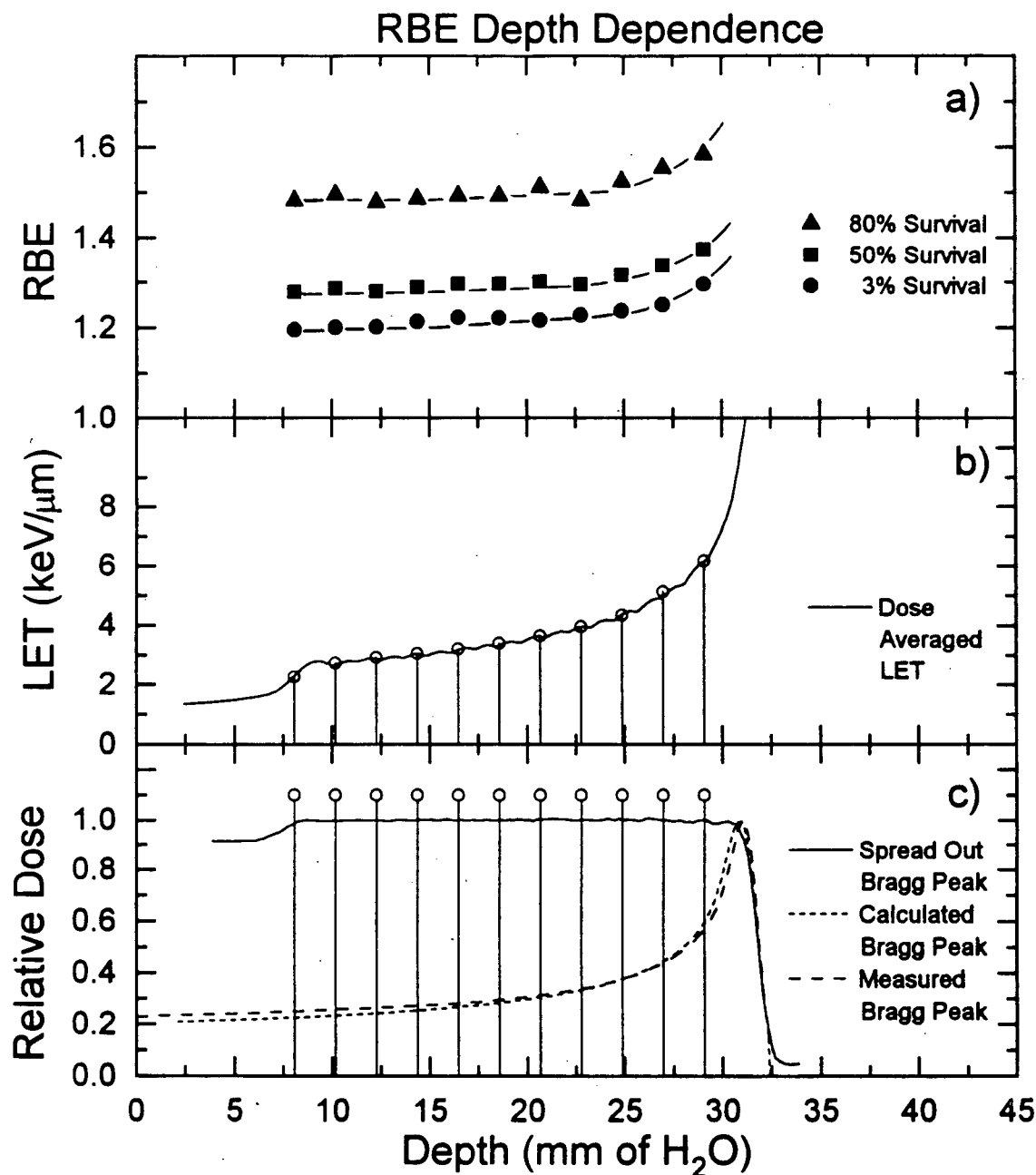
Figure 5-22 V79 WNRE RBE Depth Dependence
RBE of the 70 MeV proton beam as a function of depth (panel (a)). Points plotted are RBE values determined from fits to survival data at different depths within the peak. Survival curves were generated for each 2 mm gel slice and fitted with the LQ model. The RBE was determined at 80%, 50% and 3% survival, representing doses of approximately 1.2 Gy, 3 Gy, and 8 Gy, respectively. Panel (b) shows the dose-averaged linear energy transfer (LET_d) (determined at TRIUMF- Dr. Uwe Oelfke personal communication). Panel (c) shows the physical dose profile of the SOBP, along with the measured and Monte Carlo calculated raw Bragg peaks. The centre position of each gel slice within the SOBP is shown for reference.

5.3 Discussion

Using the cell sorting assay in conjunction with the gel slicing technique, measurements of the survival of V79-WNRE cells following irradiation with the 70 MeV, range modulated, proton beam at TRIUMF have been made. The results suggest that for this cell line, the average RBE throughout the SOBP, above doses of about 4 Gy, is equal to 1.21±0.05. This value is consistent with recently reported values in the range of 1.0-1.2 (Urano *et al.* 1980, 1984, Tsunemoto *et al.* 1985, Rosengren *et al.* 1991, Blomquist *et al.* 1993, Robertson *et al.* 1994). The dose and depth dependence of this value have also been investigated, and the results show that the RBE increases both with increasing depth and with decreasing dose.

5.3.1 RBE is Depth Dependent

In order to produce a flat physical dose profile throughout the treatment volume, the position of the proton Bragg peak is shifted in depth using a rotating absorber of variable thickness. Thus at each point in the SOBP, the proton fluence consists of a mixture of low energy (Bragg peak) and high energy protons. The proportion of dose attributable to the peak, or low energy protons rises with depth to a value of 100% at the distal edge of the stopping peak. Because the low energy protons have a larger RBE (Belli *et al.* 1989, 1991, 1993, 1994, Folkard *et al.* 1989), one would expect an increasing RBE with depth within the SOBP. In the case of higher LET charged particle beams including pions (*e.g.,* Skarsgard *et. al* 1982) and heavy ions (*e.g.,* Blakely *et al.* 1979), this can more easily be detected because the RBE for these particles within the Bragg

peak is much higher than it is for protons. The results presented in figures 5-21 and 5-22 show clearly that there is also a small RBE dependence on depth within the 70 MeV proton SOBP, which is reflected by the survival depth dependence depicted in figures 5-5 and 5-6. This can be correlated to the depth dependence of the dose averaged LET_d within the SOBP as shown in figure 5-22(b). The LET_d values shown in this figure range from 2.4 keV/μm at the beginning of the SOBP and rise to 6 keV/μm at ~2 mm upstream of the distal edge of the SOBP. Beyond this point the LET continues to rise rapidly, to a value of more than 15 keV/μm on the falling edge of the peak. The anticipated correlation between the LET_d and the RBE, *i.e.*, the increase of LET_d and RBE with increasing depth, is observed consistently for survival levels ranging from 3% to 80%.

These results are also consistent with the recent model calculations of Scholz and Kraft (1994, 1996, personal communication), and with the report of Blomquist *et al.* (1993), who reported a small increase in biological effect with increasing depth, although the result was not statistically significant. The measured RBE at the distal edge of the beam shows a substantial increase in comparison to the average RBE in the SOBP (figs. 5-21 and 5-22). This is despite the fact that this value was determined from a 2 mm slice which was located approximately 0.3-0.5 mm from the actual edge of the beam. The true RBE at the extreme end of the SOBP (including the falling edge) is likely much larger than the value which was measured (consistent with the large increase in LET_d at that point), and may be of concern when there are sensitive tissues adjacent to this part of the treatment volume. This point is reinforced by the more limited data in the first experiment (figure 5-4), which demonstrate a larger effect (larger RBE) for the slice at the

distal edge. Analysis of figure 5-1 suggests that this increased effect is due to the fact that this last slice is closer to the extreme distal edge of the stopping peak (by ~1 mm) than that for experiments 2 or 3.

5.3.2 RBE is Dose Dependent

The RBE plotted in figure 5-29 exhibits a strong dose dependence for protons, with significantly larger values at lower dose. This dose dependence was observed in all three experiments, including one that used a somewhat different physical dose profile (see fig. 5-1). The dose dependence results from a reduction in the size of the shoulder, or in other words an increased α/β ratio, in the proton survival response. Determination of the RBE at low doses (below 5 Gy) is influenced by substructure in the survival response, and thus requires that one measure accurately the survival in this region.

5.3.2.1 Substructure in the ^{60}Co Radiation Survival Response

Careful analysis of the survival response to ^{60}Co gamma rays (figs. 5-7, 5-8, 5-9 and 5-16) reveals the presence of substructure in the survival curve at doses of approximately 4-5 Gy. This substructure has previously been observed in this same cell line in response to 250 kVp X-rays, and was shown to be due, most probably, to subpopulations of sensitive and resistant cells associated with different phases of the cell cycle (Skwarchuk *et al.* 1993). The presence of this substructure results from the emergence of a more resistant cell population at higher doses, as sensitive cells are selectively killed, and results in a fit to the full dose range (or high dose range sub-set) which overestimates the degree of cell kill at low doses (Skarsgard *et al.* 1991, 1992,

1993, 1994a, 1995, Skwarchuk *et al.* 1993). To obtain an accurate description of the ^{60}Co data at all doses, a two population LQ model was fitted to the data in the same manner as in chapter 3. This model was able to characterize the response at all dose levels, and could thus be used to accurately calculate the RBE of protons as a function of proton dose.

The presence of substructure has important implications for the calculation of the RBE for these cells at low doses. To highlight these effects, the ^{60}Co data in the low dose region (0-5 Gy) and high dose region (5-14 Gy) have been fitted separately with the LQ model. The high dose fit results in an overestimation of cell kill at low doses (fig. 5-16), and illustrates the fact that survival has to be *measured* in this region, it cannot be predicted from the higher dose data regardless of how accurately those measurements are made. Because the low dose fit results in a much smaller value for α, and a larger value for β in comparison to the high dose fit (table 5-2), the RBE determined from the low dose fit is much larger at low dose than the RBE determined from the high dose parameters. Without accurate measurements of survival at low dose, a LQ fit would result in parameters like those in the high dose fit, and would yield substantially smaller low dose RBE values. For example, at 80% survival, the high dose fit parameters predict an RBE value of 1.18, no greater than the high dose RBE, and substantially lower than the correct value of approximately 1.50.

5.3.2.2 Substructure in the Proton Radiation Survival Response

Irradiation with protons showed less evidence of the cell-cycle associated substructure, at least for the data presented in figures 5-7, 5-8, 5-9, and 5-17, suggesting

there may be less variation in response among cells in different parts of the cell cycle, following proton irradiation. As a result, adequate fits to the entire response could be made with the LQ equation. However, for each of the proton survival responses shown in these figures, the measured response for the first two dose points (0.5 and 1 Gy) fell below the fit. This hypersensitivity below 1.5 Gy, is similar to the low dose hypersensitivity that was investigated in human tumour cell lines in chapter 4, and attributed to a dose-dependent increase in the radioresistance of the cell population. This phenomenon has previously been documented in the X-ray response of human cell lines using the cell sorting assay (Wouters and Skarsgard 1994, Wouters *et al.* 1995) and in rodent and human lines using a microscopic assay (Marples and Joiner 1993, Lambin *et al.* 1993, 1994a, 1994b, Singh *et al.* 1994). Based upon these data, one would not expect to observe the low dose hypersensitivity in response to ^{60}Co gamma rays in the present study (assuming the response would be similar to the X-ray response) because the lowest dose used was 0.5 Gy. However, in the proton data presented in this chapter, the hypersensitivity observed in V79-WNRE cells extends to higher doses and lower survival levels as compared to the hypersensitivity that has been observed in response to X-rays (see chapter 4). Marples *et al.* have also observed the presence of low dose hypersensitivity in V79 cells in response to treatment with plateau pions (not in the Bragg peak), but not with peak pions, or neutrons, and have thus suggested that higher LET radiations are less efficient at inducing radioresistance (Marples and Joiner 1993, Marples *et al.* 1994). If the basis of the low dose hypersensitivity that results from proton irradiation is due to a radiation-induced increase in radioresistance, then one must assume

that irradiation with protons is also less efficient at inducing radioresistance to explain the observed increased dose range of hypersensitivity. Thus, this explanation supports the LET dependence proposed by Marples.

However, based on the data presented here, the hypersensitivity can also be explained by the presence of a subpopulation of sensitive cells. Figures 5-23(a) and 5-23(b) show that the average proton response within the SOBP, shown in figure 5-17, can be adequately fit with a two population model (equation 4-2). This fit predicts that 8.2% of the cells are unusually radiosensitive to irradiation with protons, with an α value of 4.3 Gy^{-1} (see table 5-5). If we compare this sensitivity to that predicted by a fit with the induced radioresistance variable-α model (equation 4-3) (see figures 5-23(c) and 5-23(d)), this value represents a population which is more than 10 times as sensitive as the initial sensitivity of the cells predicted by the variable-α fit (table 5-5). Although these fitting results would suggest that the induced radioresistance hypothesis may be more likely, more data at low doses are required to determine these values with better certainty.

As a consequence of this apparent low dose hypersensitivity, it should be noted that the values of RBE at low dose shown in figures 5-20 and 5-21, represent *minimum* values. If the hypersensitivity observed in response to low proton doses is real (regardless of its origin), then the RBE values at doses below 1.5 Gy would be considerably larger than those shown in figures 5-20 and 5-21, which are derived from the LQ fits of the proton responses shown in figures 5-17 and 5-18. If a function that accurately characterized the initial hypersensitivity were used to calculate the RBE (*e.g.,* see fig. 5-23), much larger values at low doses would result.

V79-WNRE Survival - 70 MeV Proton SOBP
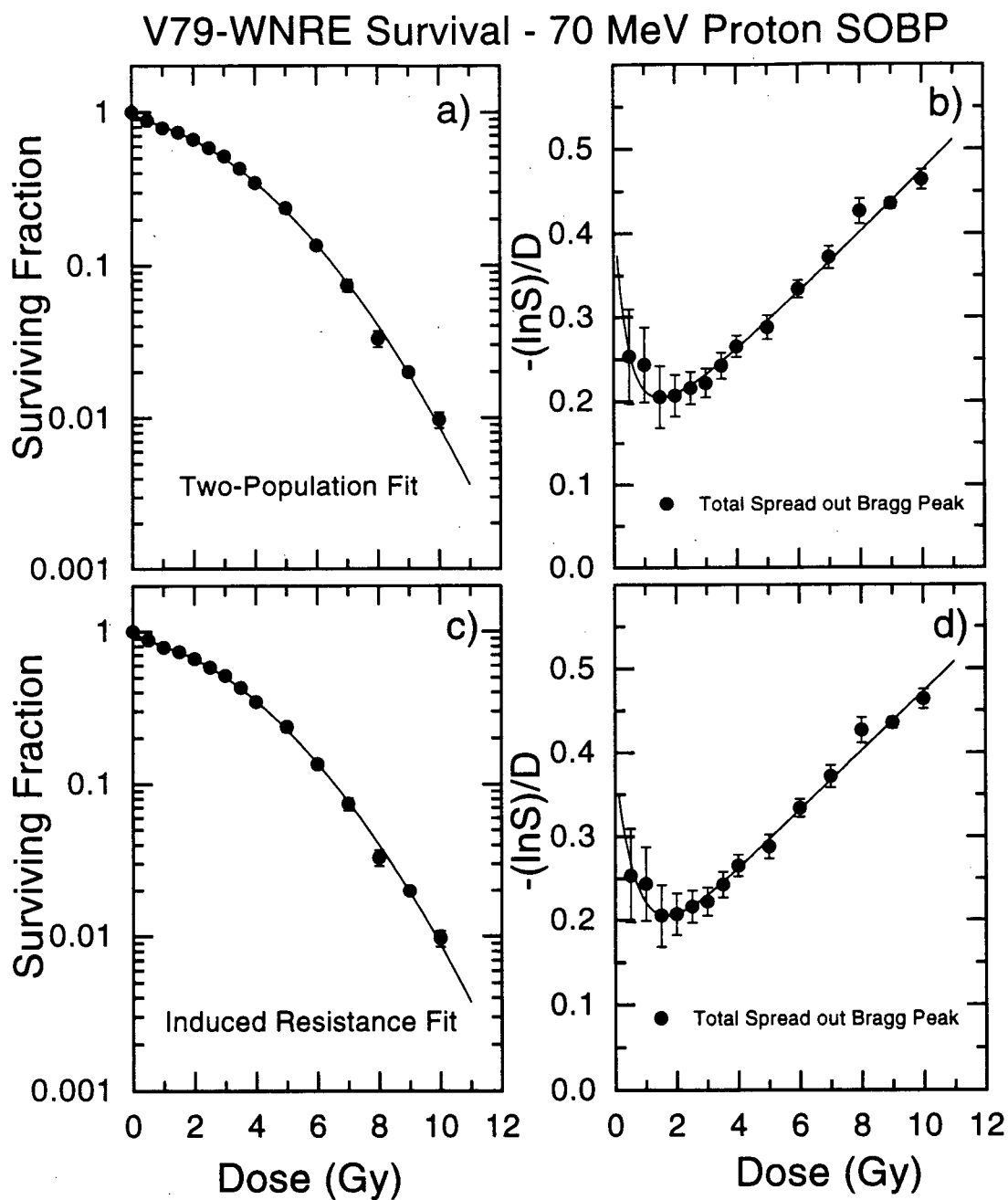
Figure 5-23 V79-WNRE Proton Survival - Low Dose Characterization
The average proton response within the SOBP from figure 5-17 is shown along with fits of two models able to characterize the hypersensitive response observed at very low doses. Panels (a) and (b) show the best fit of the TPLQ model (equation 4-2) in which the low dose hypersensitivity is hypothesized to result from a small sensitive fraction of cells. Panels (c) and (d) show the best fits of the variable-α model (equation 4-3), which proposes a radiation-induced increase in resistance of the entire population.

Table 5-5 Best-Fit Parameters for Models Describing the Low Dose Proton Survival Response
The low dose data in the average proton SOBP survival response were characterized using two models. The TPLQ model (equation 4-2) in which the low dose hypersensitivity is hypothesized to result from a small sensitive fraction of cells, and the variable-α model (equation 4-3), which proposes a radiation-induced increase in resistance of the entire population.

Model	f (%)	d_c (Gy)	α_s (Gy^{-1})	α_r (Gy^{-1})	β (Gy^{-2})
Two-Population	8.2	-	4.3	.092	.0374
Variable-α	-	.720	.381	.120	.0353

5.3.3 Cell Line Dependence?

If one considers the results with hypoxic radiosensitizers in chapter 3, then one would expect that the extent of the dose dependence of the RBE is likely to be cell line dependent. The RBE rises at low dose because there is a reduction in the size of the shoulder on the survival curve for protons. In other words, there is a selective modification (increase) of the α parameter. Cell lines with a large shoulder (*i.e.,* a low α/β ratio) would be expected to show the largest increase in proton RBE at low doses, because selective modification of the α parameter by protons would result in a larger change at low doses. In cell lines with a high α/β ratio, the α parameter contributes more to cell kill at all doses, and thus a change in this parameter would affect the RBE at all doses more equally. For the extreme case of a purely exponential response to ^{60}Co (β=0), the RBE should be independent of dose. This analysis is consistent with the results of a recent report that examined the RBE of helium ions with an LET of either 6 keV/μm or 25 keV/μm (Carlsson *et al.* 1995). These authors reported a large dose dependence of

RBE for two cell lines, both of which exhibited shouldered survival curves, and almost no dose dependence for another cell line that exhibited a nearly exponential response. This explanation based on the α/β ratio is also consistent with results observed for neutron irradiation. Irradiation with neutrons results in a large modification of the shoulder and leads to both a normal tissue dependence (Field 1976,) and tumour dependence (van Peperzeel, *et al.* 1974, Field and Hornsey 1975, Battermann *et al.* 1981) of the RBE. Recently reported *in vitro* results with fast neutrons (62.5 MeV [p$\rightarrow$Be$^+$]) described RBE values ranging from 1.5 to more than 3 in different human tumour cell lines (Britten *et al.* 1992, Warenius *et al.* 1994).

5.3.4 What Value of RBE?

The results of these studies clearly indicate that there is no single RBE value that can be quoted even for just a single cell line. The RBE is depth and dose dependent, and in all likelihood cell line dependent. This poses problems in relation to specifying the dose delivered to patients in terms of 'cobalt equivalent grays'. In the clinic, RBE values of 1.0 or 1.1 are commonly being used (Tsunemoto *et al.* 1985, Munzenrider *et al.* 1989). However, in general the RBE will depend on both the fraction size used, and possibly the tissue (normal or tumour) irradiated. And of course some of these RBE differences reflect not so much differences in the absolute effectiveness of the high LET radiations which they describe as they do differences in the absolute effectiveness of the X- or γ-rays against which they are compared - a consequence of our historical use of photons as the standard. This situation urges caution in the specification of global RBE values and in the use of 'cobalt equivalent grays'. One can easily envisage a situation where 2 adjacent

tissues that receive the same physical dose might, because of RBE differences, receive different cobalt equivalent doses. Only the physical proton dose, in grays, has a unique value and it is what the protocol should specify.

6

CONCLUSIONS

The purpose of the work described in this thesis was to obtain a better understanding of the nature of the mammalian cell survival response to low radiation doses, and to identify some of the implications of this response for clinical treatment of cancer. To this end, the cell sorting assay has been adopted for its ability to measure with high precision, the clonogenic potential of mammalian cells at high plating efficiencies where the radiation effect is small.

The first part of this work grew out of previous findings in this laboratory. Using the cell sorting assay, Skarsgard and colleagues (Skarsgard *et al.* 1991, 1992, 1993, 1994a, 1995, Skwarchuk *et al.* 1993) identified substructure in the mammalian cell survival response that was attributed to cell-cycle associated subpopulations of cells with different radiosensitivity. This had important implications for the determination of cell survival at low doses. The presence of this substructure results in progressive selection of resistant cells as the radiation dose is increased, and when the response data are fitted with the linear quadratic (LQ) model, a misfit of the data at low doses results. This early work showed that the radiation response at low dose cannot be predicted by the high dose data, it must be measured. When the response is extrapolated from high dose data, in most cases, an over-prediction of cell kill occurs. This extrapolation tends to over-predict the magnitude of the α parameter in the LQ model, and underestimate the contribution to cell kill from the β component. This has important implications for the evaluation of hypoxic cell radiosensitizers at low, clinically relevant doses. In chapter 3, it was shown that cell-cycle associated substructure is also found in the radiation responses of hypoxic cells alone and in hypoxic cells treated with either etanidazole or RB6145. The

magnitude of this substructure is different in different cell lines, and thus the efficacy of these radiosensitizers cannot be predicted from high dose data alone. Each of these radiosensitizers exhibits a unique dependence on cell line and on dose, which can be predicted in part, on the basis of the radiation response measured at low dose under hypoxic conditions alone. However, the efficacy of these agents appears to be related more to the shape, $i.e.$, the α/β ratio, of the low dose intrinsic radiosensitivity, than to the absolute sensitivity of different human tumour cell lines. Both of the radiosensitizers resulted in selective sensitization of cell lines with low α/β ratios, although the mechanisms by which this occurred were different. For etanidazole, sensitization resulted from a selective increase in the β parameter, and was most effective in cell lines in which this parameter contributed significantly to cell kill at low doses under hypoxic conditions alone. For RB6145, sensitization resulted from an increase in the α parameter, but did so only in cell lines in which $a\ priori$, this parameter played a less important a role in cell killing under hypoxic conditions alone. The intrinsic shape of the low dose response also determined the dose dependence of the efficacy of these two radiosensitizers in different cell lines, and may also explain conflicting reports which exist in the literature on the radiation dose dependence of the sensitizing effects of oxygen. With etanidazole, for which there was selective modification of the β parameter, we observed somewhat greater sensitization at higher doses. However, this only significantly influenced the dose dependence of this agent in DU145 cells, where the α-contribution is large. This is because in order to observe the dose dependence, measurements of survival must be made in the survival region for which the α parameter dominates cell kill. For example, in HT-

29 cells, the β parameter dominates cell kill at a relatively low dose, and correspondingly, no significant dose dependence was found.

This is the first work to show that the intrinsic radiosensitivity has important clinical implications for the efficacy of radiation modifying agents, and it illustrates the point that particular tumour types may be selectively treated with specific radiation modifying agents, offering the potential of tailoring individual treatment. In other words, it may be necessary to match the response characteristics of the tumour to the action characteristics of the modifying agent. The results also strongly suggest that the efficacy of radiation modifying agents should be evaluated at low radiation doses in a wide range of human tumour cell lines exhibiting different radiosensitivity, cell-cycle associated substructure, and α/β ratios.

The identification of a wide range in the intrinsic radiosensitivity characteristics of different human tumour cells is potentially of great importance to the radiation treatment of cancer. As a consequence, further studies of the intrinsic radiation response were carried out. In order to understand the mechanisms of radiosensitivity, it is imperative to know the dose response relationship for radiation. Until recently, it was very difficult to measure cell kill following irradiation with doses below 1 Gy, due to statistical limitations of the clonogenic assay. However, with the advent of new assays such as the cell sorting assay used for this work, measurement in this dose range is now possible. In chapter 4, we adapted the cell sorting assay to allow high precision measurements of survival after very low doses of X-rays, in an attempt to understand the mechanisms underlying these very different responses. This investigation revealed a marked increase in the sensitivity

of three human tumour cell lines to radiation doses below approximately 0.5 Gy, as compared to that which would be predicted by the LQ model. These studies suggested a possible relationship to overall radiosensitivity, with the most resistant cell lines, HT-29 and DU145, exhibiting larger increases in radioresistance at doses beyond the hypersensitive region, than the more sensitive A549 cell line. To eliminate, as much as possible, the possibility that low dose hypersensitivity could be explained by random error, an extensive amount of data averaging and error analysis was performed, the results of which suggested that the phenomenon was real. Mathematical modeling of the radiation response for these cell lines indicated that it is unlikely that the low dose hypersensitivity is due to a small subpopulation of sensitive cells. Rather, these results suggest that the response is due to a radiation-induced increase in radioresistance of the entire cell population. This interpretation was supported by two further studies. First, synchronous populations of HT-29 cells in G0/G1 phase of the cell-cycle also exhibited low dose hypersensitivity followed by a large increase in resistance. Second, cells primed with 0.3 Gy prior to a second dose of radiation showed no evidence of low dose hypersensitivity, but were somewhat more sensitive at high doses as compared to unprimed cells. If the population had contained a small subpopulation of sensitive cells, one would have expected the response to the second dose to be somewhat more resistant at higher doses. Instead, the cells responded as though they had received the entire dose at once, and thus exhibited no sub-lethal damage repair during the 4 hour period between the priming and second dose. This is consistent with the hypothesis that the damage which results from very low doses is either not recognized, or not repaired, to the same

extent that it is at doses beyond the sensitive region. The priming study also distinguished this phenomenon from that which has been termed the adaptive response.

The proposal that cells exhibit low dose hypersensitivity followed by an increase in resistance is consistent with a recent and fundamental change in thinking with regard to the cellular response to radiation. Rather than simply responding passively to radiation damage, there is growing evidence that the cell actively responds to damage by complex signal transduction networks. If the induction of these networks is dose dependent, then one would expect that the radiosensitivity, at different doses, might also be fundamentally different. Thus, the differences in radiosensitivity observed among different human tumour cell lines may be related to mutations in oncogenes and tumour suppressor genes that play critical and active roles in these signal transduction networks. Two explanations were offered for the observed low dose hypersensitivity. We suggested that either the constitutive repair processes that are active at doses above 1 Gy are inactive, or less efficient at doses below ~0.5 Gy, or that the ability to induce apoptosis is somewhat suppressed or down-regulated above the hypersensitive region. This latter hypothesis is supported by recent evidence that the defect in A-T cells, which results in their unusual hypersensitivity to radiation, is related to an inability to down-regulate apoptosis following irradiation (Meyn 1994). Clearly more work is required to resolve this question.

Finally, the radiation response of V79-WNRE cells to the 70 MeV proton beam at TRIUMF was measured to determine the relative biological effectiveness (RBE) of this beam, compared to ^{60}Co. In chapter 5, it was shown that the average RBE throughout the

spread out Bragg peak (SOBP) for doses above 4 Gy was equal to 1.21±.05, for V79-WNRE cells. However, further analysis of this data showed a small but significant increase in RBE with increasing depth within the spread out Bragg peak. The magnitude of this increase in RBE at the end of the stopping distribution was large enough to be of concern when critical tissues (such as the optic nerve in uveal melanoma treatments) are located in this region, distal to the stopping peak. This investigation also showed a significant dose dependence for the RBE, with values rising rapidly below 4 Gy. The importance of low dose survival measurements was once again highlighted by this work. The cell survival response for ^{60}Co irradiation exhibited substructure similar to that seen previously with this cell line in response to X-rays. However the proton response showed less evidence of this cell-cycle-dependent substructure, and also exhibited a smaller shoulder (larger α/β ratio) that resulted in the observed dose dependence of the RBE. If measurements had been made only at high dose, the cell kill resulting from low doses of ^{60}Co γ-rays would have been over-predicted, and the corresponding RBE at low doses underestimated.

The importance of the low dose response for determining radiosensitizer efficacy among different cell lines that was observed in chapter 3, would also be expected to apply to the RBE dose dependence in different cell lines. Because measurement of the radiation response at low, clinically relevant doses (*i.e.,* above the hypersensitive region) generally results in smaller α/β ratios and a more resistant response than predicted by high dose data, the RBE for protons at low doses is likely to be larger and more variable among different cell lines than one would predict without low dose measurements. One would also expect that the dose below which the RBE begins to rise would be extremely variable

from one cell line to another, dependent on the low dose α/β value determined from the ^{60}Co response, and the relative contributions of each of these parameters to cell kill. The variability in the RBE at different depths, different doses, and most likely different cell lines, cautions against the use of 'global' RBE values that are used for determination of 'cobalt equivalent grays', and suggests that radiotherapy treatment protocols would be more meaningful if they were described in 'proton grays'.

7

REFERENCES

Adams G. E., Flockart I. R., Smithen C. E., Strafford J. J., Wardman F. and Watts M. E., 1976, Electron-affinic sensitization VIII. A correlation between structures, one electron reduction potentials and efficiencies of nitroimidazoles as hypoxic cell radiosensitizers. *Radiation Research*, **67**, 9-20.

Adams G. E., Ahmed I., Sheldon P. W. and Stratford I. J., 1984a, RSU 1069, a 2-nitroimidazole containing an alkylating group: high efficiency as a radio- and chemosensitizer *in vitro* and *in vivo*. *International Journal of Radiation Oncology, Biology, Physics*, **10**, 1653-1656.

Adams G. E., Ahmed I., Sheldon P. W. and Stratford I. J., 1984b, Radiation sensitization and chemopotentiation: RSU 1069, a compound more efficient than misonidazole *in vitro* and *in vivo*. *British Journal of Cancer*, **49**, 571-577.

Alper T. 1979, Cellular Radiobiology. (Cambridge University Press, Cambridge).

Arends M. J. and Wyllie A. H., 1991, Apoptosis: mechanisms and roles in pathology. *International Review of Experimental Pathology*, **32**, 223-254.

Azzam E. I., Raaphorst G. P. and Mitchel R. E. J., 1994, Radiation induced adaptive response for protection against micronucleus formation and neoplastic transformation in C3H10T1/2 mouse embryo cells. *Radiation Research*, **138**, S28-S31.

Barendsen G. W., Koot C. J., van Kersen G. R., Bewley D. K., Field S. B. and Parnell C. J., 1966, The effect of oxygen on impairment of the proliferative capacity of human cells in culture by ionizing radiations of different LET. *International Journal of Radiation Biology*, **10**, 317-327.

Barendsen G. W. and Walter H. M. D., 1964, Effects of different ionizing radiations on human cells in culture. IV. Modification of radiation damage. *Radiation Research*, **21**, 314-329.

Barry M. A., Behnke C. A. and Eastman A., 1990, Activation of programmed cell death (apoptosis) by cisplatin, other anticancer drugs, toxins and hyperthermia. *Biochemical Pharmacology*, **40**, 2353-2362.

Battermann J. J., Breur K., Hart G. A. M. and van Peperzeel H. A., 1981, Observations on pulmonary metastases in patients after single doses and multiple fractions of fast neutrons and cobalt-60 gamma rays. *European Journal of Cancer*, **17**, 539-548.

Bedford J. S. and Griggs H. G., 1975, The estimation of survival at low doses and the limits of resolution of the single-cell-plating technique. In: *Cell Survival after Low Doses of Radiation: Theoretical and Clinical Implications*. Edited by: T. Alper (Wiley, London), pp. 34-39.

Bedforth J. S. and Cornforth M. N., 1987, Relationship between the recovery from sublethal X-ray damage and the rejoining of chromosome breaks in normal human fibroblasts. *Radiation Research,* **111,** 406-423.

BEIR V Committee, 1990, Health Effects of Exposure to Low Levels of Ionizing Radiation, BEIR V Report, Committee on the Biological Effects of Ionizing Radiations, Board of Radiation Effects Research, Commission on Life Sciences, National Research Council, (National Academy Press, Washington, D. C.).

Belli M., Cherubini R., Finotto S., Moschini G., Sapora O., Simone G. and Tabocchini M. A., 1989, RBE-LET relationship for the survival of V79 cells irradiated with low energy protons. *International Journal of Radiation Biology,* **55,** 93-104.

Belli M., Cera F., Cherubini R., Ianzini F., Moschini G., Sapora O., Simone G., Tabocchini M. A. and Tiveron P., 1991, Mutation induction and RBE-LET relationship of low-energy protons in V79 cells. *International Journal of Radiation Biology,* **59,** 459-465.

Belli M., Cera F., Cherubini R., Haque A. M., Ianzini F., Moschini G., Sapora O., Simone G., Tabocchini M. A. and Tiveron P., 1993, Inactivation and mutation induction in V79 cells by low energy protons: re-evaluation of the results at the LNL facility. *International Journal of Radiation Biology,* **63,** 331-337.

Belli M., Cera F., Cherubini R., Haque A. M. I., Ianzini F., Moschini G., Sapora O., Simone G., Tabocchini M. A. and Tiveron P., 1994, The RBE of protons for cell inactivation: the experience with V79 cells. In: *Hadrontherapy in oncology.* Edited by: U. Amaldi and B. Larsson (Elsevier Science, Amsterdam), pp. 702-705.

Bender M. A. and Gooch P. C., 1962, The kinetics of X-ray survival of mammalian cells *in vitro. International Journal of Radiation Biology,* **5,** 133-145.

Berry R. J., 1974, Population distribution in tumours and normal tissues: A guide to tissue radiosensitivity. In: *The Biological and Clinical Basis of Radiosensitivity.* Edited by: M. Friedman (Charles C. Thomas, Springfield, Illinois), pp. 141-155.

Biaglow J. E., 1983, The role of thiols in cellular response to radiation and drugs. *Radiation Research,* **95,** 437-455.

Bird R. P. and Burki H. J., 1975, Survival of synchronized Chinese hamster cells exposed to radiation of different linear-energy transfer. *International Journal of Radiation Biology,* **27,** 105-120.

Blackmore E. W., Vincent J., Chavez S., Gardey K., Lam G. K. Y., Oelfeke U., Pickles T. and Paton K. Commissioning the TRIUMF proton therapy facility. 1995, In:

Proceedings of NIRS International Seminar on the Application of Heavy Ion Accelerators to Radiation Therapy of Cancer - PTCOG XXI (Chiba, Japan, Nov. 14-16, 1994) HIMAC report (NIRS Publication), NIRS-M-103/HIMAC-008, pp. 135-140.

Blakely E. A., Tobias C. A., Yang T. C., Smith K. C. and Lyman J. T., 1979, Inactivation of human kidney cells by high-energy monoenergetic heavy-ion beams. *Radiation Research,* **80,** 122-160.

Blakely E. A., Roots R. J., Chang P. Y., Lommel L., Craise L. M., Goodwin E. H., Yee E., Dodgen D. P. and Blakely W. F., 1988, Cell-cycle dependence of X-ray oxygen effect: role of endogenous glutathione. *NCI Monographs,* **6,** 217-223.

Blomquist E., Russell K. R., Stenerlow B., Montelius A., Grusell E. and Carlsson J., 1993, Relative biological effectiveness of intermediate energy protons. Comparisons with ^{60}Co gamma-radiation using two cell lines. *Radiotherapy & Oncology,* **28,** 44-51.

Boag J. W., 1975, The statistical treatment of cell survival data. In: *Cell Survival after Low Doses of Radiation.* Edited by: T. Alper (Wiley, London), pp. 40-53.

Boothman D. A., Bouvard I. and Hughes E. N., 1989, Identification and characterization of X-ray-induced proteins in human cells. *Cancer Research,* **49,** 2871-2878.

Bridges B. A., 1969, Sensitization of organisms to radiation by sulphydryl binding agents. *Advances in Radiation Biology,* **3,** 123-176.

Britten R. A., Warenius H. M., Parkins C. and Peacock J. H., 1992, The inherent cellular sensitivity to 62.5 MeV(p-->Be+) neutrons of human cells differing in photon sensitivity. *International Journal of Radiation Biology,* **61,** 805-812.

Brock W. A., Baker F. L. and Peters L. J., 1989, Radiosensitivity of human head and neck squamous cell carcinomas in primary culture and its potential as a predictive assay of tumour radiocurability. *International Journal of Radiation Biology,* **56,** 751-760.

Brown J. M. 1984, Modification of Radiosensitivity in Cancer Treatment. (Academic Press, Tokyo), pp.139-176.

Brown J. M. and Yu N. Y., 1984, Radiosensitization of hypoxic cells *in vivo* by SR 2508 at low radiation doses: a preliminary report. *International Journal of Radiation Oncology, Biology, Physics,* **10,** 1207-1212.

Buxton G. V., 1982, Basic radiation chemistry of liquid water. In: *The study of fast processes and transient species by electron pulse radiolysis.* Edited by: J. M. Baxendale and F. Busi (D. Reidel, Dordrecht), pp. 241-260.

Calkins J., Einspenner M., Blocher D. and Greer W., 1989, Responses of two mammalian cell lines to low gamma-ray doses. *International Journal of Radiation Biology,* **56,** 869-875.

Carlsson J., Stenerlow B., Russell K. R., Grusell E., Larsson B. and Blomquist E., 1995, Cell type dependent effectiveness of tumour cell inactivation by radiation with increased ionization density. *Anticancer Research,* **15,** 273-282.

Carrano A. V., 1973, Chromosome aberrations and radiation-induced cell death. II. Predicted and observed cell survival. *Mutation Research,* **17,** 355-366.

Chadwick K. H. and Leenhouts H. P., 1973, A molecular theory of cell survival. *Physics in Medicine & Biology,* **18,** 78-87.

Chaplin D. J., Durand R. E. and Olive P. L., 1986, Acute hypoxia in tumours: implications for modifiers of radiation effects. *International Journal of Radiation Oncology, Biology, Physics,* **12,** 1279-1282.

Chaplin D. J., Douglas B. G., Grulkey W., Skarsgard L. D., Lam G. and Denekamp J., 1987, The response of mouse epidermis to fractionated doses of pi mesons. *International Journal of Radiation Oncology, Biology, Physics,* **13,** 1199-1208.

Chapman J. D., 1980, Biological models of mammalian cell inactivation by radiation. In: *Radiation Biology in Cancer Research.* Edited by: R. E. Meyn and H. R. Withers (Raven Press, New York), pp. 21-32.

Chapman J. D., Todd P. and Sturrock J., 1970, X-ray survival of cultured Chinese hamster cells resuming growth after plateau phase. *Radiation Research,* **42,** 590-600.

Chapman J. D., Reuvers A. P., Borsa A. P., Petkau J. and McCalla D. R., 1972, Nitrofurans as radiosensitizers of hypoxic mammalian cells. *Cancer Research,* **32,** 2630-2632.

Chapman J. D., Gillespie C. J., Reuvers A. P. and Dugle D. L., 1975a, Radioprotectors, radiosensitizers, and the shape of the mammalian cell survival curve. In: *Cell Survival After Low Doses of Radiation: Theoretical and Clinical Implications.* Edited by: T. Alper (Wiley, London), pp. 135-140.

Chapman J. D., Gillespie C. J., Reuvers A. P. and Dugle D. L., 1975b, The inactivation of Chinese hamster cells by X Rays: The effects of chemical modifiers on single- and double-events. *Radiation Research,* **64,** 365-375.

Chassagne D., Sancho-Garnier H., Charreau I., Eschwege F. and Malaise E. P., 1991, Progress report of a phase II and a phase III trial with etanidazole (SR-2508): a multicentre European study. *Radiotherapy & Oncology*, **20 (Suppl. 1)**, 121-127.

Chen M., Quintans J., Fuks Z., Thompson C., Kufe D. W. and Weichselbaum R. R., 1995, Suppression of Bcl-2 messenger RNA production may mediate apoptosis after ionizing radiation, tumour necrosis factor alpha, and ceramide. *Cancer Research*, **55**, 991-994.

Churchill-Davidson I., Sanger C. and Thomlinson R. H., 1955, High-pressure oxygen and radiotherapy. *Lancet*, **i**, 1091-1095.

Clarke A. R., Purdie C. A., Harrison D. J., Morris R. G., Bird C. C., Hooper M. L. and Wyllie A. H., 1993, Thymocyte apoptosis induced by p53-dependent and independent pathways. *Nature*, **362**, 849-852.

Cole S., Stratford I. J., Adams G. E., Fielden E. M. and Jenkins T. C., 1990, Dual-function 2-nitroimidazoles as hypoxic cell radiosensitizers and bioreductive cytotoxins: *in vivo* evaluation in KHT murine sarcomas. *Radiation Research*, **124**, S38-43.

Cole S., Stratford I. J., Fielden E. M., Adams G. E., Leopold W., Elliott W., Suto M. and Sebolt-Leopold J., 1992, Dual function nitroimidazoles less toxic than RSU 1069: selection of candidate drugs for clinical trial (RB 6145 and/or PD 130908). *International Journal of Radiation Oncology, Biology, Physics*, **22**, 545-548.

Crompton N. E. A., Barth B. and Kiefer J., 1990, Inverse dose-rate effect for the induction of 6-thioguanine-resistant mutants in Chinese hamster V79-S cells by ^{60}Co gamma rays. *Radiation Research*, **124**, 300-308.

Curtis S. B., 1986, Lethal and potentially lethal lesions induced by radiation-a unified repair model. *Radiation Research*, **106**, 252-270.

D'Amico A. V. and McKenna W. G., 1994, Apoptosis and a re-investigation of the biological basis for cancer therapy. *Radiotherapy & Oncology*, **33**, 3-10.

Deacon J., Peckham M. J. and Steel G. G., 1984, The radioresponsiveness of human tumours and the initial slope of the cell survival curve. *Radiotherapy & Oncology*, **2**, 317-323.

Deering R. A. and Rice R., 1962, Heavy ion irradiation of HeLa cells. *Radiation Research*, **17**, 774-786.

Deschavanne P. J., Debieu D., Fertil B. and Malaise E. P., 1986, Re-evaluation of *in vitro* radiosensitivity of human fibroblasts of different genetic origins. *International Journal of Radiation Biology,* **50,** 279-293.

Dewey W. C., Furman S. C. and Miller H. H., 1970, Comparison of lethality and chromosomal damage induced by X-rays in synchronized Chinese Hamster cells *in vitro. Radiation Research,* **43,** 561-581.

Dische S., Saunders M. I., Anderson P., Lee M., Fowler J. F., Stratford M. and Minchinton A., 1977, Clinical testing of the radiosensitizer Ro 07-0582: experience with multiple doses. *British Journal of Cancer,* **35,** 567-579.

Dische S., 1985, Chemical sensitizers for hypoxic cells: a decade of experience in clinical radiotherapy. *Radiotherapy & Oncology,* **3,** 97-115.

Dische S., Saunders M. I., Dunphy E. P., Bennett M. H., Des Rochers C., Stratford M. R., Minchinton A. I. and Orchard R. A., 1986, Concentrations achieved in human tumours after administration of misonidazole, SR-2508 and Ro 03-8799. *International Journal of Radiation Oncology, Biology, Physics,* **12,** 1109-1111.

Douglas B. G., 1983, Pion beam studies in mice and in pigs. In: *Pion and Heavy Ion Radiotherapy: Pre-clinical and Clinical Studies.* Edited by: L. D. Skarsgard (Elselvier, New York), pp. 299-314.

Douglas B. G., Grulkey W. R., Chaplin D. J., Lam G., Skarsgard L. D. and Denekamp J., 1986, Pions and pig skin: preclinical evaluation of RBE for early and late damage. *International Journal of Radiation Oncology, Biology, Physics,* **12,** 221-229.

Duncan W. and Nias A. H. W. 1977, Clinical Radiobiology. (Churchill Livingstone, Edinburgh).

Durand R. E., 1984a, Repair during multifraction exposures: spheroids versus monolayers. *British Journal of Cancer,* **49 (Suppl. 6) I,** 203-206.

Durand R. E., 1984b, Roles of thiols in cellular radiosensitivity. *International Journal of Radiation Oncology, Biology, Physics,* **10,** 1235-1238.

Durand R. E., 1986, Use of a cell sorter for assays of cell clonogenicity. *Cancer Research,* **46,** 2775-2778.

Elkind M. M. and Sutton H., 1960, Radiation response of mammalian cells grown in culture. 1. Repair of X-ray damage in surviving Chinese hamster cells. *Radiation Research,* **13,** 556-593.

Elkind M. M., Sutton-Gilbert H., Moses W. B., Alescio T. and Swain R. W., 1965, Radiation response of mammalian cells in culture. V. Temperature dependence of the repair of X-ray damage in surviving cells (aerobic and hypoxic). *Radiation Research*, **25,** 359-376.

Elkind M. M. and Whitmore G. F., 1967, The Radiobiology of Cultured Mammalian Cells. (Gordon and Breach, New York).

Fertil B., Dertinger H., Courdi A. and Malaise E. P., 1984, Mean inactivation dose: A useful concept for intercomparison of human cell survival curves. *Radiation Research*, **99,** 73-84.

Fertil B. and Malaise E. P., 1981, Inherent cellular radiosensitivity as a basic concept for human tumour radiotherapy. *International Journal of Radiation Oncology, Biology, Physics,* **7,** 621-629.

Fertil B. and Malaise E. P., 1985, Intrinsic radiosensitivity of human cell lines is correlated with radioresponsiveness of human tumours: analysis of 101 published survival curves. *International Journal of Radiation Oncology, Biology, Physics,* **11,** 1699-1707.

Field S. B., 1976, An historical survey of radiobiology and radiotherapy with fast neutrons. In: *Current Topics in Radiation Research.* Edited by: M. Ebert and A. Howard (North-Holland, Amsterdam), pp. 1-86.

Field S. B. and Hornsey, S., 1975, The RBE for fast neutrons: the link between animal experiments and clinical practice. In: *Proceedings of the 5th International Congress of Radiation Research, Seattle, Washington.* Edited by: O. F. Nygaard, H. I. Adler and W. K. Sinclair (Academic Press, New York), pp. 1125-1135.

Folkard M., Prise K. M., Vojnovic B., Davies S., Roper M. J. and Michael B. D., 1989, The irradiation of V79 mammalian cells by protons with energies below 2 MeV. Part I: Experimental arrangement and measurements of cell survival. *International Journal of Radiation Biology,* **56,** 221-237.

Fowler J. F., Morgan R. L., Silvester J. A., Bweley D. K. and Turner B. A., 1963, Pretherapeutic experiments with fast neutron beam from Medical Research Council cyclotron: VIII. General review. *British Journal of Radiology,* **36,** 188-196.

Fowler J. F., Adams G. E. and Denekamp J., 1976, Radiosensitizers of hypoxic cells in solid tumours. *Cancer Treatment Review,* **3,** 227-256.

Freyer J. P., Jarrett K., Carpenter S. and Raju M. R., 1991, Oxygen enhancement ratio as a function of dose and cell cycle phase for radiation-resistant and sensitive CHO cells. *Radiation Research,* **127,** 297-307.

Gatenby R. A., Kessler H. B., Rosenblum J. S., Coia L. R., Moldofsky P. J., Hartz W. H. and Broder G. J., 1988, Oxygen distribution in squamous cell carcinoma metastases and its relationship to outcome of radiation therapy. *International Journal of Radiation Oncology, Biology, Physics,* **14,** 831-838.

Gillespie C. J., Chapman, J. D., Reuvers, A. P., and Dugle, D. L., 1975, The Inactivation of Chinese Hamster Cells by X Rays: Synchronized and Exponential Cell Populations. *Radiation Research,* **64,** 253-364.

Goodhead D. T., 1988, Spatial and temporal distribution of energy. *Health Physics,* **55,** 231-240.

Goodhead D. T., 1989, The initial physical damage produced by ionizing radiations. *International Journal of Radiation Biology,* **56,** 623-634.

Goodhead D. T., 1994, Initial events in the cellular effects of ionizing radiations: clustered damage in DNA. *International Journal of Radiation Biology,* **65,** 7-17.

Goodhead D. T., Munson R. J., Thacker J. and Cox R., 1980, Mutation and inactivation of cultured mammalian cells exposed to beams of accelerated heavy ions. IV Biophysical interpretation. *International Journal of Radiation Biology,* **37,** 135-167.

Goodman G. B., Douglas B. G., Jackson S. M., Kornelsen R. O., Lam G. K., Ludgate C. M. and Skarsgard L. D., 1982, Pions, Vancouver. *International Journal of Radiation Oncology, Biology, Physics,* **8,** 2187-2190.

Gorczyca W., Gong J., Ardelt B., Traganos F. and Darzynkiewicz Z., 1993, The cell cycle related differences in susceptibility of HL-60 cells to apoptosis induced by various antitumour agents. *Cancer Research.* **53,** 3186-3192.

Gratzner H. G., 1982, Monoclonal antibody to 5-bromo and 5-iododeoxyuridine: A new reagent for detection of DNA replication. *Science,* **218,** 474-475.

Gray L. H., Conger A. D., Ebert M., Hornsey S. and Scott O. C. A., 1953, The concentration of oxygen dissolved in tissues at the time of irradiation as a factor in radiotherapy. *British Journal of Radiology,* **26,** 638-648.

Guillouf C., Grana X., Selvakumaran M., De Luca A., Giordano A., Hoffman B. and Liebermann D. A., 1995, Dissection of the genetic programs of p53-mediated G1

growth arrest and apoptosis: blocking p53-induced apoptosis unmasks G1 arrest. *Blood*, **85,** 2691-2698.

Hall E. J. 1994, Radiobiology for the Radiobiologist. **4,** (J. B. Lippincott Company, Philadelphia).

Hall E. J. and Roizin-Towle L. A., 1975, Hypoxic sensitizers. Radiobiological studies at the cellular level. *Radiology,* **117,** 453-457.

Hall E. J., Kellerer A. M., Rossi H. H. and Lam Y. M., 1978, The relative biological effectiveness of 160 MeV protons--II. Biological data and their interpretation in terms of microdosimetry. *International Journal of Radiation Oncology, Biology, Physics,* **4,** 1009-1013.

Hart E. J. and Platzman R. L., 1961, Radiation chemistry. In: *Mechanisms in Radiobiology.* Edited by: M. Errera and A. Forssberg (Academic Press, New York), pp. 93-257.

Hendry J. H., Potten C. S. and Merritt A., 1995, Apoptosis induced by high- and low-LET radiations. *Radiation & Environmental Biophysics,* **34,** 59-62.

Hengartner M. O. and Horvitz H. R., 1994a, The ins and outs of programmed cell death during C. elegans development. *Philosophical Transactions of the Royal Society of London - Series B: Biological Sciences.* **345,** 243-246.

Hengartner M. O. and Horvitz H. R., 1994b, C. elegans cell survival gene ced-9 encodes a functional homolog of the mammalian proto-oncogene bcl-2, *Cell,* **76,** 665-676.

Henk J. M., 1986, Late results of a trial of hyperbaric oxygen and radiotherapy in head and neck cancer: a rationale for hypoxic cell sensitizers? *International Journal of Radiation Oncology, Biology, Physics,* **12,** 1339-1341.

Hickman J. A., 1992, Apoptosis induced by anticancer drugs. *Cancer & Metastasis Reviews,* **11,** 121-139.

Hockel M., Schlenger K., Knoop C. and Vaupel P., 1991, Oxygenation of carcinomas of the uterine cervix: evaluation by computerized O_2 tension measurements. *Cancer Research,* 6098-6102.

Hockel M., Knoop C., Schlenger K., Vorndran B., Baubmann E., Mitz M., Knapstein P. G. and Vaupel P., 1993, Intratumoural pO_2 predicts survival in advanced cancer of the uterine cervix. *Radiotherapy & Oncology,* **26,** 45-50.

Hornsey S. and Silini G., 1963, Comparisons of the effects of X-rays and cyclotron neutrons on mouse ascites tumours, mouse testis and chick embryos. *British Journal of Radiology*, **36,** 92-97.

Howard A. and Pelc S. R., 1953, Synthesis of deoxyribonucleic acid in normal and irradiated cells and its relation to chromosome breakage. *Heredity*, **6,** 261-273.

Iliakis G., 1991, The role of DNA double-strand breaks in ionizing radiation-induced killing of eukaryotic cells. *BioEssays*, **13,** 641-648.

Iliakis G. E., Cicilioni O. and Metzger L., 1991, Measurement of DNA double-strand breaks in CHO cells at various stages of the cell cycle using pulsed field gel electrophoresis: calibration by means of ^{125}I decay. *International Journal of Radiation Biology*, **59,** 343-357.

International Commission on Radiological Protection, 1991, Recommendations of the ICRP, ICRP Report. (Pergamon, Oxford).

Isaacs W. B., Carter B. S. and Ewing C. M., 1991, Wild-type p53 suppresses growth of human prostate cancer cells containing mutant p53 alleles. *Cancer Research*, **51,** 4716-4720.

Jeggo P. A. and Kemp L. M., 1983, X-ray sensitive mutants of Chinese hamster ovary cell line. *Mutation Research*, **112,** 313-327.

Jenkins T. C., Naylor M. A., O'Neill P., Threadgill M. D., Cole S., Stratford I. J., Adams G. E., Fielden E. M., Suto M. J. and Stier M. A., 1990, Synthesis and evaluation of alpha - [[(2-haloethyl) amino] methyl] - 2 - nitro - 1 H- imidazole-1- ethanols as prodrugs of alpha-[(1-aziridinyl)methyl]-2- nitro-1H-imidazole-1-ethanol (RSU-1069) and its analogues which are radiosensitizers and bioreductively activated cytotoxins. *Journal of Medicinal Chemistry.* **33,** 2603-2610.

Joiner M. C., 1994, Induced radioresistance: an overview and historical perspective. *International Journal of Radiation Biology*, **65,** 79-84.

Joiner M. C. and Johns H., 1988, Renal damage in the mouse: The response to very small doses per fraction. *Radiation Research*, **114,** 385-398.

Joshi G. P., Nelson W. J., Revell S. H. and Shaw C. A., 1982, X-ray chromosomal damage in live mammalian cells, and improved measurements of its effects on their colony forming ability. *International Journal of Radiation Biology*, **41,** 161-181.

Kastan M. B., Onyekwere O., Sidransky D., Vogelstein B. and Craig R. W., 1991, Participation of p53 protein in the cellular response to DNA damage. *Cancer Research*, **51**, 6304-6311.

Kastan M. B., Zhan Q., el-Deiry W. S., Carrier F., Jacks T., Walsh W. V., Plunkett B. S., Vogelstein B. and Fornace A. J.,Jr., 1992, A mammalian cell cycle checkpoint pathway utilizing p53 and GADD45 is defective in ataxia-telangiectasia. *Cell*, **71**, 587-597.

Kellerer A. M. and Rossi H. H., 1972, The theory of dual radiation action. *Current Topics in Radiation Research Quarterly*, **8**, 85-158.

Kemp L. M., Sedgwick S. G. and Jeggo P. A., 1984, X-ray sensitive mutants of Chinese hamster ovary cells deficient in double-strand break rejoining. *Mutation Research*, **132**, 189-196.

Kennedy K. A., Rockwell S. and Sartorelli A. C., 1980, Preferential, activation of mitomycin C to cytotoxic metabolites by hypoxic tumor cells. *Cancer Research*, **40**, 2356-2360.

Kerr J. F., Wyllie A. H. and Currie A. R., 1972, Apoptosis: a basic biological phenomenon with wide-ranging implications in tissue kinetics. *British Journal of Cancer*, **26**, 239-257.

Koch C. J., 1975, Measurements of very low oxygen tensions in liquids; does the extrapolation number of mammalian cell curves decrease after X-irradiation under anoxic conditions? In: *Cell Survival after Low Doses of Radiation: Theoretical and Clinical Implications*. Edited by : T. Alper (Wiley, London), pp. 150-157.

Koch C. J. and Kruuv J., 1972, Measurements of very low oxygen tensions in unstirred liquids. *Analytical Chemistry*, **44**, 1258-1263.

Koh W. J., Rasey J. S., Evans M. L., Grierson J. R., Lewellen T. K., Graham M. M., Krohn K. A. and Griffin T. W., 1992, Imaging of hypoxia in human tumours and [F-18] Fluoromisonidazole. *International Journal of Radiation Oncology, Biology, Physics*, **22**, 199-212.

Korbelik M. and Skov K. A., 1989, Inactivation of hypoxic cells by cisplatin and radiation at clinically relevant doses. *Radiation Research*, **119**, 145-156.

Koval T. M., 1984, Multiphasic survival response of a radioresistant lepidopteran insect cell line. *Radiation Research*, **98**, 642-648.

Kuerbitz S. J., Plunkett B. S., Walsh W. V. and Kastan M. B., 1992, Wild-type p53 is a cell cycle checkpoint determinant following irradiation. *Proceedings of the National Academy of Sciences,* **89,** 7491-7495.

Lambin P., Marples B., Fertil B., Malaise E. P. and Joiner M. C., 1993, Hypersensitivity of a human tumour cell line to very low radiation doses. *International Journal of Radiation Biology,* **63,** 639-650.

Lambin P., Fertil B., Malaise E. P. and Joiner M. C., 1994a, Multiphasic survival curves for cells of human tumour cell lines: induced repair or hypersensitive subpopulation? *Radiation Research,* **138,** S32-S36.

Lambin P., Malaise E. P. and Joiner M. C., 1994b, The effect of very low radiation doses on the human bladder carcinoma cell line RT112. *Radiotherapy & Oncology,* **32,** 63-72.

Larsson B., 1961, Pretherapeutic physical experiments with high energy protons. *British Journal of Radiology,* **34,** 143-151.

Lavin M. F., Khanna K. K., Beamish H., Teale B., Hobson K. and Watters D., 1994, Defect in radiation signal transduction in ataxia -telangiectasia. *International Journal of Radiation Biology,* **6,** S151-S156.

Lea D. E., 1955, *Action of Radiations on Living Cells* (Cambridge University Press, London and New York).

Lee D. J., Cosmatos D., Marcial V. A., Fu K. K., Rotman M., Cooper J. S., Ortiz H. G., Beitler J. J., Abrams R. A. and Curran W. J., 1995, Results of an RTOG phase III trial (RTOG 85-27) comparing radiotherapy plus etanidazole with radiotherapy alone for locally advanced head and neck carcinomas. *International Journal of Radiation Oncology, Biology, Physics,* **32,** 567-576.

Lee J. M. and Bernstein A., 1993, p53 mutations increase resistance to ionizing radiation. *Proceedings of the National Academy of Sciences,* **90,** 5742-5746.

Lehman T. A., Bennett W. P., Metcalf R. A., Welsh J. A., Ecker J., Modali R. V., Ullrich S., Romano J. W., Appella E. and Testa J. R., 1991, p53 mutations, ras mutations, and p53-heat shock 70 protein complexes in human lung carcinoma cell lines. *Cancer Research,* **51,** 4090-4096.

Li C. Y., Suardet L. and Little J. B., 1995, Potential role of WAF1/Cip1/p21 as a mediator of TGF-β cytoinhibitory effect. *The Journal of Biological Chemistry,* **270,** 4971-4974.

Ling C. C., Michaels B., Epp E. R. and Peterson E. C., 1980, Interaction of misonidazole and oxygen in the radiosensitization of mammalian cells. *International Journal of Radiation Oncology, Biology, Physics,* **6,** 583-589.

Ling C. C., Chen C. H. and Li W. X., 1994, Apoptosis induced at different dose rates: implication for the shoulder region of cell survival curves. *Radiotherapy & Oncology,* **32,** 129-136.

Littbrand B. and Revesz L., 1969, The effect of oxygen on cellular survival and recovery after radiation. *British Journal of Radiology,* **42,** 914-924.

Little J. B., 1994, Failla Memorial Lecture. Changing views of cellular radiosensitivity. *Radiation Research,* **140,** 299-311.

Lord E. M., Harwell L. and Koch C. J., 1993, Detection of hypoxic cells by monoclonal antibody recognizing 2-nitroimidazole adducts. *Cancer Research,* **53,** 5721-5726.

Lowe S. W., Schmitt E. M., Smith S. W., Osborne B. A. and Jacks T., 1993, p53 is required for radiation-induced apoptosis in mouse thymocytes. *Nature,* **362,** 847-849.

Mabuchi K., Soda M., Ron E., Tokunaga M., Ochikubo S., Sugimoto S., Ikeda T., Terasaki M., Preston D. L. and Thompson D. E., 1994, Cancer incidence in atomic bomb survivors. Part I: Use of the tumour registries in Hiroshima and Nagasaki for incidence studies. *Radiation Research,* **137,** S1-S16.

Maity A., McKenna W. G. and Muschel R. J., 1994, The molecular basis for cell cycle delays following ionizing radiation: a review. *Radiotherapy & Oncology,* **31,** 1-13.

Malaise E. P., Fertil B., Deschavanne P. J., Chavaudra N. and Brock W. A., 1987, Initial slope of radiation survival curves is characteristic of the origin of primary and established cultures of human tumour cells and fibroblasts. *Radiation Research,* **111,** 319-333.

Marples B., Lam G. K., Zhou H. and Skov K. A., 1994, The response of Chinese hamster V79-379A cells exposed to negative pi-mesons: evidence that increased radioresistance is dependent on linear energy transfer. *Radiation Research,* **138,** S81-S84.

Marples B. and Joiner M. C., 1993, The response of Chinese hamster V79 cells to low radiation doses: evidence of enhanced sensitivity of the whole cell population. *Radiation Research,* **133,** 41-51.

Marples B. and Joiner M. C., 1995, The elimination of low-dose hypersensitivity in Chinese hamster V79-379A cells by pretreatment with X rays or hydrogen peroxide. *Radiation Research,* **141,** 160-169.

McIlwrath A. J., Vasey P. A., Ross G. M. and Brown R., 1994, Cell cycle arrests and radiosensitivity of human tumour cell lines: dependence on wild-type p53 for radiosensitivity. *Cancer Research,* **54,** 3718-3722.

McKenna W. G., Iliakis G., Weiss M. C., Bernhard E. J. and Muschel R. J., 1991, Increased G2 delay in radiation-resistant cells obtained by transformation of primary rat embryo cells with the oncogenes H-ras and v-myc. *Radiation Research,* **125,** 283-287.

McMillan T. J. and Peacock J. H., 1994, Molecular determinants of radiosensitivity in mammalian cells. *International Journal of Radiation Biology,* **65,** 49-55.

Mendelsohn M. L., 1960, The growth fraction: a new concept applied to tumours. *Science,* **132,** 1496.

Meyn R. E., Stephens L. C., Ang K. K., Hunter N. R., Brock W. A., Milas L. and Peters L. J., 1993a, Heterogeneity in the development of apoptosis in irradiated murine tumours of different histologies. *International Journal of Radiation Biology,* **64,** 583-591.

Meyn R. E., Stephens L. C., Voehringer D. W., Story M. D., Mirkovic N. and Milas L., 1993b, Biochemical modulation of radiation-induced apoptosis in murine lymphoma cells. *Radiation Research,* **64,** 583-591.

Meyn M. S., 1995, Ataxia-telangiectasia and cellular responses to DNA damage. *Cancer Research,* **55,** 5991-6001.

Meyn M. S., Strasfeld L. and Allen C., 1994, Testing the role of p53 in the expression of genetic instability and apoptosis in ataxia-telangiectasia. *International Journal of Radiation Biology,* **66,** S141-149.

Moore B. A., Palcic B. and Skarsgard L. D., 1976, Radiosensitizing and toxic effects of the 2-nitroimidazole Ro-07-0582 in hypoxic mammalian cells. *Radiation Research,* **67,** 459-473.

Mothersill C., Harney J., Cottell D., Parsons K., Murphy D. M. and Seymour C. B., 1995, Primary explants of human uroepithelium show an unusual response to low-dose irradiation with Cobalt-60 gamma rays. *Radiation Research,* **142,** 181-187.

Moulder J. E. and Rockwell S., 1984, Hypoxic fractions of solid tumours: Experimental techniques, methods of analysis and a survey of existing data. *International Journal of Radiation Oncology, Biology, Physics,* **10,** 695-712.

Munzenrider J. E., Verhey L. J., Gragoudas E. S., Seddon J. M., Urie M., Gentry R., Birnbaum S., Ruotolo D. M., Crowell C. and McManus P., 1989, Conservative treatment of uveal melanoma: local recurrence after proton beam therapy. *International Journal of Radiation Oncology, Biology, Physics,* **17,** 493-498.

Nakano H. and Shinohara K., 1994, X-ray-induced cell death: apoptosis and necrosis. *Radiation Research,* **140,** 1-9.

Nias A. H. W. 1990, An Introduction to Radiobiology. (John Wiley & Sons, Chichester).

Nunez M. I., Villalobos M., Olea N., Valenzuela M. T., Pedraza V., McMillan T. J. and Ruiz de Almodovar J. M., 1995, Radiation-induced DNA double-strand break rejoining in human tumour cells. *British Journal of Cancer,* **71,** 311-316.

O'Connor P. M., Jackman J., Jondle D., Bhatia K., Magrath I. and Kohn K. W., 1993, Role of the p53 tumour suppressor gene in cell cycle arrest and radiosensitivity of Burkitt's lymphoma cell lines. *Cancer Research,* **53,** 4776-4780.

Okunieff P., Hockel M., Dunphy E. P., Karlheinz S., Knoop C. and Vaupel P., 1993, Oxygen tension distributions are sufficient to explain the local response of human breast tumours treated with radiation alone. *International Journal of Radiation Oncology, Biology, Physics,* **26,** 631-636.

Olive P. L., 1992, DNA organization affects cellular radiosensitivity and detection of initial DNA strand breaks. *International Journal of Radiation Biology,* **62,** 389-396.

Olive P. L., 1995, Use of the comet assay to detect hypoxic cells in murine tumours and normal tissues exposed to bioreductive drugs. *Acta Oncologica,* **34,** 301-305.

Olive P. L., Durand R. E., Le Riche J., Olivotto I. A. and Jackson S. M., 1993a, Gel electrophoresis of individual cells to quantify hypoxic fraction in human breast cancers. *Cancer Research.* **53,** 733-736.

Olive P. L., Frazer G. and Banath J. P., 1993b, Radiation-induced apoptosis measured in TK6 human B lymphoblast cells using the comet assay. *Radiation Research,* **136,** 130-136.

Olive P. L., Vikse C. M. and Durand R. E., 1994, Hypoxic fractions measured in murine tumours and normal tissues using the comet assay. *International Journal of Radiation Oncology, Biology, Physics,* **29,** 487-491.

Olive P. L. and Durand R. E., 1992, Detection of hypoxic cells in a murine tumour with the use of the comet assay. *Journal of the National Cancer Institute*, **84**, 707-711.

Olivieri G., Bodycote J. and Wolff S., 1984, Adaptive response of human lymphocytes to low concentrations of radioactive thymidine. *Science*, 594-597.

Oostveen E. A. and Speckamp W. N., 1987, Mitomycin analogs. I. Indoloquinones as (potential) bisalkylating agents. *Tetrahedron*, **43**, 255-262.

Overgaard J., Hansen H. S., Jorgensen K. and Hansen M. H., 1986, Primary radiotherapy of larynx and pharynx carcinoma - an analysis of some factors influencing local control and survival. *International Journal of Radiation Oncology, Biology, Physics*, **12**, 515-521.

Overgaard J., 1994, Clinical evaluation of nitroimidazoles as modifiers of hypoxia in solid tumours. *Oncology Research*, **6**, 509-518.

Palcic B., 1984, *In vivo* and *in vitro* mechanisms of radiation sensitization, drug synthesis and screening: can we learn it all from the high dose data? *International Journal of Radiation Oncology, Biology, Physics*, **10**, 1185-1193.

Palcic B., Moore B. A. and Skarsgard L. D., 1974, *In vitro* studies of anoxic cell sensitizers. Presented at the Sensitizer Workshop, *Fifth International Congress of Radiation Research*, Seattle, Wash., July 21, 1974.

Palcic B., Faddegon B., Jaggi B. and Skarsgard L. D., 1983, Automated low dose assay system for survival measurements of mammalian cells *in vitro*. *Journal of Tissue Culture Methods*, **8**, 103-107.

Palcic B., Brosing J. W. and Skarsgard L. D., 1984a, Survival measurements at low doses: Oxygen enhancement ratio. *British Journal of Cancer*, **46**, 980-984.

Palcic B., Faddegon B. and Skarsgard L. D., 1984b, The effect of misonidazole as a hypoxic radiosensitizer at low dose. *Radiation Research*, **100**, 340-347.

Palcic B. and Skarsgard L. D., 1984, Reduced oxygen enhancement ratio at low doses of ionizing radiation. *Radiation Research*, **100**, 328-339.

Palcic B. and Jaggi B., 1986, The use of solid state sensor technology to detect and characterize live mammalian cells growing in tissue culture. *International Journal of Radiation Biology*, **50**, 345-352.

Payne C. M., Bjore C. G.,Jr. and Schultz D. A., 1992, Change in the frequency of apoptosis after low- and high-dose X-irradiation of human lymphocytes. *Journal of Leukocyte Biology,* **52,** 433-440.

Phillips, T. L., Fu, K. K. and Lane, L. J., 1975, The effect of hypoxia and dose-rate on the shape of survival curves for EMT6 tumour and B14FAF cells *in vitro.* In: *Cell Survival after Low Doses of Radiation: Theoretical and Clinical Implications.* Edited by: T. Alper (Wiley, London), pp. 158-166.

Powell S. N. and McMillan T. J., 1994, The repair fidelity of restriction enzyme-induced double strand breaks in plasmid DNA correlates with radioresistance in human tumour cell lines. *International Journal of Radiation Oncology, Biology, Physics,* **29,** 1035-1040.

Powers W. E. and Tolmach L. J., 1963, A multicomponent X-ray survival curve for mouse lymphosarcoma cells irradiated *in vivo. Nature,* **197,** 710-711.

Prasad A. V., Mohan N., Chandrasekar B. and Meltz M. L., 1994, Activation of nuclear factor kappa B in human lymphoblastoid cells by low-dose ionizing radiation. *Radiation Research,* **138,** 367-372.

Prasad A. V., Mohan N., Chandrasekar B. and Meltz M. L., 1995, Induction of transcription of "immediate early genes" by low-dose ionizing radiation. *Radiation Research,* **143,** 263-272.

Press W. H., Flannery B. P., Teukolsky S. A. and Vetterling W. T., 1989, *Numerical Recipes.* (Cambridge University Press, Cambridge), pp. 523-528.

Preston D. L., Kusumi S., Tomonaga M., Izumi S., Ron E., Kuramoto A., Kamada N., Dohy H., Matsuo T. and Matsui T., 1994, Cancer incidence in atomic bomb survivors. Part III. Leukemia, lymphoma and multiple myeloma, 1950-1987. *Radiation Research,* **137,** S68-S97.

Puck T. T. and Marcus P. I., 1956, Action of X-rays on mammalian cells. *Journal of Experimental Medicine,* **103,** 653-666.

Raju M. R., Amols H. I., Bain E., Carpenter S. G., Cox R. A. and Robertson J. B., 1978a, A heavy particle comparative study. Part III: OER and RBE. *British Journal of Radiology,* **51,** 712-719.

Raju M. R., Bain E., Carpenter S. G., Cox R. A. and Robertson J. B., 1978b, A heavy particle comparative study. Part II: cell survival versus depth. *British Journal of Radiology,* **51,** 704-711.

Raju M. R., 1980, *Heavy Particle Radiotherapy,* (Academic Press, New York), pp. 188-251.

Raju M. R., 1995, Proton radiobiology, radiosurgery and radiotherapy. *International Journal of Radiation Biology,* **67,** 237-259.

Revesz, L., Littbrand, B., Midander, J. and Scott, O. C. A., 1975, Oxygen effects in the shoulder region of the cell survival curves. In: *Cell Survival after Low Doses of Radiation: Theoretical and Clinical Implications.* Edited by: T. Alper (Wiley, London), pp. 141-149.

Robertson, J. B., Eaddy, J. M., Archambeau, J. O., Coutrakon, G. B., Miller, D. W., Moyers, M. F., Siebers, J. V., Slater, J. M. and Dicello, J. F., 1994, Variation of measured proton relative biological effectiveness as a function of initial proton energy. In: *Hadrontherapy in Oncology.* Edited by: U. Amaldi and B. Larsson (Elsevier Science), pp. 706-711.

Rodrigues N. R., Rowan A., Smith M. E. F., Kerr I. B., Bodmer W. F., Gannon J. V. and Lane D. P., 1990, p53 mutations in colorectal cancer. *Proceedings of the National Academy of Sciences,* **87,** 7555-7559.

Rofstad E. K., Wahl A. and Brustad T., 1987, Radiation sensitivity *in vitro* of cells isolated from human tumour surgical specimens. *Cancer Research,* **47,** 106-110.

Ron E., Preston D. L., Mabuchi K., Thompson D. E. and Soda M., 1994, Cancer incidence in atomic bomb survivors. Part IV: Comparison of cancer incidence and mortality. *Radiation Research,* **137,** S98-112.

Rosengren B., Wulff L., Carlsson E., Carlsson J., Montelius A., Russell K. and Grusell E., 1991, Backscatter radiation at tissue-titanium interfaces. Analyses of biological effects from ^{60}Co and protons. *Acta Oncologica,* **30,** 859-866.

Ruiz de Almodovar J. M., Nunez M. I., McMillan T. J., Olea N., Mort C., Villalobos M., Pedraza V. and Steel G. G., 1994, Initial radiation-induced DNA damage in human tumour cell lines: a correlation with intrinsic cellular radiosensitivity. *British Journal of Cancer,* **69,** 457-462.

Savitsky K., Bar-Shira A., Gilad S., Rotman G., Ziv Y., Vanagaite L., Tagle D. A., Smith S., Uziel T. and Sfez S., 1995, A single ataxia telangiectasia gene with a product similar to PI-3 kinase. *Science,* **268,** 1749-1753.

Scholz M. and Kraft G., 1994, Calculation of heavy ion inactivation probabilities based on track structure, X ray sensitivity and target size. *Radiation Protection Dosimetry,* **52,** 29-33.

Scholz M. and Kraft G., 1996, Track structure and the calculation of biological effects of heavy charged particles. *Advances in Space Research,* **18,** 5-14.

Schwartz J. L., Jordan R., Sedita B. A., Swenningson M. J., Banath J. P. and Olive P. L., 1995, Different sensitivity to cell killing and chromosome mutation induction by gamma rays in two human lymphoblastoid cell lines derived from a single donor: possible role of apoptosis. *Mutagenesis,* **10,** 227-233.

Seong J., Chang O. S. and Kim G. E., 1995, Adaptive response to ionizing radiation induced by low doses of gamma rays in human cell lines. *International Journal of Radiation Oncology, Biology, Physics,* **33,** 869-874.

Serrano M., Hannon G. J. and Beach D., 1993, A new regulatory motif in cell-cycle control causing specific inhibition of cyclin D/CDK4. *Nature,* **366,** 704-707.

Shadley J. D., 1994, Chromosomal adaptive response in human lymphocytes. *Radiation Research,* **138,** S9-12.

Shibamoto Y., Streffer C., Sasai K., Oya N. and Abe M., 1992, Radiosensitization efficacy of KU-2285, RP-170 and etanidazole at low radiation doses: assessment by *in vitro* cytokinesis-block micronucleus assay. *International Journal of Radiation Biology,* **61,** 473-478.

Shimizu Y., Kato H., Schull W. J., Preston D. L., Fujita S. and Pierce D. A., 1989, Studies of the mortality of A-bomb survivors. 9. Mortality, 1950-1985: Part 1. Comparison of risk coefficients for site-specific cancer mortality based on the DS86 and T65DR shielded kerma and organ doses. *Radiation Research,* **118,** 502-524.

Shimizu Y., Kato H. and Schull W. J., 1990, Studies of the mortality of A-bomb survivors. 9. Mortality, 1950-1985: Part 2. Cancer mortality based on the recently revised doses (DS86). *Radiation Research,* **121,** 120-141.

Shinohara K. and Nakano H., 1993, Interphase death and reproductive death in X-irradiated MOLT-4 cells. *Radiation Research,* **135,** 197-205.

Sinclair W. K., 1966, The shape of radiation survival curves of mammalian cells cultured *in vitro.* In: *Biophysical Aspects of Radiation Quality,* Technical Report Series No. 58 (International Atomic Energy Agency, Vienna), pp. 21-43.

Sinclair W. K., 1972, Cell cycle dependence of the lethal radiation response in mammalian cells. *Current Topics in Radiation Research Quarterly,* **7,** 264-285.

Sinclair W. K. and Morton R. A., 1966, X-ray sensitivity during the cell generation cycle of cultured Chinese hamster cells. *Radiation Research,* **29,** 450-474.

Singh B., Arrand J. E. and Joiner M. C., 1994, Hypersensitive response of normal human lung epithelial cells at low radiation doses. *International Journal of Radiation Biology*, **65**, 457-464.

Skarsgard L. D., Pujara C. M., and Richardson S., 1966, The effect of high LET radiations on recovery and radiation sensitivity throughout the cell cycle in mammalian cells. *Third International Congress of Radiation Research*, Cortina d'Ampezzo, Italy, June 26-July 2, 1966 (Abstract), p.204.

Skarsgard L. D., Kihlman B. A., Parker L., Pujara C. M. and Richardson S., 1967, Survival, chromosome abnormalities, and recovery in heavy ion and X-irradiated mammalian cells. *Radiation Research*, **7**, 208-221.

Skarsgard L. D., Henkelman R. M. and Eaves C. J., 1980, Pions for radiotherapy at TRIUMF. *Journal of the Canadian Association of Radiologists*, **31**, 3-12.

Skarsgard L. D., Palcic B., Douglas B. G. and Lam G. K., 1982, Radiobiology of pions at TRIUMF. *International Journal of Radiation Oncology, Biology, Physics*, **8**, 2127-2132.

Skarsgard L. D., Palcic B. and Lam G. K. Y., 1983, RBE mapping in pion beams using the gel technique. In: *Pion and Heavy Ion Radiotherapy: Pre-clinical and Clinical Studies*. Edited by: L. D. Skarsgard (Elsevier, New York), pp. 197-210.

Skarsgard L. D., Harrison I., Durand R. E. and Palcic B., 1986, Radiosensitization of hypoxic cells at low doses. *International Journal of Radiation Oncology, Biology, Physics*, **12**, 1075-1078.

Skarsgard L. D., Harrison I. and Durand R. E., 1991, The radiation response of asynchronous cells at low dose: evidence of substructure. *Radiation Research*, **127**, 248-256.

Skarsgard L. D., Skwarchuk M. W. and Wilson D. J., 1992, Substructure in the cell survival response at low dose: Effect on the fitted parameters α and β. In: *Biophysical Modeling of Radiation Effects*. Edited by: K. H. Chadwick, G. Moschini and M. Varma (Institute of Physics Publishing, Bristol), pp. 277-284.

Skarsgard L. D., Wilson D. J. and Durand R. E., 1993, Survival at low dose in asynchronous and partially synchronized Chinese hamster V79-171 cells. *Radiation Research*, **133**, 102-107.

Skarsgard L. D., Skwarchuk M. W. and Wouters B. G., 1994a, The survival of asynchronous V79 cells at low radiation doses: modeling the response of mixed cell populations. *Radiation Research*, **138**, S72-75.

Skarsgard L. D., Wouters B. G., Lam G. K. Y., Durand R. E. and Sy A. 1994b, RBE determinations for the 70MeV proton beam at TRIUMF using cultured V79-WNRE cells. *20th PTCOG Meeting, Chester, U. K.* (Abstract).

Skarsgard L. D., Skwarchuk M. W., Wouters B. G. and Durand R. E., 1995, Substructure in the radiation survival response at low dose in human tumour cells. *(Submitted to Radiation Research).*

Skarsgard L. D. and Palcic B., 1974, Pretherapeutic research programs at π⁻ meson facilities. In: *Volume 2 of the Proceedings of the XIII International Congress of Radiology, (Madrid, Spain, October 15-20, 1973),* International Congress Series No. 39, *Radiology,* **2,** 447-454.

Skarsgard L. D. and Harrison I., 1991, Dose dependence of the oxygen enhancement ratio (OER) in radiation inactivation of Chinese hamster V79-171 cells. *Radiation Research,* **127,** 243-247.

Skov K. A., Koch C. J. and Marples B., 1994, Effect of etanidazole on absolute sensitivity and increased radioresistance in hypoxic cells at low doses. *Radiation Oncology Investigations,* **2,** 164-170.

Skov K. A. and MacPhail S., 1994, Low concentrations of nitroimidazoles: effective radiosensitizers at low doses. *International Journal of Radiation Oncology, Biology, Physics,* **29,** 87-93.

Skwarchuk M. W., Wouters B. G., and Skarsgard L. D., 1993, Substructure in the radiation survival response at low dose: asynchronous and partially synchronized V79-WNRE cells. *International Journal of Radiation Biology,* **64,** 601-612.

Solary E., Bertrand R. and Pommier Y., 1994, Apoptosis induced by DNA topoisomerase I and II inhibitors in human leukemic HL-60 cells. *Leukemia &. Lymphoma.* **15,** 21-32.

Soldatenkov V. A., Prasad S., Notario V. and Dritschilo A., 1995, Radiation-induced apoptosis of Ewing's sarcoma cells: DNA fragmentation and proteolysis of poly(ADP-ribose) polymerase. *Cancer Research.* **55,** 4240-4242.

Stapper N. J., Stuschke M., Sak A. and Stuben G., 1995, Radiation-induced apoptosis in human sarcoma and glioma cell lines. *International Journal of Cancer,* **62,** 58-62.

Steel G. G., 1967, Cell loss as a factor in the growth rate of human tumours. *European Journal of Cancer,* **3,** 381-387.

Steel G. G., 1988, The radiobiology of human tumour cells. In: *Megavoltage Radio-therapy 1937-1987*. Edited by: P. N. Plowman and A. N. Harnett (British Journal of Radiology), pp. 116-120.

Steel G. G. and Peacock J. H., 1989, Why are some human tumours more radiosensitive than others? *Radiotherapy & Oncology*, **15**, 63-72.

Stephens L. C., Hunter N. R., Ang K. K., Milas L. and Meyn R. E., 1993, Development of apoptosis in irradiated murine tumours as a function of time and dose. *Radiation Research*, **135**, 75-80.

Stone R. S., 1948, Neutron therapy and specific ionization. *American Journal of Roentgenology*, **59**, 771-785.

Su L. N. and Little J. B., 1993, Prolonged cell cycle delay in radioresistant human cell lines transfected with activated ras oncogene and/or simian virus 40 T-antigen. *Radiation Research*, **133**, 73-79.

Szumiel I., 1994, Ionizing radiation-induced cell death. *International Journal of Radiation Biology*, **66**, 329-341.

Taylor A. M. R., Harnden D. G., Arlett S. A., Harcourt S. A., Lehmann A. R., Stevens S. and Bridges B. A., 1975, Ataxia telangiectasia: a human mutation with abnormal radiation sensitivity. *Nature*, **258**, 427-429.

Tepper J., Verhey L., Goitein M. and Suit H. D., 1977, *In vivo* determinations of RBE in a high energy modulated proton beam using normal tissue reactions and fractionated dose schedules. *International Journal of Radiation Oncology, Biology, Physics*, **2**, 1115-1122.

Terasima T. and Tolmach L. J., 1961, Changes in X-ray sensitivity of HeLa cells during the division cycle. *Nature*, **190**, 1210-1211.

Thacker J., 1994, Cellular radiosensitivity in ataxia-telangiectasia. *International Journal of Radiation Biology*, **66**, S87-96.

Thomlinson R. H. and Gray L. H., 1955, The histological structure of some human lung cancers and the possible implications for radiotherapy. *British Journal of Cancer*, **9**, 539-549.

Thompson D. E., Mabuchi K., Ron E., Soda M., Tokunaga M., Ochikubo S., Sugimoto S., Ikeda T. and Terasaki M., 1994, Cancer incidence in atomic bomb survivors. Part II: Solid tumours, 1958-1987. *Radiation Research*, **137**, S17-S67.

Tobias C. A., 1985, The repair-misrepair model in radiobiology: comparison to other models. *Radiation Research,* **104,** S77-S95.

Tsunemoto H., Morita S., Ishikawa T., Furukawa S., Kawachi K., Kanai T., Ohara H., Kitagawa T. and Inada T., 1985, Proton therapy in Japan. *Radiation Research,* **104,** S235-S243.

Tubiana M., Dutreix J., Wambersie A. and Translated by D. R. Bewley, 1990, Introduction to Radiobiology. (Taylor & Francis, Philadelphia).

UNSCEAR Report A/43/45, 1988, United Nations Scientific Committee on the Effects of Atomic Radiation, General Assembly document, 43rd Session, Supplement No. 45. (United Nations, New, York).

Urano M., Goitein M., Verhey L., Mendiondo O., Suit H. D. and Koehler A., 1980, Relative biological effectiveness of a high energy modulated proton beam using a spontaneous murine tumour *in vivo. International Journal of Radiation Oncology, Biology, Physics,* **6,** 1187-1193.

Urano M., Verhey L. J., Goitein M., Tepper J. E., Suit H. D., Mendiondo O., Gragoudas E. S. and Koehler A., 1984, Relative biological effectiveness of modulated proton beams in various murine tissues. *International Journal of Radiation Oncology, Biology, Physics,* **10,** 509-514.

van Peperzeel H. A., Breur K., Broerse J. J. and Barendsen G. W., 1974, RBE values of 15 MeV neutrons for responses of pulmonary metastases in patients. *European Journal of Cancer,* **10,** 349-355.

Vaupel P., Schlenger K., Knoop C. and Hockel M., 1991, Oxygenation of human tumours:evaluation of tissue oxygen distribution in breast cancers by computerized O_2 tension measurements. *Cancer Research,* **51,** 3316-3322.

Vynckier S., Bonnett D. E. and Jones D. T. L., 1991, Code of practice for clinical proton dosimetry. *Radiotherapy & Oncology,* **20,** 53-63.

Ward J. F., 1988, DNA damage produced by ionizing radiation in mammalian cells: identities, mechanisms of formation and reparability. *Progress in Nucleic Acid Research and Molecular Biology,* **35,** 95-125.

Ward J. F., 1990, The yield of DNA double-strand breaks produced intracellularly by ionizing radiation: a review. *International Journal of Radiation Biology,* **57,** 1141-1150.

Warenius H. M., Britten R. A. and Peacock J. H., 1994, The relative cellular radiosensitivity of 30 human *in vitro* cell lines of different histological type to

high LET 62.5 MeV (p-->Be+) fast neutrons and 4 MeV photons. *Radiotherapy & Oncology*, **30,** 83-89.

Wasserman T. H., Lee D. J., Cosmatos D., Coleman N., Phillips T., Davis L., Marcial V. and Stetz J., 1991, Clinical trials with etanidazole (SR-2508) by the Radiation Therapy Oncology Group (RTOG). *Radiotherapy & Oncology*, **20 (Suppl. 1),** 129-135.

Watts M. E., Hodgkiss R. J., Jones N. R. and Fowler J. F., 1986, Radiosensitization of Chinese hamster cells by oxygen and misonidazole at low X-ray doses. *International Journal of Radiation Biology*, **50,** 1009-1021.

Weichselbaum R. R., Epstein J., Little J. B. and Kornblith P., 1976a, Inherent cellular radiosensitivity of human tumours of varying clinical curability. *American Journal of Roentgenology*, **127,** 1027-1032.

Weichselbaum R. R., Epstein J., Little J. B. and Kornblith P. L., 1976b, *In vitro* cellular radiosensitivity of human malignant tumours. *European Journal of Cancer,* **12,** 47-51.

Weichselbaum R. R., Nove J. and Little J. B., 1980, X-ray sensitivity of human tumour cells *in vitro. International Journal of Radiation Oncology, Biology, Physics,* **6,** 437-440.

Weichselbaum R. R., Beckett M. A., Vijayakumar S., Simon M. A., Awan A. M., Nachman J., Panje W. R., Goldman M. E., Tybor A. G. and Moran W. J., 1990, Radiobiological characterization of head and neck and sarcoma cells derived from patients prior to radiotherapy. *International Journal of Radiation Oncology, Biology, Physics,* **19,** 313-319.

Weichselbaum R. R., Hallahan D., Fuks Z. and Kufe D., 1994, Radiation induction of immediate early genes: effectors of the radiation-stress response. *International Journal of Radiation Oncology, Biology, Physics,* **30,** 229-234.

Weininger J., Guichard M., Joly A. M., Malaise E. P. and Lachet B., 1978, Radiosensitivity and growth parameters *in vitro* of three human melanoma strains. *International Journal of Radiation Biology,* **34,** 285-290.

West C. M., Davidson S. E. and Hunter R. D., 1989, Evaluation of surviving fraction at 2 Gy as a potential prognostic factor for the radiotherapy of carcinoma of the cervix. *International Journal of Radiation Biology,* **56,** 761-765.

Whillans D. W. and Hunt J. W., 1982, A rapid mixing comparison of the mechanisms of radiosensitization by oxygen and misonidazole in CHO cells. *Radiation Research,* **90,** 126-141.

Whillans D. W. and Rauth A. M. ,1980, An experimental and analytical study of oxygen depletion in stirred cell suspensions. *Radiation Research*, **84,** 97-114.

Whitaker S. J., Ung Y. C. and McMillan T. J., 1995, DNA double-strand break induction and rejoining as determinants of human tumour cell radiosensitivity. A pulsed-field gel electrophoresis study. *International Journal of Radiation Biology*, **67,** 7-18.

Wideroe R., 1971, Various examples from cellular kinetics showing how radiation quality can be analyzed and calculated by the two-component theory of radiation. In: *Biophysical Aspects of Radiation Quality*, Proceedings Series STI/PUB/286, Edited by: M. Krippner (International Atomic Energy Agency, Vienna), pp. 311-330.

Wilson R. R., 1946, Radiological use of fast protons. *Radiology*, **47**, 487-491.

Wilson D. F. and Cerniglia G. J., 1992, Localization of tumours and evaluation of their state of oxygenation by phosphorescence imaging. *Cancer Research*, **52,** 3988-3993.

Withers H. R., Mason K., Reid B. O., Dubravsky N., Barkley H. T., Brown B. W. and Smathers J. B., 1974, Response of mouse intestine to neutrons and gamma rays in relation to dose fractionation and division cycle. *Cancer,* **34,** 39-47.

Wolff S., Afzal V., Wiencke J. K., Olivieri G. and Michaeli A., 1988, Human lymphocytes exposed to low doses of ionizing radiations become refractory to high doses of radiation as well as to chemical mutagens that induce double-strand breaks in DNA. *International Journal of Radiation Biology & Related Studies in Physics, Chemistry & Medicine*, **53,** 39-47.

Wolff S., 1992, Failla Memorial Lecture. Is radiation all bad? The search for adaptation. *Radiation Research,* **131,** 117-123.

Woloschak G. E., Chang-Lu C.-M. and Shearin-Jones P., 1990, Regulation of protein kinase C by ionizing radiation. *Cancer Research,* **50,** 3963-3967.

Wouters B. G., Sy A. M. and Skarsgard L. D., 1995, Low dose hypersensitivity and increased radioresistance in a panel of human tumour cell lines with different radiosensitivity. *(Submitted to Radiation Research).*

Wouters B. G. and Skarsgard L. D., 1994, The response of a human tumour cell line to low radiation doses: evidence of enhanced sensitivity. *Radiation Research,* **138,** S76-S80.

Wyllie A. H., 1992, Apoptosis and the regulation of cell numbers in normal and neoplastic tissues: an overview. *Cancer & Metastasis Reviews*, **11,** 95-103.

Xiong Y., Hannon G. J., Zhang H., Casso D., Kobayashi R. and Beach D., 1993, p21 is a universal inhibitor of cyclin kinases. *Nature,* **366,** 701-704.

Yuan J., Shaham S., Ledoux S., Ellis H. M. and Horvitz H. R., 1993, The C. elegans cell death gene ced-3 encodes a protein similar to mammalian interleukin-1 beta-converting enzyme. *Cell,* **75,** 641-652.

Zeman E. M., Brown J. M., Lemmon M. J., Hirst V. K. and Lee W. W., 1986, SR 4233: A new bioreductive agent with high selective toxicity for hypoxic mammalian cells. *International Journal of Radiation Oncology, Biology, Physics,* **12,** 1239-1242.

Zeman E. M., Lemmon M. J. and Brown J. M., 1990, Aerobic radiosensitization by SR 4233 *in vitro* and *in vivo. International Journal of Radiation Oncology, Biology, Physics,* **18,** 125-132.

8

APPENDICES

8.1 Experimental Errors

The uncertainty associated with measurements of plating efficiency in the cell sorter assay results from biological variation, statistical error, and other experimental errors. The uncertainty in the measured plating efficiency (p.e.) is defined as the standard deviation, σ_m, and for each dose point can be found by:

$$\sigma_m = \sqrt{\frac{\sum_{i=1}^{n}(\overline{p.e.} - p.e._i)^2}{n-1}}$$

Equation 8-1

where n is the number of repeated measurements at each dose point (m denotes the *measured* error). In order to compare these values at different dose levels, the relative error is used. This is simply the measured deviation divided by the measured plating efficiency:

$$Relative\ error = \frac{\sigma_m}{\overline{p.e.}}$$

Equation 8-2

Provided there are significant numbers of individual measurements, the relative error provides a good estimate of the uncertainty which results from errors in cell sorting, colonies scored, and the binomial variance associated with a limited sampling of the population. Measurement of plating efficiency involves selecting cells from a population containing those with clonogenic ability and those without. In this situation the binomial distribution applies. This distribution describes the probability of selecting a representative proportion of these cells, such that the measured probability of clonogenicity (the measured plating efficiency) will reflect the true probability of clonogenicity. When a sample from this population is examined (*e.g.*, a single

measurement) the measured plating efficiency is equal to the number of colonies counted divided by the number of cells at risk (c), and is the best estimate of the true probability of clonogenicity. This measurement has an associated error due to limited sampling given by the binomial function:

$$\sigma_b = \sqrt{\frac{p.e.(1 - p.e.)}{c}}$$

Equation 8-3

(b denotes the *binomial* error). In the application of the cell sorter assay, the number of cells plated is adjusted to produce approximately 500 colonies per Petri dish. Thus,

$$c(p.e.)=500$$

Equation 8-4

and the binomial error becomes:

$$\sigma_b = \sqrt{\frac{p.e.^2(1 - p.e.)}{500}}$$

Equation 8-5

The corresponding relative binomial error can then be found:

$$\frac{\sigma_b}{p.e.} = \sqrt{\frac{(1 - p.e)}{(500)}}$$

Equation 8-6

The appropriate value to use in these equations is the measured plating efficiency rather than the measured survival values, which are normalized by the zero dose control plating efficiency. This is because the plating efficiency describes the true probability of clonogenicity and thus the variance in this value includes the variance due to sampling from a cell population containing cells which do not have colony forming ability regardless of treatment.

The residual error (σ_r) between the measured and binomial error is due to all other errors including cell sorting errors, colony counting errors, and other biological errors.

This value can be found by subtracting the binomial variance from the measured variance:

$$\sigma_{r.}^{2} = \sigma_{m}^{2} - \sigma_{b}^{2}$$

Equation 8-7

and the corresponding residual relative error is simply:

$$\frac{\sigma_r}{p.e.} = \frac{\sqrt{\sigma_m^2 - \sigma_b^2}}{p.e.}$$

Equation 8-8

In all cases these relative errors refer to the deviation among *individual* measurements (*i.e.*, individual Petri-dishes), and are thus specific to the protocol for which the assay is applied (*i.e.*, the number of colonies produced per Petri dish). The relative errors in the *mean* values for any of the above defined errors are reduced by a factor equal to the square root of the number of measurements which are made at each dose point.

The increased precision of the FACS cell sorting assay is primarily due to a knowledge of the actual numbers of cells at risk with a high degree of accuracy. This therefore contributes only a small amount to the residual uncertainty. When cells are plated in the conventional manner, from a volume containing an average number of cells/ml, the Poisson distribution applies to the number of cells plated. Thus, the actual number of cells plated is equal to:

$$c \pm \sqrt{c}$$

Equation 8-9

When the relative error from equation 8-9 is combined with the relative binomial error from the distribution of clonogenic cells (equation 8-5), one arrives at the value:

$$\sigma_{col} = \sqrt{\frac{1}{c} + \frac{1 - p.e.}{c(p.e.)}} = \sqrt{\frac{p.e. + 1 - p.e.}{c(p.e.)}} = \sqrt{\frac{1}{c(p.e.)}}$$

Equation 8-10

which is the commonly quoted relative Poisson error in the number of *colonies* counted. However, it should be pointed out that this value is always an underestimate of the true error in the conventional assay. This is because both of the quantities used to determine the value for the number of cells at risk (plating a given *volume* from a population with an average number of *cells/ml*) also have significant uncertainties associated with them. It also does not include any random biological error, which can contribute significantly to the actual measured error.